

Welsh School of Pharmacy

CARDIFF UNIVERSITY



**NANO GEL-BASED CARRIERS FOR
TOPICAL DELIVERY**

By

NOR HAYATI ABU SAMAH

A thesis submitted to Cardiff University in accordance with the
requirements for the degree of

Doctor of Philosophy

June 2011

UMI Number: U584538

All rights reserved

INFORMATION TO ALL USERS

The quality of this reproduction is dependent upon the quality of the copy submitted.

In the unlikely event that the author did not send a complete manuscript and there are missing pages, these will be noted. Also, if material had to be removed, a note will indicate the deletion.



UMI U584538

Published by ProQuest LLC 2013. Copyright in the Dissertation held by the Author.
Microform Edition © ProQuest LLC.

All rights reserved. This work is protected against
unauthorized copying under Title 17, United States Code.



ProQuest LLC
789 East Eisenhower Parkway
P.O. Box 1346
Ann Arbor, MI 48106-1346

ACKNOWLEDGEMENTS

First and foremost, I wish to express my appreciation to my supervisor, Dr Charles Heard, for his kindness, supervision, and thoughtful suggestions.

I wish to thank Dr Anthony Hann for generously giving me the permission to use the electron microscope facilities in School of Biosciences, and his wonderful ideas and helpful advice regarding the microscope works. I am also greatly indebted to these individuals – Lindy Goddard and Janice Knowlden from Tenovous Centre of Cancer Research, Guy Pitt from Electron Microscope Unit (School of Biosciences) and not to forget all the technical and support staffs at the Welsh School of Pharmacy.

I also owe a debt of gratitude to my colleagues in the Skin and Natural Product Research Group (present and past) especially David Houston, whom I had worked with in the same laboratory (1.35) for more than 3 years, during both good and hard times. Special thanks to Ministry of Higher Education (Malaysia) and Faculty of Pharmacy (Universiti Teknologi MARA) for their financial support.

Finally, but by no means last in my thoughts, I would like to particularly thank my parents – Abu Samah Md Ali and Sharifah Aminah Syed Hussein, for their never-ending love, encouragement and prayers throughout my years as a student. Not to forget all my dear friends who always support me, “terima kasih and thank you”.

LIST OF ABBREVIATIONS AND SYMBOLS

~	approximate
μm	micrometre
AAc	acrylic acid
APS	ammonium persulfate
BA	butyl acrylate
CA	citric acid
CA-adjusted poly(NIPAM-co-BA)	pH adjusted with CA – copolymer poly(<i>N</i> -isopropylacrylamide) <i>co</i> -butyl acrylate
cLog <i>P</i>	calculated logarithm of the octanol/water partition coefficient ratio
CLSM	confocal laser scanning microscopy
COX	cyclooxygenase
DMSO	dimethyl sulfoxide
DSC	differential scanning calorimeter
DTT	dithiothreitol
EDTA	ethylene diamine tetraacetic acid
EE	encapsulation efficiency
EIA	enzyme immunoassay
EP	emulsion polymerisation
<i>g</i>	gravity
g	gram
h	hour
HaCaT	human keratinocytes
HBSBS	Hanks' balanced salt buffer solution
HBHBS solution	HEPES-buffered Hanks' balanced salt solution
HEPES	<i>N</i> -(2-hydroxyethyl)piperazine- <i>N'</i> -(2-ethanesulfonic acid)
HPLC	high performance liquid chromatography
HRP	horseradish-peroxidase
<i>J</i> _{ss}	steady state flux
KPS	potassium persulfate
KTTKS	lysine-threonine-threonine-lysine-serine
kV	kilovolt
Kx	a thousand times (microscope magnification)
L	litre
LCST	lower critical solution temperature
LOD	limit of detection
M	molarity
MAA	methacrylic acid

Magn	magnification
MC-DSC	multi-cell differential scanning calorimeter
Palmitoyl-KTTKS	palmitoyl-lysine-threonine-threonine-lysine-serine
MBA	<i>N,N'</i> -methylenebis-acrylamide
min	minute
mL	millilitre
MTX	methotrexate
MW	molecular weight
NIPAM	<i>N</i> -isopropylacrylamide
NMR	nuclear magnetic resonance
nm	nanometre
PAGE	polyacrylamide gel electrophoresis
PBS	phosphate buffered saline
PolyNIPAM	poly(<i>N</i> -isopropylacrylamide)
Poly(NIPAM-co-AAc)	copolymer poly(<i>N</i> -isopropylacrylamide) <i>co</i> -acrylic acid
Poly(NIPAM-co-BA)	copolymer poly(<i>N</i> -isopropylacrylamide) <i>co</i> -butyl acrylate
<i>r</i>	reactivity ratio
<i>R</i>	regression
RIPA	radio immune precipitation assay
rpm	revolutions per minute
RT	room temperature
s	seconds
SC	stratum corneum
SD	standard deviation
SDS	sodium dodecyl sulfate
SEM	scanning electron microscope
SFEP	surfactant-free emulsion polymerisation
SR	swelling ratio
T	temperature
TBS	Tris-buffered saline
TEM	transmission electron microscope
TEMED	<i>N, N,N',N'</i> -tetramethylethylenediamine
TFA	trifluoroacetic acid
Tween® 20	polyoxyethylene-sorbitan monolaurate
UA	uranyl acetate
VAA	vinylacetic acid
VPTT	volume phase transition temperature
w/v	weight/volume
w/w	weight/weight

PUBLICATIONS FROM THIS THESIS

Full Papers

Samah, N.A., Heard, C.M., 2011. Topically applied KTTKS: a review. *Int. J. Cosmet. Sci.* (corrected proof).

Samah, N.A., Williams, N., Heard, C.M., 2010. Nanogel particulates located within diffusion cell receptor phases following topical application demonstrates uptake into and migration across skin. *Int. J. Pharm.* 401, 72-78.

Singka, G.S.L., Samah, N.A., Zulfakar, M.H., Yurdasiper, A., Heard, C.M., 2010. Enhanced topical delivery and anti-inflammatory activity of methotrexate from an activated nanogel. *Eur. J. Pharm. Biopharm.* 76, 275-281.

Conference Presentations

Singka, G.S.L., Samah, N.A., Zulfakar, M.H., Yurdasiper, A., Heard, C.M. Enhanced topical delivery and anti-inflammatory activity of methotrexate from an activated nanogel. 25th Annual Postgraduate Research Day, Cardiff University, November 2010 (Poster).

Samah, N.A., Denyer, S.P. and Heard, C.M. Polymer based temperature- & pH-sensitive nanogel carrier: Delivery of nanogel particles into the skin. WSP Postgraduate Research Day, Cardiff University. March 2010 (Poster).

Samah, N.A., White A.W., Heard, C.M. Cutaneous delivery of Lysine-Threonine-Threonine-Lysine-Serine (KTTKS). APS Skin Forum, University of London. July 2008 (Poster).

Samah, N.A., Yurdasiper, A., White, A.W., Denyer, S.P. and Heard, C.M. Polymer-based temperature-sensitive carrier for Cosmeceuticals. WSP Postgraduate Research Day, Cardiff University. March 2009 (Poster).

ABSTRACT

This thesis investigated the potential of multiple stimuli-responsive nanogels as carriers in topical drug administration, with a view to developing a multi-responsive topical delivery system. Firstly, temperature-responsive *N*-isopropylacrylamide (NIPAM) was co-polymerised with a butyl acrylate monomer to yield poly(NIPAM-co-BA), which was loaded with a model permeant, methotrexate. An *in vitro* study of the loaded nanogel showed that it was capable of delivering methotrexate across the epidermis in levels that significantly reduce the biosynthesis of prostaglandin E₂ (PGE₂), a key inflammation mediator. Moreover, reduced lag time and enhanced delivery by the addition of sodium carbonate to the nanogel were observed. However, Western blotting for cyclooxygenase-2 (COX-2) in *ex vivo* skin, found the nanogel to be pro-inflammatory; thus the observed reduced level of PGE₂ was due to the enhanced delivery of methotrexate, which overwhelmed the inflammatory effect produced by the nanogel. Next, a temperature- and pH-responsive polyNIPAM copolymerised with acrylic acid known as poly(NIPAM-co-AAc)(5%) nanogel was synthesised. An *in vitro* migration study demonstrated that particles of the poly(NIPAM-co-AAc)(5%) were capable of penetrating the porcine skin and migrating across the epidermis, as shown by the presence of the particulates in the diffusion cell receptor phases. Furthermore, the nanogels were shown to enhance the delivery of loaded drugs across the epidermis in comparison to saturated solutions of the corresponding drugs. Western blotting for COX-2 demonstrated that the nanogel did not induce significant inflammatory reactions post-topical application, suggesting its compatibility with skin. A preliminary investigation examined a single-compartment system comprised of poly(NIPAM-co-AAc)(5%) nanogel and pH modulator-containing liposome, designed to remain stable until its application onto the skin. However, the composite system proved unsuccessful, primarily due to the liposome instability. Overall, this novel smart topical drug delivery system is within reach, provided the pH modulator-loaded liposome can be adequately stabilised.

TABLE OF CONTENTS

DECLARATION.....	I
ACKNOWLEDGEMENTS.....	II
LIST OF ABBREVIATIONS AND SYMBOLS.....	III
PUBLICATIONS FROM THIS THESIS.....	V
ABSTRACT.....	VI
TABLE OF CONTENTS	VII
LIST OF FIGURES	XV
LIST OF TABLES	XXVII
LIST OF EQUATIONS.....	XXX
CHAPTER 1 GENERAL INTRODUCTION.....	1
1.1 OVERVIEW.....	2
1.2 SKIN: MORPHOLOGY AND FUNCTIONS.....	3
1.3 TOPICAL DELIVERY	5
1.3.1 Modes of Topical Delivery	6
1.3.2 Routes of Penetration	9
1.3.3 Factors Affecting Drug Delivery to the Skin.....	12
1.3.3.1 Physicochemical Factors.....	12
1.3.3.2 Physiological Factors	14
1.3.4 Mathematical Models of Skin Permeation.....	17
1.3.5 Strategies and Innovations for Enhancement of Topical Drug Delivery.....	18
1.3.5.1 Chemical Approach	18
1.3.5.2 Physical Approach	19
1.4 NANOTECHNOLOGY.....	20
1.4.1 Properties and Benefits of Nanoparticles.....	20
1.4.2 Hydrogels.....	21
1.4.2.1 Nanogels.....	24
1.5 POLYNIPAM-BASED RESPONSIVE NANOGELS.....	25
1.5.1 Swelling and De-swelling Behaviours of Nanogels	25
1.5.2 Effect of Temperature	26
1.5.3 Effect of pH.....	29
1.5.4 Effect of Co-monomers	30
1.5.5 Effect of Cross-linking Agents.....	32

1.6	NANOGELS IN DRUG DELIVERY SYSTEMS	32
1.6.1	Nanogels in Topical Drug Delivery	34
1.7	LIPOSOMES	35
1.7.1	The Use of Liposomes in Transdermal Applications	37
1.7.2	Mode of Action: Vesicle-skin Interactions	37
1.8	RESEARCH HYPOTHESIS AND AIMS	39
1.8.1	Hypothesis	39
1.8.1.1	Controlled Nanogel Activation	39
1.8.1.2	A Stimulus-responsive Topical Drug Delivery System: Nanogel and Liposome	41
1.8.2	Aims	43
CHAPTER 2 SYNTHESIS AND CHARACTERISATION OF TEMPERATURE-SENSITIVE POLYNIPAM-BASED NANOGELS		45
2.1	INTRODUCTION	46
2.1.1	Nanogel Synthesis: EP	46
2.2	MATERIALS AND METHODS	51
2.2.1	Materials	51
2.2.2	Methods	51
2.2.2.1	Nanogel Synthesis	51
2.2.2.1.1	PolyNIPAM	51
2.2.2.1.2	Copolymer PolyNIPAM <i>co</i> -Butyl Acrylate: Poly(NIPAM- <i>co</i> -BA)	54
2.2.2.1.3	Citric Acid-adjusted Poly(NIPAM- <i>co</i> -BA)	54
2.2.2.2	Nanogel Purification	56
2.2.2.3	Physicochemical Characterisation	56
2.2.2.3.1	Particle Size and Size Distribution	57
2.2.2.3.2	Stimulus-responsive Properties	58
2.2.2.3.2.1	Temperature	58
2.2.2.3.2.2	Temperature Cycling	59
2.2.2.3.2.3	pH	60
2.2.2.3.3	Thermal Analysis: Phase Transition	60
2.2.2.3.4	Morphology Determination by SEM and TEM	62
2.2.2.3.4.1	SEM	62
2.2.2.3.4.2	TEM	63
2.2.2.3.4.2.1	Preparation of Ploloform ^o -coated Copper Grids	64
2.2.2.3.4.2.2	TEM Imaging	65
2.2.2.3.4.3	Particle Size Analysis by SEM and TEM	65
2.2.2.4	Data and Statistical Analysis	66
2.3	RESULTS AND DISCUSSION	66
2.3.1	Physicochemical Characterisation	67
2.3.1.1	Particle Size and Size Distribution	67

2.3.1.2	Temperature-responsive Effect.....	71
2.3.1.3	pH-responsive Effect	75
2.3.1.4	Thermal Analysis: Phase Transition	76
2.3.1.5	Size and Morphology.....	77
2.3.1.5.1	SEM	78
2.3.1.5.2	TEM.....	81
2.4	CONCLUSION.....	83
CHAPTER 3 PROBING ENHANCED TOPICAL DRUG DELIVERY BY POLY(NIPAM-CO-BA) NANOGEL AS A CARRIER 84		
3.1	INTRODUCTION.....	85
3.2	MATERIALS AND METHODS	88
3.2.1	Materials.....	88
3.2.2	Methods	89
3.2.2.1	Preparation of MTX-loaded Poly(NIPAM-co-BA) Nanogel.....	89
3.2.2.2	Preparation of Water Saturated with Na ₂ CO ₃	92
3.2.2.3	Thermal Analysis: Phase Transition	92
3.2.2.4	Test Membranes: Porcine Full-thickness, Heat-separated Porcine Epidermis and Silastic [®] ...	93
3.2.2.4.1	Heat-separated Porcine Epidermis	93
3.2.2.4.2	Silastic [®] Membrane	94
3.2.2.4.3	Porcine Full-thickness Skin	94
3.2.2.5	<i>In vitro</i> Permeation Study.....	95
3.2.2.5.1	HPLC Analysis	97
3.2.2.6	Determination of PGE ₂ in Porcine Skin <i>Ex vivo</i>	98
3.2.2.6.1	<i>In vitro</i> Skin Permeation.....	98
3.2.2.6.2	EIA.....	99
3.2.2.7	Data and Statistical Analysis.....	100
3.3	RESULTS AND DISCUSSION.....	101
3.3.1	Thermal Analysis: Phase Transition	101
3.3.2	Permeation of MTX across Test Membranes	102
3.3.2.1	Silastic [®] Membrane	102
3.3.2.2	Heat-separated Porcine Epidermal Membrane	102
3.3.3	Modulation of Skin PGE ₂ Level	104
3.3.4	Proposed Mechanism	106
3.4	CONCLUSION.....	108
CHAPTER 4 SYNTHESIS AND CHARACTERISATION OF PH- AND TEMPERATURE-SENSITIVE POLY(NIPAM-CO-AAC) NANOGELS..... 110		
4.1	INTRODUCTION.....	111
4.2	MATERIALS AND METHODS	112
4.2.1	Materials.....	112

4.2.2	Methods	113
4.2.2.1	Synthesis of Poly(NIPAM-co-AAc) Nanogels	113
4.2.2.2	Nanogel Purification	114
4.2.2.3	Physicochemical Characterisation	115
4.2.2.3.1	Effect of Temperature and pH	115
4.2.2.3.2	Thermal Analysis: Phase Transition.....	115
4.2.2.3.3	Swelling Behaviour: Measurement of Swelling Ratio (SR)	115
4.2.2.3.4	Morphology Determination by SEM and TEM	117
4.2.2.3.4.1	SEM.....	117
4.2.2.3.4.2	TEM.....	117
4.2.2.3.4.2.1	Ionic Functional Groups Distribution: Droplet Negative-staining.....	117
4.2.2.3.4.2.2	Effect of pH.....	119
4.2.2.3.4.3	SEM and TEM Particle Size Analysis.....	120
4.2.2.4	Data and Statistical Analysis	120
4.3	RESULTS AND DISCUSSION.....	121
4.3.1	Physicochemical Characterisation	121
4.3.1.1	Particle Size and Size Distribution	121
4.3.1.2	Temperature-responsive Effect.....	123
4.3.1.3	pH-responsive Effect	128
4.3.1.4	Thermal Analysis: Phase Transition	130
4.3.1.5	Swelling Behaviour: Effect of Temperature and Ionic Strength	131
4.3.1.6	Size and Morphology.....	138
4.3.1.6.1	SEM	138
4.3.1.6.2	TEM.....	139
4.3.1.6.2.1	TEM: Droplet Negative-staining.....	142
4.3.1.6.2.2	pH-responsive Effect.....	146
4.4	CONCLUSION.....	150
CHAPTER 5 PROBING THE UPTAKE AND MIGRATION OF NANOGEL PARTICULATES ACROSS SKIN		
151		
5.1	INTRODUCTION.....	152
5.2	MATERIALS AND METHODS	155
5.2.1	Materials.....	155
5.2.2	Methods	155
5.2.2.1	Thermal Analysis: Phase Transition in the Presence of pH Modulator (CA).....	156
5.2.2.2	<i>In vitro</i> Migration of Nanogel Particulates across Porcine Epidermis.....	157
5.2.2.2.1	Preparation of Poly(NIPAM-co-AAc) and PolyNIPAM Nanogels.....	157
5.2.2.2.2	Migration of Nanogel Particulates across Skin <i>In vitro</i>	157
5.2.2.2.3	TEM Analysis	159
5.2.2.3	Membrane Integrity Validation - <i>In vitro</i> Permeation of MTX.....	160
5.2.2.3.1	Preparation of Saturated Aqueous Solution of MTX.....	160

5.2.2.3.2	<i>In vitro</i> Skin Permeation of MTX	160
5.2.2.3.3	Quantitative Analysis	161
5.2.2.4	Data and Statistical Analysis	162
5.3	RESULTS AND DISCUSSION.....	162
5.3.1	Thermal Analysis: Phase Transition	162
5.3.2	Evidence of Nanogel Particulates in Receptor Phase	164
5.3.3	Validation of Skin Membrane Integrity Post-application of Nanogels	170
5.3.4	Proposed Mechanism: Penetration of Nanogel Particulates	171
5.3.4.1	Mechanical Massage	172
5.3.4.2	Hair Follicle: A Geared Pump Mechanism	173
5.4	CONCLUSION.....	178
CHAPTER 6 DELIVERY OF MODEL PERMEANTS USING A TEMPERATURE- AND PH- SENSITIVE POLY(NIPAM-CO-AAC) NANOGEL		
179		
6.1	INTRODUCTION.....	180
6.1.1	Loading of Model Compounds into Poly(NIPAM-co-AAC)(5%)	180
6.1.2	Model Compounds	182
6.2	MATERIALS AND METHODS	185
6.2.1	Materials.....	185
6.2.2	Methods	186
6.2.2.1	Preparation of KTTKS, Palmitoyl-KTTKS and Caffeine Solutions	186
6.2.2.2	Preparation of KTTKS, Palmitoyl-KTTKS and Caffeine Loaded-Poly(NIPAM-co-AAC)(5%) Nanogel	186
6.2.2.2.1	Peptides (KTTKS and Palmitoyl-KTTKS)	187
6.2.2.2.2	Caffeine	187
6.2.2.3	Determination of EE	188
6.2.2.4	Quantitative Analysis.....	188
6.2.2.4.1	KTTKS	188
6.2.2.4.2	Palmitoyl-KTTKS	189
6.2.2.4.3	Caffeine	190
6.2.2.5	<i>In vitro</i> Permeation of Permeants across Heat-separated Porcine Epidermal Membranes from Loaded-poly(NIPAM-co-AAC)(5%) Nanogel.....	191
6.2.2.6	Data and Statistical Analysis	192
6.3	RESULTS AND DISCUSSION.....	193
6.3.1	Loading of KTTKS, Palmitoyl-KTTKS and Caffeine into Poly(NIPAM-co-AAC)(5%) Nanogel	193
6.3.2	<i>In vitro</i> Permeation of Permeants across Heat-separated Porcine Epidermal Membrane from Loaded-poly(NIPAM-co-AAC)(5%) Nanogels	196
6.3.3	Proposed Mechanism	201
6.4	CONCLUSION.....	203

CHAPTER 7 PROBING THE EFFECTS OF TOPICALLY APPLIED POLYNIPAM-BASED NANOGELS ON SKIN INFLAMMATION	204
7.1 INTRODUCTION.....	205
7.1.1 Biocompatibility of PolyNIPAM-based Polymers.....	205
7.1.1.1 Monomer and co-monomers: NIPAM, AAc and BA.....	205
7.1.1.2 PolyNIPAM-based Polymers.....	206
7.1.2 Determining the Modulation of Skin Inflammation.....	207
7.2 MATERIALS AND METHODS.....	209
7.2.1 Materials.....	209
7.2.2 Methods.....	210
7.2.2.1 Western Blot Analysis.....	210
7.2.2.1.1 Sample Preparation: Skin Lysates.....	211
7.2.2.1.1.1 Protein Estimation.....	213
7.2.2.1.1.2 Protein Denaturation.....	213
7.2.2.1.2 Gel Electrophoresis.....	214
7.2.2.1.2.1 SDS-PAGE.....	214
7.2.2.1.2.2 Protein Blotting.....	217
7.2.2.1.3 Immunohistochemistry.....	218
7.2.2.1.3.1 Membrane Blocking.....	218
7.2.2.1.3.2 Primary and Secondary Antibody Conjugation.....	219
7.2.2.1.3.3 Detection of Protein.....	219
7.2.2.1.3.4 Loading Control.....	220
7.2.2.1.4 Data Analysis.....	220
7.3 RESULTS AND DISCUSSION.....	220
7.3.1 Western Blotting Determinations of COX-2 Expression.....	221
7.3.1.1 Poly(NIPAM-co-AAc)(5%) Nanogel.....	221
7.3.1.2 Poly(NIPAM-co-BA) Nanogel.....	223
7.4 CONCLUSION.....	225
CHAPTER 8 PREPARATION, CHARACTERISATION AND LOADING OF LIPOSOMES AS CARRIERS OF PH MODULATOR	227
8.1 INTRODUCTION.....	228
8.1.1 Preparation of Liposomes.....	228
8.1.2 Loading Compounds into Liposomes.....	229
8.1.3 Sphingomyelin Liposomes.....	230
8.2 MATERIALS AND METHODS.....	233
8.2.1 Materials.....	233
8.2.2 Methods.....	234
8.2.2.1 Preparation of Liposomes.....	234
8.2.2.2 Determination of EE.....	235

8.2.2.3	HPLC Analysis of CA.....	236
8.2.2.4	Characterisation of Liposomes.....	237
8.2.2.4.1	Vesicle Size and Size Distribution.....	237
8.2.2.4.2	Release of CA from Degrading Spingomyelin Liposome Vesicles.....	238
8.2.2.4.3	Evaluation of Liposome Stability.....	238
8.2.2.4.3.1	Vesicle Size and Size Distribution.....	239
8.2.2.4.3.2	TEM.....	240
8.2.2.4.4	Thermal Analysis: Phase Transition.....	240
8.2.2.5	Data Analysis.....	241
8.2.3	RESULTS AND DISCUSSION.....	241
8.2.3.1	EE of Liposome.....	241
8.2.3.2	Liposome Characterisation.....	241
8.2.3.2.1	Vesicle Size and Size Distribution.....	241
8.2.3.2.2	Release of CA from Degrading Sphingomyelin Liposome Vesicles.....	242
8.2.3.3	Evaluation of Liposome Stability.....	244
8.2.3.3.1	Vesicle Size and Size Distribution.....	244
8.2.3.3.2	TEM Investigation.....	248
8.2.3.4	Thermal Analysis: Phase Transition.....	256
8.3	CONCLUSION.....	256
CHAPTER 9 COMPOSITE TOPICAL DELIVERY SYSTEM: PH MODULATOR-LOADED LIPOSOME AND DRUG-LOADED POLY(NIPAM-CO-AAC) NANOGEL..... 258		
9.1	INTRODUCTION.....	259
9.1.1	Formulation Design of a pH Modulator-loaded Liposome and Drug-loaded Poly(NIPAM-co-AAc) Nanogel – Skin Composite System.....	261
9.2	MATERIALS AND METHODS.....	262
9.2.1	Materials.....	262
9.2.2	Methods.....	263
9.2.2.1	Effect of pH Modulator and Temperature Concomitantly on Poly(NIPAM-co-AAc)(5%) Nanogel.....	263
9.2.2.2	CA-loaded Liposome – activated – poly(NIPAM-co-AAc)(5%) Nanogel – skin Composite System.....	264
9.2.2.2.1	Particle Size Distribution and Stability Evaluation.....	264
9.2.2.2.2	TEM Investigation.....	266
9.2.2.3	Data Analysis.....	266
9.3	RESULTS AND DISCUSSION.....	267
9.3.1	Effect of pH Modulator and Temperature Concomitantly on Poly(NIPAM-co-AAc)(5%) Nanogel.....	267
9.3.2	CA-loaded Liposome – activated – poly(NIPAM-co-AAc)(5%) – skin Composite System.....	272
9.3.2.1	Stability Evaluation.....	272

9.3.2.1.1	Particle Size & Size Distribution	272
9.3.2.1.2	TEM Investigation	274
9.4	CONCLUSION.....	280
CHAPTER 10	 GENERAL DISCUSSION	281
10.1	GENERAL DISCUSSION.....	282
10.2	FUTURE WORK	286
10.3	CONCLUDING REMARKS	287
REFERENCES	288

LIST OF FIGURES

Figure 1-1: An illustrative diagram of a cross-section of the human skin, showing in details epidermal and dermal layers.....	5
Figure 1-2: Illustration of the potential targets for some examples of compounds that can be delivered through the skin. The magnified illustration represents blood vessels embedded within the dermis. Adapted from (Brown et al., 2006).....	8
Figure 1-3: A simplified diagram of skin structure and possible routes of penetration for exogenous compounds. Adapted from (Benson, 2005).....	11
Figure 1-4: Schematic representation of permeation routes through the SC via intercellular (lipid matrix between the corneocytes) and transcellular (across the corneocytes and the intercellular lipid domain).....	12
Figure 1-5: General factors influence permeability and penetration of a compound across the skin.	13
Figure 1-6: Schematic diagram of major possible steps involved in the absorption of a solute across the skin. Adapted from (Siddiqui et al., 1985).	16
Figure 1-7: Illustration of the difference between macrogels and microgels/nanogels. Adapted from (Thorne et al., 2011).....	22
Figure 1-8: General classifications of hydrogel-based polymers.	23
Figure 1-9: Structure of polyNIPAM chain and identification of its hydrophilic and hydrophobic segments.....	25
Figure 1-10: Schematic illustration of temperature-induced phase transitions in a polyNIPAM chain and a nanogel triggered by changes in environmental temperature. Adapted from (Das, 2008; Galaev and Mattiasson, 2007).....	28
Figure 1-11: Schematic representation of pH-triggered swollen and collapsed states of (A) anionic and (B) cationic nanogel particles. Adapted from (Nur et al., 2010).....	30
Figure 1-12: Chemical structures of several co-monomers that have been suggested in the literature for copolymerisation with polyNIPAM (Schild, 1992).	31
Figure 1-13: Size ranges of polymers for different modes of drug administration (Das, 2008).	34

Figure 1-14: Schematic diagram represents a liposome formed from a bilayer of phospholipid molecules. Adapted from (Balazs and Godbey, 2011).	36
Figure 1-15: Possible mechanisms of action of liposomes intended for cutaneous delivery. Adapted from (El Maghraby et al., 2008).	39
Figure 1-16: Schematic representation on the proposed mechanism of pH-activated drug-loaded nanogel particles.	42
Figure 1-17: Schematic diagram of a proposed pH modulator-loaded liposome – skin – drug-loaded nanogel composite system.....	43
Figure 2-1: The schematic illustrates several steps involve during synthesis of gel particles by SFEP. Adapted from (Galaev and Mattiasson, 2007; Gracia and Snowden, 2007; Saunders and Vincent, 2006).....	49
Figure 2-2: Schematic illustration of the experimental set up for polyNIPAM-based nanogel synthesis.	53
Figure 2-3: Images of a reaction mixture taken during the initial stage of polymerisation. ..	54
Figure 2-4: Proposed synthetic scheme for poly(NIPAM-co-BA) nanogel by SFEP technique using MBA as cross-linker and KPS as initiator at 70°C.	55
Figure 2-5: Typical particle size distribution curve produced by a laser light diffraction analyser, Malvern Mastersizer 2000.	58
Figure 2-6: A typical thermogram of homopolymer polyNIPAM in de-ionised water obtained from MC-DSC showing LCST.	62
Figure 2-7: Illustration of a sample mounted on a specimen stub for SEM.....	63
Figure 2-8: Uncoated copper grid of 200 squares mesh used to mount sample for TEM. Scale bar: 1.0 mm.	64
Figure 2-9: Mean hydrodynamic diameter of polyNIPAM-based nanogels dispersed in de-ionised water measured at RT by a laser light diffraction analyser (n=3, \pm SD).....	69
Figure 2-10: Particle size distribution curves of polyNIPAM-based nanogels dispersed in de-ionised water, measured at RT by a laser light diffraction analyser.	70
Figure 2-11: Mean hydrodynamic diameter, as a function of temperature for polyNIPAM-based nanogels dispersed in de-ionised water measured by a laser light diffraction analyser; span and uniformity values correspond to polydispersity of each measurement (n=3, \pm SD).....	71

Figure 2-12: De-swelling (%) of polyNIPAM-based nanogels in de-ionised water, calculated over two temperature ranges, 2 – 4°C → 32°C and 2 – 4°C → 37 °C (n=3, ± SD).....	73
Figure 2-13: Reversibility of hydrodynamic diameter (A) polyNIPAM (200 rpm), (B) polyNIPAM (300 rpm), (C) poly(NIPAM-co-BA) and (D) CA-adjusted poly(NIPAM-co-BA) dispersed in de-ionised water, as a function of alternating temperatures (25°C → 60°C → 25°C) (n=3, ± SD). In all cases, $p < 0.0001$ between treatments	74
Figure 2-14: Particle size distribution curves for (A) poly(NIPAM-co-BA) and (B) CA-adjusted poly(NIPAM-co-BA) nanogels in different pH environments, measured by a laser diffraction analyser.....	76
Figure 2-15: Thermograms of poly(NIPAM-co-BA) and CA-adjusted poly(NIPAM-co-BA) nanogels in de-ionised water measured by MC-DSC.	77
Figure 2-16: SEM images of freeze-dried CA-adjusted poly(NIPAM-co-BA) particles taken at different magnifications.	79
Figure 2-17: SEM images of freeze-dried poly(NIPAM-co-BA) particles at different magnifications. Most of the particles self-assembled to form a continuous film on drying with no spheres apparent.	80
Figure 2-18: Mean particle diameters of poly(NIPAM-co-BA) and CA-adjusted poly(NIPAM-co-BA) nanogels determined according to SEM images (n=30, ± SD). $p=0.0001$	80
Figure 2-19: TEM images of (A & B) poly(NIPAM-co-BA) and (C & D) CA-adjusted poly(NIPAM-co-BA) particles.....	82
Figure 2-20: Mean particle diameters of poly(NIPAM-co-BA) and CA-adjusted poly(NIPAM-co-BA) nanogels measured based on TEM images (n=150, ± SD). $p=0.0001$	82
Figure 3-1: Chemical structure and physicochemical data for MTX.	86
Figure 3-2: Scheme illustrating biosynthesis of PGE ₂ . Adapted from (Nakatani and Kudo, 2002).....	87
Figure 3-3: Solubilisation of MTX – (A) MTX in de-ionised water followed by (B) pH adjustment to 12 (C) then to neutral.	89
Figure 3-4: Preparation of MTX-loaded poly(NIPAM-co-BA) nanogel.	91
Figure 3-5: MTX-loaded poly(NIPAM-co-BA) nanogel maintained at different temperatures – (A) RT (25°C); (B) 32°C; and (C) 2 – 4°C.	91
Figure 3-6: A typical glass Franz-type diffusion cell.	95

- Figure 3-7:** HPLC chromatogram for MTX dissolved in PBS. 97
- Figure 3-8:** Schematic of EIA for detection of PGE₂. Adapted from (Cayman Chemical Company, 2011). 100
- Figure 3-9:** MC-DSC thermograms for aqueous dispersions of poly(NIPAM-co-BA) nanogel in the presence of saturated and half-saturated aqueous solutions of Na₂CO₃. Aqueous dispersion of Na₂CO₃ -free poly(NIPAM-co-BA) nanogel served as control. 101
- Figure 3-10:** Permeation profiles of MTX from loaded poly(NIPAM-co-BA) nanogel across heat-separated porcine epidermis: No Na₂CO₃ – no added Na₂CO₃; saturated Na₂CO₃ – skin dosed with 25 µL saturated aqueous solution of Na₂CO₃; and half-saturated Na₂CO₃ – skin dosed with 25 µL half-saturated aqueous solution of Na₂CO₃ (n≥3, ± SD). 103
- Figure 3-11:** Bar chart comparing concentrations of PGE₂ (ng mL⁻¹) from different treatment groups, (n=3, ± SD). Skin dosed with: A – MTX-loaded poly(NIPAM-co-BA) nanogel alone; B – MTX-loaded poly(NIPAM-co-BA) nanogel, followed by 25 µL saturated aqueous solution of Na₂CO₃; control (base) – 25 µL saturated aqueous solution of Na₂CO₃ alone; and control (H₂O) – de-ionised water alone. *p*<0.0001 between treatments..... 106
- Figure 3-12:** Schematic representation of MTX-loaded poly(NIPAM-co-BA) preparation for topical drug delivery and a proposed enhanced drug delivery mechanism by the nanogel as a carrier in the presence of a base (Na₂CO₃)..... 108
- Figure 4-1:** Proposed synthetic scheme for poly(NIPAM-co-AAc) nanogel by SFEP technique using MBA as cross-linker and KPS as initiator at 70°C. 114
- Figure 4-2:** UA droplet negative-staining procedure for TEM..... 119
- Figure 4-3:** Particle size profiles of poly(NIPAM-co-AAc)(2%) and poly(NIPAM-co-AAc)(5%) nanogels in de-ionised water, determined at RT by a laser light diffraction analyser; polyNIPAM served as control; polydispersity of each sample represents by span and uniformity values (n=3, ± SD). **p*=0.0001, vs. control; ***p*=0.0006, vs. control; and ****p*<0.0314 between nanogels 122
- Figure 4-4:** Particle size distribution curves for poly(NIPAM-co-AAc)(2%) and poly(NIPAM-co-AAc)(5%) nanogels in de-ionised water, measured at RT using a laser light diffraction analyser. PolyNIPAM served as control..... 122
- Figure 4-5:** Mean hydrodynamic particle diameter, as a function of temperature for poly(NIPAM-co-AAc)(2%) and poly(NIPAM-co-AAc)(5%) nanogels in de-ionised water,

- measured by a laser light diffraction analyser; polyNIPAM acted as a control nanogel; span and uniformity values represent polydispersity ($n=3, \pm SD$)..... 124
- Figure 4-6:** Images of aqueous dispersions of poly(NIPAM-co-AAc)(2%) and poly(NIPAM-co-AAc)(5%) taken after 30 min of storage at designated temperatures, 2 – 4°C → 60°C. 125
- Figure 4-7:** De-swelling of poly(NIPAM-co-AAc)(2%) and poly(NIPAM-co-AAc)(5%) nanogels in de-ionised water, calculated over temperature ranges of (i) 2 – 4°C → 32°C and (ii) 2 – 4°C → 37°C; polyNIPAM served as a control nanogel ($n=3, \pm SD$). 126
- Figure 4-8:** Reversibility of hydrodynamic diameter (A) poly(NIPAM-co-AAc)(2%) and (B) poly(NIPAM-co-AAc)(5%) in de-ionised water, as a function of alternating temperatures (25°C → 60°C → 25°C). $p<0.0001$ between treatments 127
- Figure 4-9:** Mean hydrodynamic particle diameter, as a function of pH for poly(NIPAM-co-AAc) nanogels measured at RT using a laser light diffraction analyser; solutions of varied pH were prepared in the absence of NaCl as ionic strength contributor; span and uniformity represent polydispersity of the particles ($n=3, \pm SD$). 129
- Figure 4-10:** De-swelling factor, as a function of pH for poly(NIPAM-co-AAc)(2%) and poly(NIPAM-co-AAc)(5%) nanogels ($n=3, \pm SD$). 130
- Figure 4-11:** MC-DSC thermograms of poly(NIPAM-co-AAc)(2%) and poly(NIPAM-co-AAc)(5%) nanogel in de-ionised water. PolyNIPAM served as control. 131
- Figure 4-12:** SR as a function of time for poly(NIPAM-co-AAc) nanogels dispersed in pH 5 acetate buffer, maintained at 2 – 4°C over a period of 5 days; polyNIPAM served as control and NaCl (0.01 – 1.00 M) used as the background electrolyte in all measurements ($n=4, \pm SD$). 134
- Figure 4-13:** SR as a function of time for poly(NIPAM-co-AAc) nanogels dispersed in pH 5 acetate buffer, maintained at RT over a period of 5 days; polyNIPAM served as control and NaCl (0.01 – 1.00 M) used as the background electrolyte in all measurements ($n=4, \pm SD$)..... 135
- Figure 4-14:** SR as a function of time for poly(NIPAM-co-AAc) nanogels dispersed in de-ionised water (absence of NaCl), maintained at 2 – 4°C and RT over a period of 5 days; polyNIPAM served as control ($n=4, \pm SD$)..... 136
- Figure 4-15:** SR as a function of ionic strength for poly(NIPAM-co-AAc) nanogels in pH 5 acetate buffer, maintained at 2 – 4°C and RT for 3 days; polyNIPAM served as control

and NaCl (0.01 – 1.00 M) used as the background electrolyte for the acetate buffer (n=4, ± SD).	137
Figure 4-16: Mean particle diameters of poly(NIPAM-co-AAc)(2%) and poly(NIPAM-co-AAc)(5%) nanogels determined according to SEM images (n=30, ± SD). $p=0.0342$	138
Figure 4-17: SEM images of freeze-dried nanogels – (A & B) poly(NIPAM-co-AAc)(2%) and (C) poly(NIPAM-co-AAc)(5%) particles.....	139
Figure 4-18: Mean particle diameters of poly(NIPAM-co-AAc)(2%) and poly(NIPAM-co-AAc)(5%) nanogels determined according to TEM images; polyNIPAM served as control (n=150, ± SD). * $p=0.0001$, vs. control; ** $p=0.0001$, vs. control; and *** $p=0.2419$ between nanogels.	140
Figure 4-19: TEM images of poly(NIPAM-co-AAc)(2%) and poly(NIPAM-co-AAc)(5%) particles; polyNIPAM served as control.	141
Figure 4-20: TEM images of poly(NIPAM-co-AAc) nanogels of varied AAc content (2, 5 and 10%), negatively stained with aqueous UA 2%; polyNIPAM served as control.	144
Figure 4-21: Mean particle diameter, as a function of pH for poly(NIPAM-co-AAc)(2%) and poly(NIPAM-co-AAc)(5%) nanogels determined according to TEM images; polyNIPAM served as control (n=150, ± SD).....	146
Figure 4-22: TEM micrographs of poly(NIPAM-co-AAc)(2%) and poly(NIPAM-co-AAc)(5%) nanogels in a buffer solution of pH 2, negatively-stained with aqueous UA 2%; polyNIPAM served as control.	147
Figure 4-23: TEM micrographs of poly(NIPAM-co-AAc)(2%) and poly(NIPAM-co-AAc)(5%) nanogels in a buffer solution of pH 5, negatively-stained with aqueous UA 2%; polyNIPAM served as control.	148
Figure 4-24: TEM micrographs of poly(NIPAM-co-AAc)(2%) and poly(NIPAM-co-AAc)(5%) nanogels in a buffer solution of pH 10, negatively-stained with aqueous UA 2%; polyNIPAM served as control.	149
Figure 5-1: Chemical structure and physicochemical data for CA.	154
Figure 5-2: Schematic diagram of the experimental design.	156
Figure 5-3: Sketch of a Franz diffusion cell set up for <i>in vitro</i> investigation of poly(NIPAM-co-AAc)(5%) particulate migration across heat-separated porcine epidermis. PolyNIPAM nanogel served as control.	159

-
- Figure 5-4:** Sketch of a Franz diffusion cell set up to determine *in vitro* permeation of MTX across the same skin membranes used in Section 5.2.2.2.2. 161
- Figure 5-5:** HPLC chromatogram for MTX dissolved in de-ionised water. 162
- Figure 5-6:** MC-DSC thermogram of an aqueous dispersion of poly(NIPAM-co-AAc)(5%) in the presence of a pH modulator (aqueous solution of CA, 5%); aqueous dispersions of pH modulator-free poly(NIPAM-co-AAc)(5%) and polyNIPAM served as control. 163
- Figure 5-7:** Receptor phases of *in vitro* of porcine epidermis dosed with – (A & B) poly(NIPAM-co-AAc)(5%) and (C – E) poly(NIPAM-co-AAc)(5%), followed by aqueous solution of CA (5% w/v), sampled at 24 h, stained with aqueous UA 2% and characterised by TEM; (→ Nanogel particle; → Skin debris). 165
- Figure 5-8:** Receptor phases of *in vitro* of porcine epidermis dosed with – (A & B) polyNIPAM alone; (C & D) aqueous solution of CA (5% w/v); and (E & F) de-ionised water, sampled at 24 h, stained with aqueous UA 2% and characterised by TEM; (C – F) samples served as negative controls for the *in vitro* investigation of migration of nanogel particles across porcine epidermis (→ Nanogel particle; → Skin debris). 166
- Figure 5-9:** TEM images of (A) poly(NIPAM-co-AAc)(5%) and (B) polyNIPAM nanogels used for the *in vitro* investigation of migration of nanogel particles across porcine epidermis. 166
- Figure 5-10:** Receptor phases of *in vitro* of porcine epidermis dosed with – (A) poly(NIPAM-co-AAc)(5%) and (B & C) polyNIPAM nanogels, sampled at 24 h, stained with aqueous UA 2% and characterised by TEM; (A – C) samples served as positive controls for the *in vitro* investigation of migration of nanogel particles across porcine epidermis, where the nanogels were applied on defected membranes (i.e. torn). 167
- Figure 5-11:** Receptor phases of *in vitro* of porcine epidermis dosed with – (A & B) aqueous solution of CA (5% w/v); and (C & D) de-ionised water, sampled at 24 h, stained with aqueous UA 2% and characterised by TEM; (A – D) samples served as negative controls for the *in vitro* investigation of migration of nanogel particles across porcine epidermis (→ Skin debris; → Lipid). 168
- Figure 5-12:** Nanogel particles observed in receptor phase by TEM, 24 h post-*in vitro* permeation study (n=3, ± SD); polyNIPAM served as a control nanogel. * $p=0.0434$, vs. control; ** $p=0.0004$, vs. control; and *** $p=0.3659$ 170
-

- Figure 5-13:** Total mass of MTX ($\mu\text{g cm}^{-2}$) recovered in receptor phase after 24 h ($n=3, \pm \text{SD}$) *in vitro* permeation across porcine epidermis. Membranes were previously treated with polyNIPAM nanogel alone; poly(NIPAM-co-AAc)(5%) nanogel alone; poly(NIPAM-co-AAc)(5%) nanogel and aqueous solution of CA (5% w/v); aqueous solution of CA (5% w/v) alone; and de-ionised water alone. $p=0.6478$ between treatments. 171
- Figure 5-14:** Nanoparticle migration via skin surface (SC), furrows and hair follicle infundibulum. Adapted from (Prow et al., 2011). 172
- Figure 5-15:** Structures of terminal hair follicle – ORS (outer root sheath); IRS (inner root sheath); CL (companion layer); FS (fibrous sheath); SG (sebaceous gland); and AP (arrector pili)..... 174
- Figure 5-16:** Penetration depth and capacity in relation to particle size within hair follicles; APC (antigen-presenting cells). 177
- Figure 6-1:** Summary of techniques available for nanogel loading – (A) polymerisation encapsulation and (B) post-fabrication. 182
- Figure 6-2:** Chemical structures of (A) KTTKS; (B) palmitoyl-KTTKS; and (C) caffeine..... 184
- Figure 6-3:** HPLC chromatogram for KTTKS dissolved in de-ionised water..... 189
- Figure 6-4:** HPLC chromatogram for palmitoyl-KTTKS dissolved in de-ionised water. 190
- Figure 6-5:** HPLC chromatogram for caffeine dissolved in de-ionised water. 190
- Figure 6-6:** EE(%) for poly(NIPAM-co-AAc)(5%) nanogel loaded with an aqueous solution of KTTKS at 4°C ($n=4, \pm \text{SD}$); polyNIPAM served as control. $p=0.1757$ 194
- Figure 6-7:** EE(%) for poly(NIPAM-co-AAc)(5%) nanogel loaded with a saturated aqueous solution of palmitoyl-KTTKS at 4°C ($n=4, \pm \text{SD}$); polyNIPAM served as control. $p=0.0578$ 195
- Figure 6-8:** EE(%) for poly(NIPAM-co-AAc)(5%) nanogel loaded with a saturated aqueous solution of caffeine at 4°C and RT ($n=4, \pm \text{SD}$); polyNIPAM served as control. $*p=0.0070$, vs. control (4°C) and $**p=0.8521$, vs. control (RT) 195
- Figure 6-9:** Cumulative permeation profiles for caffeine from loaded-poly(NIPAM-co-AAc)(5%) nanogel with and without the addition of CA solution (5% w/v); caffeine was loaded into the nanogel at 4°C environment; loaded-polyNIPAM nanogel and saturated solution of caffeine served as controls ($n=4, \pm \text{SD}$). 199

- Figure 6-10:** Cumulative permeation profiles for caffeine from loaded-poly(NIPAM-co-AAc)(5%) nanogel with and without the addition of CA solution (5% w/v); caffeine was loaded into the nanogel at RT environment; loaded-polyNIPAM nanogel and saturated solution of caffeine served as controls (n=4, \pm SD). 199
- Figure 6-11:** Schematic presentation of a post-fabrication loading of a model drug into nanogel particles, followed by its delivery or removal triggered by multiple stimuli... 202
- Figure 7-1:** Schematic showing COX pathway – COX-1 and COX-2 enzymes. Adapted from (Maroon et al., 2006)..... 208
- Figure 7-2:** Components of XCell *SureLock*[™] Mini - Cell electrophoresis system apparatus. 214
- Figure 7-3:** Gel electrophoresis set up demonstrating the electrophoresis stage. Sample wells were marked with a marker pen to aid loading of samples..... 216
- Figure 7-4:** Assembly of Western blot ‘gel sandwich’ 217
- Figure 7-5:** COX-2 protein expression by Western blot analysis. Porcine full-thickness skin was treated with the following – control (de-ionised water); NIPAM monomer (1% w/v); AAc monomer (0.05% v/v); aqueous solution of CA (5% w/v); polyNIPAM; poly(NIPAM-co-AAc)(5%); poly(NIPAM-co-AAc)(5%) followed by CA solution; and MTX – negative control at 6 h. The results were normalised using β -actin and level in control was arbitrarily assigned a value of 100%, (n=3, \pm SD). $p < 0.5123$ between treatment groups 222
- Figure 7-6:** Western blotting and densitometric analysis of COX-2 protein expression. Porcine full-thickness skin was treated for 9 h with the following – control (de-ionised water); NIPAM monomer (1% w/v); polyNIPAM; poly(NIPAM-co-BA); and MTX (negative control); Results were normalised using β -actin and level in control was arbitrarily assigned a value of 100% (n=3, \pm SD). (* $p=0.8905$, ** $p=0.1458$, *** $p=0.0035$ and **** $p=0.0060$, vs. control treatment) 225
- Figure 8-1:** Hydrophilic and hydrophobic compounds encapsulation by a liposome vesicle. Adapted from (Pattnaik and Ray, 2009)..... 230
- Figure 8-2:** Chemical structure of sphingomyelin. 230
- Figure 8-3:** Schematic diagram of pH-modulator loaded-liposome vesicles in a proposed single compartment system. 233
- Figure 8-4:** Flow chart describing the procedures for EE determination of CA. 236

-
- Figure 8-5:** HPLC chromatogram showing the retention time for CA dissolved in de-ionised water at ~7 min. 237
- Figure 8-6:** Vesicle size analysis of CA-loaded liposome measured by laser light diffraction analyser at room temperature; unloaded liposome served as control; span and uniformity data represent polydispersity of the samples (n=3, ± SD). $p < 0.0001$ vs. control 242
- Figure 8-7:** pH of CA-loaded liposome, as a function of time (min). Value at the baseline (0 min) obtained while the suspension was maintained at 2 – 4°C, followed by heat application of 32°C for 48 h; unloaded liposome served as control (n=4, ± SD). $p < 0.0001$, vs. control 243
- Figure 8-8:** Mean hydrodynamic diameter of CA-loaded liposome vesicles (green) following maintenance at 2 – 4°C for 30 days; unloaded liposome served as control (purple) (n=3, ± SD)..... 246
- Figure 8-9:** Mean hydrodynamic diameter of CA-loaded liposome vesicles (green) following maintenance at RT (~25°C) for 30 days; unloaded liposome served as control (purple) (n=3, ± SD). 247
- Figure 8-10:** Mean hydrodynamic diameter of CA-loaded liposome determined after 1 h storage at 2 – 4°C, 32°C and 40°C; unloaded liposome served as control (n=3, ± SD). $p < 0.0001$ between treatments..... 248
- Figure 8-11:** TEM images of CA-loaded liposome vesicles maintained at 2 – 4°C taken on day-0 (baseline) and day-7; samples were negatively-stained with aqueous UA 2%. 250
- Figure 8-12:** TEM images of unloaded liposome (control) maintained at 2 – 4°C taken on day-0 (baseline) and day-7; samples were negatively-stained with aqueous UA 2%. 251
- Figure 8-13:** TEM images of CA-loaded liposome maintained at RT taken on day-0 (baseline) and day-7; samples were negatively-stained with aqueous UA 2%. 252
- Figure 8-14:** TEM images of unloaded liposome (control) maintained at RT taken on day-0 (baseline) and day-7; samples were negatively-stained with aqueous UA 2%. 253
- Figure 8-15:** TEM images of CA-loaded liposome taken on day-0 (baseline) and day-7 of storage at 32°C; samples were negatively-stained with aqueous UA 2%. 254
- Figure 8-16:** TEM images of unloaded liposome (control) taken on day-0 (baseline) and day-7 of storage at 32°C; samples were negatively-stained with aqueous UA 2%. 255

-
- Figure 8-17:** MC-DSC thermograms of CA-loaded and unloaded liposomes in de-ionised water..... 256
- Figure 9-1:** Multiple compartment systems – (A & B) SnapPack and (C) TanDerm™ (Rosen, 2005)..... 260
- Figure 9-2:** Particle size distribution curves illustrating poly(NIPAM-co-AAc)(5%) nanogel, unloaded liposome and freshly prepared mixture of both measured at RT using a laser light diffraction system..... 265
- Figure 9-3:** Images of diluted mixtures of poly(NIPAM-co-AAc)(5%) and CA solution (5% w/v) after maintained at various temperatures. From left at (A) 2 – 4°C; (B) RT (~25°C); (C) 32°C; and (D) 37°C. 269
- Figure 9-4:** Images of poly(NIPAM-co-AAc)(5%) suspension at – (A) 32°C; (B) 5 min after cooling down at RT; and (C) after gently shaken to re-disperse the agglomerates. 269
- Figure 9-5:** Images of poly(NIPAM-co-AAc)(5%) dispersed in de-ionised water in absence of CA solution maintained at (A) 32°C and (B) 37°C. 270
- Figure 9-6:** Mean hydrodynamic diameters of poly(NIPAM-co-AAc)(5%) dispersed in de-ionised water, followed by addition of CA solution (5% w/v) and maintained at different temperatures; nanogel sample in the absence of CA served as control (n=3, ± SD). * $p=0.0001$ and ** $p=0.0001$, vs. control. 271
- Figure 9-7:** Particle size distribution curve for a mixture containing a nanogel and liposome – (A) CA-loaded liposome and poly(NIPAM-co-AAc)(5%) and (B) unloaded liposome and poly(NIPAM-co-AAc)(5%) maintained at 2 – 4°C measured on day-0 and day-30. Sample (B) containing the unloaded liposome served as control..... 273
- Figure 9-8:** Particle size distribution curve for a mixture containing a nanogel and liposome – (A) CA-loaded liposome and poly(NIPAM-co-AAc)(5%) and (B) unloaded liposome and poly(NIPAM-co-AAc)(5%) maintained at RT measured on day-0 and day-30. Sample (B) containing the unloaded liposome served as control. 274
- Figure 9-9:** TEM images of a proposed single compartment system where poly(NIPAM-co-AAc)(5%) and CA-loaded liposome exist within a single formulation, maintained at 32°C for 1 h; samples containing unloaded liposome served as control; all samples were negatively-stained with aqueous UA 2% (→ Nanogel; → Liposome). 276
-

-
- Figure 9-10:** TEM images of control (A & B) CA-loaded liposome – polyNIPAM and (C & D) unloaded liposome – polyNIPAM systems maintained at 32°C for 1 h; all samples were negatively-stained with aqueous UA 2% (→ Nanogel; → Liposome)..... 277
- Figure 9-11:** TEM images of a proposed single compartment system where poly(NIPAM-co-AAc)(5%) and CA-loaded liposome exist within a single formulation, maintained at 2 – 4°C for 24 h; all samples were negatively-stained with aqueous UA 2% (→ Nanogel; → Liposome). 278
- Figure 9-12:** TEM images of control (A & B) CA-loaded liposome – polyNIPAM and (C & D) unloaded liposome – polyNIPAM systems maintained at 2 – 4°C for 1 h; all samples were negatively-stained with aqueous UA 2% (→ Nanogel; → Liposome)..... 279

LIST OF TABLES

Table 2-1: The molecular structures of monomers, cross-linking agent and initiator employed during polyNIPAM-based nanogels preparation.....	48
Table 2-2: PolyNIPAM-based nanogels made up to a total preparation volume of 250 mL with de-ionised water (Lopez et al., 2004; Pelton and Chibante, 1986; Yurdasiper et al., 2008).....	55
Table 2-3: Storage conditions for polyNIPAM-based nanogels to investigate temperature-responsive effect.	59
Table 2-4: Particle size profiles of polyNIPAM-based nanogel particles, measured at RT by a laser light diffraction analyser; polydispersity of the samples reflected by span and uniformity values (n=3, \pm SD).	70
Table 2-5: Phase transitions of poly(NIPAM-co-BA) and CA-adjusted poly(NIPAM-co-BA) nanogels dispersed in de-ionised water measured by MC-DSC (n=3 \pm SD).	77
Table 3-1: Dosing regimens for <i>in vitro</i> permeation of MTX loaded-poly(NIPAM-co-BA) nanogel across heat-separated porcine epidermal and Silastic® membranes (n \geq 3).	96
Table 3-2: Dosing regimens for <i>in vitro</i> permeation of MTX loaded-poly(NIPAM-co-BA) nanogel across porcine full-thickness skin (n=3).....	99
Table 3-3: Phase transitions of aqueous dispersions of poly(NIPAM-co-BA) nanogel in the presence of saturated and half-saturated aqueous solutions of Na ₂ CO ₃ measured by MC-DSC; Aqueous dispersion of Na ₂ CO ₃ -free poly(NIPAM-co-BA) served as control (n=3 \pm SD).....	102
Table 3-4: Lag time, steady state flux (J_{ss}) and cumulative permeation after 12 h (Q_{12}) data for MTX across heat-separated porcine epidermal membranes (n \geq 3, \pm SD).....	104
Table 4-1: Poly(NIPAM-co-AAc) nanogels made-up to a total preparation volume of 250 mL with de-ionised water (da Silva and Ganzarolli de Oliveira, 2007; Kratz et al., 2000; Pelton and Chibante, 1986).....	113
Table 4-2: Phase transitions of poly(NIPAM-co-AAc)(2%) and poly(NIPAM-co-AAc)(5%) nanogels in de-ionised water measured by MC-DSC; polyNIPAM served as control (n=3 \pm SD).....	131

Table 4-3: Comparison of theoretical radial density profiles of functional monomers and cross-linker in a particle with experimental observation of a radial functional groups distribution by TEM images. Adapted from (Hoare and McLean, 2006; Hoare and Pelton, 2007; Hoare and Pelton, 2008a).....	145
Table 5-1: Dosing regimens for <i>in vitro</i> migration study of nanogel particles across heat-separated porcine epidermis.....	158
Table 5-2: Phase transition of poly(NIPAM-co-AAc)(5%) nanogel in the presence of a pH modulator (aqueous solution of CA, 5%); aqueous dispersions of poly(NIPAM-co-AAc)(5%)- and polyNIPAM-free pH modulator served as control (n=3 ± SD).	164
Table 5-3: Surface structure of a (A & B) human and (C) porcine hair follicle with a zigzag formation of the cuticular layers along the hair shaft which serves as a basis for a geared pump delivery; image (B) is the magnified version of the image (A).....	176
Table 6-1: Physicochemical properties of KTTKS, palmitoyl-KTTKS and caffeine.	184
Table 6-2: Gradient elution for HPLC analysis of KTTKS.....	189
Table 6-3: Dosing regimens for <i>in vitro</i> permeation of KTTKS- and palmitoyl-KTTKS from loaded nanogels across heat-separated porcine epidermis (n=4).....	191
Table 6-4: Dosing regimens for <i>in vitro</i> permeation of caffeine from loaded-nanogels across heat-separated porcine epidermis (n=4).....	192
Table 6-5: Loading levels of model permeants into poly(NIPAM-co-AAc)(5%) at different temperatures; polyNIPAM served as control (n=4, ±SD)	196
Table 6-6: Lag time, steady state flux (J_{SS}) and cumulative permeation data of caffeine from caffeine-loaded nanogels prepared at 4°C and RT, across the heat-separated porcine epidermal membranes after 12 h (Q_{12}), 24 h (Q_{24}), and 48 h (Q_{48}) of <i>in vitro</i> permeation study (n=4 ± SD). * <i>p</i> value vs. control group (i.e. saturated aqueous solution of caffeine)	200
Table 7-1: Physicochemical properties of NIPAM, AAc and BA monomers.....	206
Table 7-2: Treatments applied for the protein immunoblot study.....	212
Table 7-3: Cocktail of protease inhibitors added to the RIPA buffer for lysis of tissue samples.	212
Table 7-4: Separating and stacking gels used in SDS-PAGE analysis. The preparation can be used to prepare two SDS-PAGE gels.....	215

Table 8-1: Vesicle size analysis of CA-loaded liposome following maintenance at 2 – 4°C for 30 days; unloaded liposome served as control (n=3, ± SD).....	246
Table 8-2: Vesicle size analysis of CA-loaded liposome following maintenance at RT for 30 days; unloaded liposome served as control (n=3, ± SD).....	247
Table 8-3: Vesicle size analysis of CA-loaded liposome following maintenance at 2 – 4°C, 32°C and 40°C for 1 h; unloaded liposome served as control (n=3, ± SD).....	248
Table 9-1: Storage conditions for polyNIPAM-based nanogel particles to investigate temperature-responsive effect.	264
Table 9-2: Particle analysis profile of poly(NIPAM-co-AAc)(5%) nanogel followed by addition of CA solution (5% w/v) and maintained either at 2 – 4°C or RT (n=3, ± SD); nanogel sample in the absence of CA served as control.....	271

LIST OF EQUATIONS

Equation 1-1	13
Equation 1-2	17
Equation 1-3	17
Equation 1-4	18
Equation 1-5	29
Equation 2-1	57
Equation 2-2	66
Equation 2-3	72
Equation 3-1	90
Equation 4-1	117
Equation 4-2	128

CHAPTER 1 | General Introduction

1.1 OVERVIEW

Topical administration is an approach used to deliver pharmaceutical, dermatological and cosmetic actives through the principle barrier of skin, stratum corneum (SC). Despite great interest in this field, it is still limited due to the restrictive physicochemical properties of the potential drugs or active candidates to partition into and diffuses across the SC by topical application. Advanced drug carriers such as liposomes and nanoparticles could solve the problem. Drug carriers of nanoscale (<1000 nanometre, nm) dimensions were first reported, back in the early 70's and since then, they have rapidly evolved in the pharmaceutical field (Otto and M. de Villiers, 2009). Due to their submicron size and additional properties such as biodegradability and multiple-stimuli sensitivity, they are primarily used to improve methods of delivery over conventional formulations such as creams or ointments.

Nanogels are three-dimensional (3-D) polymeric networks which undergo conformational changes according to environmental factors, such as temperature or pH, if dispersed in a suitable solvent such as water. To date, limited work has been published on the use of nanogel particles as drug carriers for topical administration. In this study, nanogels based on *N*-isopropylacrylamide (known as NIPAM) as a primary monomer were copolymerised with co-monomers of different functionalities. Hypothetically, the smart nanogels would result and demonstrate improved delivery of compounds across the SC. Ultimately such nanogels would be formulated with thermally labile liposome vesicles containing entrapped pH modulator, to yield a novel composite highly potent smart topical drug delivery system.

1.2 Skin: Morphology and Functions

Skin is a complex organ and primarily functions as a protective barrier, sensory organ and is also involved in homeostasis maintenance. The average temperature of healthy human skin is about 32 – 34°C (Agarwal et al., 2007), and it is expected to rise as we advance from the skin surface to the interior part. **Figure 1-1** presents a cross-section illustration of the normal human skin. Based on a transdermal drug delivery perspective, human skin is comprised of four main layers: the outermost layer of the tissue (non-viable epidermis) – the stratum corneum (SC); the viable epidermis; the overlying dermis; and the innermost subcutaneous tissues (hypodermis).

The SC layer is generated by the epidermis and is about 10 to 20 µm thick in a dried state (Mendelsohn et al., 2006; Williams, 2003). The layer is a non-viable epidermis and consists of 10 – 20 flattened, stacked, hexagonal and cornified cells, surrounded by an extracellular lamellar lipid matrix of mostly ceramides, free fatty acids and cholesterol (Mendelsohn et al., 2006; Prausnitz et al., 2004). The arrangement is usually depicted in the so-called “brick and mortar” architecture. Its hydrophobic nature is primarily responsible for its highly resistant property against permeation of most exogenous molecules or entities (e.g. chemicals and microbes). Due to that property, it is usually regarded as a separate membrane in topical and transdermal drug delivery even though it is a part of an epidermal layer.

The viable epidermis, estimated to be 50 to 150 µm thick, consists primarily of actively dividing cells, keratinocytes, which slowly evolve outwards to form four distinct layers of cells which, from outside to the inside order, are the SC, stratum granulosum, stratum spinosum and the stratum basale (Foldvari, 2000; Steinsträsser and Merkle, 1995). Langerhans cells, melanocytes and Merkel cells are among other cells that are also scattered throughout the epidermis region. Those cells contain a variety of active enzymes including esterases, proteases and lipases which play a crucial role in the physiologic degradation of keratinocytes to form the multi-layered epidermis (Boderke et al., 1997; Steinsträsser and Merkle, 1995).

The major component of human skin is the dermal layer. Typically, it is 3 to 5 mm thick (Mendelsohn et al., 2006), and rich with blood and lymphatic vessels as well as nerve endings (Foldvari, 2000). The elasticity and resilience of the dermal structure depend on its 3-D meshwork comprised primarily of types I (80% – 85%) and III collagen (10% – 15%), in addition to glycosaminoglycans (GAGs) and elastin (Chung et al., 2001; Diegelmann, 2001; Oikarinen, 2004). Other than scattered fibroblasts, macrophages and mast cells in the dermis, there are a number of associated appendages such as hair follicles, sebaceous glands and sweat ducts present in the membrane (Williams, 2003).

The subcutaneous tissue is located beneath the dermis and is composed of fibrous connective tissue in which fat and elastic fibres are intermingled (Paige, 2005). The layer also contains blood and lymph vessels, the base of hair follicles and nerves. The hypodermis is usually considered insignificant in terms of the permeation of exogenous compounds, as the compounds are assumed to have entered the circulatory system before they manage to reach this layer even though the adipose tissue could retain the compound and serve as a depot (Williams, 2003).

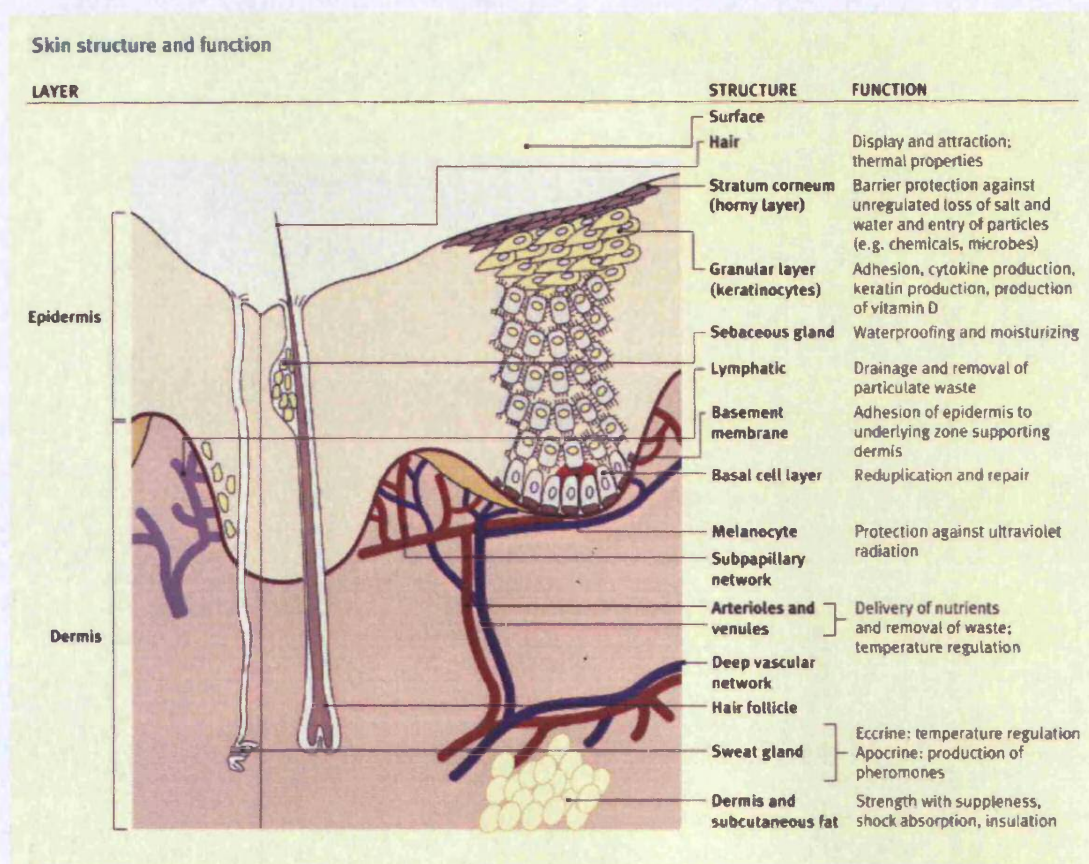


Figure 1-1: An illustrative diagram of a cross-section of the human skin, showing in details epidermal and dermal layers.

Reprinted from Surgery (Oxford) 28, Venus, M., Waterman, J., McNab, I., Basic physiology of the skin, 469-472, Copyright (2011), with permission from Elsevier [OR APPLICABLE SOCIETY COPYRIGHT OWNER].

1.3 Topical Delivery

Some drugs intended for skin therapy are currently delivered to their sites of action by the conventional oral route. For example, methotrexate (MTX) has to be taken orally for moderate to severe psoriasis treatment – psoriasis is a chronic inflammatory disease that is commonly associated with the skin. Even though the drug formulated for oral administration is easier to formulate and can attain rapid onset of action, there are several issues that need to be dealt with, for example systemic side effects and the hepatic first-pass metabolism (i.e. therapeutic dose of a drug is greatly reduced prior to reaching the systemic circulation).

Skin has been considered as a promising alternative route for the delivery of active ingredients particularly drugs, as it manages to avoid the variable absorption and metabolic breakdown associated with oral treatments as the compound enters the systemic circulation without passing through the liver. As the mode of drug delivery becomes specific due to direct application at the intended site for the skin therapy, lower dose of drugs can be utilised due to increase bioavailability. As a result, possible systemic side effects can be prevented or minimised (e.g. intestinal irritation cause by conventional oral formulations). In addition, it is the most accessible route of administration, non-invasive and offers a large surface area for absorption of applied drugs.

Nonetheless, delivery through the skin has several disadvantages including the potential of localised irritation and hypersensitivity due to the active ingredients or additives in the formulations (Berti and Lipsky, 1995; Desai, 2007) and limited contact time for the formulation, as most of the formulations easily wiped away from the site of application (Desai, 2007). Furthermore, the delivered drugs could possibly reach systemic circulation and produce undesirable side effects (Desai, 2007) and there is no specific measurements for applying an accurate dose for formulations such as creams, ointments or gels (based on consumers consideration), which may lead to excessive use or under dose (Desai, 2007). The pharmacological treatments of various skin diseases exhibit some difficulties, particularly when the superficial layer of the SC is not the target site, and drug penetration into the deeper skin layers is required. As a result, it may cause delay onset of action of the active ingredients due to the difficulty for the compounds to diffuse through the skin to reach the target tissues (Berti and Lipsky, 1995).

1.3.1 Modes of Topical Delivery

Modes of delivery of a compound across the skin can be categorised into topical, transdermal and transcutaneous. Examples of compounds that can be delivered through several potential target sites in the skin are shown in **Figure 1-2**. There are several requirements to be met in order for an active compound

formulated for delivery via the skin to offer excellent effects – it has to be potent; low molecular weight (MW); highly skin permeable; has no significant interaction with the skin components; and stable against skin action (e.g. metabolism activities by enzymes) (Flynn, 2002).

When the target sites of therapy are restricted within the skin layers (SC, appendages, epidermis and dermis) with minimal or no permeation, this type of delivery is regarded as topical. Cosmetics (e.g. moisturisers and anti-aging peptides), dermatologicals (e.g. benzoyl peroxide and tretinoin), and drugs (e.g. corticosteroids and antibiotics), are classes of compounds that are commonly intended for various skin conditions such as diseases, anti-aging, etc. They are formulated into appropriate dosage form systems such as gels, creams and ointments in order to attain their delivery into the target sites in the skin. Most cosmetic and dermatological products commonly target the SC and/or epidermis, whereas drug formulations for example, MTX for psoriasis treatment is intended to be localised in the epidermis (i.e. stratum spinosum and stratum basale layers) (Siddiqui et al., 1985).

Topical delivery systems also cover formulations that require their active ingredients to be delivered only onto the surface of the skin. These include antiseptics, antibiotics and cosmetic products (e.g. sunscreen and deodorant). Systemic effects are unnecessary for topical formulations and thus, permeation beyond the dermal layer is undesirable. However, a small amount of the compounds could be possibly absorbed systemically, as further penetration beyond the viable epidermis may offer access to the dermal microvasculature (transdermal) or deeper skin tissues (transcutaneous) (Lau et al., 2008).

Transdermal delivery refers to a compound that traverses through the multi-layered structure of the skin and into the systemic circulation to illicit its pharmacological effect. Drugs such as hormones, opioids and antihypertensives are commonly delivered via a transdermal route. Fentanyl, a potent opioid member indicated for management of moderate to severe chronic pain is one of the drugs successfully formulated for transdermal therapy. The United States Food and Drug

Administration (US FDA) approved its transdermal patch formulation system, Duragesic® for commercial use in 2005 (US Food & Drug Administration, 2005).

For transcutaneous delivery, it is intended that the compounds are delivered across the skin into the underlying tissues for example muscles or joint capsules. Members of non-steroidal anti-inflammatory drugs (NSAIDs) (e.g. ketoprofen and ibuprofen) are suitable for transcutaneous delivery, as they can offer pain relief for conditions such as joint pain or arthritis (Renwick et al., 2001).

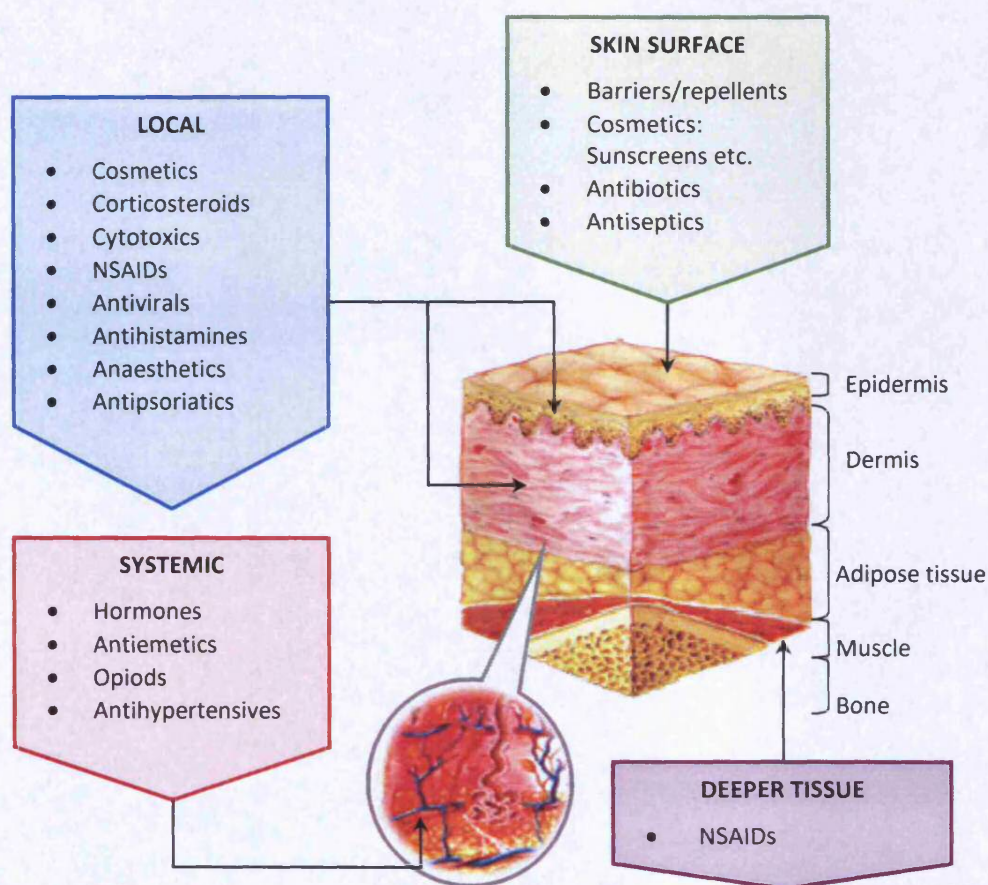


Figure 1-2: Illustration of the potential targets for some examples of compounds that can be delivered through the skin. The magnified illustration represents blood vessels embedded within the dermis. Adapted from (Brown et al., 2006).

1.3.2 Routes of Penetration

The external layer of the skin (SC) is considered as an effective barrier, essential for protection of the internal milieu from the external environment. Permeation through this barrier usually signifies permeation through the skin, due to its overwhelming rate limiting step in the dermal or transdermal delivery of drugs. However, there are several potential routes of access for exogenous compounds, from the surface of the skin to reach sub-epidermal tissue region – the transappendageal or shunt route; the transcellular route; and the intercellular pathway.

Transappendageal or shunt route involves the diffusion of compounds into the skin through sweat gland pores (diameter: 60 – 80 μm) (Sato et al., 1989) and hair follicles with associated sebaceous glands (diameter: 10 – 70 μm) (Lauer et al., 1996), as illustrated in [Figure 1-3](#), routes A and C. Initially, this route was considered to be negligible, as evidence suggested that the fractional area offered is very small and not more than 0.1% (Lauer et al., 1996). However, the density and proportions of the skin appendages vary greatly according to the body regions (Knorr et al., 2009), where the largest surface was found on the forehead, ~13.7 % of the skin surface. These structures may offer a potential route for drug delivery as they originate in the dermal tissue but are accessible as they can be found on the surface of the skin (Stracke and Schneider, 2010; Williams, 2003). Therefore, the compounds could directly reach the dermis without having to traverse the 'intact' barrier of the SC.

Studies have suggested that the follicular penetration route may be especially relevant in the penetration pathways for hydrophilic and high molecular weight molecules (Baroli, 2010; Mitragotri, 2003, 2007), as well as by particle-based drug delivery systems (e.g. liposomes) (Knorr et al., 2009). A pump mechanism is suggested to be one of the responsible mechanisms for the particle-based drug delivery systems penetration – the movement of hair follicles may act as a geared pump due to the zigzag structure of the cuticular layers along the hair shaft, where particles of a similar size to hair cuticles are pushed deep into the follicles (Lademann

et al., 2009; Lademann et al., 2007). The follicular penetration will be discussed in greater detail in CHAPTER 5.

Additionally, the hair follicles represent an efficient reservoir for topically applied substances, which is comparable to the reservoir of the SC on a number of body sites (Lademann et al., 2011; Otberg et al., 2004). For example, hair follicles of the calf region are comparable with those at the scalp (Otberg et al., 2004). The reservoir of the hair follicles is usually located deep in the skin tissue up to 2000 μm and their reservoir depletion occurs only through the slow processes of sebum secretion and hair growth (Knorr et al., 2009; Lademann et al., 2008). The reservoir of the SC in contrast, is mainly located in the uppermost cell layers of the SC ($\sim 5 \mu\text{m}$), where it only provides a short-term reservoir due to continuous depletion from textile contact, washing and physiological process of desquamation.

Intercellular pathway relates to compounds that pass through the continuous lipid domains of the SC between the keratinocytes into the viable epidermis (Williams, 2003). This route is considered to be the predominant pathway for penetration of exogenous compounds through the skin (Hadgraft, 2004; Rosen, 2005). Generally, it is accepted that the compounds traversing the SC through this structured lipoidal pathway are dependent upon their physicochemical properties and thus, most lipophilic compounds will follow this pathway (Mitragotri, 2007). This pathway is very tortuous and much longer in distance than the thickness of the SC (Williams, 2003). Additionally, it was proposed that, the permeation of polar compounds was mediated via the intercellular route (Rosen, 2005). The laminar organisation discontinuities within the intercellular lipids (imperfections in the SC lipid bilayers) create aqueous regions, or micro-channels, that act as polar pathways (Mitragotri, 2003). The structural defects are usually observed in lipid lamellar systems as grain boundaries, fault-dislocations or nanoscale pinholes. The precise size of these defects depends on the type of defect which may span a length scale of 1 to 10 nm.

Transcellular route is often regarded as providing a pathway for polar compounds, possibly through hydrophilic regions present in the lipid layers of the SC (Williams, 2003). The compounds diffuse through the keratinocytes (keratin-filled

corneocytes) which provide an aqueous-based porous pathway but still need to partition into the hydrophobic domains of the lipid layers. The intercellular and transcellular pathways are shown in [Figure 1-3](#), route B and in detail in [Figure 1-4](#).

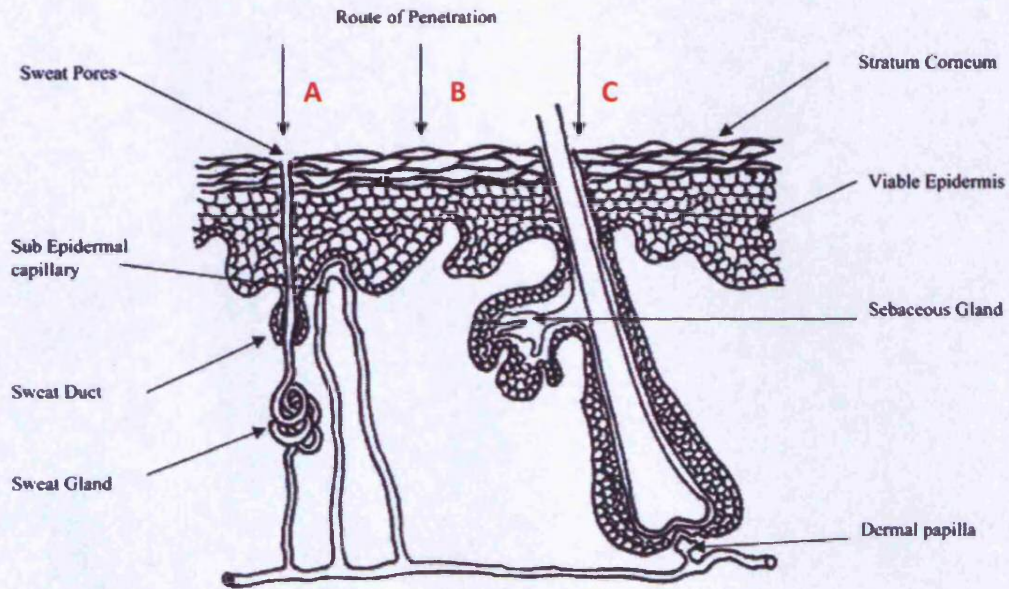


Figure 1-3: A simplified diagram of skin structure and possible routes of penetration for exogenous compounds. Adapted from (Benson, 2005).

(A) Sweat gland pore; (B) directly across SC (transcellular and intercellular); and/or (C) hair follicle with its associated sebaceous gland.

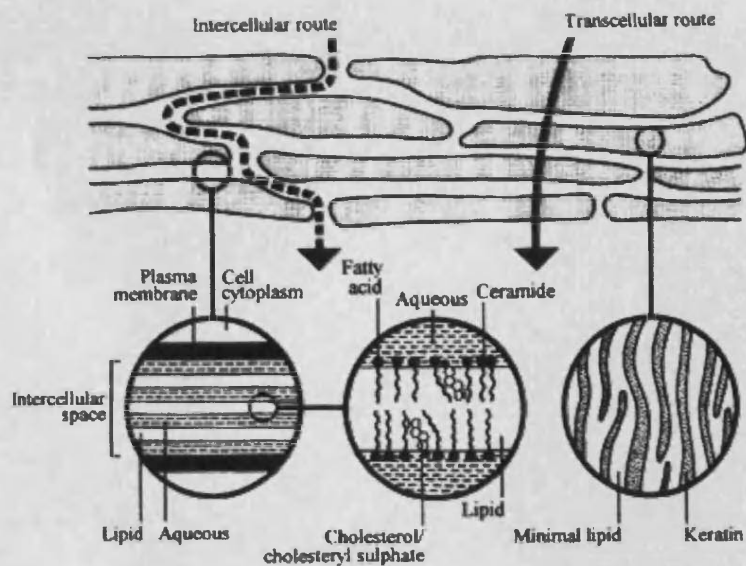


Figure 1-4: Schematic representation of permeation routes through the SC via intercellular (lipid matrix between the corneocytes) and transcellular (across the corneocytes and the intercellular lipid domain).

Percutaneous absorption: drugs-cosmetics-mechanisms-methodology by BRONAUGH, ROBERT L. Copyright 2011 Reproduced with permission of INFORMA HEALTHCARE - BOOKS in the format Dissertation via Copyright Clearance Center.

1.3.3 Factors Affecting Drug Delivery to the Skin

1.3.3.1 Physicochemical Factors

The delivery of drugs to the intended target site in the body, in the right dose, and at the right time, by topical application presents a number of significant challenges. Drugs may often have limited solubility, suffer poor distributions and experience breakdown before they reach their target sites due to metabolism. There are several issues to consider when formulating a compound as a topical or transdermal ingredient, particularly its passive permeation and penetration ability across the skin. **Figure 1-5** summarises factors that may generally influence passive delivery of a particular compound across the skin.

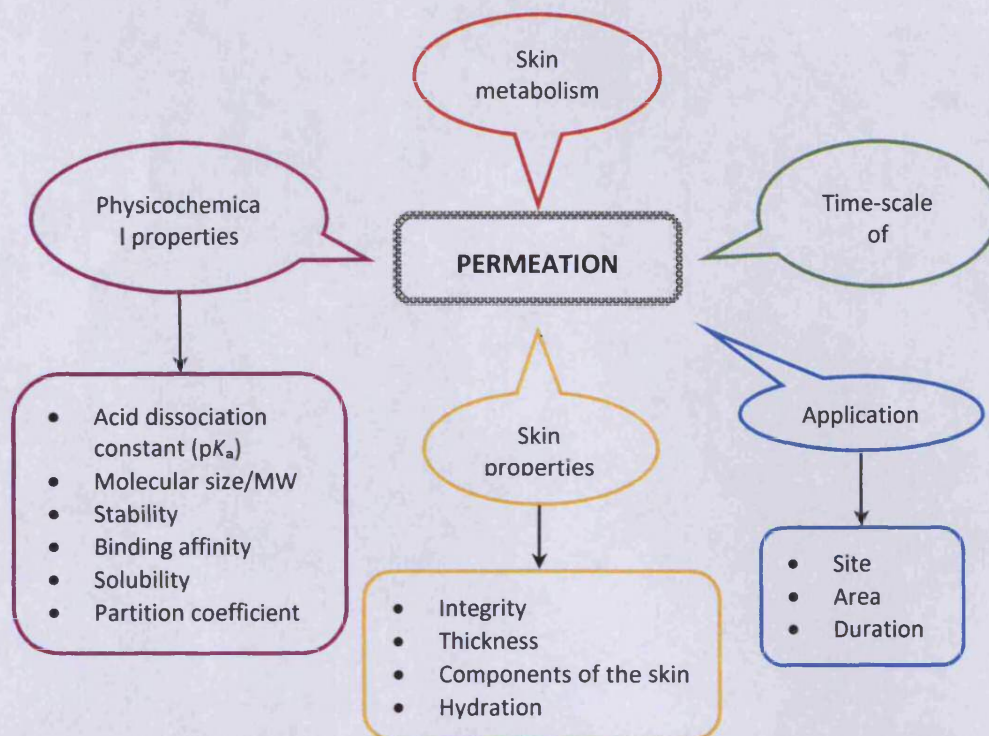


Figure 1-5: General factors influence permeability and penetration of a compound across the skin.

Compounds intended for transcutaneous delivery should ideally possess physicochemical properties within the listed ranges:

- (i) $\log P_{(\text{octanol}/\text{water})}$ in the range of $\sim 1 - 3$ (Gorouhi and Maibach, 2009; Prausnitz et al., 2004; Williams, 2003) – $\log P$ is a measure of the partition coefficient, which is the ratio of a compound concentration between two phases and is calculated as follows:

$$\log P_{(\text{octanol}/\text{water})} = \log \left[\frac{\text{solute}_{(\text{octanol})}}{\text{solute}_{(\text{water})}} \right]$$

Equation 1-1

$\log P$ is preferably applies to small chemical compounds with less polar side chains.

- (ii) MW < 500 (Brown et al., 2006; Lau et al., 2008; Williams, 2003) – it is suggested that an inverse relationship existed between transdermal flux and MW of the compounds. This effect is much more relevant for larger molecules such as peptides and proteins.
- (iii) Aqueous solubility > 100 $\mu\text{g mL}^{-1}$ (Williams, 2003) – lipophilic compounds are ideal candidates for transdermal delivery, however, it is necessary for the compounds to possess some aqueous solubility to provide sufficient concentration since most formulations are generally formulated in an aqueous form. In addition, beyond the optimum lipophilicity, permeation decreases due to the aqueous environment of the viable epidermis.
- (iv) Melting point < 200°C (Gorouhi and Maibach, 2009) – most of compounds with high melting points are relatively lipophilic and may have lower aqueous solubility at ambient temperature and pressure.
- (v) Daily dose < 10 mg day^{-1} (Williams, 2003) – generally limited for compounds which are potent, as one simply cannot transfer high amount of any compound across a small surface area within a short period of time (Guy, 1996).
- (vi) Polar centres of ≤ 4 (Gorouhi and Maibach, 2009; Pugh et al., 1996) – may pose potential interactions such as hydrogen bonding or van der Waals force between the compounds and skin components which may retard the diffusivity of the compounds, resulting lower permeability across the skin.

1.3.3.2 Physiological Factors

The major obstacle facing transdermal delivery is the skin anatomy itself. Between the area of application and the site of action, there are numerous barriers and issues to be dealt with as summarised in [Figure 1-6](#). Once the formulation is applied onto the skin, active compounds must partition into the outermost layer of

the skin, the SC. The layer imposes the major rate-limiting barrier to the permeation of the majority of exogenous compounds (Prausnitz et al., 2004). The structure constitutes only 10% of the entire skin, but contributes a significant role (80%) in the cutaneous barrier function (Pouillot et al., 2008). Comprised of corneocytes (dead cells) in a lipoidal matrix, the barrier is essentially lipophilic in nature and a highly selective membrane for passive permeation of exogenous compounds, especially those that are polar and hydrophilic.

Following the transdermal pathway, the compounds must permeate through the membrane without significantly interacting with keratinocytes and enzymes present in the skin. The spectrum of enzymes and metabolic reactions in the skin are comparable with those found in other tissues for example the liver (Bronaugh and Maibach, 2005; Hadgraft and Guy, 1989; Narawane and Lee, 1994). However, the enzymes activities detected in the skin are low, reported as only 10% of the liver activity (Bronaugh and Maibach, 2005). A great variety of endogenous enzymes such as deaminases and esterases are present in the extracellular compartment of the SC, sebaceous glands and near hair follicles (Pouillot et al., 2008; Williams, 2003), although different anatomical sites of the skin have different levels of enzymatic activities .

Further evidence has highlighted the epidermis as the main site of metabolism in the skin and an important limiting factor for the dermal delivery of drugs (Hadgraft and Guy, 1989; Steinsträsser and Merkle, 1995; Williams, 2003). The epidermis consists of actively dividing cells which slowly evolve outwards to form a layer of dead cells, the SC (Steinsträsser and Merkle, 1995). An essential component of the differentiation process is the physiologic degradation of the keratinocyte components (e.g. proteins or lipids) by lytic enzymes in the viable layer of the epidermis (Boderke et al., 1997; Steinsträsser and Merkle, 1995). At the same time, these enzymes are functionally capable of reacting on exogenous compounds (Steinsträsser and Merkle, 1995). Therefore, the viable epidermis potentially represents an enzymatic barrier for topically applied compounds, as reduced availability of the compounds would affect their optimum benefits.

In addition to the above factors, skin flora which reside on the skin may also impose a barrier to the compounds by reducing their availability prior to entering the skin. Normal human skin is colonised by a range of microorganisms including staphylococci, micrococci and propionibacteria (Davison et al., 2009). The skin flora possess a wide range of enzymes capable of metabolising some topically applied molecules. Furthermore, the compounds could potentially serve as a food substrate for the skin flora. Microorganisms for example *Staphylococcus epidermidis* may metabolise topically applied compounds prior to penetrating the tissues (Williams, 2003).

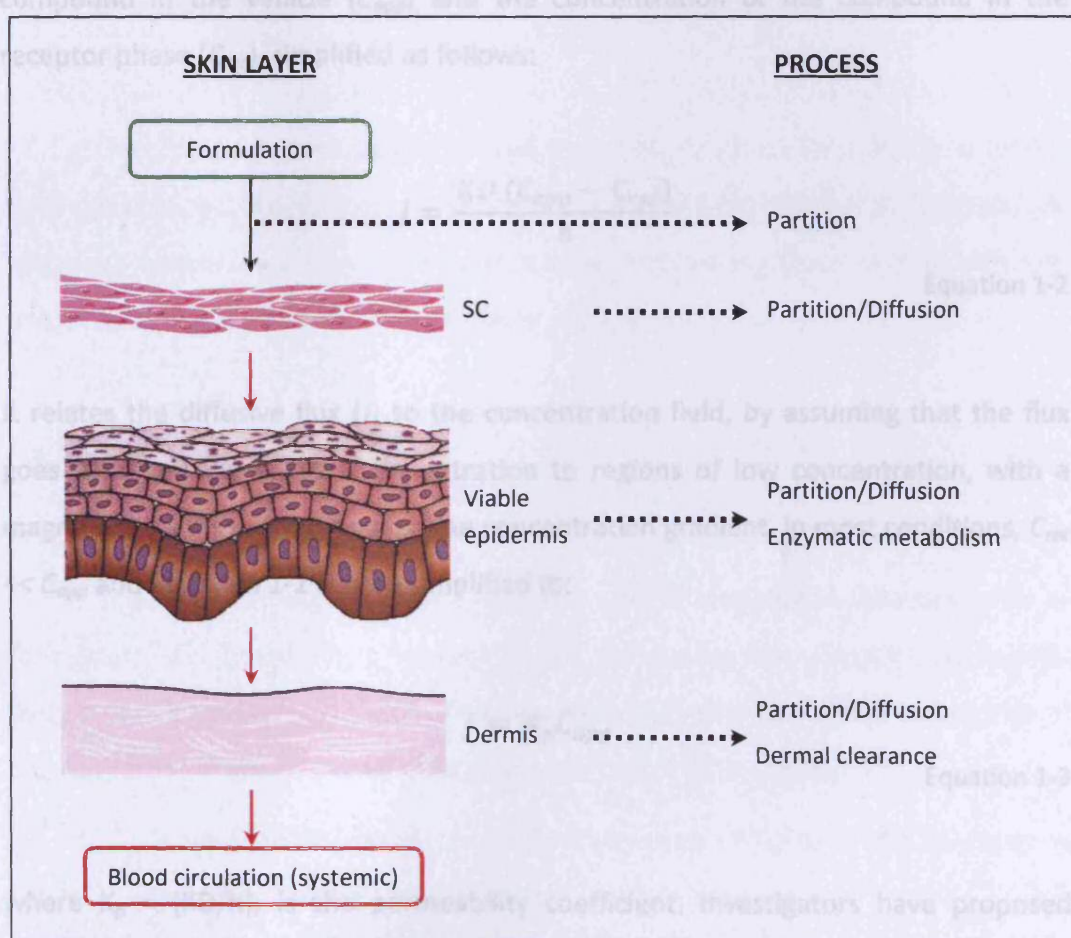


Figure 1-6: Schematic diagram of major possible steps involved in the absorption of a solute across the skin. Adapted from (Siddiqui et al., 1985).

The absorption involves the passage of the solute from the surface of the skin – partitions out of its vehicle into the SC layer, and subsequently diffuses through the SC and underlying epidermis and through the dermis. The dermis contains blood vessels that can take up transdermally administered solutes for systemic circulation.

1.3.4 Mathematical Models of Skin Permeation

Mathematical models can be used for estimating the permeation of an exogenous compound across human skin. Percutaneous absorption of a compound applied on the skin is governed by diffusion, and can be described by Fick's first law of diffusion (Hadgraft, 2004). The model describes the steady state flux per area of a section (J_{ss}) in terms of the partition of the compound between the skin and the applied formulation (partition coefficient, K), its diffusion coefficient (D) in the membrane of diffusional path length (thickness, h), the applied concentration of the compound in the vehicle (C_{app}) and the concentration of the compound in the receptor phase (C_{rec}), simplified as follows:

$$J = \frac{KD (C_{app} - C_{rec})}{h}$$

Equation 1-2

It relates the diffusive flux (J) to the concentration field, by assuming that the flux goes from regions of high concentration to regions of low concentration, with a magnitude that is proportional to the concentration gradient. In most conditions, $C_{rec} \ll C_{app}$ and Equation 1-2 can be simplified to:

$$J = K_p C_{app}$$

Equation 1-3

where $K_p = (KD/h)$, is the permeability coefficient. Investigators have proposed equations that associate drug flux through human skin with the various physicochemical characteristics of the compounds for the best data fitting. One of the most commonly utilised models is the Potts and Guy equation (Potts and Guy, 1992):

$$\text{Log } K_p = 0.71 \log P_{(\text{octanol/water})} - 0.0061 \text{ MW} - 2.74$$

Equation 1-4

The Equation 1-4 relates a compound MW and its $\log P_{(\text{octanol/water})}$ for estimation of a permeability of a solute (K_p , cm h^{-1}) from an aqueous environment. The $\log P$ value can be predicted from numerous software packages and online algorithms or determined based on Equation 1-1.

1.3.5 Strategies and Innovations for Enhancement of Topical Drug Delivery

Over the past years, advances and improvements have been made in topical drug delivery technology and these can be broadly subdivided into 'physical' or 'chemical' approaches. Their role is to increase the driving force of drug diffusion and/or enhance the permeability of the intact skin.

1.3.5.1 Chemical Approach

The chemical approach includes the use of chemical enhancers such as surfactants (e.g. Tween® or propylene glycol), fatty acids (e.g. palmitic acid or oleic acid), and solvents (e.g. ethanol). They can reversibly alter the barrier properties of the skin through several possible mechanisms (Aungst et al., 1990):

- (i) Reversibly disrupting the packed structure of lipids in the SC layer to enhance 'fluidity'.
- (ii) Increase skin/vehicle partitioning of a permeant.
- (iii) Increase solvent transport into or across the skin.

For the latter mechanism it has been suggested that eicosapentaenoic acid (EPA), ethanol and 1,8-cineole exert an enhancing effect by a 'pull' or co-permeation mechanism (Heard et al., 2006; Heard and Screen, 2008). Co-permeation

mechanism (Heard et al., 2006; Heard and Screen, 2008). Co-permeation enhancement effect refers to concomitant transport of vehicle and permeant across the skin barrier, where the movement of vehicle facilitates the movement of the active solutes. This phenomenon has been established in multiple works involving co-formulation of NSAIDs (ketoprofen and ibuprofen) with essential fatty acids (EPA and docosahexaenoic acid, DHA) (Heard et al., 2006; Heard and Screen, 2008). However, the success of chemical enhancers is limited to low molecular mass permeants and their inclusion in the formulation may enhance the absorption of components other than the permeants, which can lead to skin damage and irritancy problems (Prausnitz et al., 2004).

Chemical strategies based on formulation include the use of loaded carriers such as emulsions, liposomes and nanogel particles. They can be customised based on size and chemical composition. Other methods involve adjustment of the thermodynamic activity of permeants e.g. supersaturated systems or modification of the active compounds in a manner designed for chemical or enzymatic action: pro-drugs and the related technique of co-drugs (Brown et al., 2006; Lau et al., 2008).

1.3.5.2 Physical Approach

Physical enhancement generally utilise external energy to physically reduce biological barrier of the SC to promote penetration of exogenous compounds (Brown et al., 2006). They can be classified based on energy force use to assist the delivery – electrical (i.e. iontophoresis, electroporation); mechanical (e.g. microneedles and abrasion); and miscellaneous methods (e.g. ultrasound and laser wave) (Brown et al., 2006). These approaches are preferable for large and hydrophilic molecules such as peptides and proteins. However, the devices developed for physical methods are quite costly, complicated and may pose potential safety risks (electrical components). Furthermore, some of these techniques are usually associated with discomfort sensation and mechanical damage to the skin barrier (Lau et al., 2008).

There were suggestions on a combination of chemical and physical enhancers in order to get synergistic effects of those two techniques. For example, a study demonstrated enhanced transdermal permeation of insulin by combining iontophoresis with chemical enhancers in comparison to the individual techniques (Pillai et al., 2004).

1.4 Nanotechnology

Nanotechnology is a relatively new area which has attracted global interests, where it can be defined as the study of matter at the scale of atoms or molecules. In the United States (US), the Federal funding for nanotechnology has increased from approximately \$464 million in 2001 to nearly \$1.5 billion for the 2009 fiscal year (ObservatoryNANO, 2008). The same phenomenon can be observed in the European Union (EU) and Japan which invested approximately \$1.05 billion and \$950 million, respectively in nanotechnology. The technology is widely applied in medicine and pharmaceutical fields.

Different definitions of nanomaterials have been proposed by various organisations typically range from about 1 nanometre (nm) – 100 nm dimension (Scientific Committee on Emerging and Newly Identified Health Risks, 2010). Even though this scale is generally accepted, it is very difficult to clearly define the top end of the range, as there is no scientific evidence to qualify the appropriateness of the 100 nm limit, i.e. no data are available to indicate that a specific size associated with special properties due to the nanoscale. Others, such as the US FDA proposed an upper limit of 1,000 nm for pharmaceutical fields (Scientific Committee on Emerging and Newly Identified Health Risks, 2010; US Food and Drug Administration, 2010).

1.4.1 Properties and Benefits of Nanoparticles

Nanoscale technology is an exciting area of scientific development which offers potentials in various areas especially in medicine, computing, textiles, and

cosmetic products. Nanotechnology may be able to overcome some of the problems associated with the drug delivery area. The nano-sized structures can be designed as drug delivery vehicles which may offer significant benefits over conventional delivery mechanisms. These benefits include better stability, the possibility of transporting hydrophilic and hydrophobic drugs, high loading capacity due to greatly increased surface area, greater bioavailability, systems that allow controlled and sustained release rates or release upon an external stimulus, and the possibility to exploit a range of patient-friendly delivery routes, e.g. oral, cutaneous or inhalation.

In cosmetics, nanotechnology-based materials are widely used. Currently, they are primarily utilised as ultra violet filters (e.g. titanium dioxide and zinc oxide) and delivery carriers (e.g. hydrogels, liposomes, niosomes and nanostructured lipids) (ObservatoryNANO, 2008). Amongst the available nanomaterials already described in the literature, hydrogels have already proved their value in diverse biomedical applications. These materials can be tailored in size, composition and stimuli-responsive properties as carriers for drug delivery purposes.

In this chapter, we especially aim to highlight some of the most important properties of hydrogels particularly nanogels (<1 μm) with an emphasis towards their application to enhance the transport of active compounds into and across the principal skin barrier, the SC.

1.4.2 Hydrogels

Hydrogels are a type of polymer material consisting of 3-D cross-linked network chains, which are capable of absorbing large amounts of water (Langer and Peppas, 2003). They are known as smart polymers due to their ability to display a reversible dramatic physicochemical change in response to small changes in their environments (Aguilar et al., 2007). Moreover, their high water content and low surface tension contribute to their biocompatibility.

Hydrogels are variably classified as shown in [Figure 1-8](#). They can be simply classified based on their cross-linking chemistry, either physically or chemically cross-

linked (Thorne et al., 2011). The physically cross-linked gels are polymeric networks that are bound together via polymer chain entanglements and/or non-covalent interactions (typically hydrogen bonding, electrostatic or hydrophobic force) between the polymer chains. These types of gels can be reversibly dissolved under certain circumstances that would weaken those attractive forces such as changes in temperature. The chemically cross-linked gels, on the other hand, have improved stability due to the formation of covalent bonds between different polymer chains throughout the networks. These gels are usually prepared through a monomer polymerisation in the presence of a cross-linking agent.

Hydrogels can also be either neutral or ionic, based on the nature of the functional groups (Peppas et al., 2000). Additionally, they can also be categorised on the basis of their dimensions, as macrogels, microgels or nanogels. Macrogels have a large, cross-linked structure often referred to as a 'bowl of jelly', typically range in size from millimetres (mm) or larger (Thorne et al., 2011). Microgels or nanogels instead, are much smaller, discrete particles with cross-linked polymeric networks (Nolan, 2005; Thorne et al., 2011). **Figure 1-7** illustrates the fundamental difference between those structures. This chapter is concerned with nanogel particles dispersed in aqueous media.

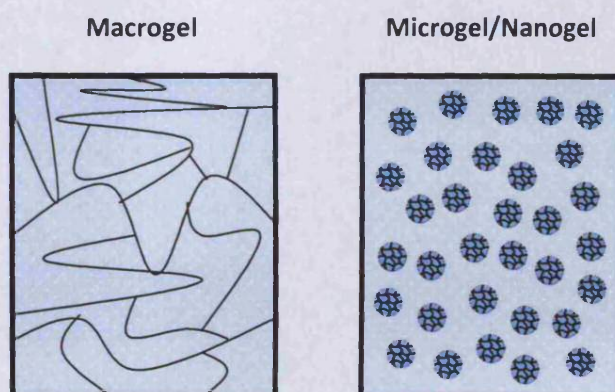


Figure 1-7: Illustration of the difference between macrogels and microgels/nanogels. Adapted from (Thorne et al., 2011).

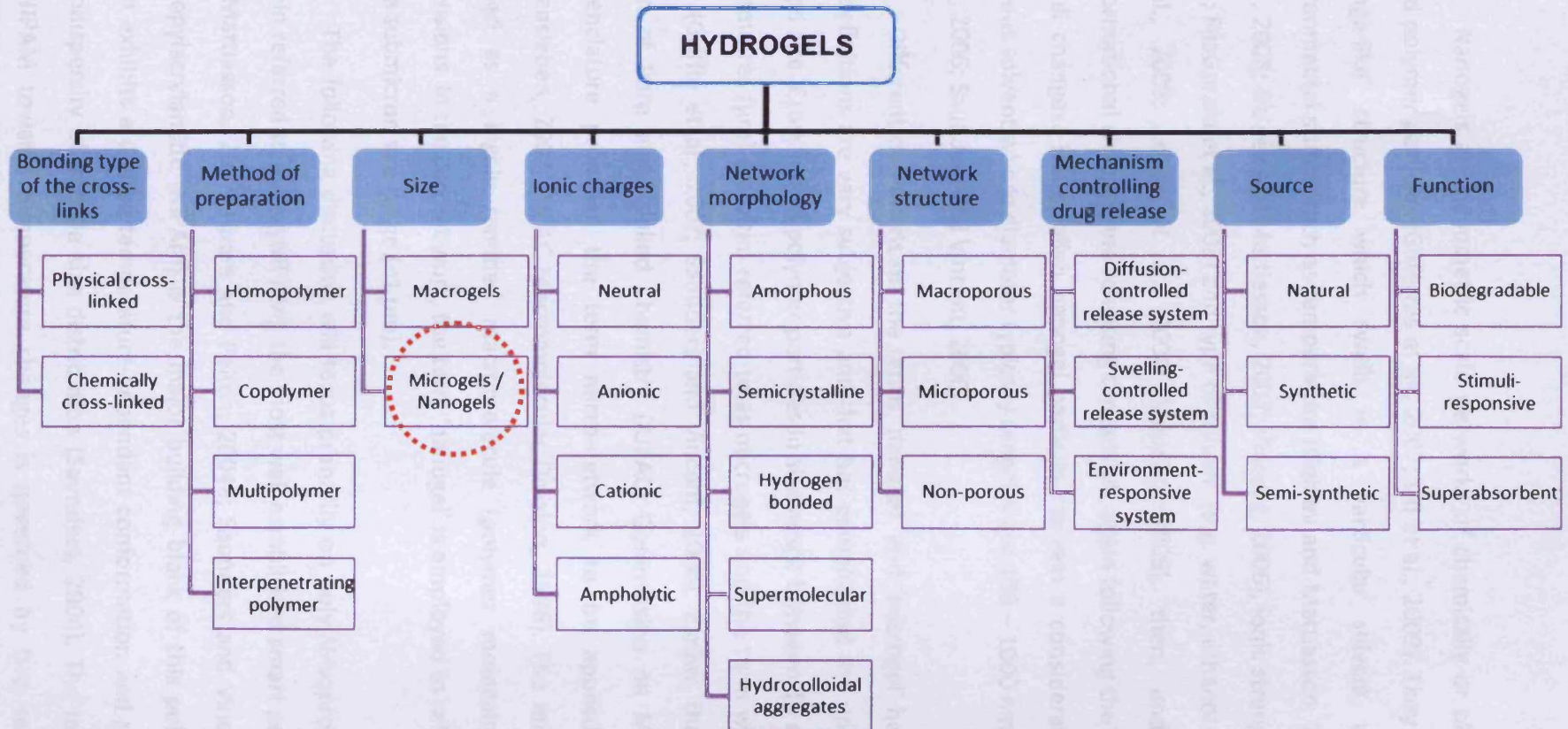


Figure 1-8: General classifications of hydrogel-based polymers.

Red circle represents the hydrogel of interest.

1.4.2.1 Nanogels

Nanogels are nanometric scale networks of chemically or physically cross-linked polymer particles (Guterres et al., 2007; Oh et al., 2009). They have a porous 'sponge-like' structure which swells in a particular solvent under specific environmental stimuli such as temperature (Galaev and Mattiasson, 2007), pH (Don et al., 2008; Galaev and Mattiasson, 2007; Vincent, 2006), ionic strength (Don et al., 2008; FitzGerald et al., 2008) and type of solvent (e.g. water, ethanol or buffer) (Das et al., 2006; Lopez et al., 2004; Vincent, 2006), then, undergoing rapid conformational changes and releasing the solvent again following the environmental stimuli changes. The swollen nanogel particles contain a considerable amount of aqueous solvent whose diameter typically ranges from 100 – 1000 nm at ~ 25°C (Das et al., 2006; Saunders and Vincent, 2006).

Different definitions on the terms 'nanogel' and 'microgel' have been used. The definitions are very subjective and that has complicated the understanding of the gel size. Cross-linked polymer particles in size range between 10 nm and several micrometres (μm) are often referred to as microgels and the term was first used in 1949 (Griffin et al., 2007; Saunders and Vincent, 2006). Earlier, the International Union of Pure and Applied Chemistry (IUPAC) Commission on Macromolecular Nomenclature proposed the term micro-network to be applied on microgel (Hallensleben, 2004; IUPAC Macromolecular Division, 1996). The micro-network is defined as a highly ramified macromolecule (polymer molecule) of colloidal dimensions. In the current work, the term 'nanogel' is employed to refer to polymers in the submicron size range ($<1 \mu\text{m}$).

The following discussion will focus primarily on poly(*N*-isopropylacrylamide) (herein referred to as polyNIPAM), the most well established smart polymer (Galaev and Mattiasson, 2007; Hoare and Pelton, 2004a; Saunders and Vincent, 2006). *N*-isopropylacrylamide (NIPAM) is the major building block of this polymer network which exhibits a unique temperature-dependant conformation and produce a high monodispersity of particle size distribution (Saunders, 2004). The response of the polyNIPAM towards temperature changes is governed by two segments of its

polymer chain, which are the hydrophilic amide residue ($-\text{CONH}-$) and the hydrophobic isopropyl moiety [$-\text{CH}(\text{CH}_3)_2$], as shown in **Figure 1-9**. Further roles played by these two moieties in response to temperature changes will be discussed in Section 1.5.2.

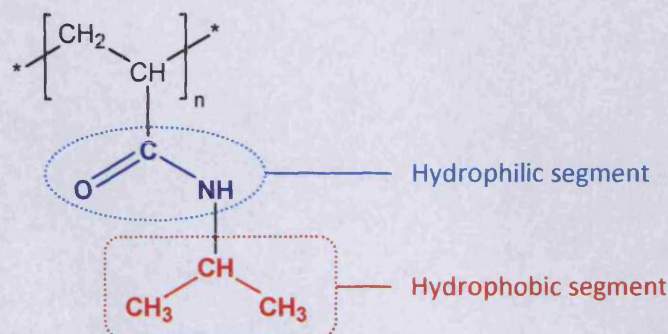


Figure 1-9: Structure of polyNIPAM chain and identification of its hydrophilic and hydrophobic segments.

1.5 PolyNIPAM-based Responsive Nanogels

1.5.1 Swelling and De-swelling Behaviours of Nanogels

Swelling and de-swelling of nanogel particles in water is primarily controlled by several factors including concentrations of cross-linker and monomers used during synthesis, charge density (for polyelectrolyte gels), and environmental parameters (e.g. pH, ionic strength and temperature) (Galaev and Mattiasson, 2007; Kabanov and Vinogradov, 2008; Saunders and Vincent, 2006). A nanogel particle can change in volume up to 100-fold when its surrounding conditions vary continuously (Woodward et al., 2003).

The classical theory of gel swelling was proposed many years ago by Flory and Rehner (Flory and Rehner, 1943). The theory assumes uniform distributions of polymer segments and cross-linker throughout the polymer network. The physical dimension of a cross-linked nanogel particle is set by a balance between the osmotic

pressure and the polymer elasticity (Galaev and Mattiasson, 2007). A nanogel placed in a suitable aqueous medium (e.g. polyNIPAM nanogel dispersed in water), takes in solvent molecules to balance the solvent chemical potential inside and outside of the gel. Swelling continues until the sum of elastic forces between the crosslink is equal to the osmotic force. However, the above theory is only applicable to neutral nanogels or small polyNIPAM nanogels with uniform cross-linker distribution (Kratz et al., 2000).

1.5.2 Effect of Temperature

Temperature-sensitive gels dispersed in a suitable solvent show critical solution behaviour, where a phase transition is induced by exceeding a certain temperature (Galaev and Mattiasson, 2007). The temperature at which a non-cross-linked polymer drastically undergoes a phase transition from a 'hydrophilic' state to a 'hydrophobic' state is known as the lower critical solution temperature (LCST) (Das, 2008; Lee et al., 2008). When the polymer chains are cross-linked into a network, the response appears as a volume collapse (conformational change) due to the release of their content (Saunders, 2004; Wang et al., 2008). This transition temperature is called the volume phase transition temperature (VPTT). Generally, the VPTT is close to the LCST of the corresponding solution of non-cross-linked polymer (Schmidt et al., 2005). For example, the experimental LCST value of a linear form polyNIPAM polymer in aqueous solvent is $\sim 32^{\circ}\text{C}$ (Hoare and Pelton, 2004a; Schild, 1992), and when the NIPAM cross-linked into a polyNIPAM by a cross-linking agent, its VPTT is between $32 - 34^{\circ}\text{C}$ (Hoare and Pelton, 2004a).

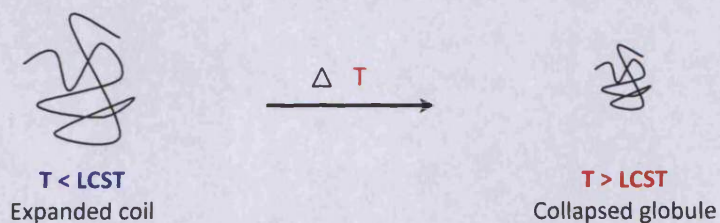
Figure 1-10 shows the temperature-induced conformational transitions of a single polyNIPAM chain (coil \leftrightarrow globule) and cross-linked polyNIPAM nanogel (swelling \leftrightarrow de-swelling). The behaviour of a polymer in a solvent depends on polymer-solvent, polymer-polymer, and solvent-solvent interactions (Das, 2008; Pinkrah et al., 2004; Schild, 1992). The swelling and de-swelling phenomena are caused by a reversible formation and cleavage of the van der Waals attractive forces

and hydrogen bonds with temperature changes (Das, 2008; Kawaguchi et al., 1992; Wu et al., 1994).

At temperatures lower than the LCST ($T < \text{LCST}$), the polymer is highly solvated due to the extensive formation of hydrogen bonds between the hydrophilic amide residues ($-\text{CONH}-$) on the polymer chains and the surrounding water molecules (Crowther and Vincent, 1998; Galaev and Mattiasson, 2007; Lin et al., 2006). In addition, solvent-solvent interactions in water become strong, where water molecules are highly ordered forming a 'cage-like' structure around the hydrophobic isopropyl groups of the polyNIPAM, known as a 'hydrophobic effect' (Das, 2008). This effect acts to increase hydration and solubility of the nanogel in water. Thus, the polymer-solvent interactions are more dominant than the polymer-polymer interactions, leads to extensive swelling conformation of the nanogel in water (Agbugba et al., 1998; Lee et al., 2008; Lin et al., 2006; Pinkrah et al., 2004).

Above the LCST ($T > \text{LCST}$), not only the hydrogen bonds between the polymer and the water molecules become weakened or broken, but also between water molecules themselves. The hydrophobic interactions among the isopropyl moieties [$-\text{CH}(\text{CH}_3)_2$] of the polymer, i.e. polymer-polymer interactions grow stronger than the polymer-solvent interactions (Agbugba et al., 1998; Lee et al., 2008; Lin et al., 2006). These altogether lead to favoured expel of water from inside of the polymer network into the environmental media resulting in a phase separation (Agbugba et al., 1998; Das, 2008; Lin et al., 2006). The phase separation is described by the appearance of two phases; one is composed of collapsed gel that has expelled most of its associated water, and the other is the water itself. The above-mentioned response of polyNIPAM to temperature changes is believed to change the surface of the polymer from a hydrophilic (swollen) state to a hydrophobic (de-swelling) state (Kawaguchi et al., 1992; Pinkrah et al., 2004). The de-swelling of nanogel particles is a reversible process thus, the particles return to their original swollen condition upon cooling (Galaev and Mattiasson, 2007).

PolyNIPAM Chain



PolyNIPAM Nanogel

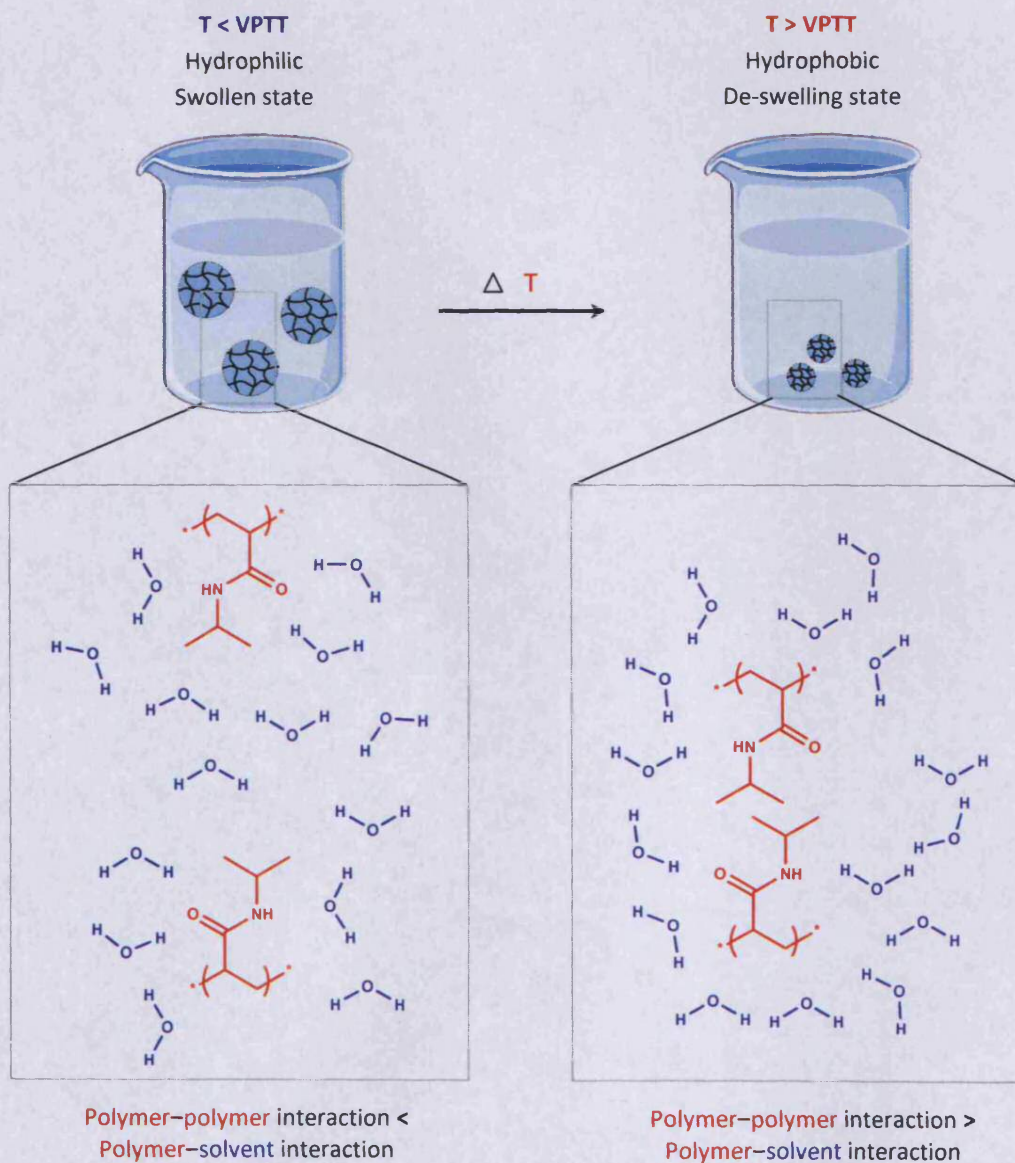


Figure 1-10: Schematic illustration of temperature-induced phase transitions in a polyNIPAM chain and a nanogel triggered by changes in environmental temperature. Adapted from (Das, 2008; Galaev and Mattiasson, 2007).

1.5.3 Effect of pH

Nanogels which are sensitive to pH changes are prepared by copolymerising either acidic or basic functional groups into the polymer network (Galaev and Mattiasson, 2007; Nur et al., 2010). Variations in pH induce a change in ionisation of the polymer networks and a corresponding change in their swelling capacity. Their swelling mechanism is controlled by the internal osmotic pressure powered by the mobile counter-ions contained within the particles, which balance the internal electrostatic repulsion (Galaev and Mattiasson, 2007; Gracia and Snowden, 2007). The swelling based on the balance between osmotic pressure inside and outside of the particles as described by Equation 1-5 (Gracia and Snowden, 2007):

$$\Pi_{in} + \Pi_{el} = \Pi_{out}$$

Equation 1-5

Π_{in} : The osmotic pressure of the mobile ions inside the nanogels.

Π_{el} : The elastic pressure of the polymer network.

Π_{out} : The osmotic pressure of the mobile ions in the bulk solution.

Nanogels copolymerised with a weak acid or base functional group (i.e. pH-dependant group) have more complex swelling mechanism than neutral nanogels (Gracia and Snowden, 2007). The ionisation of nanogels is determined by either acid dissociation constant (pK_a) or base dissociation constant (pK_b) of the respected functional groups. However, these values are functions of the local charge group in which a higher charge density may suppress the ionisation.

Under the pK_a of the nanogel network ($pH < pK_a$), the swelling of anionic nanogel particles reduces due to the protonation of the ionised carboxylate groups ($-\text{COO}^- + \text{H}^+ \rightarrow -\text{COOH}$) (Galaev and Mattiasson, 2007; Gracia and Snowden, 2007; Nur et al., 2010). However, above the pK_a of the nanogel network ($pH > pK_a$), the

degree of ionisation increases and thus, the number of fixed charges increases, resulting in increased electrostatic repulsions between the internal, dissociated carboxyl groups ($-\text{COOH} \rightarrow -\text{COO}^- + \text{H}^+$). This, in turn, results in the particles becoming increasingly hydrophilic and will swell to a greater degree. This behaviour is consistent with the typical behaviour of conventional weak polyelectrolytes, whose hydrodynamic size increases with an increase in the degree of dissociation. The reverse is the case for cationic nanogels with functional groups such as amines, which swell at lower pH (Murthy et al., 2003). A schematic presentation of the differential swelling of anionic and cationic nanogels in acidic and alkaline environments is shown in **Figure 1-11**.

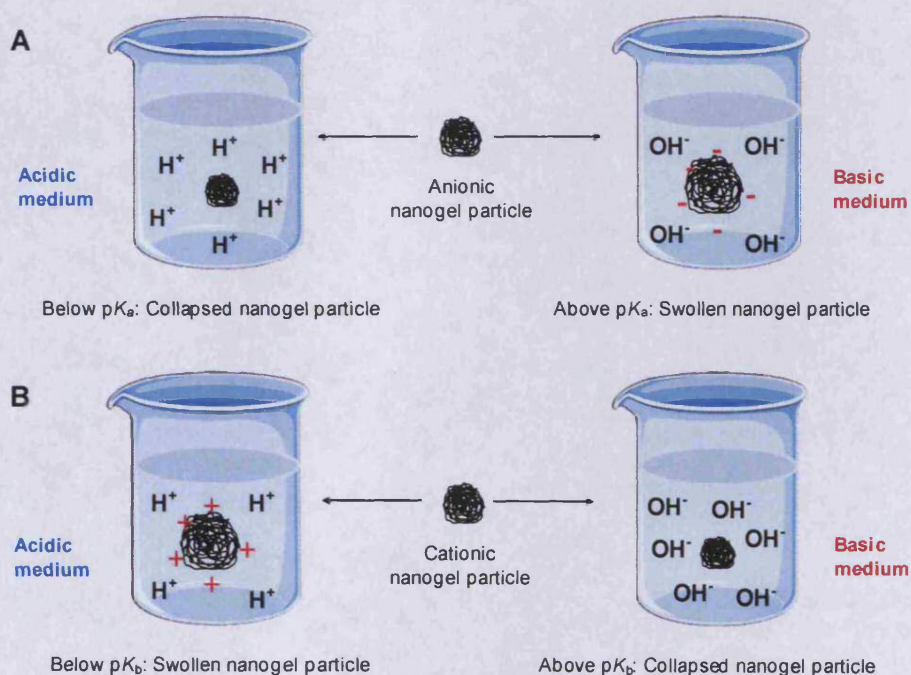


Figure 1-11: Schematic representation of pH-triggered swollen and collapsed states of (A) anionic and (B) cationic nanogel particles. Adapted from (Nur et al., 2010).

1.5.4 Effect of Co-monomers

Nanogels can be customised to possess certain desired properties by varying the monomers used in the synthesis. The combination of monomers, which respond

to different stimuli or have ranging hydrophobic properties, creates nanogels that exhibit physicochemical properties which are composite of those of the comonomers employed in their preparation (Galaev and Mattiasson, 2007; Gracia and Snowden, 2007). **Figure 1-12** shows the monomers commonly used for manipulating properties of polyNIPAM polymer.

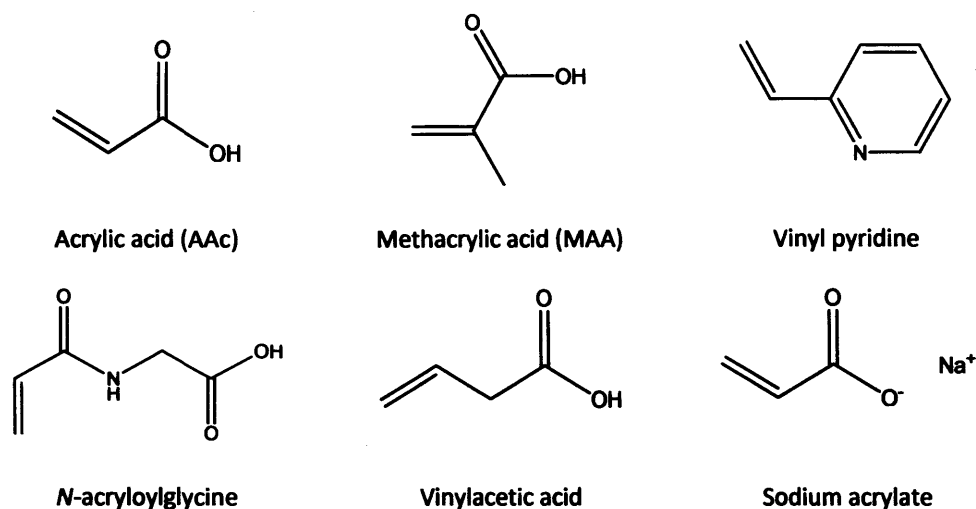


Figure 1-12: Chemical structures of several co-monomers that have been suggested in the literature for copolymerisation with polyNIPAM (Schild, 1992).

The rule of thumb is that the incorporation of a suitable hydrophilic or hydrophobic constituent would either lower or increase the VPTT of the resulting copolymer (Amalvy et al., 2004; Bromberg and Ron, 1998; Gracia and Snowden, 2007). This phenomenon can be explained by the alteration of the hydrophobic-hydrophilic balance in the cross-linked polymer network (Das, 2008; Gracia and Snowden, 2007). Thus, the upper limit to the content of a second monomer (co-monomer) is the requirement that the resulting polymer not to be soluble in water at the polymerisation temperature to allow its precipitation (Pelton, 2000). Typically, incorporation of the hydrophilic monomer increases and broadens the VPTT. On the other hand, incorporation of the hydrophobic monomers generally decreases the VPTT.

An anionic nanogel can be prepared with monomers such as acrylic acid (AAc) or methacrylic acid (MAA) which contribute negative charges to the nanogel

particles (Saunders and Vincent, 1999; Zhang et al., 2004), while cationic monomers (e.g. 2-aminoethylmethacrylate hydrochloride or vinylbenzylisothiuronium) contribute positive charges to form a cationic nanogel (Zhang et al., 2004). The addition of only a small amount of monomers, typically between 1 – 5% w/w can have a remarkable effect on the whole properties of the resultant nanogel particles (Galaev and Mattiasson, 2007; Schild, 1992).

1.5.5 Effect of Cross-linking Agents

The use of a cross-linking agent for synthesis of polyNIPAM-based nanogels is crucial because the agent helps to maintain 3-D network structures and prevents the nanogels from dissolving in water at low temperatures by restricting the extent of their swelling capacities (Das et al., 2006; Don et al., 2008; Khare and Peppas, 1995). As a general rule, the swelling ratio of the polymer decreases as the amount of a cross-linking agent increases (Peppas et al., 2000; Vincent, 2006; Wu et al., 1994). A relatively low amount of the agent which is typically up to ~ 10% w/w of the total monomer concentration is required in order to produce a porous open structure gel (Dowding et al., 2000; Gracia and Snowden, 2007). High density of cross-linking in a nanogel particle would restrict the flexibility of the nanogel network and thus, the particle has a relative compact conformation even in its swollen state. However, the transition temperature of nanogels is not significantly dependant on the cross-linker density (Gracia and Snowden, 2007; Wu et al., 1994).

1.6 Nanogels in Drug Delivery Systems

Polymer particles with controlled size, size distribution and morphology are found to be diversely beneficial particularly in pharmaceutical, biotechnology and biomedical application fields (Das, 2008; Galaev and Mattiasson, 2007; Oh et al., 2008). The nanogels of our interest are intended for dermatology and cosmetology applications, where skin is the target site. As can be seen in [Figure 1-13](#), the

recommended size of polymer particles for transdermal delivery should be less than 1 μm (Tinkle et al., 2003). The dimension aspect is very crucial, as it critically influences the response time of polymer particles towards environmental stimuli, which is attractive when aiming for triggered drug delivery (Lin et al., 2006). The response is usually in the form of a conformational transition which brings about changes in their physical properties such as particle size and surface charge density (Gracia and Snowden, 2007). The time required for changes in particle size, i.e. swelling and de-swelling of polyNIPAM particles depend on the inverse square of a linear dimension of the particles (Gracia and Snowden, 2007; Schmidt et al., 2005). Thus, the nanometre dimension would provide very high surface area to volume ratios which allows rapid diffusion of a given stimulus to facilitate a response throughout the particles over very short time scales.

The nanogel particles may serve as potential carriers in drug delivery system due to their tunable chemical and 3-D physical structures with good mechanical properties (Oh et al., 2008). The particles offer smart activation delivery systems in comparison to the conventional topical preparations such as creams or ointments. They are responsive towards environmental changes such as pH, temperature or ionic strengths. Active ingredients can be loaded into the nanogel particles under one set of conditions, where they are swollen the most and expel the actives once their structures collapse due to changes in their environmental medium (Gan et al., 2010). In addition, the properties of nanogel particles can be tailored according to desired stimuli (Galaev and Mattiasson, 2007). This can be achieved by polymerisation of monomers with different functional groups. For example, a hydrophilic acrylic acid (AAc) monomer can be copolymerised into the temperature-sensitive polyNIPAM to obtain poly(NIPAM-co-AAc), a nanogel that is responsive to both, external pH and temperature stimuli (Snowden et al., 1996).

Furthermore, the nanogel offers a cost-effective carrier for topical delivery systems. For example, the raw materials require for the synthesis of the nanogel are generally cheaper than liposomes. Moreover, there is no need for application of external forces to assist movement of the particles into the skin layers. In addition,

the mode of delivery by such particles can be designed either for sustained-release or dose-dumping (Huang and Brazel, 2001).

Delivery

Ocular

Nasal

Pulmonary

Oral

Intratumoral

Intramuscular

Intravenous

Transdermal

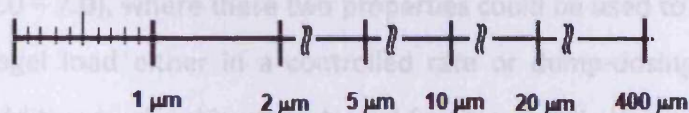


Figure 1-13: Size ranges of polymers for different modes of drug administration (Das, 2008).

1.6.1 Nanogels in Topical Drug Delivery

Nanogel particles can be designed as carriers for drug or compound of interest due to their open network structure and their ability to undergo conformational transitions (swelling \leftrightarrow de-swelling) upon interaction with suitable stimuli including temperature, pH and ionic strength. These stimuli can be used to modulate the release of drugs from the particles. Even though there is a wealth of publications regarding the applications of polyNIPAM-based polymers in drug delivery, less knowledge is known regarding its application for skin. Studies done by Lopez *et al* among a few publications, suggested that polyNIPAM-based polymers have potential in drug release to the skin. They investigated two types of polyNIPAM-based polymers for loading of several selected model compounds including ibuprofen and salicylamide for dermal and transdermal delivery: (i) temperature-sensitive co-polymer of polyNIPAM *co*-butyl acrylate – poly(NIPAM-*co*-BA) (90/10) (Lopez *et al.*, 2004) and (ii) temperature- and pH-responsive co-polymer of polyNIPAM *co*-butyl acrylate *co*-methacrylic acid – poly(NIPAM-*co*-BA-*co*-MAA) (85/10/5) for wound management application (Lopez *et al.*, 2005). The authors

concluded that the incorporation of compounds into the polymers and the subsequent release depends on the octanol/water partition coefficient ($\text{Log } P$) and solubility of the respective compounds.

Under certain conditions, the polymers would be suitable for controlled or triggered drug delivery via the cutaneous route. With optimisation of their network composition, size and morphology, nanogels can be tailor-made to sense and respond to environmental changes in order to ensure spatial and stimuli-triggered drug release. The nanogels properties could be designed by manipulating skin physiological environments such as temperature (average surface temperature, $\sim 32^\circ\text{C}$) and/or pH (4.0 – 7.0), where these two properties could be used to modulate the release of nanogel load either in a controlled rate or dump-dosing manner. External stimuli in addition to the skin physiological features could also be beneficial to the stimuli-modulated nanogel system.

1.7 Liposomes

Liposomes were discovered in the work of Alex Bangham and colleagues at the Agricultural Research Council Institute of Animal Physiology at Babraham, Cambridge in the 1960s (Bangham et al., 1965). Liposomes can be defined as microscopic spherical lipid bilayer vesicles that fully encapsulate an aqueous volume (Ranade and Hollinger, 2003), with diameters ranging from 80 nm – 100 μm (Bhalerao and Raje Harshal, 2003). The lipid components are usually phospholipid, with or without cholesterol and the lipids may be arranged in one or more concentric bilayers. The lipid composition affects the properties of the resulting liposomes. For example, the addition of relatively small amounts of cholesterol tends to stabilise the vesicles due to tighter membrane packing. Consequently, the vesicles would be somewhat more rigid and less permeable to encapsulated compounds than vesicles lacking cholesterol.

Figure 1-14 shows an illustration of the general structure of a liposome. The interior of a liposome contains water and therefore, molecules which are hydrophilic

in nature can be encapsulated in the interior part, while lipophilic molecules can be entrapped in the hydrophobic portion of the phospholipid bilayer region (Ranade and Hollinger, 2003). Due to their unique properties, liposomes can serve as carriers for many types of molecules including both hydrophilic and lipophilic compounds. In fact, a single liposome vesicle can carry both types of molecules or combinations of each type of molecule. The vesicles can be classified in various ways including method of preparation, size and lipid composition or by lamellarity (how many bilayers are formed by the phospholipids).

Liposomes with compositions that imitate the lipid content of skin (e.g. ceramides, cholesterol, fatty acids) have been reported to have high compatibility with skin tissue (Guterres et al., 2007). In neither the US nor the EU are there restrictions concerning the use of liposomes in foods, cosmetics and pharmaceuticals.

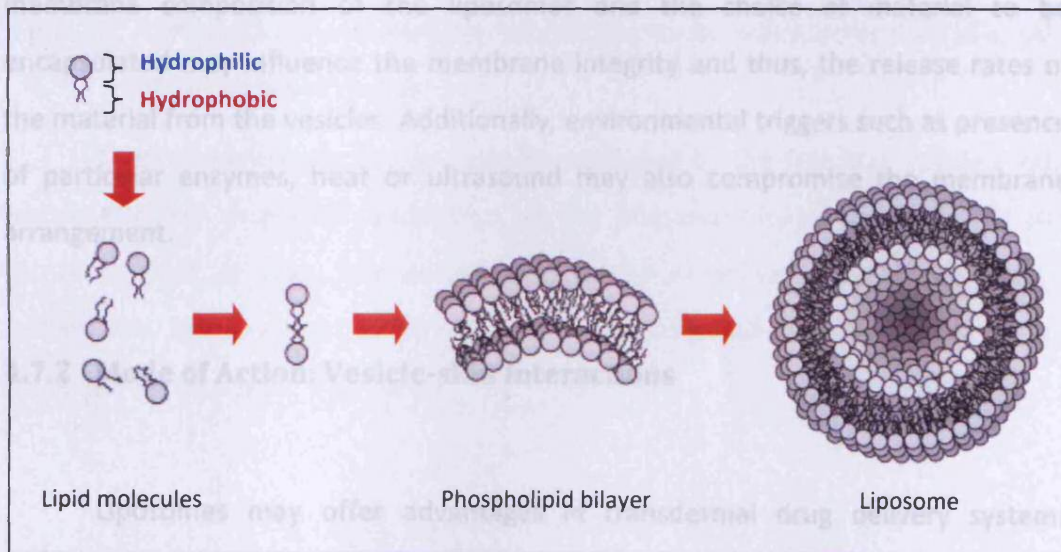


Figure 1-14: Schematic diagram represents a liposome formed from a bilayer of phospholipid molecules. Adapted from (Balazs and Godbey, 2011).

1.7.1 The Use of Liposomes in Transdermal Applications

The applicability of liposomes as drug carriers for topical application was first proposed in 1980 (Mezei and Gulasekharan, 1980). They discovered that when triamcinolone was encapsulated in a liposome before being applied to skin, enhanced drug disposition in the epidermis and dermis by 4- to 5-fold were achieved, in comparison to a standard ointment. Since then, many efforts have been made in order to enhance understanding of the potentiality of liposomes. Liposome technology is widely used for topical application in cosmetic- and dermatological-related products, where it offers several advantages to the encapsulated materials including the potential enhancement of flux accompanied with greater and deeper deposition in the skin layers (El Maghraby et al., 2008). Additionally, it also improves stability by providing protection through the formation of a membrane barrier between the entrapped component and its environment (Xia and Xu, 2005). The membrane composition of the liposomes and the choice of material to be encapsulated may influence the membrane integrity and thus, the release rates of the material from the vesicles. Additionally, environmental triggers such as presence of particular enzymes, heat or ultrasound may also compromise the membrane arrangement.

1.7.2 Mode of Action: Vesicle-skin Interactions

Liposomes may offer advantages in transdermal drug delivery systems because of their improved penetration into skin compared to most conventional formulations such as creams, ointments or gels (Maghraby et al., 2006; Verma et al., 2003). There are several possible mechanisms used by the vesicles for transdermal or dermal delivery as summarised in [Figure 1-15](#) (El Maghraby et al., 2008):

- (i) Scheme A represents a free permeant process, where the permeant permeates through the skin independently after initial release from the

liposome. The vesicles are regarded only as carriers that control the permeant release.

- (i) Scheme B suggests a possible penetration enhancement effect by the liposomes. The vesicles do not penetrate intact, but they disintegrate on the skin surface and individual lipid molecules can penetrate the SC resulting fluidisation and modification of the SC lipids. This provides fewer barriers for the permeant to travel across the SC.
- (ii) Scheme C – the liposomes may penetrate into and through the skin layers as intact vesicles. According to this process, adsorption and fusion of the liposomes on the skin surface may occur with a consequent mixing of the liposomal bilayer with intercellular skin lipids lead to enhancement of the permeant partition into the skin and/or direct transfer of the permeant to the SC.
- (iii) Scheme D represents a transappendageal penetration mechanism, where the liposomes are postulated to be transported into the skin through shunt routes.

These different mechanisms can be explained by the fact that vesicle – skin interactions are primarily dependant on the physicochemical properties of the liposomes such as their lipid composition, phase transition state and elasticity. Additionally, those properties may also potentially influence drug deposition by the liposomes in the deeper skin layers.

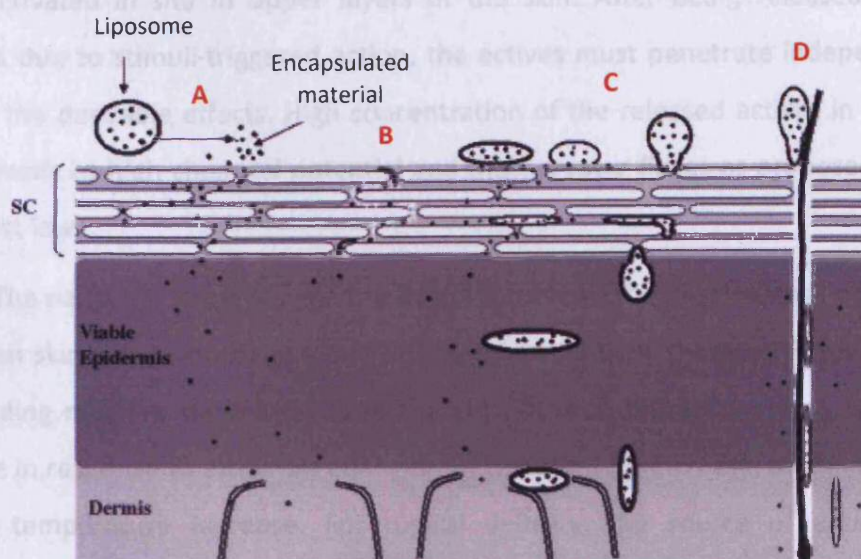


Figure 1-15: Possible mechanisms of action of liposomes intended for cutaneous delivery. Adapted from (El Maghraby et al., 2008).

(A) Free permeant mechanism; (B) penetration enhancing process of liposome components; (C) penetration of intact vesicles into and/or through the intact SC; and (D) intact vesicles through skin appendages (e.g. hair follicles).

Scheme (C) is the desired mechanism for the liposome vesicles proposed in this thesis.

1.8 Research Hypothesis and Aims

1.8.1 Hypothesis

1.8.1.1 Controlled Nanogel Activation

Specific swelling and drug release properties exhibited by the nanogel particles in aqueous solutions, in response to external stimuli may have potentials in topical drug delivery applications. Depending on types of monomer, nanogels possess functional groups in their networks that are selectively responsive to a particular external stimulus. An attempt was made to formulate polyNIPAM-based nanogel particles as suitable “carriers” for dermatology and cosmetology applications via skin. The concept referring to the particles only served as a transporter bringing the actives into the skin by crossing beyond the SC layer, and

being activated *in situ* in upper layers of the skin. After being released by the particles due to stimuli-triggered action, the actives must penetrate independently to yield the desirable effects. High concentration of the released actives in the skin region, leads to high chemical potential and thus, greater fluxes as proposed by the Fick's first law.

The nanogels were designed to be responsive to the physiological properties of human skin (i.e. temperature and pH) by releasing their therapeutic load to the surrounding medium once applied to the skin. In drug therapy, release of a drug could be in response to either an endogenous temperature increase, or an externally applied temperature increase. For topical delivery, the source of endogenous temperature is originated from the skin with an average reported surface temperature of 32°C. PolyNIPAM may offer much potential for drug delivery area of research, as it undergoes a sharp conformational transition in the form of volume changes at a narrow temperature range of 32 – 34°C, close to the skin physiological temperature.

Incorporation of co-monomers containing acidic or basic functionalities into polyNIPAM nanogels yields particles with a pH-driven swelling property. From a topical delivery perspective via the cutaneous route, temperature- and pH-sensitive nanogels would provide enhancement of drug release from the particles. The human skin usually presents slightly acidic SC environment as a part of its protective function with pH ranging from 4.0 – 7.0 (Lambers et al., 2006), mostly due to the effect of sebum secreted by the skin glands and cosmetic-related product application. The acidic property is essential in creating a resistance to permeation of pathogenic organisms (bacteria and fungi) and skin flora proliferation. Thus, the acidic environment of the skin theoretically would also be capable of activating the nanogels. An external pH modulator such as citric acid (CA) or ascorbic acid could also be beneficial in modulation of the release of loaded drugs from the ionic nanogel particles.

1.8.1.2 A Stimulus-responsive Topical Drug Delivery System: Nanogel and Liposome

Applying temperature and pH-activation principles together, the concept of a single compartment system is proposed, consisting of two components, i.e. nanogel and pH modulator-loaded liposome in a single formulation without any interaction takes place until required or necessary as illustrated in [Figure 1-16](#). The reaction between the nanogel and liposome is assumed to take place in the upper layer of the skin, SC. We have synthesised a temperature- and pH-responsive polymer, which is a copolymer of NIPAM and AAc of submicron size, poly(NIPAM-co-AAc) nanogel. The nanogel behaviours towards LCST can be manipulated for a temperature-sensitive release mechanism. Since the swelling and de-swelling occur over a relatively narrow temperature range, one may release or “dump-dose” at this specific temperature range, substances which have been previously loaded into the gel. If a drug is loaded below the LCST, it can be squeezed out above the LCST due to the pressure generated during gel collapse.

To attain maximum release of the particles' content to the media, an external pH modulator was utilised, in addition to weak acidic environment provided by the skin. Thermally labile sphingomyelin liposome vesicles were selected to encapsulate the pH modulator within its interior aqueous space below its LCST ($T < 37^{\circ}\text{C}$), with the aim to prevent the pH modulator from interacting/activating the nanogel particles under storage condition as shown in [Figure 1-17](#). Hypothetically, the membranes of the liposome vesicles become highly leaky following warming, shortly after application onto the human skin. Eventually the vesicles rupture and liberate their content into surrounding media creating acidic environment. This leads to enhanced activation of the nanogel particles represented by de-swelling of the particles due to release of their content into the surrounding medium. Moreover, further collapse of the particles reflected by reduction in size may contribute to deeper penetration of the particles and thus, higher distribution of their therapeutic loads in the skin layers.

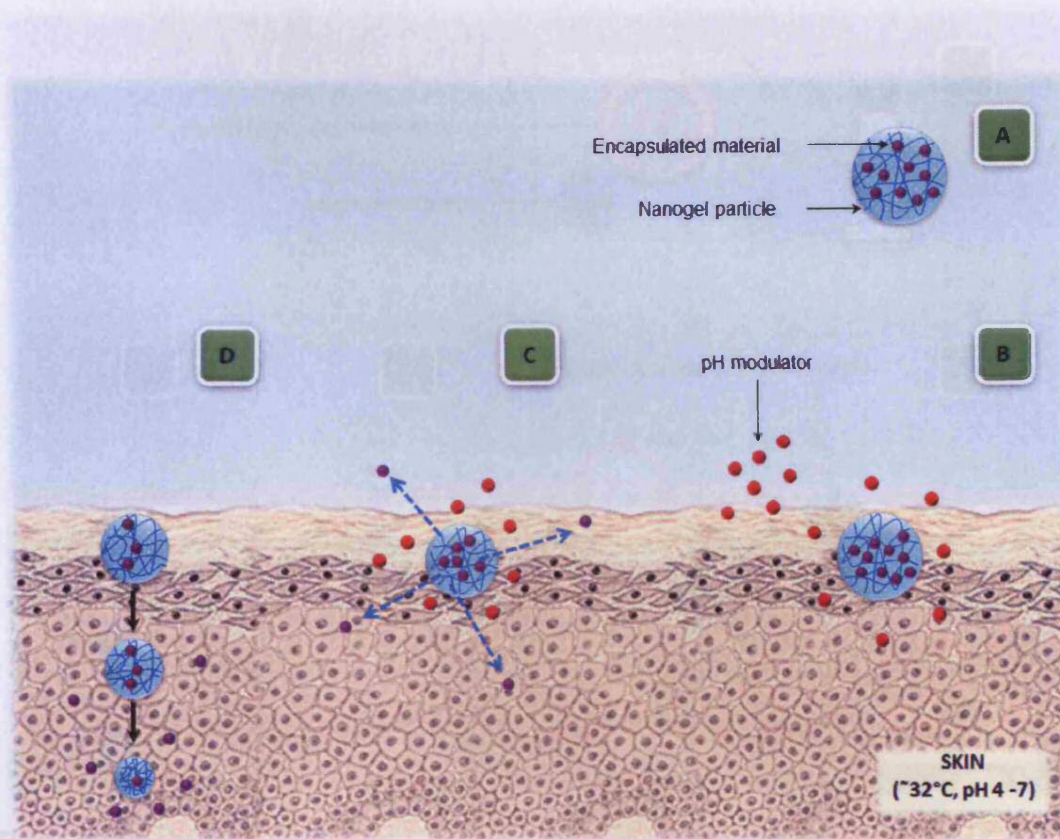


Figure 1-16: Schematic representation on the proposed mechanism of pH-activated drug-loaded nanogel particles.

(A) Drug molecules are loaded into the nanogel particles at a particular temperature using a post-fabrication method; (B) the drug-loaded nanogel is applied onto the skin, followed by the addition of external pH modulator (acidic in nature); (C) acidic environment is created due to the presence of external pH modulator, in addition to the skin slightly acidic nature which initiate the activation of the nanogel particles; and (D) the activated particles start to release their content into the surrounding medium due to internal osmotic pressure build up following collapse of the particle network. Further collapse and release of their content may take place due to the particles' response to the skin surface temperature (32°C, thermal stimulus). Drug molecules are expelled at high pressure that may suggest the drug particles will be forced across the SC layer. Additional collapse of the particles may contribute to their further penetration into the skin layers.

Enhanced topical drug delivery may be achieved using a novel system based on the concept of a single compartment smart nanogel and liposome formulation.

The aims were:

- (i) To synthesise a series of stimulus-responsive polyNIPAM-based nanogels of nanometre scale particles and characterise them particularly on their

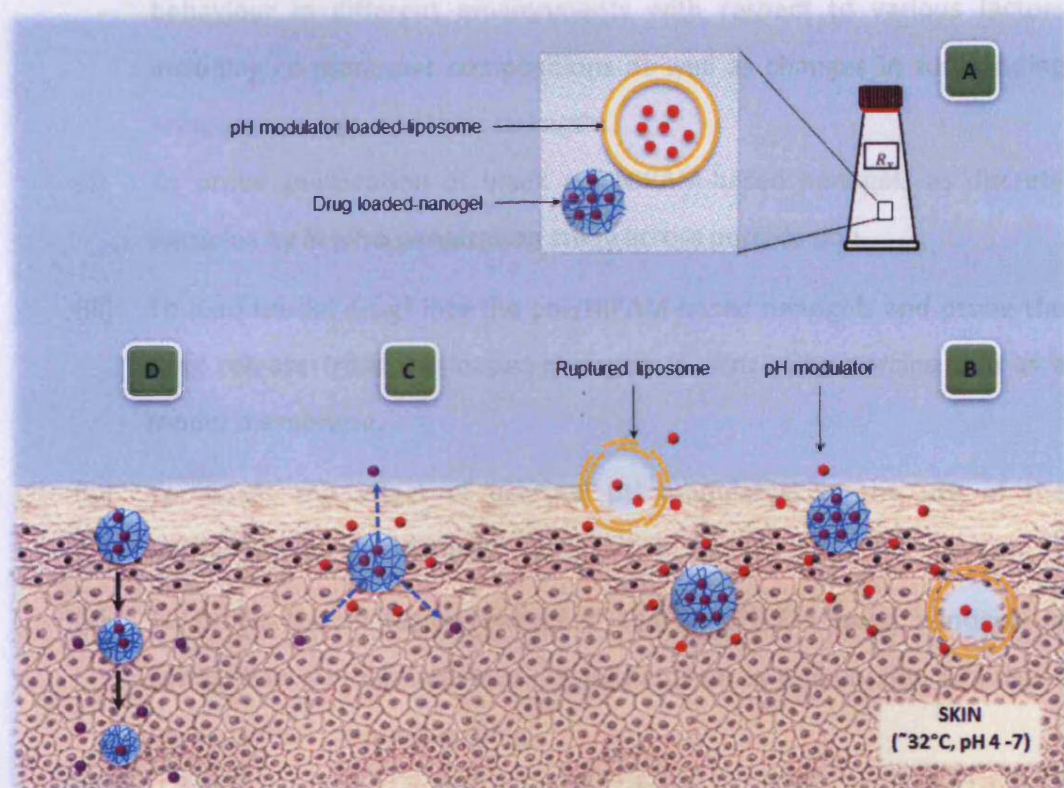


Figure 1-17: Schematic diagram of a proposed pH modulator-loaded liposome – skin – drug-loaded nanogel composite system.

(A) Stable pH modulator loaded-liposome and drug-loaded nanogel present in a single formulation at a suitable storage condition; (B) following warming, shortly after application onto the human skin (32°C), the liposome vesicles rupture and releasing their content, creating an acidic environment; (C) the acidic condition leads to activation of the nanogel particles, triggering the collapse of the spheres and release of their content into the surrounding medium; and (D) the collapse of the nanogel can also be triggered by a thermal stimulus originated from the skin. The activation of the nanogel particles simultaneously by pH and thermal stimuli is expected to enhance their content release into the skin.

1.8.2 Aims

Enhanced topical drug delivery may be achieved using a novel system based on the concept of a single compartment smart nanogel and liposome formulation.

The aims were:

- (i) To synthesise a series of stimulus-responsive polyNIPAM-based nanogels of nanometre scale particles and characterise them particularly on their

behaviour in different environments with respect to various factors including co-monomer compositions as well as changes in surrounding temperature, pH, and ionic strengths.

- (ii) To probe permeation of blank polyNIPAM-based nanogels as discrete particles by *in vitro* penetration study across porcine skin.
- (iii) To load model drugs into the polyNIPAM-based nanogels and probe the drug release from the loaded-nanogels *in vitro* using porcine skin as a model membrane.
- (iv) To assess the effect of external pH modulators in the use of the polyNIPAM-based nanogels.
- (v) To probe the biological effects of the polyNIPAM-based nanogels in comparison to their individual components on *ex vivo* porcine skin tissue using protein immunoblotting.
- (vi) To synthesise and characterise pH modulator-loaded sphingomyelin liposomes.
- (vii) To develop a stable single compartment composite system containing a drug-loaded nanogel and pH modulator-loaded liposome.

CHAPTER 2 | Synthesis and
Characterisation of Temperature-sensitive
PolyNIPAM-based Nanogels

2.1 INTRODUCTION

Responsive nanogels can be prepared by several methods depending on the nature of the monomers involved. These include emulsion polymerisation (EP), inverse EP, living free-radical polymerisation and synthesis by radiation (Galaev and Mattiasson, 2007; Gracia and Snowden, 2007). In this chapter, we are going to focus on EP, the most widely used method to prepare aqueous polyNIPAM nanogels (Saunders and Vincent, 2006).

2.1.1 Nanogel Synthesis: EP

EP is more efficient and effective in avoiding macroscopic network formation and typically produces a range of particles of submicron diameters (100 – 1000 nm) (Galaev and Mattiasson, 2007; Gracia and Snowden, 2007). It can be performed in the presence or absence of a surfactant:

- (i) Presence of added surfactant (conventional EP) or
- (ii) Absence of added surfactant (surfactant-free EP, SFEP).

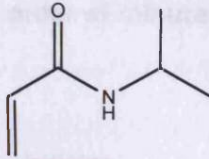
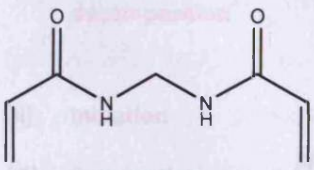
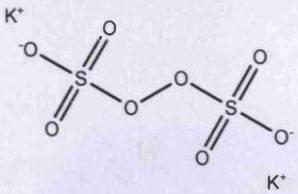
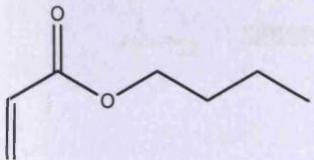
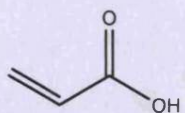
Conventional EP is able to produce nanogel particles with a diameter of <150 nm. The presence of surfactant molecules such as sodium dodecyl sulfate (SDS) or potassium pentadecanoate enhances the stabilisation of precursor particles, leading to rapid inhibition of the particle growth during the polymerisation process, thus producing small particles (Galaev and Mattiasson, 2007; Panayiotou et al., 2007). However, a problem with this technique is the difficulty of completely removing the residual surfactant molecules employed, post-synthesis (Lin et al., 2006). The presence of surfactants in the final product is undesirable, as it might affect the overall properties of the product in various ways depending on the nature of the polymer and surfactant involved and compromises its potential applications. For instance, an aqueous solution of polyNIPAM containing SDS might seriously affect the temperature-sensitive property of the final polymer even at a low concentration (1% w/v) (Eliassaf, 1978; Galaev and Mattiasson, 2007; Tam et al., 1994) - the

solution failed to demonstrate any phase separations even upon boiling due to the SDS molecules bound to the polyNIPAM particles, preventing aggregation of the collapsed particles.

SFEP is preferable to the conventional technique, as it does not suffer from residual surfactant contamination (Lin et al., 2006; Panayiotou et al., 2007). It is well known as a standard technique of synthesis for polyNIPAM-based nanogels (Galaev and Mattiasson, 2007; Gracia and Snowden, 2007). PolyNIPAM is the most extensively investigated within the class of stimuli-responsive polymers due to its temperature-sensitive property (Gracia and Snowden, 2007; Pelton, 2000). The synthesis of polyNIPAM by SFEP of NIPAM in water at $\sim 70^{\circ}\text{C}$ in the presence of *N,N'*-methylenebis-acrylamide (MBA) as a cross-linker was first reported in 1986 (Pelton and Chibante, 1986). **Table 2-1** presents the molecular structures of the primary monomer (NIPAM), co-monomers, cross-linker and initiator employed in preparation of nanogels used in the current studies.

NIPAM is the major building block for temperature-sensitive nanogels (Gracia and Snowden, 2007; Pelton, 2000). In SFEP, the continuous phase must have a high dielectric constant (e.g. water) and an ionic initiator such as potassium persulfate (KPS) or ammonium persulfate (APS) (Lin et al., 2006). MBA is the most commonly used cross-linking agent for SFEP, and is also used in other applications for example polyacrylamide gels for electrophoresis (Schild, 1992). The polymerisation process is usually conducted at a temperature between $60 - 70^{\circ}\text{C}$, in order to initiate the decomposition of the persulfate initiator to generate free radicals (Gracia and Snowden, 2007; Lee et al., 2008; Pelton, 2000), and also to facilitate the growing polyNIPAM chains in undergoing precipitation to form colloidal particles (Galaev and Mattiasson, 2007; Gracia and Snowden, 2007). It was reported that the polymerisation reactions of polyNIPAM-based nanogels were very fast and high conversions were obtained within the first hour (h) of synthesis (Zhang et al., 2008). Many gels were prepared by carrying out the polymerisation for 2 h (Griffin et al., 2007; Lee et al., 2008; Zhang et al., 2008), 4 h (Hellweg, 2003; Pelton and Chibante, 1986; Zhang et al., 2008), or 6 h (Hoare and Pelton, 2008b; Keerl and Richtering, 2007; Zhang et al., 2008).

Table 2-1: The molecular structures of monomers, cross-linking agent and initiator employed during polyNIPAM-based nanogels preparation.

Structure	Name/Abbreviation	Function
	<i>N</i> -isopropylacrylamide (NIPAM)	Main monomer <ul style="list-style-type: none"> Neutral thermo-responsive component
	<i>N,N'</i> -methylenebisacrylamide (MBA)	Cross-linker
	Potassium persulfate (KPS)	Anionic initiator
	Butyl acrylate (BA)	Co-monomer <ul style="list-style-type: none"> Hydrophobic component
	Acrylic acid (AAc)	Anionic co-monomer <ul style="list-style-type: none"> Hydrophilic component pH-responsive component

The steps involved during the SFEP are illustrated in **Figure 2-1**. It starts with a thermal decomposition of the persulfate initiator to form sulfate radicals (Saunders and Vincent, 2006). The water-soluble sulfate radicals initiate water-soluble NIPAM monomers which then grow in the solution until they reach a critical chain length, after which the growing chains collapse to become unstable 'precursor particles'. The precursor particles follow one of two competing processes; either they deposit onto an existing stable polymer particle or they aggregate with other precursor particles until they form a particle sufficiently large to be stable (Gracia and Snowden, 2007; Panayiotou et al., 2007; Pelton, 2000). In the absence of surfactant molecules, the sulfate groups of the sulfate radicals also act as a surfactant by giving

electrostatic stabilisation to the precursor particles (Lin et al., 2006; Odian, 2004). Chain termination may also occur when the growing radical chain encounters oxygen atoms (Panayiotou et al., 2007). The particle nucleation period for SFEP is rapid, in the order of minutes (min) which contributes to a narrow particle size distribution.

- (i) **Initiator decomposition** $S_2O_8^{2-} \xrightarrow{\Delta} 2(\bullet SO_4^-)$ Thermal decomposition: the initiator decomposes and forms two radicals.
- (ii) **Initiation** $M + \bullet SO_4^- \rightarrow \bullet MSO_4^-$ Each radical then reacts with a monomer.
- (iii) **Propagation** $M + \bullet MSO_4^- \rightarrow \bullet M_{x+1}SO_4^-$ This further reacts with other monomers to form a polar head and polymeric tail as shown below:

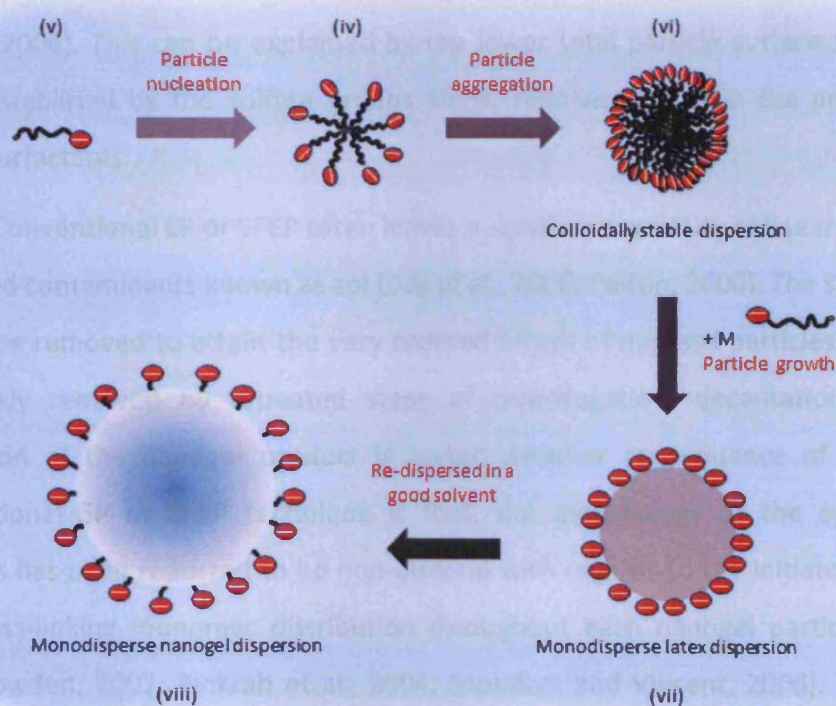


Figure 2-1: The schematic illustrates several steps involve during synthesis of gel particles by SFEP. Adapted from (Galaev and Mattiasson, 2007; Gracia and Snowden, 2007; Saunders and Vincent, 2006).

[M represents an ethenyl monomer (chemical formula $-\text{CH}=\text{CH}_2$); latex defined as a stable dispersion of polymer particles in an aqueous medium].

Although SFEP does not suffer from the residual surfactant contamination, it does suffer from the difficulty of preparing small nanoparticles (<50 nm in diameter). A simple SFEP procedure normally produces polyNIPAM nanogel particles with a diameter in the order of ~700 nm (Gracia and Snowden, 2007). Insufficient surface charges (sulfate groups originated from the initiator), leads to the formation of larger nanoparticles, due to reduced stabilisation at a high concentration of precursor particles during the polymerisation process. The copolymerisation of NIPAM with an ionic monomer can solve the problem, as introducing ionic groups at the particle surface should increase electrostatic stabilisation and create adsorptive sites for the molecules with the opposite charges (Zhang et al., 2004).

Moreover, the number of particles produced by the SFEP technique is generally lower by up to two orders of magnitude compared to the conventional EP (O dian, 2004). This can be explained by the lower total particle surface areas that can be stabilised by the sulfate groups alone, relative to that in the presence of added surfactants.

Conventional EP or SFEP often leaves a significant quantity of linear or slightly branched contaminants known as sol (Das et al., 2006; Pelton, 2000). The sol fraction should be removed to attain the very ordered arrays of nanogel particles. It can be effectively removed by repeated steps of centrifugation, decantation and re-dispersion of the nanogel product in water. Another consequence of using the conventional EP or SFEP technique is that, the morphology of the synthesised particles has been reported to be non-uniform with regards to the initiator residues and cross-linking monomer distribution throughout each nanogel particle (Gracia and Snowden, 2007; Pinkrah et al., 2004; Saunders and Vincent, 2006). This could happen if the cross-linker agent and monofunctional monomer have significantly different reactivity ratios during the polymerisation process (Saunders and Vincent, 2006). With polyNIPAM, for example, MBA was shown to be consumed faster than NIPAM during synthesis, resulting in nanoparticles with high cross-linked density in their core (Bradley et al., 2005; Pinkrah et al., 2004).

The aim of this study was to synthesise a series of submicron size, cross-linked temperature-sensitive gels by the SFEP technique. The gels, which are here on

be addressed as nanogels throughout this thesis are composed of polyNIPAM as the primary monomer and are intended as carriers for topical delivery applications. The physicochemical properties of the synthesised nanogels were also characterised.

2.2 MATERIALS AND METHODS

2.2.1 Materials

NIPAM (99%), BA (99%), KPS (99.9%), hydrochloric acid (HCl), glass wool, chloroform and high performance liquid chromatography (HPLC)-grade solvents were purchased from Fisher Scientific (Loughborough, UK). Citric acid anhydrous (CA, 99.5%), MBA, sodium hydroxide (NaOH) and Whatman® qualitative filter paper Grade 4 were supplied by Sigma-Aldrich Company Ltd. (Poole, UK). Polyvinyl butyral (Pioloform®) was purchased from Agar Scientific Ltd. (Stansted, UK). All chemicals used were of analytical grade and were used as received without any further purification.

2.2.2 Methods

2.2.2.1 Nanogel Synthesis

2.2.2.1.1 PolyNIPAM

PolyNIPAM nanogel synthesis was carried out by a single-step SFEP reaction according to [Table 2-2](#). The reaction was carried out in a fume cupboard and the apparatus set up as illustrated in [Figure 2-2](#). NIPAM, MBA and de-ionised water (150 mL) were added together in a beaker and stirred for ~15 min. The mixture was continuously stirred and immersed in a water bath heated to the polymerisation

temperature of $\sim 70^{\circ}\text{C}$. The flask was continuously purged with nitrogen gas to maintain anoxic conditions, as oxygen could act as a free-radical scavenger that might interfere with the polymerisation process. After stabilising for 30 min at $\sim 70^{\circ}\text{C}$, polymerisation was initiated by the addition of a hot pre-dissolved persulfate initiator (made-up beforehand in 100 mL of de-ionised water). The nitrogen flow was maintained for ~ 2 h after the addition of the initiator. The colour of the solution turned from colourless to sky blue until it reached an ultimate ivory white hue, indicating successful polymerisation as shown in [Figure 2-3](#) (Lin et al., 2006; Pelton and Chibante, 1986).

In this reaction system, the NIPAM, MBA, and KPS were all water-soluble; therefore, in the initial state of the reaction, the reaction mixture was homogeneous, but it soon became heterogeneous, producing nanogel particles as precipitates, with the solution turning into ivory white (Lin et al., 2006). Unsuccessful preparation could be indicated as either a clear solution of dissolved polymer (i.e. sub-precipitation) or the polymer precipitated as macroscopic aggregates (Pelton and Chibante, 1986).

The reaction mixture was allowed to proceed for a further 6 h. Once completed, the crude product mixture was left to cool to room temperature (RT, $\sim 25^{\circ}\text{C}$) under constant stirring overnight prior to purification.

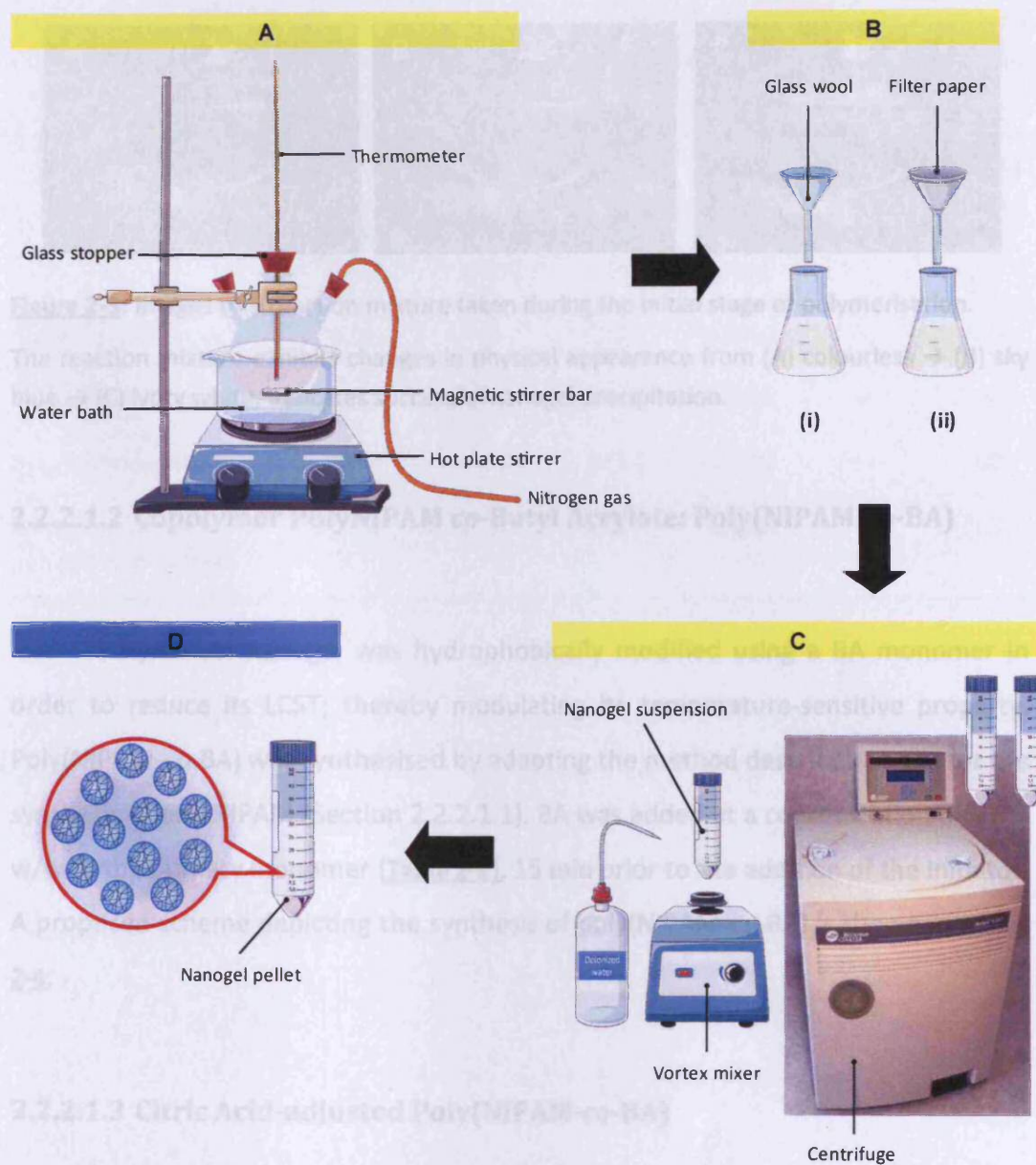


Figure 2-2: Schematic illustration of the experimental set up for polyNIPAM-based nanogel synthesis.

(A) Polymerisation; (B) purification by filtration (glass wool, then filter paper); (C) purification by repeated centrifugation, decantation and re-dispersion; and (D) final product, nanogel pellet.

The CA adjusted poly(NIPAM-co-BA) nanogel was prepared in a similar way to the poly(NIPAM-co-BA) but with a slight modification (Table 2-2). The reaction solution was made up of NIPAM monomer and MBA in de-ionised water, then adjusted to pH 2 by the drop-wise addition of 0.6 M aqueous CA. This was monitored using a digital PH209 Bench pH meter (Haine Instruments Ltd., Leighton Buzzard, UK) before the addition of the BA monomer.



Figure 2-3: Images of a reaction mixture taken during the initial stage of polymerisation.

The reaction mixture exhibits changes in physical appearance from (A) colourless → (B) sky blue → (C) ivory white, indicates successful nanogel precipitation.

2.2.2.1.2 Copolymer PolyNIPAM *co*-Butyl Acrylate: Poly(NIPAM-*co*-BA)

PolyNIPAM nanogel was hydrophobically modified using a BA monomer in order to reduce its LCST; thereby modulating its temperature-sensitive property. Poly(NIPAM-*co*-BA) was synthesised by adapting the method described above for the synthesis of polyNIPAM (Section 2.2.2.1.1). BA was added at a concentration of 7.5% w/w to the primary monomer (**Table 2-2**), 15 min prior to the addition of the initiator. A proposed scheme depicting the synthesis of poly(NIPAM-*co*-BA) is shown in **Figure 2-4**.

2.2.2.1.3 Citric Acid-adjusted Poly(NIPAM-*co*-BA)

The purpose of adding CA to the synthetic mixture was to determine the influence of an acidic environment of the reaction mixture during the polymerisation process on the properties of the resulting poly(NIPAM-*co*-BA) nanogel.

The CA adjusted poly(NIPAM-*co*-BA) nanogel was prepared in a similar way to the poly(NIPAM-*co*-BA) but with a slight modification (**Table 2-2**). The reaction solution was made up of NIPAM monomer and MBA in de-ionised water, then adjusted to pH 2 by the drop-wise addition of 0.6 M aqueous CA. This was monitored using a digital PH209 Bench pH meter (Hanna Instruments Ltd., Leighton Buzzard, UK) before the addition of the BA monomer.

Table 2-2: PolyNIPAM-based nanogels made up to a total preparation volume of 250 mL with de-ionised water (Lopez et al., 2004; Pelton and Chibante, 1986; Yurdasiper et al., 2008).

Nanogel / Abbreviation	Components					Stirring Rate (rpm)
	NIPAM (mol)	BA (mol)	MBA (mol)	KPS (mol)	CA (μL)	
PolyNIPAM (200 rpm)	0.02	—	0.001	0.0002	—	300
PolyNIPAM (300 rpm)	0.02	—	0.001	0.0002	—	200
Poly(NIPAM-co-BA)	0.02	0.002	0.001	0.0002	—	300
CA-adjusted poly(NIPAM-co-BA)	0.02	0.002	0.001	0.0002	√	300

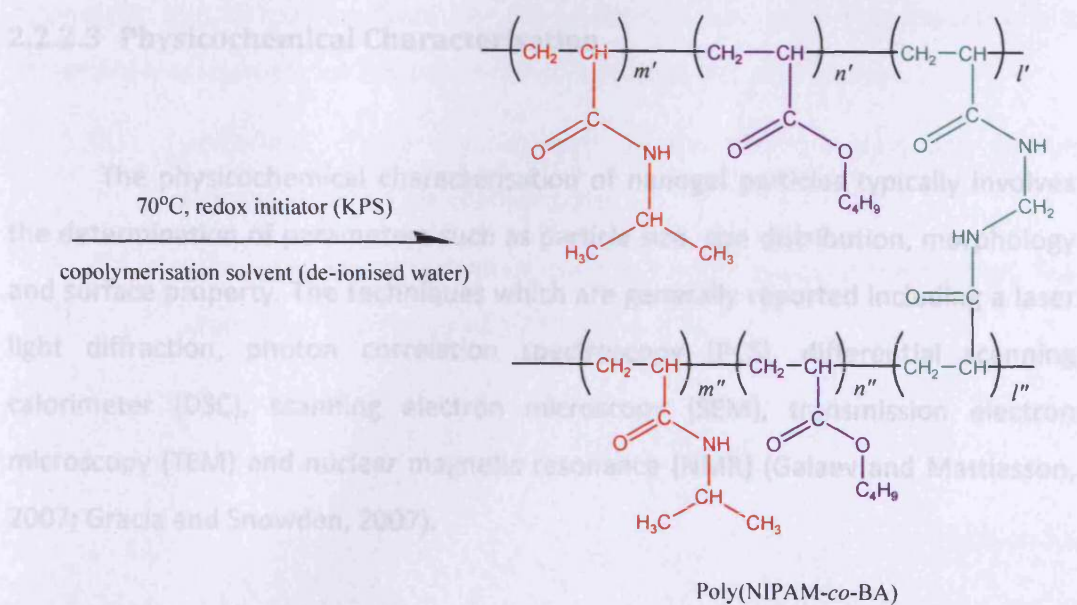
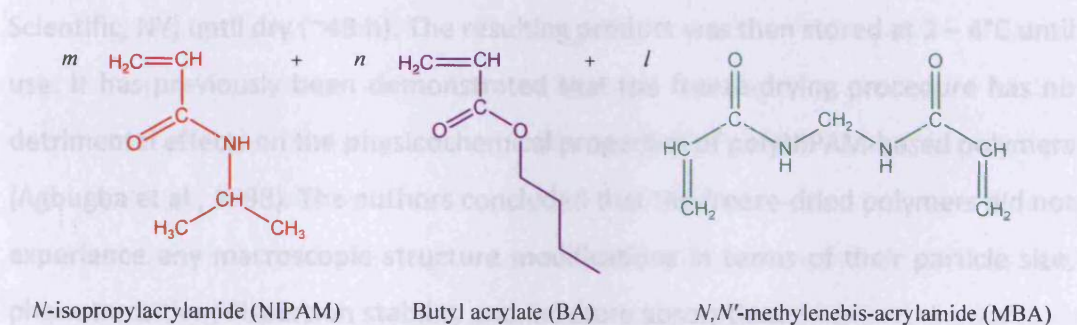


Figure 2-4: Proposed synthetic scheme for poly(NIPAM-co-BA) nanogel by SFEP technique using MBA as cross-linker and KPS as initiator at 70°C.

2.2.2.2 Nanogel Purification

The nanogel suspensions were initially cold-filtered through glass wool and filter paper to eliminate large aggregates or clumps. Residual monomers and other low molecular weight impurities were then removed by repeated steps of centrifugation [15,000 $\times g$, 20°C for 1 h in a temperature-controlled Beckman Coulter Avanti® J-25 centrifuge (Beckman Coulter Inc., Fullerton, CA)], decantation and re-dispersion in de-ionised water (up to 5 times).

For ease of storage, the nanogels were then subjected to freeze-drying. After the final centrifugation/decantation step, the nanogel pellets were placed in a freezer of -20°C for 1 h, then placed into a MicroModulyo 230 freeze-dryer (Thermo Scientific, NY) until dry (~48 h). The resulting product was then stored at 2 – 4°C until use. It has previously been demonstrated that the freeze-drying procedure has no detrimental effects on the physicochemical properties of polyNIPAM-based polymers (Agbugba et al., 1998). The authors concluded that the freeze-dried polymers did not experience any macroscopic structure modifications in terms of their particle size, phase transition, dispersion stability and moisture absorption.

2.2.2.3 Physicochemical Characterisation

The physicochemical characterisation of nanogel particles typically involves the determination of parameters such as particle size, size distribution, morphology and surface property. The techniques which are generally reported including a laser light diffraction, photon correlation spectroscopy (PCS), differential scanning calorimeter (DSC), scanning electron microscopy (SEM), transmission electron microscopy (TEM) and nuclear magnetic resonance (NMR) (Galaev and Mattiasson, 2007; Gracia and Snowden, 2007).

2.2.2.3.1 Particle Size and Size Distribution

Particle diameter and size distribution of the purified nanogel particles were determined by a laser light diffraction system: Malvern Mastersizer 2000 (Malvern Instruments Ltd., Malvern, UK). The technique is based on the principle that particles passing through a laser beam will scatter light at an angle that is directly related to their size – large particles scatter at low angles, whereas small particles scatter at high angles. Suspensions are mostly prepared with water, but other solvents can also be used (e.g. ethanol). The limitations of this method generally apply to non-spherical particles, and for materials with a low refractive index with respect to the dispersive medium (Malvern Instruments Ltd., 2007).

Figure 2-5 is an example of a typical particle size distribution curve obtained with Malvern Mastersizer 2000. The fundamental size distribution derived by this technique was volume-based, and expressed in terms of the volume of equivalent spheres ($D_{N\%}$) and weighted mean of the volume distribution (average particle diameter by mass – hydrodynamic diameter) (Malvern Instruments Ltd., 2007). The hydrodynamic diameter refers to how a particle diffuses within a fluid. As the laser light diffraction system was used for the analysis, two values that would give a rough equivalent on particle polydispersity are uniformity and span. Polydispersity is a dimensionless measure for the broadness of a particle size distribution:

- (i) Uniformity – the measurement of the absolute deviation of the distribution from the median point.
- (ii) Span – the measurement of the width of the particles distribution. The span value is determined by Equation 2-1:

$$\text{Span} = \frac{D_{90\%} - D_{10\%}}{D_{50\%}}$$

Equation 2-1

where $D_{N\%}$ ($N=10, 50, 90$) means that, the volume percentage of particles with diameters up to $D_{N\%}$ equals to $N\%$. The smaller the span value the narrower the particle size distribution.

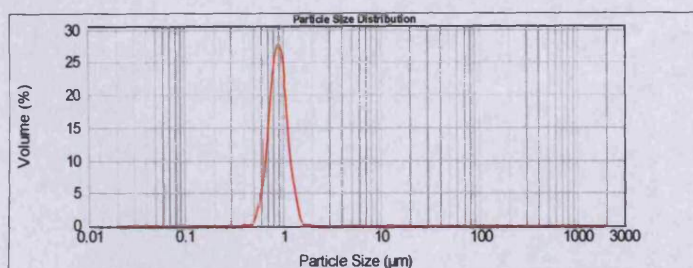


Figure 2-5: Typical particle size distribution curve produced by a laser light diffraction analyser, Malvern Mastersizer 2000.

Nanogel dispersions of 0.1% w/v were prepared by dilution of the swollen nanogel with de-ionised water in capped glass vials, and left to equilibrate for 1 h at ambient temperature on a SB1 Stuart® blood tube rotator (Bibby Scientific Ltd., Stone, UK). The samples were measured at ambient temperature and the data obtained were analysed automatically using a Mastersizer 2000 version 5.00 software supplied by the manufacturer (Malvern Instruments Ltd., Malvern, UK) Each sample was analysed in triplicate ($n=3$).

2.2.2.3.2 Stimulus-responsive Properties

2.2.2.3.2.1 Temperature

Laser light diffraction system has been widely used to observe and evaluate the temperature-induced swelling/de-swelling behaviour of the polyNIPAM-based polymers. To study the response of the nanogel particles to a temperature stimulus, the freeze-dried nanogels were dispersed in de-ionised water to 0.1% w/v in capped glass vials and left to mix for 30 min at ambient temperature on the laboratory

Stuart® Flask Shaker-SF1 (Bibby Scientific Ltd., Staffordshire, UK). The samples were stored at designated temperatures as listed in **Table 2-3**, allowing at least 1 h for temperature equilibrium and rapidly characterised using Malvern Mastersizer 2000. No further temperature measurements were made once the samples were removed from the incubation environment. De-ionised water was used as the dispersant medium and treated similarly as each test sample. Three measurements of each sample were taken to check for repeatability (n=3).

Table 2-3: Storage conditions for polyNIPAM-based nanogels to investigate temperature-responsive effect.

Temperature (°C)	Rationale	Storage
2 – 4	Storage condition	Laboratory refrigerator (Osborne Refrigerators Ltd., Bognor Regis, UK)
~25	RT – handling and analysis	Laboratory bench
32	Average skin surface temperature	Laboratory incubator (Weiss Gallenkamp, Loughborough, UK)
37	Average physiological temperature	Laboratory incubator
50	High skin temperature condition (e.g. blistering)	Laboratory incubator
60	Maximal heat effect	Laboratory incubator

2.2.2.3.2.2 Temperature Cycling

The effect of temperature cycling on the particle size was determined by alternating the temperature of nanogel suspensions between RT (~25°C) and 60°C, in order to check the reversibility of the swelling/de-swelling of the nanogel particles in response to changes in the solution temperature. Firstly, the freeze-dried samples were dispersed in de-ionised water at 0.1% w/v and analysed with Malvern Mastersizer 2000. Following that, the samples were left to equilibrate at 60°C in the laboratory incubator for 1 h and instantaneously characterised using Malvern

Mastersizer 2000. Then, the samples were left to cool to RT for 1 h before subjected to the particle size characterisation in order to check the reversibility of the swelling/de-swelling. No further temperature measurements were done once the sample removed from the incubator. Replicates of three were prepared for each sample (n=3).

2.2.2.3.2.3 pH

The response of the nanogel particles to pH was also investigated. This was to verify that the ionisable groups originating from the persulfate initiator had no significant response to pH that could contribute to the swelling/de-swelling behaviour of the nanogel particles. Results from Section 2.2.2.3.2.1 demonstrated that poly(NIPAM-co-BA) exhibited the most desirable response towards a thermal stimulus. Therefore, for the following studies in this chapter, only the poly(NIPAM-co-BA) and CA-adjusted poly(NIPAM-co-BA) were further investigated unless mentioned otherwise.

Solutions of various pH values (pH 2, 4, 5.8, 6, 8, and 10) were prepared through the drop-wise addition of either HCl (0.1 M) or NaOH (0.1 M) in de-ionised water, and monitored using PH209 Bench pH meter. Nanogel dispersions of 0.1% w/v were prepared by mixing the freeze-dried nanogels in the solutions of variable pH on a laboratory Stuart® Flask Shaker-SF1 for 1 h. No further pH adjustment was carried out on the resulting mixtures prior to analysis using Malvern Mastersizer 2000. The measurements were performed in triplicate at RT (n=3).

2.2.2.3.3 Thermal Analysis: Phase Transition

The de-swelling behaviour of the nanogels was investigated by thermal analysis using the technique differential scanning calorimetry. The instrument operates by measuring change in the heat capacity of a sample relative to a control,

over a predetermined temperature range and temperature gradient. Heat flow is measured by simultaneously monitoring the temperature difference between the sample and a reference material. This has previously been used in numerous polymer studies including polyNIPAM-based polymers (Kawaguchi et al., 1992; Ma et al., 2005; Minoo-Rabeeh-Hobabi et al., 2007).

The thermal analysis was performed using a multi-cell differential scanning calorimeter (MC-DSC) instrument with operating software MC-DSCRun version 2.5.0 for Windows (TA Instruments, Lindon, UT). This fully automated calorimeter is well-suited for analysing liquid samples. It runs one reference and three samples simultaneously in reusable, Hastelloy® ampoules sealed with O-rings to prevent loss of volatile components. Samples were prepared by diluting concentrated swollen poly(NIPAM-co-BA) and CA-adjusted poly(NIPAM-co-BA) nanogels in de-ionised water (50% w/v) and equilibrated at 2 – 4°C for 1 h. Approximately 1 mL of each hydrated sample was then transferred into the ampoule using a pipette. A nanogel-free solution of the same composition, i.e. de-ionised water, was placed in the reference ampoule. The samples were determined in replicates of three (n=3). A thermal scan was performed on the hydrated nanogels from 4 – 60°C at a scanning rate of 1°C min⁻¹, with an equilibrium period of 2 min.

Figure 2-6 is an example of a typical thermogram obtained with the MC-DSC. In this study, the LCST value was taken as the abscissa of the maximum of the endothermic transition peak (Eeckman et al., 2004). TA Instruments Universal Analysis 2000 software package for Windows (version 2.5.0) supplied by the instrument manufacturer was used for data acquisition and analysis.

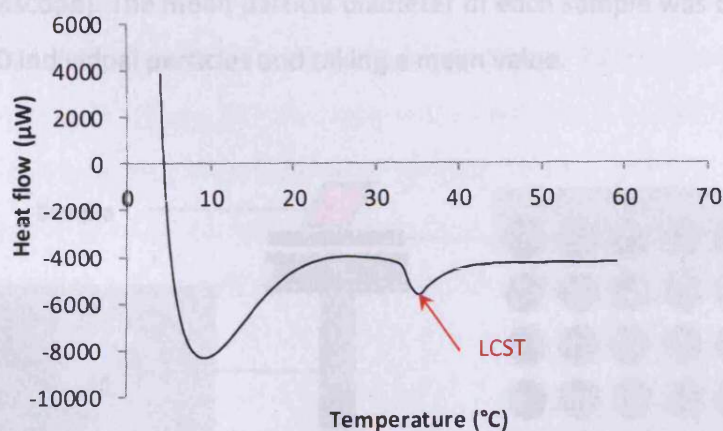


Figure 2-6: A typical thermogram of homopolymer polyNIPAM in de-ionised water obtained from MC-DSC showing LCST.

2.2.2.3.4 Morphology Determination by SEM and TEM

SEM and TEM studies are necessary for morphological characterisation of polymer particles of submicron size. These techniques offer the advantage that the fine structure including shape, size and uniformity of the sample of interest can be examined in great detail and of high resolution.

2.2.2.3.4.1 SEM

The surface morphology of the nanogel particles was investigated using a Phillips SEM-XL Series-20 SEM operated at 15 kilovolts (kV) accelerated voltage. Prior to viewing, it was essential that the samples were in a completely dried state, as the high vacuum conditions in the SEM chamber would cause hydrated specimens to boil, thereby destroying the integrity of the sample surface. Thus, the freeze-dried nanogels were left overnight in a high-pressure vacuum evaporator (Vacuum Edward Auto 306). After drying, each sample was carefully mounted on a pin-type aluminium specimen stub using a double-sided carbon adhesive tab as shown in [Figure 2-7](#). Prior to imaging, the samples were coated with gold for 30 – 40 s in a sputter coating unit

(JFC-1200 EMscope). The mean particle diameter of each sample was determined by measuring 30 individual particles and taking a mean value.

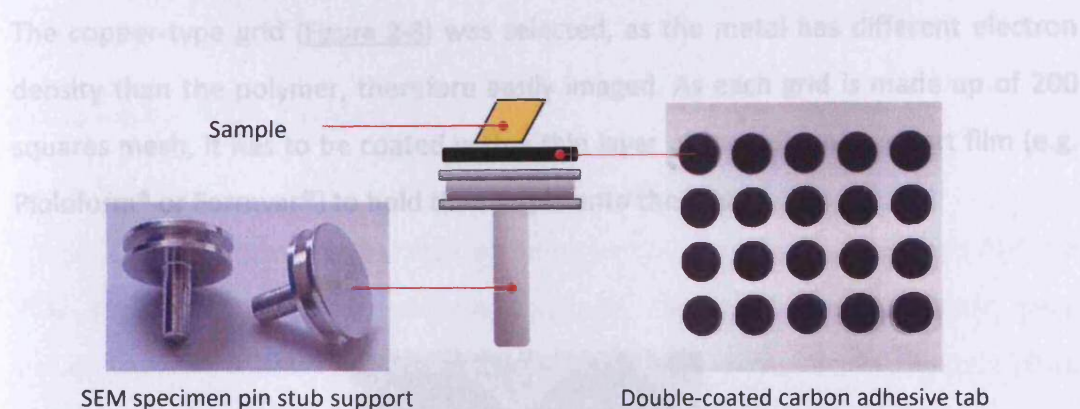


Figure 2-7: Illustration of a sample mounted on a specimen stub for SEM.

2.2.2.3.4.2 TEM

TEM has been widely used in studies involving polymers. It allows visualisation of a sample at higher resolution as compared to SEM. Initially, TEM was intended for studying in detail both, the internal and surface structure of nanogel particles. However, the nanogels were unsuitable for cross-sectional imaging (internal structural view), as the samples must be:

- (i) fixed either chemically (e.g. glutaraldehyde) or physically (cryofixation) to preserve fine structure,
- (ii) stained to enhance image contrast,
- (iii) dehydrated to remove water from the samples through wash steps of increasing ethanol concentrations,
- (iv) embedded in resin so that it can be cut into ultra-thin sections with a microtome, and
- (v) photographed under the high vacuum of an electron microscope.

Initial attempts to prepare samples for cross-sectional imaging were unsuccessful due to the fact that changes brought about by the fixing, dehydration and embedding steps were substantial, and almost destroyed the whole structure of

the studied nanogels. Thus, the nanogel particles could only be examined externally (surface structure) by directly dispersing the samples onto TEM coated-copper grids. The copper-type grid (**Figure 2-8**) was selected, as the metal has different electron density than the polymer, therefore easily imaged. As each grid is made up of 200 squares mesh, it has to be coated with a thin layer of transparent support film (e.g. Pioloform® or Formvar®) to hold the sample onto the grid.

TEM images of the nanogel particles were obtained using a Phillips EM 208 TEM operated at 80 kV accelerated voltage. The freeze-dried nanogels were suspended in de-ionised water (1% w/v). Approximately 20 µl of each sample was transferred onto a Pioloform®-coated copper grid. The residual water was removed by blotting with a filter paper, and the grids were washed with distilled water at room temperature before microscopic observation. At least three replicates were prepared for each sample load. The images (derived as magnified) selected were sufficient to examine in detail the general morphology of the samples under study. The mean particle diameter of each

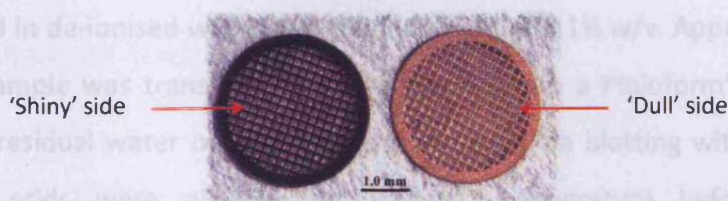


Figure 2-8: Uncoated copper grid of 200 squares mesh used to mount sample for TEM. Scale bar: 1.0 mm.

2.2.2.3.4.2.1 Preparation of Pioloform®-coated Copper Grids

Pioloform® is used to coat the grid, as it is suitable for application in TEM operated up to 100 kV. Pioloform® solution (0.8% w/v in chloroform) was poured into a clean dry film-casting funnel to the level that could cover 3/4 of a glass microscope slide. The slide was wiped with a lint-free tissue (e.g. Velin tissue) to remove dust before placing it vertically into the casting funnel. After a few seconds (s), the Pioloform® solution was slowly drained out of the funnel, allowing the solution to cling to the slide as the fluid level drops. The slide was allowed to dry at RT before being scored with a razor blade. Breathing on both sides of the slide prior to immersion in water aids the release of the film. The slide was slowly dipped vertically into distilled water (prepared beforehand in a clean glass container and its surface was 'dusted' by drawing a piece of Velin tissue across the container) and the film from each side was released, and floated onto the surface of the water. The grids were placed onto the Pioloform® film with their dull side facing down. The grids

on the film were removed from the water by lifting them up with a Parafilm® strip and left to dry on a filter paper in a petri dish.

2.2.2.3.4.2.2 TEM Imaging

TEM images of the nanogel particles were obtained using a Phillips EM 208 TEM operated at 80 kV accelerated voltage. The freeze-dried nanogels were suspended in de-ionised water at a concentration of 0.1% w/v. Approximately 10 µL of each sample was transferred using a pipette onto a Pioloform®-coated copper grid. The residual water on the grids was removed via blotting with a filter paper, and the grids were air-dried at ambient temperature before microscopic observation. At least three replicates were prepared for each sample ($n \geq 3$). The magnifications (termed as magn) selected were sufficient to examine in detail the general morphology of the samples under study. The mean particle diameter of each nanogel sample was determined by measuring 150 individual particles and taking a mean value.

2.2.2.3.4.3 Particle Size Analysis by SEM and TEM

Particle diameter obtained from the SEM images was determined using a software package supplied by the manufacturer of SEM-XL Series-20, Phillips. To maintain consistency, the measurement was restricted only to the SEM images of 10Kx magnification.

Quantitative measurement of the TEM micrographs was done using a commercial digital image processing software known as ImageJ (Image processing and analysis in JAVA) version 1.45b (National Institute of Health, Bethesda, MD). The software measured the areas of the particles in captured images of 13Kx magnification. Particle diameter (D) was determined from the projected area (A) on the image as shown in Equation 2-2:

$$D = \sqrt{\frac{A}{\pi}} \times 2$$

Equation 2-2

where the particle diameter is defined as the diameter of a sphere of equivalent cross-sectional area on the images.

2.2.2.4 Data and Statistical Analysis

The data obtained were recorded and analysed using Excel 2007 (Microsoft Office, Microsoft Corp., Redmond, WA) and expressed as a mean \pm standard deviation (SD). Statistical analysis was performed with InStat[®] for Macintosh, version 3.00 (GraphPad Software Inc., San Diego, CA). Significant differences between two means were made using Student's *t*-test. Confidence interval was 95% where $p < 0.05$ was considered to be significant.

2.3 RESULTS AND DISCUSSION

For the preliminary study, a series of nanogels as listed in [Table 2-2](#) were synthesised since the aim was to determine a suitable nanogel matrix to serve as a carrier for topical delivery applications. NIPAM was selected as the primary component of the synthesised nanogels because of the wealth of literature and database available on the properties of polyNIPAM-based polymers (Das, 2008; Hellweg, 2003; Saunders and Vincent, 1996; Schild, 1992).

2.3.1 Physicochemical Characterisation

2.3.1.1 Particle Size and Size Distribution

Figure 2-9 presents the mean hydrodynamic diameter of the synthesised nanogels. A series of nanogel particles with diameter ranges in a nanometric scale were successfully synthesised. The synthesis of particles in nanometre range is desirable, as a reduction in their dimension may significantly improve their response time to changes in external stimuli due to large surface areas. In addition, it is necessary for the particles to be in the nanoscale size for absorption into skin as discussed in CHAPTER 1.

Different stirring rates applied during the nanogel synthesis proved to have produced significantly different sizes of polyNIPAM particles. The nanogel prepared at 300 rpm exhibited a smaller mean hydrodynamic diameter (559 ± 4 nm) than the one prepared at 200 rpm (666 ± 12 nm) ($p=0.0001$). A high stirring rate applied during the synthetic step may have caused break down of the suspension droplets and thus, reduced the diameter of nanogel particles produced (Panayiotou et al., 2007).

The copolymer poly(NIPAM-co-BA) was prepared with the aim to modulate the thermal-responsive property of the polyNIPAM nanogel. BA monomer is one of the most commonly used hydrophobic co-monomers and generally decreases the phase transition temperature of the polyNIPAM by compromising the balance of hydrophobic and hydrophilic monomers present in the polymer (Gracia and Snowden, 2007). The hydrophobic monomer could reduce the hydrogen bonding between the water molecules and the hydrophilic amide groups of the NIPAM segment; thus, there is less energy required to break the hydrogen bonds in comparison to unmodified polyNIPAM nanogels upon increase in temperature.

The poly(NIPAM-co-BA) would be expected to experience pronounced deswelling at a temperature range lower than the LCST of polyNIPAM (32 – 34°C), and therefore exhibit higher sensitivity towards a thermal stimulus. The mean

hydrodynamic diameter of the poly(NIPAM-co-BA) was found to be 432 ± 4 nm, whereas the polyNIPAM (300 rpm) had a mean hydrodynamic diameter of 559 ± 4 nm. Even though BA was previously shown to increase the size of polyNIPAM particles (Wu et al., 1994), the poly(NIPAM-co-BA) demonstrated a significantly smaller hydrodynamic diameter compared to the polyNIPAM (300 rpm) at RT ($p < 0.0001$), due to the enhanced response towards external temperature changes contributed by the BA monomer.

A further copolymer, poly(NIPAM-co-BA), was prepared which was modified with CA by adjusting pH of the monomer mixture to 2, before commencing polymerisation. The CA-adjusted-poly(NIPAM-co-BA) nanoparticles were shown to have a significantly larger hydrodynamic diameter (886 ± 7 nm) in comparison to the poly(NIPAM-co-BA) prepared in the absence of the acid (432 ± 4 nm) at RT ($p < 0.0001$). The pH value of the polymerisation medium was reported to influence the nucleation step and the nanogel stability (Zha et al., 2007). Potassium persulfate, used as the initiator in the current work, is an inorganic salt and is soluble in both acidic and basic aqueous media. In the precipitation polymerisation process for synthesising polyNIPAM nanogels, the recommended pH range for persulfate salts is from 2 to 12. The reaction mixture with pH beyond or less than the recommended limits typically leads to partially or totally flocculated nanogel particles.

It was reported previously that decreasing the reaction pH value led to an increase in the particle size of polyNIPAM nanogels based on persulfate salts as initiator (Zha et al., 2007). This is because the dissociation degree of the sulfate acid groups ($pK_a = 1.89$) resulting from the decomposition of KPS during the polymerisation decreased with the reaction pH value. The low concentration of persulfate radicals caused a reduction in the formation of precursor particles. This further reduced the colloidal stabilisation of the nucleated particles through an electrostatic mechanism, thus increasing the final particle size of the nanogels (detailed polymerisation mechanism in Section 2.1.1).

Table 2-4 presents the minimum and maximum diameters of the measured nanogels, which represent their particle size distributions. Those values were illustrated as particle size distribution curves as shown in **Figure 2-10**, in which the

nanogels exhibited normal and considerably narrow particle size distributions. The particle distribution can be further assessed based on polydispersity, represented by span and uniformity values. For example, the particle size distribution of the CA-adjusted poly(NIPAM-co-BA) was narrower than the poly(NIPAM-co-BA) with the span value of 0.57 ± 0.004 and 0.92 ± 0.04 respectively, as illustrated in **Figure 2-10(C)**. Overall, the polydispersity values of the studied samples were considerably low, which indicate minimum variations in particle size.

In conclusion, the particle size of polyNIPAM-based nanogels depends on several factors including the cross-linker density, monomer and co-monomer composition/concentration, chemical nature of the solvent (e.g. pH) as well as stirring rate applied during synthesis (Chai et al., 2003; Panayiotou et al., 2007). On top of that, it is very interesting to note that the glassware used during the synthesis may have some contribution to the size of the final product. It was found that, large polymer particles ($>1 \mu\text{m}$) were obtained if the polymerisations were carried out in a flat-bottomed glass flask in comparison to a round-bottomed flask (Tauer, 2003). Therefore, the hydrodynamics of the reaction mixtures were important.

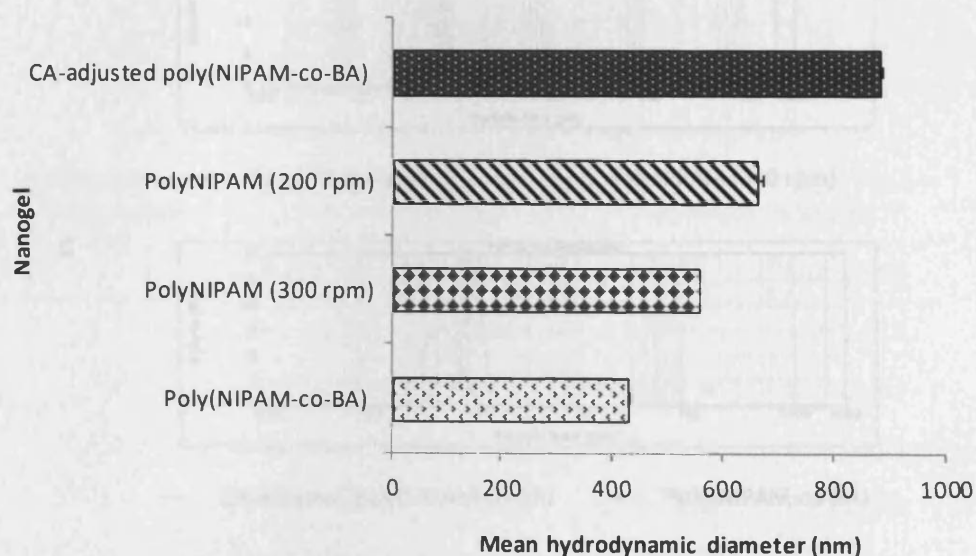


Figure 2-9: Mean hydrodynamic diameter of polyNIPAM-based nanogels dispersed in de-ionised water measured at RT by a laser light diffraction analyser ($n=3, \pm \text{SD}$).

Table 2-4: Particle size profiles of polyNIPAM-based nanogel particles, measured at RT by a laser light diffraction analyser; polydispersity of the samples reflected by span and uniformity values ($n=3$, \pm SD).

Nanogel	Particle Diameter (nm)		Span	Uniformity
	Minimum	Maximum		
PolyNIPAM (200 rpm)	426 ± 14	951 ± 47	0.83 ± 0.07	0.23 ± 0.01
PolyNIPAM (300 rpm)	384 ± 5	753 ± 16	0.68 ± 0.04	0.22 ± 0.01
Poly(NIPAM-co-BA)	263 ± 3	638 ± 14	0.92 ± 0.04	0.18 ± 0.001
CA-adjusted poly(NIPAM-co-BA)	642 ± 7	$1,132 \pm 7$	0.57 ± 0.004	0.18 ± 0.001

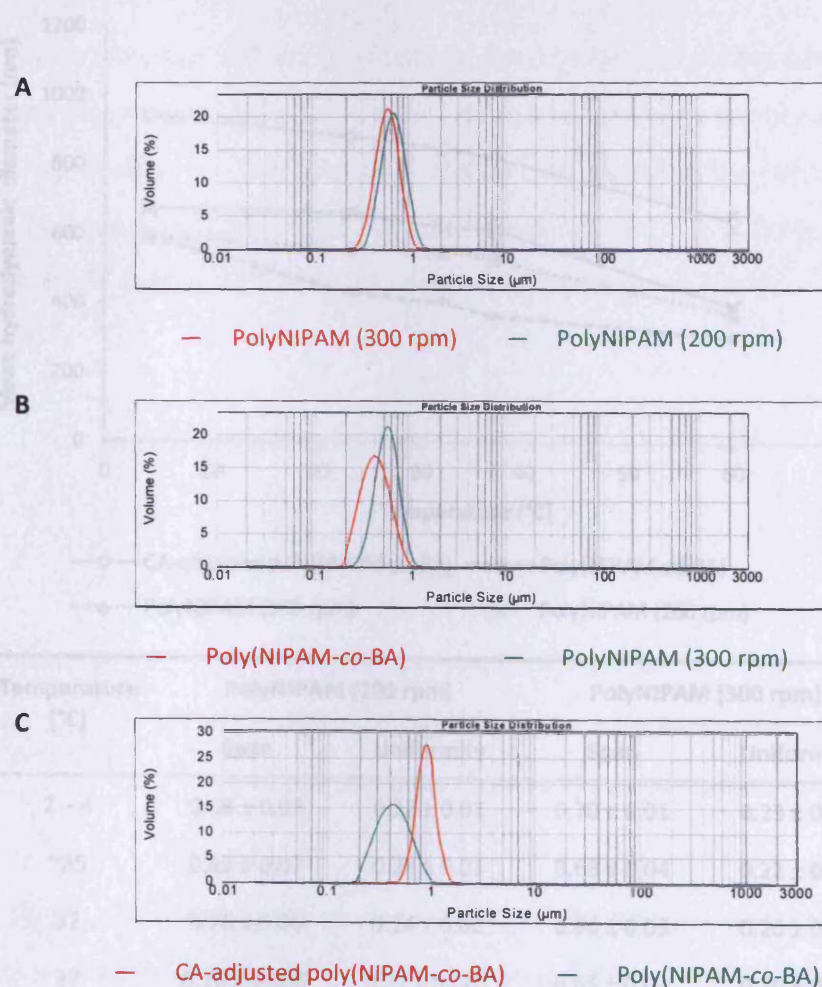
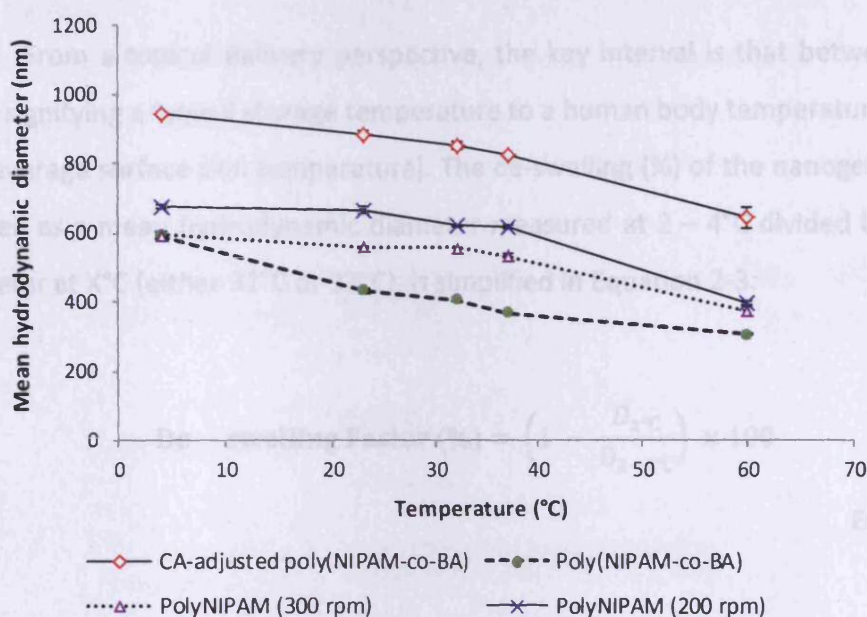


Figure 2-10: Particle size distribution curves of polyNIPAM-based nanogels dispersed in de-ionised water, measured at RT by a laser light diffraction analyser.

2.3.1.2 Temperature-responsive Effect

In principle, nanogel particles should undergo volume collapse and experience size reduction as the temperature of their environment increases (Saunders et al., 2009). As displayed in **Figure 2-11**, over the range of 4 – 60°C the particles of each nanogel underwent a de-swelling event, thereby exhibiting a typical temperature-sensitivity.



Temperature (°C)	PolyNIPAM (200 rpm)		PolyNIPAM (300 rpm)	
	Span	Uniformity	Span	Uniformity
2 – 4	0.68 ± 0.03	0.22 ± 0.01	0.70 ± 0.01	0.23 ± 0.02
~25	0.83 ± 0.07	0.23 ± 0.01	0.68 ± 0.04	0.22 ± 0.01
32	0.76 ± 0.06	0.24 ± 0.02	0.64 ± 0.03	0.20 ± 0.01
37	0.70 ± 0.003	0.22 ± 0.001	0.65 ± 0.04	0.20 ± 0.01
60	1.31 ± 0.02	0.41 ± 0.01	1.06 ± 0.12	0.33 ± 0.04

Figure 2-11: Mean hydrodynamic diameter, as a function of temperature for polyNIPAM-based nanogels dispersed in de-ionised water measured by a laser light diffraction analyser; span and uniformity values correspond to polydispersity of each measurement (n=3, ± SD).

Temperature (°C)	Poly(NIPAM-co-BA)		CA-adjusted Poly(NIPAM-co-BA)	
	Span	Uniformity	Span	Uniformity
2 – 4	0.79 ± 0.03	0.17 ± 0.001	0.55 ± 0.002	0.17 ± 0.001
~25	0.92 ± 0.04	0.18 ± 0.001	0.57 ± 0.004	0.18 ± 0.001
32	0.84 ± 0.04	0.18 ± 0.003	0.59 ± 0.02	0.18 ± 0.003
37	0.99 ± 0.01	0.18 ± 0.01	0.60 ± 0.01	0.18 ± 0.01
60	0.60 ± 0.003	0.20 ± 0.01	0.63 ± 0.04	0.20 ± 0.01

Figure 2-11: CONTINUE

From a topical delivery perspective, the key interval is that between 4 and 37°C, signifying a typical storage temperature to a human body temperature via 32°C (the average surface skin temperature). The de-swelling (%) of the nanogel particles, defined as a mean hydrodynamic diameter measured at 2 – 4°C divided by a mean diameter at X°C (either 32°C or 37°C), is simplified in Equation 2-3:

$$\text{De – swelling Factor (\%)} = \left(1 - \frac{D_{X^\circ\text{C}}}{D_{2-4^\circ\text{C}}} \right) \times 100$$

Equation 2-3

- De-swelling (%) : De-swelling of a particle, 2 – 4°C to X°C
- $D_{2-4^\circ\text{C}}$: Mean hydrodynamic diameter of particles measured at 2 – 4°C
- $D_{X^\circ\text{C}}$: Mean hydrodynamic diameter of particles measured at X°C.

Figure 2-12 presents the de-swelling (%) of the nanogel particles graphically. The hydrodynamic diameter of the poly(NIPAM-co-BA) at 2 – 4°C was 593 ± 9 nm, reduced to 432 ± 4 nm at ambient temperature, i.e. around 27.1% de-swelling over 21°C temperature change (2 – 4°C → 25°C). The particle demonstrated further de-swelling of 4.3% (432 ± 4 nm → 406 ± 5 nm), as the temperature of the nanogel suspension was increased from 25°C to 32°C, and 6.4% (406 ± 5 nm → 369 ± 1 nm)

from 32°C to 37°C. As a result, the poly(NIPAM-co-BA) particles exhibited a total hydrodynamic diameter reduction by 37.8% over the 33°C temperature range, which was considered very significant ($p < 0.0001$). Even though the CA-adjusted poly(NIPAM-co-BA) only experienced a total de-swelling of 12.7% ($944 \pm 3 \text{ nm} \rightarrow 824 \pm 11 \text{ nm}$) within the same temperature range, the nanogel still experienced a significant de-swelling ($p < 0.0001$). The polyNIPAM (300 rpm) and polyNIPAM (200 rpm) nanogels underwent the least volume reduction with 10.6% and 9.3% respectively. Therefore, the poly(NIPAM-co-BA) was found to experience the highest de-swelling event among the investigated nanogels ($p < 0.0001$). BA has previously been successfully used to reduce the VPTT of a polyNIPAM polymer (Gracia and Snowden, 2007); thus, the current nanogel would be expected to demonstrate greater sensitivity when absorbed into the skin.

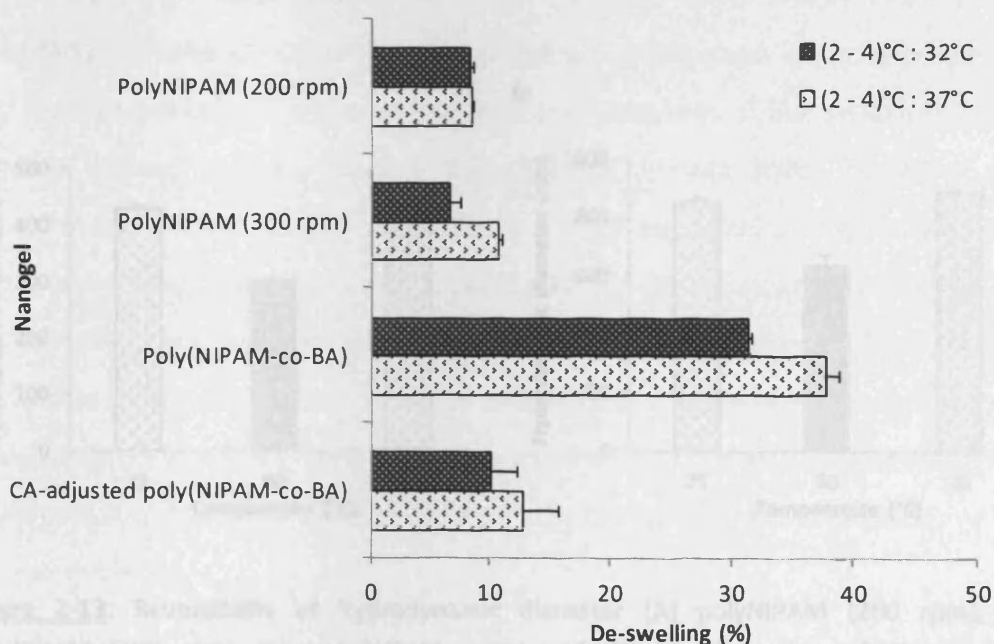


Figure 2-12: De-swelling (%) of polyNIPAM-based nanogels in de-ionised water, calculated over two temperature ranges, 2 – 4°C → 32°C and 2 – 4°C → 37 °C ($n=3$, \pm SD).

Another characteristic feature that makes polyNIPAM-based nanogel particles interesting is their capacity to change their volume reversibly when the temperature of suspending medium is modified (Jagur-Grodzinski, 2010; Panayiotou

et al., 2007). This was confirmed by repetitive measurements of the hydrodynamic diameter of nanospheres, by changing the temperature alternately between RT ($\sim 25^{\circ}\text{C}$) and 60°C . All synthesised nanogels successfully responded towards the temperature cycling (**Figure 2-13**).

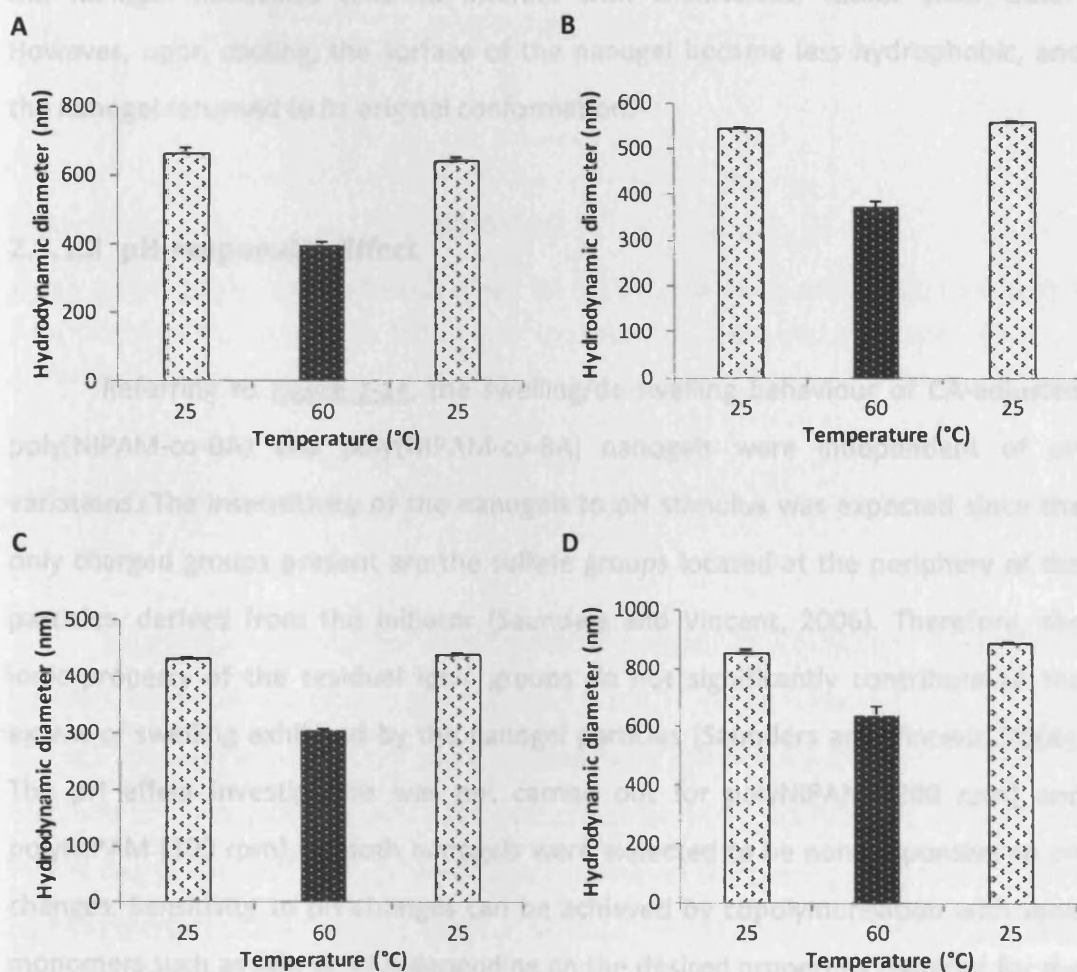


Figure 2-13: Reversibility of hydrodynamic diameter (A) polyNIPAM (200 rpm), (B) polyNIPAM (300 rpm), (C) poly(NIPAM-co-BA) and (D) CA-adjusted poly(NIPAM-co-BA) dispersed in de-ionised water, as a function of alternating temperatures ($25^{\circ}\text{C} \rightarrow 60^{\circ}\text{C} \rightarrow 25^{\circ}\text{C}$) ($n=3$, \pm SD). In all cases, $p < 0.0001$ between treatments

In addition, visual inspection also indicated the apparent reversibility of the swelling transition, as the transparent solutions became completely turbid at 60°C , and returned to their original appearance once the temperature lowered to RT. At

RT, the nanogel particles were in their swollen form. However, as the temperature increased, the nanogel particles collapsed and release their content. It could be explained by a decrease in the hydrogen bonding between the amide groups of the polymer and water molecules of the solvent at 60°C. This brought changes to the nature of the nanogel surface from a hydrophilic state to a hydrophobic state, where the nanogel molecules tend to interact with themselves, rather than water. However, upon cooling, the surface of the nanogel became less hydrophobic, and the nanogel returned to its original conformation.

2.3.1.3 pH-responsive Effect

Referring to [Figure 2-14](#), the swelling/de-swelling behaviour of CA-adjusted poly(NIPAM-co-BA) and poly(NIPAM-co-BA) nanogels were independent of pH variations. The insensitivity of the nanogels to pH stimulus was expected since the only charged groups present are the sulfate groups located at the periphery of the particles, derived from the initiator (Saunders and Vincent, 2006). Therefore, the ionic property of the residual ionic groups do not significantly contribute to the extent of swelling exhibited by the nanogel particles (Saunders and Vincent, 2006). The pH effect investigation was not carried out for polyNIPAM (200 rpm) and polyNIPAM (300 rpm), as both nanogels were expected to be non-responsive to pH changes. Sensitivity to pH changes can be achieved by copolymerisation with ionic monomers such as AAc or VAA depending on the desired properties required for the nanogel networks.

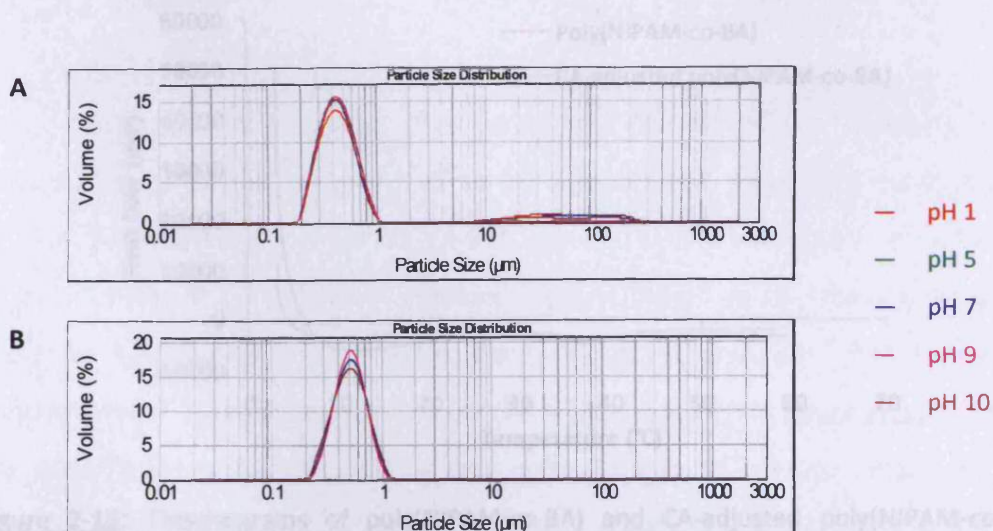


Figure 2-14: Particle size distribution curves for (A) poly(NIPAM-*co*-BA) and (B) CA-adjusted poly(NIPAM-*co*-BA) nanogels in different pH environments, measured by a laser diffraction analyser.

2.3.1.4 Thermal Analysis: Phase Transition

Figure 2-15 presents the thermograms of poly(NIPAM-*co*-BA) and CA-adjusted poly(NIPAM-*co*-BA) nanogels. **Table 2-5** listed the LCST values for both nanogel types. The LCST of poly(NIPAM-*co*-BA) and CA-adjusted poly(NIPAM-*co*-BA) was reported as 36°C and 37°C respectively, with no significant difference ($p=0.7846$) between them. This is due to the fact that, both nanogels contained the same types of monomers (NIPAM and BA) of the same concentration. Thus, no difference should be observed. However, the poly(NIPAM-*co*-BA) experienced the phase transition within a narrow temperature range (31 – 42°C) in comparison to the CA-adjusted poly(NIPAM-*co*-BA) (29 – 46°C). This could be due to a factor of dimension. Since the poly(NIPAM-*co*-BA) was significantly smaller than the CA-adjusted poly(NIPAM-*co*-BA); thus it required less time to attain absolute phase transition during the thermal scan analysis of 1°C min⁻¹.

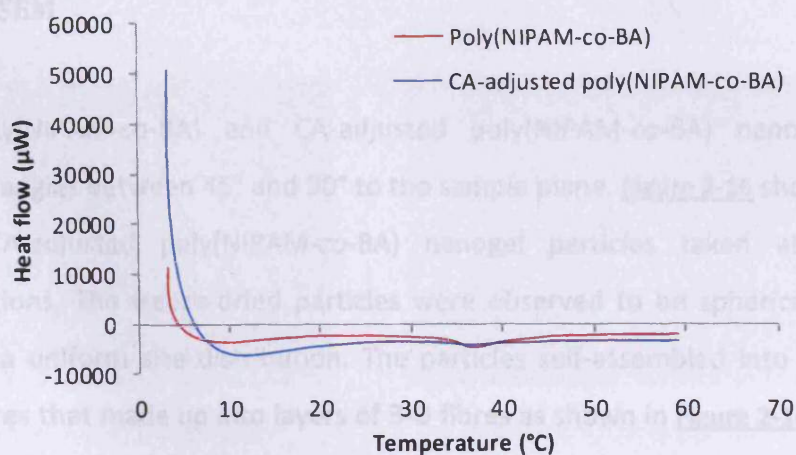


Figure 2-15: Thermograms of poly(NIPAM-co-BA) and CA-adjusted poly(NIPAM-co-BA) nanogels in de-ionised water measured by MC-DSC.

Table 2-5: Phase transitions of poly(NIPAM-co-BA) and CA-adjusted poly(NIPAM-co-BA) nanogels dispersed in de-ionised water measured by MC-DSC ($n=3 \pm SD$).

Sample	LCST (°C)
Poly(NIPAM-co-BA)	36 ± 2
CA-adjusted Poly(NIPAM-co-BA)	37 ± 0.0004

2.3.1.5 Size and Morphology

Poly(NIPAM-co-BA) and CA-adjusted poly(NIPAM-co-BA) were subjected to microscopy investigation. No further studies were done on polyNIPAM (200 rpm) or polyNIPAM (300 rpm), as they were proven to be less sensitive towards thermal stimulus in comparison to the poly(NIPAM-co-BA) nanogel. Even though the CA-adjusted poly(NIPAM-co-BA) has the largest hydrodynamic particle diameter, it was subjected to microscope investigation, as a similar type of co-monomer (BA) was incorporated into the polymer, making it comparable to the poly(NIPAM-co-BA).

2.3.1.5.1 SEM

Poly(NIPAM-*co*-BA) and CA-adjusted poly(NIPAM-*co*-BA) nanogels were viewed at angles between 45° and 90° to the sample plane. **Figure 2-16** shows images of the CA-adjusted poly(NIPAM-*co*-BA) nanogel particles taken at different magnifications. The freeze-dried particles were observed to be spherical in shape and have a uniform size distribution. The particles self-assembled into a sheet of nanospheres that made up into layers of 3-D fibres as shown in **Figure 2-16(A)**. As for the poly(NIPAM-*co*-BA) nanogel, it was quite difficult to capture images of the particles, since most of them tended to form a continuous film on drying with no spheres apparent (**Figure 2-17**). This is due to its smaller size in comparison to the CA-adjusted poly(NIPAM-*co*-BA) which could be seen as discrete spheres. The mean particle diameter of each sample is presented graphically in **Figure 2-18**. The result is consistent with the findings obtained from the laser diffraction particle size analysis (Section 2.3.1.1), where the CA-adjusted poly(NIPAM-*co*-BA) particles were significantly larger than the poly(NIPAM-*co*-BA) ($p < 0.0001$). However, the diameter determined from the SEM micrographs are comparatively smaller than those reported by the laser diffraction method: 35- and 24-fold smaller for the CA-adjusted poly(NIPAM-*co*-BA) and poly(NIPAM-*co*-BA) correspondingly. This could be explained in that the SEM deals with completely dried samples, whereas the laser diffraction analysis represents the hydrodynamic size measured at their hydrated state.

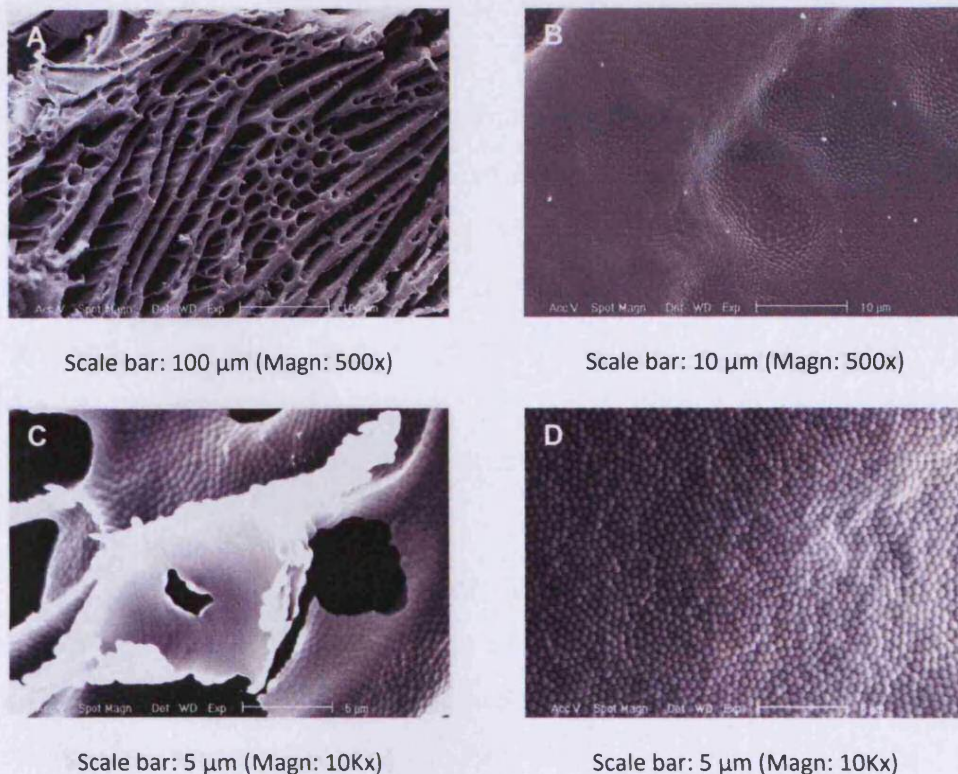


Figure 2-16: SEM images of freeze-dried CA-adjusted poly(NIPAM-co-BA) particles taken at different magnifications.

- (A) : The nanogel particles self-assembled into a sheet of nanospheres that made up into layers of 3-D fibres.
- (B – D) : Distinctive nano-sized particles that self-assembled into a sheet of spheres taken at different magnifications.

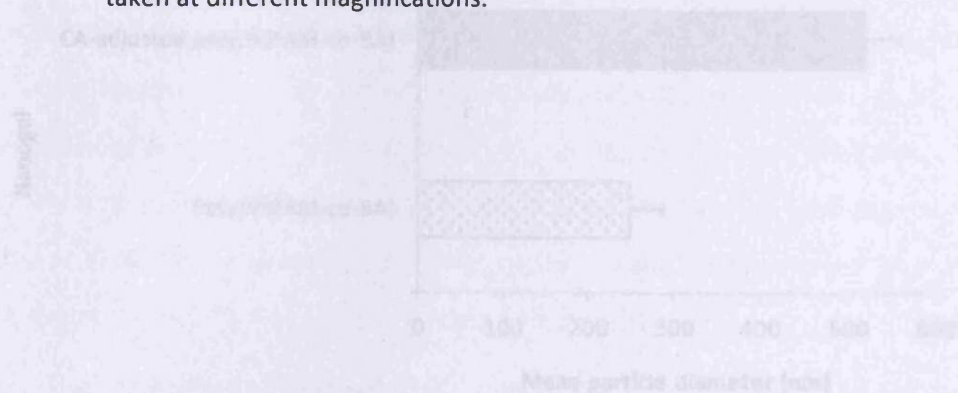


Figure 2-15: Mean particle diameters of poly(NIPAM-co-BA) and CA-adjusted poly(NIPAM-co-BA) nanogels determined according to SEM images ($n=40$, \pm SD). $p=0.0003$

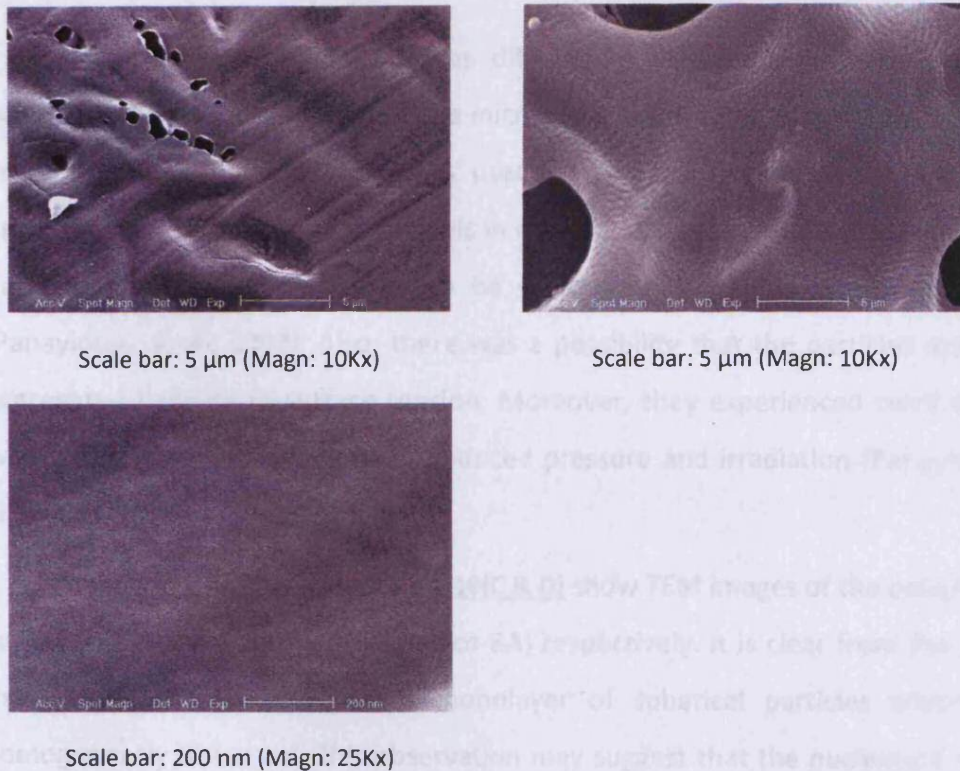


Figure 2-17: SEM images of freeze-dried poly(NIPAM-co-BA) particles at different magnifications. Most of the particles self-assembled to form a continuous film on drying with no spheres apparent.

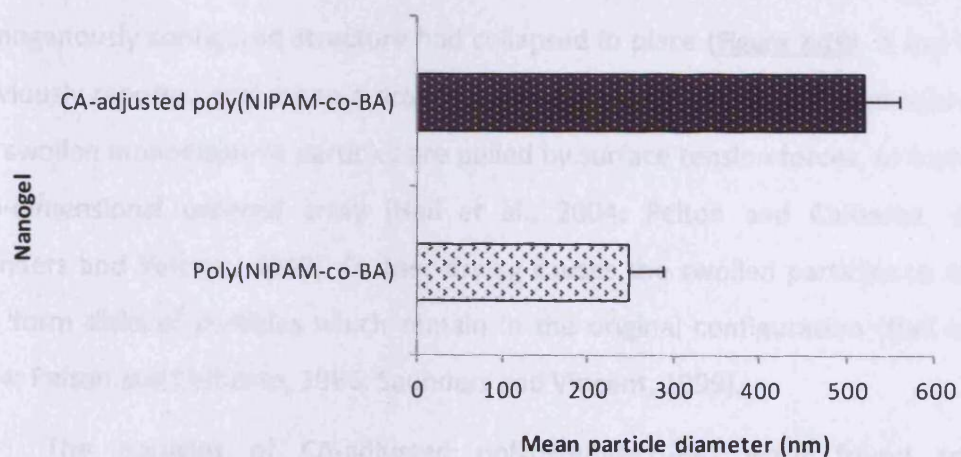


Figure 2-18: Mean particle diameters of poly(NIPAM-co-BA) and CA-adjusted poly(NIPAM-co-BA) nanogels determined according to SEM images ($n=30, \pm SD$). $p=0.0001$

2.3.1.5.2 TEM

As mentioned earlier, it was difficult to capture sharp images of the poly(NIPAM-co-BA) using SEM, as the microscope has optical microscopy resolution limited to about 0.2 μm . TEM was used instead, to investigate the shape and uniformity of the synthesised nanogels in detail. It allows a visual assessment of the particles but the samples need to be dried and viewed in a collapsed state (Panayiotou et al., 2007). Also, there was a possibility that the particles may have aggregated because of surface tension. Moreover, they experienced swell and deswell in the electron beam due to reduced pressure and irradiation (Panayiotou et al., 2007).

Figure 2-19(A & B) and **Figure 2-19(C & D)** show TEM images of the poly(NIPAM-co-BA) and CA-adjusted poly(NIPAM-co-BA) respectively. It is clear from the images that they self-assembled into a monolayer of spherical particles which were homogeneously dispersed. This observation may suggest that the nucleation process during synthesis was successful and that the purification process selected for these nanogels was efficient in removing impurities. Similar micrographs were also presented by Pelton and Chibante (Pelton and Chibante, 1986).

Detailed observations of the colloidal particles reveal that their homogeneously configured structure had collapsed in place (**Figure 2-19**). It has been previously reported that when a drop of dilute latex is placed on a microscope grid, the swollen monodisperse particles are pulled by surface tension forces, to form the two-dimensional ordered array (Hall et al., 2004; Pelton and Chibante, 1986; Saunders and Vincent, 1999). Further drying causes the swollen particles to shrink and form disks of particles which remain in the original configuration (Hall et al., 2004; Pelton and Chibante, 1986; Saunders and Vincent, 1999).

The particles of CA-adjusted poly(NIPAM-co-BA) were found to be significantly larger ($p < 0.0001$) than those of poly(NIPAM-co-BA), as shown in **Figure 2-20**. Moreover, the particles in dry state were smaller than those in the hydrated state (Section 2.3.1.1) due to shrinking, as a result of drying process.

2.4 CONCLUSION

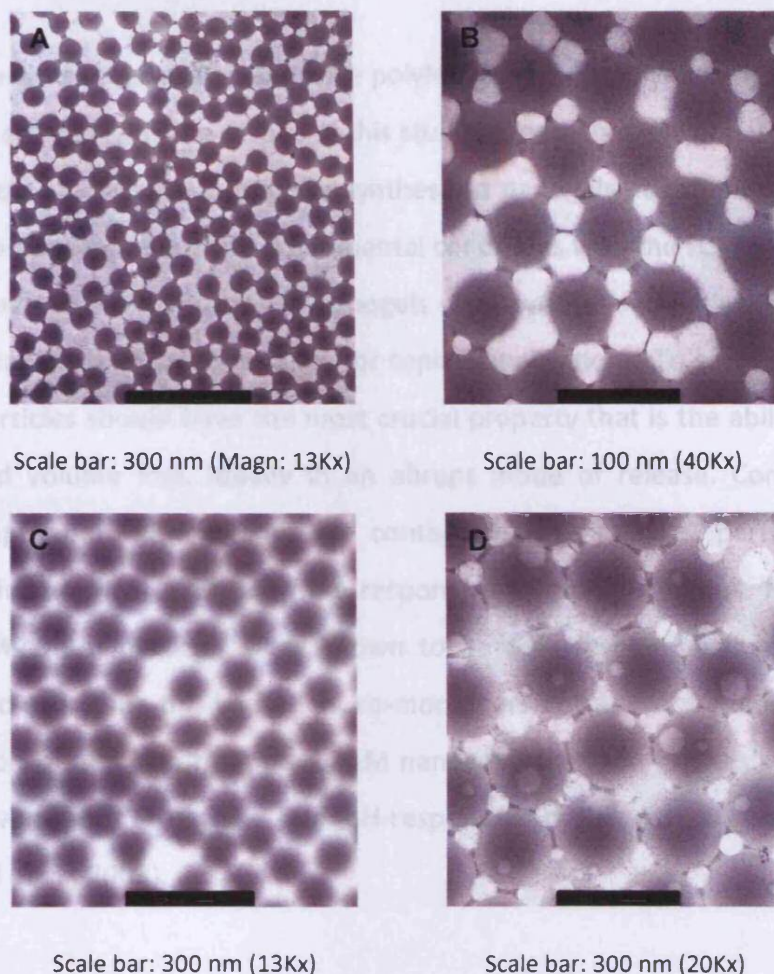


Figure 2-19: TEM images of (A & B) poly(NIPAM-co-BA) and (C & D) CA-adjusted poly(NIPAM-co-BA) particles.

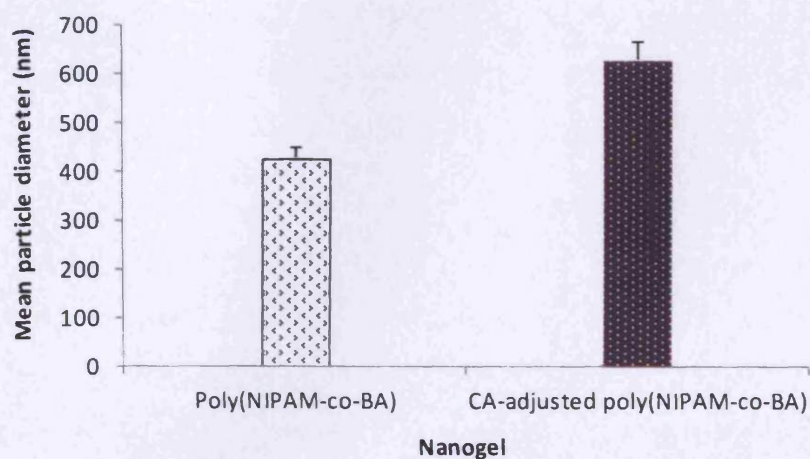


Figure 2-20: Mean particle diameters of poly(NIPAM-co-BA) and CA-adjusted poly(NIPAM-co-BA) nanogels measured based on TEM images ($n=150$, \pm SD). $p=0.0001$

2.4 CONCLUSION

A series of thermally-responsive polyNIPAM-based polymers in a nanometric scale were synthesised. The results of this study suggest that the poly(NIPAM-co-BA) was the most responsive among the synthesised nanogels. It exhibited the highest swelling/de-swelling under the experimental conditions with the LCST value found to be 36°C. The thermally-responsive nanogels were synthesised with a view towards their applicability as delivery carriers for topical applications. To serve this role, the nanogel particles should have the most crucial property that is the ability to exhibit pronounced volume loss, ideally in an abrupt mode of release. Considering the desired application, the removal of content by the nanogel particles can be enhanced further, if the particles are responsive to multiple stimuli. However, the poly(NIPAM-co-BA) particles were shown to be only responsive towards thermal stimulus. To overcome this limitation, co-monomers of acidic or basic functionalities can be incorporated into the polyNIPAM nanogel during the synthesis step to yield particles with both, thermal- and pH-responsive properties (Nur et al., 2010; Woodward et al., 2003).

CHAPTER 3 | Probing Enhanced
Topical Drug Delivery by Poly(NIPAM-co-BA)
Nanogel as a Carrier

3.1 INTRODUCTION

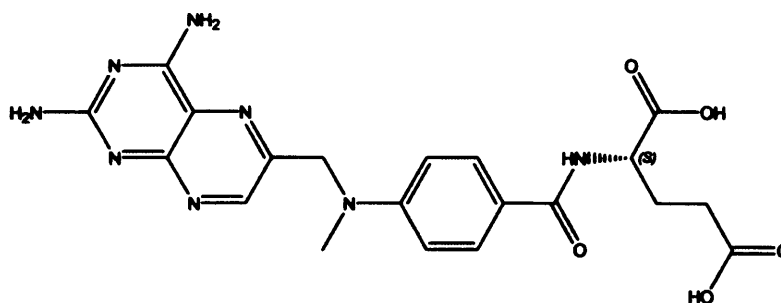
The stimulus-responsive nature of nanogels is attractive and has potential uses in many applications, including pharmaceuticals (Murray and Snowden, 1995). Depending on the chemical nature of the monomers used, nanogels undergo volume phase transition in response to external stimuli, such as temperature (Hoare and Pelton, 2004b), ionic strength (Neyret and Vincent, 1997) and solvent type (Kaneda and Vincent, 2004). This stimuli-induced behaviour, of absorbing solvated materials into the particles such as drugs under a set of conditions, then release when environmental conditions change, can be beneficial in drug delivery (Lopez et al., 2004; Zhang et al., 2006).

The current work concerns a novel topical drug delivery system involving a cross-linked poly(NIPAM-co-BA) nanogel loaded with a model permeant. The nanogel was prepared by the incorporation of BA co-monomer into a temperature-sensitive polyNIPAM network, as discussed in CHAPTER 2. PolyNIPAM polymer is well known to exhibit a thermo-responsive behaviour and unique feature of undergoing lattice collapse in water at 32 – 34°C, which is close to the human body temperature (~37°C). The BA co-monomer was included to enhance the sensitivity of the polyNIPAM particles towards changes in their environment by reducing its VPTT. This would trigger release of content from inside of the nanogel network into the surrounding medium (skin), resulting phase separation at a temperature range lower than 32 – 34°C. Such condition would result in a high concentration gradient in the skin which according to the Fick's first law of diffusion, would be expected to be followed by enhanced skin permeation (Williams, 2003).

To test the above hypothesis, MTX was selected as a model permeant for loading into the nanogel particles. To date, most of the studies related to topical delivery of MTX emphasise on the role of lipid vesicular systems (e.g. liposomes) or physical enhancement techniques (e.g. iontophoresis) (Alvarez-Figueroa et al., 2001; Trotta et al., 2004). Investigations related to the stimuli-responsive polymers as carriers for MTX were limited and revolved around a systemic delivery. For example,

biodegradable, pH-responsive chitosan based-nanogel particles have been examined as a mean to achieve targeted pH-mediated intracellular release for cancer therapeutics of MTX (Zhang et al., 2006).

MTX is a potent immunomodulating drug indicated as a second line treatment for severe psoriasis and currently, only oral forms are available with a weekly recommended dosage of between 10 – 25 mg. It is a structural analogue of folic acid (vitamin B₃), an important trace element necessary for DNA synthesis and cellular division. MTX acts by competitively inhibiting dihydrofolate reductase, the enzyme responsible for folic acid metabolism, thus selectively interfering with DNA synthesis in psoriatic epidermal cells and subsequently decreasing the epidermal cellular mitosis. Despite its efficacy, the use of MTX is greatly limited due to its systemic toxicity (e.g. hepatic toxicity, bone marrow suppression and nausea) and one way to limit the side effects is by formulating MTX into a topical product. The drug has been the subject of much research in this respect, although a product has yet to be marketed (Ali et al., 2008; Collins and Rogers, 1992; Eskicirak et al., 2006; Weinstein et al., 1981). One reason for generally poor clinical effect is insufficient percutaneous penetration of MTX to the basal layer of epidermis in order to exert its pharmacological action (McCullough et al., 1976). **Figure 3-1** shows chemical structure of MTX. It is hydrophilic in nature, has high molecular weight and commonly presents in the ionised form at a physiological pH (~pH 7.3 – 7.4), which largely contribute to its poor penetration.



Chemical Formula : C₂₀H₂₂N₈O₅ **cLog P** : -1.85

MW : 454.44 **pK_a** : 4.7

Figure 3-1: Chemical structure and physicochemical data for MTX.

Prostaglandin E₂ (PGE₂) is the major product of arachidonic acid metabolism by COX-2 in various tissues as shown in **Figure 3-2**. It is synthesised *de novo* and does not exist preformed in any cellular reservoir (Zulfakar et al., 2010). Increases in the levels of PGE₂ expression have been associated in the pathophysiology of many inflammatory diseases (e.g. psoriasis and rheumatoid arthritis) and cancer. In a study conducted to analyse the profiles of inflammatory mediators in normal, sensitive and diseased skin (psoriasis and eczema), PGE₂ level was reported to be increased by 4.7-fold in suctioned blister fluids of psoriatic and eczema skin compared to normal skin (Reilly et al., 2000). Thus, PGE₂ is a suitable biological marker to probe modulations within the inflammation process.

3.2.1 Materials

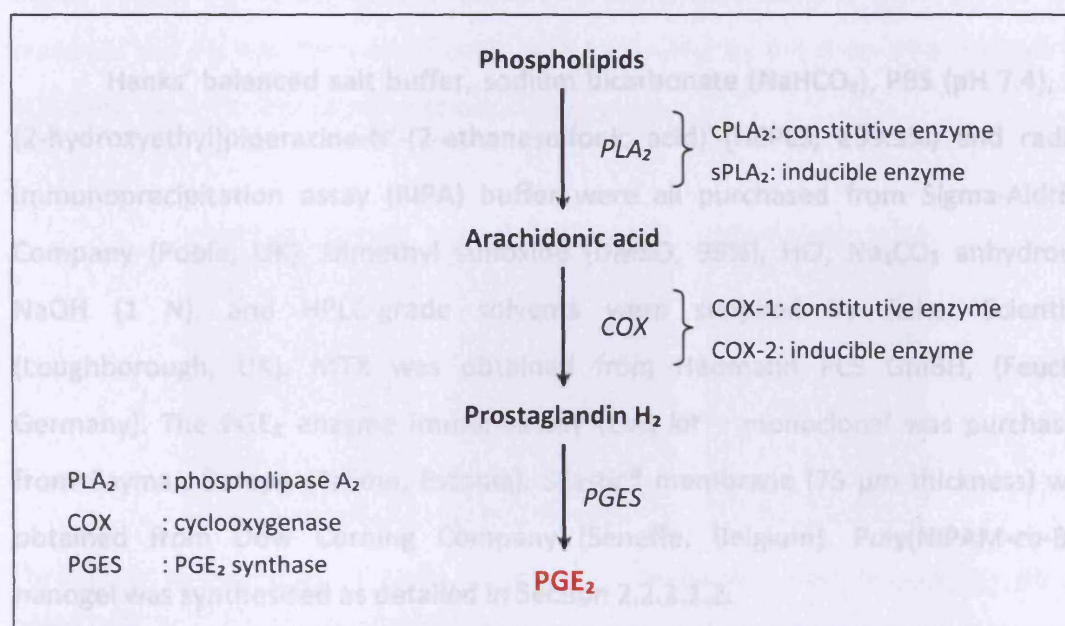


Figure 3-2: Scheme illustrating biosynthesis of PGE₂. Adapted from (Nakatani and Kudo, 2002).

A recent observation suggested that the addition of a base (triethylamine) to the poly(NIPAM-co-BA) nanogel produced large enhancements of the topical delivery of naproxen across skin (Yurdasiper et al., 2008). However, the use of triethylamine was found to be unsuitable due to it being highly pro-inflammatory (Ness, 1994; Yurdasiper et al., 2008). In the current study, poly(NIPAM-co-BA) nanogel particles were loaded with MTX. The delivery of MTX was then determined

from the nanogel applied onto heat-separated porcine epidermal membranes *in vitro*, and the effect of base sodium carbonate (Na_2CO_3) determined – Na_2CO_3 is widely used in the cosmetic industry as a pH regulator, and is certified as safe for use by the Cosmetic Ingredient Review (CIR) Expert Panel (Cosmetic Ingredient Review, 2010). Similar treatments were applied to Silastic® and *ex vivo* porcine skin membranes, where the skin was assayed for the key inflammation mediator, PGE_2 .

3.2 MATERIALS AND METHODS

3.2.1 Materials

Hanks' balanced salt buffer, sodium bicarbonate (NaHCO_3), PBS (pH 7.4), *N*-(2-hydroxyethyl)piperazine-*N'*-(2-ethanesulfonic acid) (HEPES, $\geq 99.5\%$) and radio-immunoprecipitation assay (RIPA) buffer were all purchased from Sigma-Aldrich Company (Poole, UK). Dimethyl sulfoxide (DMSO, 99%), HCl, Na_2CO_3 anhydrous, NaOH (1 N), and HPLC-grade solvents were supplied by Fisher Scientific (Loughborough, UK). MTX was obtained from Heumann PCS GmbH, (Feucht, Germany). The PGE_2 enzyme immunoassay (EIA) kit – monoclonal was purchased from Cayman Europe (Tallinn, Estonia). Silastic® membrane (75 μm thickness) was obtained from Dow Corning Company (Seneffe, Belgium). Poly(NIPAM-co-BA) nanogel was synthesised as detailed in Section 2.2.2.1.2.

Freshly excised porcine ears were obtained from a local abattoir prior to steam cleaning and immersed in iced HEPES-buffered Hanks' balanced salt (HBHBS) solution upon excision. The solution was made up of Hanks' balanced salt buffer (9.7 g), HEPES (6 mg), and NaHCO_3 (0.35 g) in 1 L de-ionised water to facilitate extended skin viability; thus maintaining skin metabolism activities during transportation from the abattoir to the laboratory. The skin was used within 3 h of slaughter.

3.2.2 Methods

3.2.2.1 Preparation of MTX-loaded Poly(NIPAM-co-BA) Nanogel

To enable high MTX loading into the nanogel particles, it was important that MTX was in a solution form at high concentration, although MTX is generally known to be poorly soluble across a range of regular solvents. Various solvents were examined including DMSO, to poor effect. However, by trial and error, a dissolution method for MTX was developed in-house. First, MTX was suspended in de-ionised water and the pH adjusted by the drop-wise addition of 1 N NaOH, monitored by the digital PH209 Bench pH meter. The yellow suspension clarified once pH 12 was reached, the pH was then readjusted back to neutral by the drop-wise addition of HCl, with the MTX remaining in solution ([Figure 3-3](#)).



Figure 3-3: Solubilisation of MTX – (A) MTX in de-ionised water followed by (B) pH adjustment to 12 (C) then to neutral.

MTX was physically entrapped in blank poly(NIPAM-co-BA) particles using an encapsulation method in which the nanogel particles were in a swollen state when put into contact with the material to be loaded (further discussion regarding nanogel loading in CHAPTER 6). The MTX solution was added to the purified unloaded nanogel in equal volumes (1:1) and placed in an ultrasonic bath (Sonicor Inc., Wallingford, CT) for 1 h, before being left for 24 h at RT, light protected on the SB1 Stuart® blood tube rotator. The mixture was then centrifuged (Beckman Coulter

Avanti® J-25, 30,000 x g for 1 h at 15°C) and a yellow-coloured sediment product was isolated, with the decanted supernatant a noticeably lighter shade of yellow relative to the concentrated solution prior to the loading step, indicating that the nanogel had successfully absorbed MTX (**Figure 3-4**). To determine the amount of MTX loaded into the nanogel, the supernatant obtained after centrifugation was assayed by an HPLC system and determine based on Equation 3-1. The difference in the average MTX concentration between the original solution (7.40 mg mL⁻¹) and the supernatant (5.04 mg mL⁻¹) was taken to be the amount loaded into the nanogel, i.e. 2.36 mg mL⁻¹. Since 2 mL of MTX was added to 2 g of the swollen nanogel, the amount of MTX entrapped in the nanoparticles was 2.36 mg g⁻¹, providing an entrapment efficiency (EE) of 31.9%.

$$EE (\%) = \frac{C_{total} - C_{out}}{C_{total}} \times 100$$

Equation 3-1

- EE (%) : Percentage encapsulation efficiency of a compound inside the nanogel
- C_{total} : Total concentration of the compound presents inside and outside of the nanogel
- C_{out} : Concentration of the compound presents in the outside of the nanogel

The MTX-loaded poly(NIPAM-co-BA) nanogel displayed a bright yellow colour at RT, and when its environment temperature increased to 32°C, the colour of the gel changed from yellow to almost white, indicating the release of MTX into its surrounding medium as shown in **Figure 3-5**. When the temperature was decreased to 2 – 4°C, the gel restored its colour.

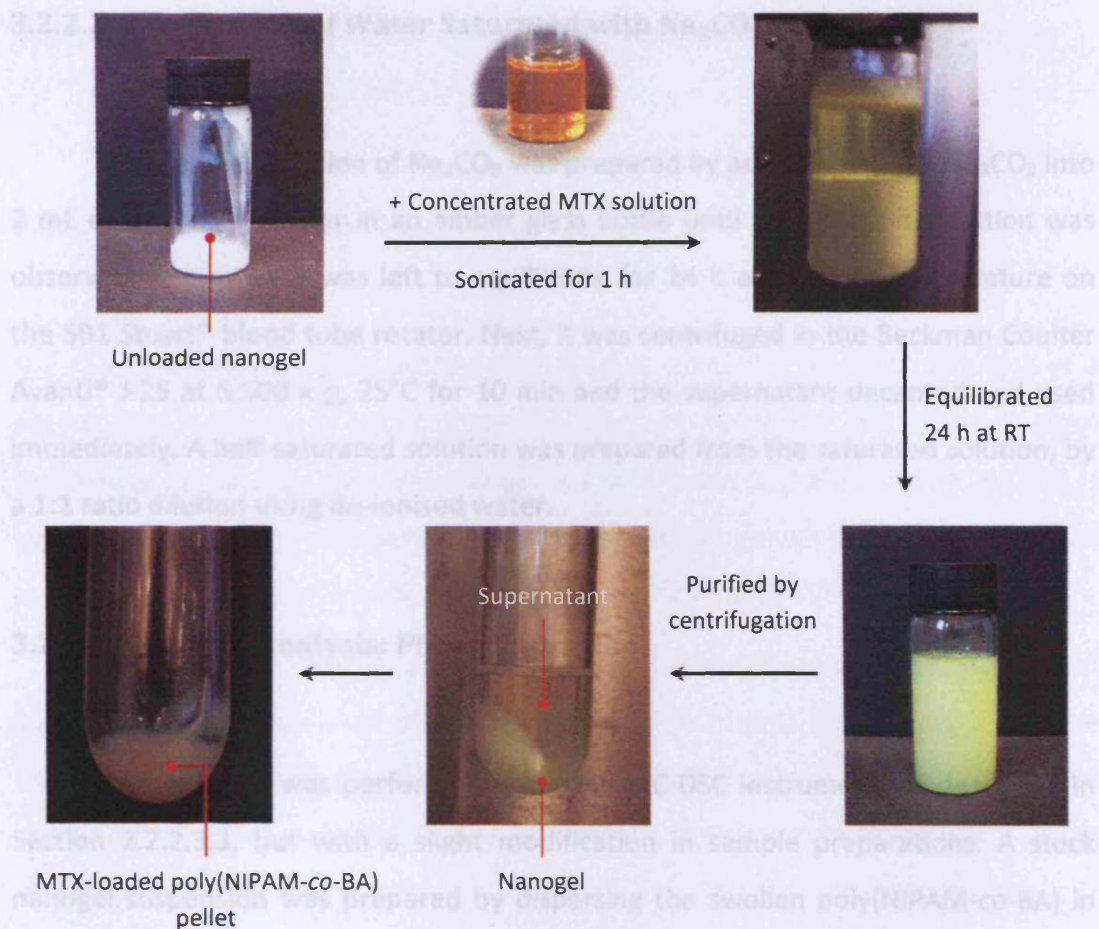


Figure 3-4: Preparation of MTX-loaded poly(NIPAM-co-BA) nanogel.

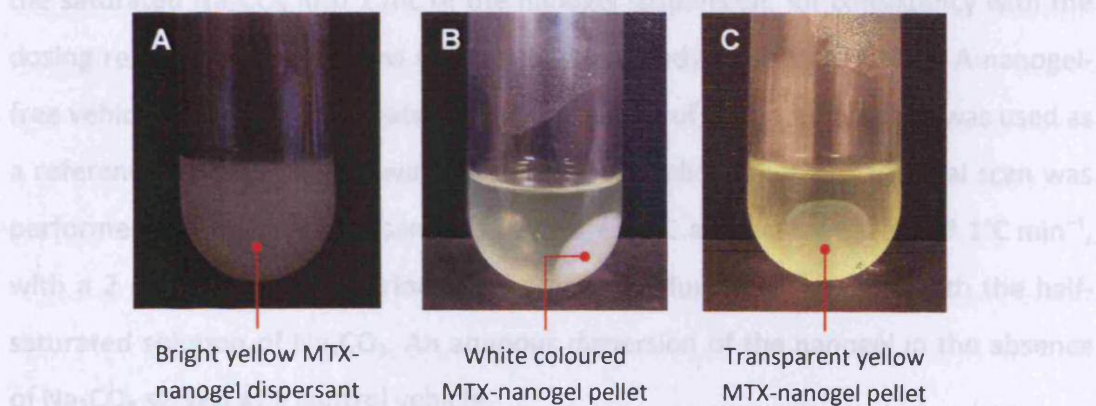


Figure 3-5: MTX-loaded poly(NIPAM-co-BA) nanogel maintained at different temperatures – (A) RT (25°C); (B) 32°C; and (C) 2 – 4°C.

3.2.2.2 Preparation of Water Saturated with Na₂CO₃

A saturated solution of Na₂CO₃ was prepared by adding excess of Na₂CO₃ into 2 mL of de-ionised water in an amber glass bottle until no further dissolution was observed. The mixture was left to equilibrate for 24 h at ambient temperature on the SB1 Stuart® blood tube rotator. Next, it was centrifuged in the Beckman Coulter Avanti® J-25 at 5,500 x g, 25°C for 10 min and the supernatant decanted and used immediately. A half-saturated solution was prepared from the saturated solution, by a 1:1 ratio dilution using de-ionised water.

3.2.2.3 Thermal Analysis: Phase Transition

DSC analysis was performed using the MC-DSC instrument, as described in Section 2.2.2.3.3, but with a slight modification in sample preparations. A stock nanogel suspension was prepared by dispersing the swollen poly(NIPAM-co-BA) in de-ionised water, at a concentration of 50% w/v. The pH regulator, Na₂CO₃, was prepared in two concentrations – saturated and half-saturated aqueous solutions. The samples for MC-DSC analysis were prepared by adding approximately 25 µL of the saturated Na₂CO₃ into 1 mL of the nanogel suspension, for consistency with the dosing regimen of the *in vitro* skin permeation study in Section 3.2.2.5. A nanogel-free vehicle (i.e. de-ionised water with the addition of saturated Na₂CO₃) was used as a reference and the sample was determined in triplicate (n=3). A thermal scan was performed on the hydrated samples from 4 – 60°C at a scanning rate of 1°C min⁻¹, with a 2 min equilibrium period. The same procedure was repeated with the half-saturated solution of Na₂CO₃. An aqueous dispersion of the nanogel in the absence of Na₂CO₃ served as a control vehicle.

3.2.2.4 Test Membranes: Porcine Full-thickness, Heat-separated Porcine Epidermis and Silastic®

3.2.2.4.1 Heat-separated Porcine Epidermis

In the current study, porcine ear skin was used. The skin from this area of a pig has been validated to be a comparable substitute for human skin due to its close similarities in the anatomy, physiology and biochemistry (Lademann et al., 2011; Vardaxis et al., 1997), with permeability values close to that of the human skin (Dick and Scott, 1992; Schmook et al., 2001; Simon and Maibach, 2000).

One of the criteria for a topical product to offer effective dermatological and cosmetic applications is its ability to penetrate the intact SC of skin. Thus, the appropriate membrane model for drug delivery is a heat-separated epidermis (SC along with attached viable epidermis). In addition, the site of action of MTX is in the viable epidermis.

Heat-separated epidermal membranes are an established model (Williams, 2003). Such membranes have been used in many research laboratories to model *in vitro* skin permeation and penetration (Contri et al., 2011; Goldovsky et al., 2006; Mahalingam et al., 2008). However, it is worth noting there are several potential limitations to the use of this type of membrane. For example, there may be loss of hair follicles from the epidermal membrane following the separation process, where hair follicles are left on the separated dermis. This could result in uneven distribution of hair follicles within the membrane. Moreover, the technique may also create holes on the heat-separated epidermal membrane, thus providing an accessible route for any particles or exogenous molecules across the membrane, bypassing the SC. Such pitfalls generally arise from erroneous preparation and microscopic examination prior to use is therefore essential. Apart than that, the process of heat-separation may cause modulation within the skin barrier function including thermal leaching of lipids from the SC (Contri et al., 2011; Heard and Screen, 2008). These limitations may affect the final permeation/penetration data.

The membranes were prepared by an established technique (Kligman and Christophers, 1963) – the porcine ears were firstly cleaned thoroughly under cold running water, and then the full thickness skin was excised from the dorsal side by blunt dissection using a scalpel. Any hairs were trimmed as short as possible using a pair of electric clippers prior to being cut into sections of 3 × 3 cm, then immersed in water heated to ~60°C for 1 min. The epidermal membrane was then gently liberated from the underlying dermis with the aid of forceps and examined by a magnifying lens to check for any physical damage. These were then floated onto aluminium foil and dried gently using soft tissues.

3.2.2.4.2 Silastic® Membrane

In this study, Silastic® membrane served as a non-porous model membrane (Houk and Guy, 1988). The Silastic® sheet was washed under running de-ionised water before being cut into 3 x 3 cm sections and soaked in a fresh PBS solution (receptor phase) overnight.

3.2.2.4.3 Porcine Full-thickness Skin

For the bioassay of PGE₂, full-thickness skin membranes were used in order to retain skin viability, with the membranes continually bathed in iced HBHBS solution until use. The porcine ear skin was processed as described above (Section 3.2.2.4.1) prior to being cut into sections of 2 × 2 cm, with care taken to choose the areas of the ear which were free from scarring or other noticeable defects which can compromise barrier integrity or provide resistance to permeating compounds. The full thickness membranes were immediately immersed in iced HBHBS solution prior to mounting on diffusion cells.

3.2.2.5 *In vitro* Permeation Study

The glass Franz-type diffusion cell is an established tool for determining *in vitro* skin permeation (Williams, 2003). It is comprised of two compartments as shown in **Figure 3-6**:

- (i) The donor (upper chamber) – for application of the permeant/sample and
- (ii) The receptor (lower chamber) of a fixed volume – contains drug sink, and is fitted with a sampling arm to allow receptor fluid to be collected.

The diffusional area and receptor phase volume of each cell were measured carefully (0.95 cm² nominal diffusional area and 4.3 mL receptor phase volume) and later to be used for quantitative analysis of the parameters concerning the permeated material through the skin.

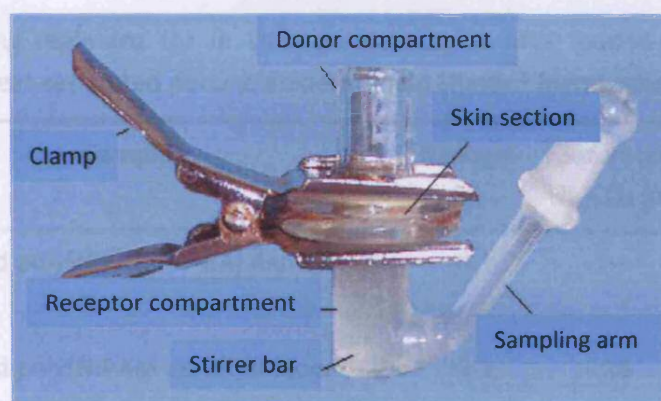


Figure 3-6: A typical glass Franz-type diffusion cell.

The porcine epidermis or Silastic® membrane was mounted onto a pre-greased receptor compartment of scrupulously clean diffusion cell with the SC side of the epidermal membrane facing upwards. Pinch clamp was affixed and the receptor compartment filled with temperature-equilibrated (~32°C), degassed PBS (receptor phase) using a syringe. PBS provided an adequate sink for MTX. Care was exercised to avoid any air bubbles trapped between the underside of the membrane and de-ionised water, by inverting the receptor chamber while filling in the

compartment. A micro magnetic stirrer bar was added and the complete assembly placed on a submersible magnetic stirring plate (Variomag, Daytona Beach, FL) set up in a thermostatically controlled water bath (Fisher Scientific, Loughborough, UK), maintained at $\sim 37^{\circ}\text{C}$ (the core temperature *in vivo*), providing a skin surface temperature of $\sim 32^{\circ}\text{C}$.

After 15 min, a finite dose of nanogel was applied to the surface of the skin using a blunt glass rod which was dipped momentarily into the MTX-loaded poly(NIPAM-co-BA) and then massaged gently onto the membrane (20 circular motions) to ensure uniform distribution without tearing the skin. Refining this method, the approximate weight of nanogel dosed was found to be consistently ~ 0.1 g. Both the sampling arm and donor compartments were occluded with Parafilm™ to minimise contamination and prevent evaporation, which cause changes in concentration of the samples. Three dosing procedures were used, as listed in **Table 3-1**.

Table 3-1: Dosing regimens for *in vitro* permeation of MTX loaded-poly(NIPAM-co-BA) nanogel across heat-separated porcine epidermal and Silastic® membranes ($n \geq 3$).

	Sample	Nanogel (g)	Saturated Na_2CO_3 (μL)	Half-saturated Na_2CO_3 (μL)
(i)	MTX-loaded poly(NIPAM-co-BA) nanogel alone	~ 0.1	–	–
(ii)	MTX-loaded poly(NIPAM-co-BA) nanogel, followed by saturated aqueous solution of Na_2CO_3	~ 0.1	25	–
(iii)	MTX-loaded poly(NIPAM-co-BA) nanogel, followed by half-saturated aqueous solution of Na_2CO_3 (not Silastic® membrane)	~ 0.1	–	25

Three replicates were prepared for each dosing regimen ($n \geq 3$). Sampling was carried out over a period of 12 h with the entire receptor phase being removed using a Pasteur pipette and replaced with fresh, pre-warmed PBS ($\sim 32^{\circ}\text{C}$). Each cell had a

dedicated pipette to avoid cross-contamination. A 1 mL sample of the removed receptor solution was retained for quantitative analysis.

3.2.2.5.1 *In vitro* Skin Permeation

3.2.2.5.1 HPLC Analysis

MTX in the receptor phase samples was analysed by reversed-phase liquid chromatography using an Agilent 1100 series automated system with Agilent ChemStation software. The HPLC method was developed in-house: Luna[®] C₁₈ ODS 150 × 4.6 mm, 5 μm column (Phenomenex Inc., Macclesfield, UK), mobile phase of 3:1 potassium phosphate buffer (0.1 M, pH 6.5)/methanol over 15 min with a flow rate set at 1 mL min⁻¹. Sample injection volume was 20 μL and detection was by UV at λ = 305 nm, with a resultant MTX retention time of ~8 min as shown in **Figure 3-7**. For calibration, a stock solution of MTX (500 μg mL⁻¹) was prepared in PBS and a standard calibration curve obtained over the range of 4 - 500 μg mL⁻¹. Excellent linearity was achieved as evidenced by *R*² of 1.000, with a limit of detection (LOD) of 7.27 ng mL⁻¹.

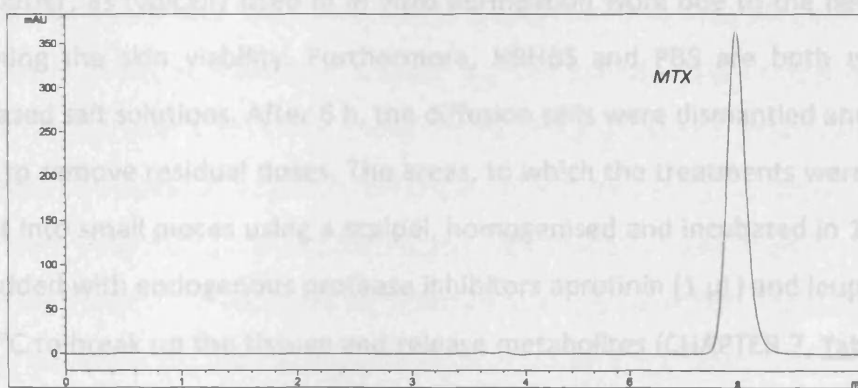


Figure 3-7: HPLC chromatogram for MTX dissolved in PBS.

3.2.2.6 Determination of PGE₂ in Porcine Skin *Ex vivo*

3.2.2.6.1 *In vitro* Skin Permeation

MTX is known to be anti-inflammatory and one way of observing this effect is by determining modulation in levels of the inflammatory marker, PGE₂ (Zulfakar et al., 2010). Meanwhile, this bioassay can also indirectly indicate the extent of MTX delivery into the skin, as any reduction in PGE₂ level must be a consequence of MTX activity on the keratinocytes. For the bioassay for PGE₂, full thickness skin membranes were used. To facilitate extended skin viability, and thus maintaining skin metabolism and any arachidonic acid activities, the freshly excised porcine ears were immersed in iced HBHBS solution during transportation from the abattoir to the laboratory – the skin was used within 3 h of slaughter. The full thickness skin was cut into approximately 2 × 2 cm sections and placed in HBHBS solution, then mounted into Franz diffusion cells, as described in Section 3.2.2.5. The skin was dosed in triplicate (n=3) according to dosing types in [Table 3-2](#).

For this study, degassed HBHBS was selected as the receptor phase instead of PBS buffer, as typically used in *in vitro* permeation work due to the necessity of maintaining the skin viability. Furthermore, HBHBS and PBS are both essentially water based salt solutions. After 6 h, the diffusion cells were dismantled and the skin washed to remove residual doses. The areas, to which the treatments were applied, were cut into small pieces using a scalpel, homogenised and incubated in 1 mL RIPA buffer added with endogenous protease inhibitors aprotinin (1 µL) and leupeptin (10 µL) at 4°C to break up the tissues and release metabolites (CHAPTER 7, [Table 7-3](#) for inhibitors preparation). The samples were then centrifuged at 14,000 rpm, 4°C for 15 min in a Heraeus Multifuge 3 S-R centrifuge (Beckman Coulter Inc., Fullerton, CA) twice and the resulting supernatant kept frozen at -20°C prior to enzyme immunoassay (EIA).

Table 3-2: Dosing regimens for *in vitro* permeation of MTX loaded-poly(NIPAM-co-BA) nanogel across porcine full-thickness skin (n=3).

	Sample	Nanogel (g)	Saturated Na ₂ CO ₃ (μL)	Half-saturated Na ₂ CO ₃ (μL)
(i)	MTX-loaded poly(NIPAM-co-BA) nanogel alone	~0.1	–	–
(ii)	MTX-loaded poly(NIPAM-co-BA) nanogel, followed by saturated aqueous solution of Na ₂ CO ₃	~0.1	25	–
(iii)	Saturated aqueous solution of Na ₂ CO ₃ alone (base control)	–	20	–
(iv)	20 μL de-ionised water alone (control)	–	–	–

3.2.2.6.2 EIA

PGE₂ levels were determined using the EIA kit in accordance with the instructions supplied by the manufacturer. The EIA is based on the competition between a constant amount of tracer molecules (PGE₂ linked to acetylcholinesterase) and free PGE₂ in a sample for a limited amount of PGE₂ monoclonal antibody as illustrated in [Figure 3-8](#). The amount of the tracer molecules bound to the antibody is inversely proportional to the amount of free PGE₂ present in the sample. Incubated together overnight at 4°C, the PGE₂- or tracer-antibody complex then bound to IgG pre-coated in the well. The plate was washed to remove any unbound reagents followed by the addition of a reagent containing the substrate for acetylcholinesterase into the well and incubated for 1 h at ambient temperature with gentle shaking. The enzymatic reaction produced a distinct yellow substance which absorbs strongly at 412 nm. Using a Sunrise™ spectrophotometric plate reader (Tecan UK Ltd., Reading, UK), the intensity of the colour is proportional to the amount of the bound tracer complex.

3.3 RESULTS AND DISCUSSION

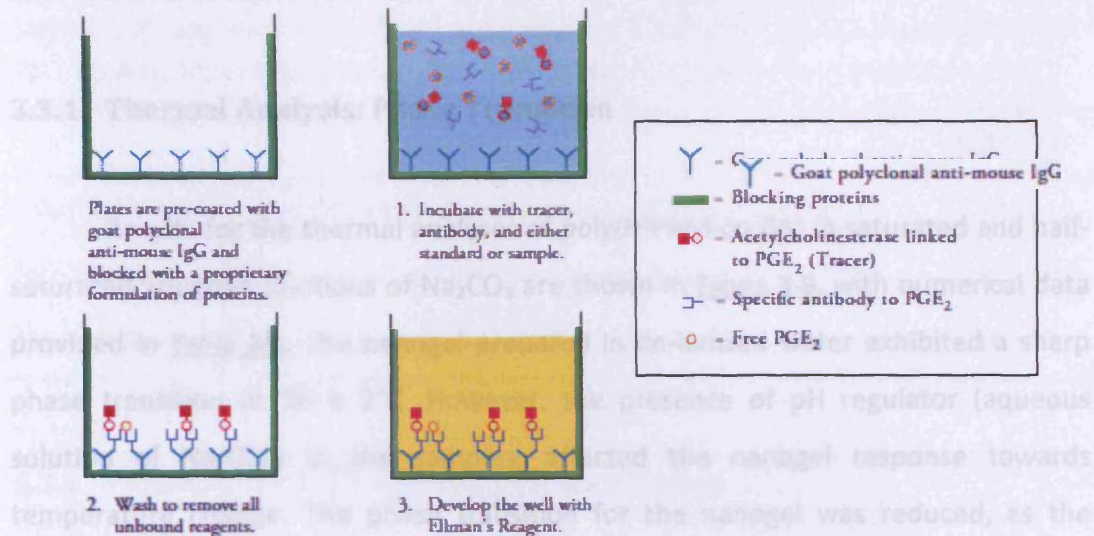


Figure 3-8: Schematic of EIA for detection of PGE₂. Adapted from (Cayman Chemical Company, 2011).

3.2.2.7 Data and Statistical Analysis

Cumulative amounts of MTX permeated per unit area ($\mu\text{g cm}^{-2}$) were plotted against time (h), with lag time and steady state flux (J_{SS}) were determined by standard methods – the flux (J) was calculated from the slope in the linear region (steady state) of the plot and the lag time was determined from the x-intercept of the linear portion of the above plot. The data were analysed using Excel 2007 (Microsoft Office, Microsoft Corp., Redmond, WA) and presented in the text as a mean \pm SD. The MTX delivery and PGE₂ modulation data were analysed statistically using an unpaired, two-tailed Student's *t*-test with Welch correction. The test was conducted using InStat® for Macintosh, version 3.00 (GraphPad Software Inc., San Diego, CA). Confidence interval was set at 95% and $p < 0.05$ was defined as statistically significant.

Figure 3-9: MC-OSC thermograms for aqueous dispersions of poly(NIPAM-co-BA) nanogel in the presence of saturated and half-saturated aqueous solutions of Na₂CO₃. Aqueous dispersion of Na₂CO₃-free poly(NIPAM-co-BA) nanogel served as control.

3.3 RESULTS AND DISCUSSION

3.3.1 Thermal Analysis: Phase Transition

Results for the thermal analyses of poly(NIPAM-co-BA) in saturated and half-saturated aqueous solutions of Na_2CO_3 are shown in **Figure 3-9**, with numerical data provided in **Table 3-3**. The nanogel prepared in de-ionised water exhibited a sharp phase transition at $36 \pm 2^\circ\text{C}$. However, the presence of pH regulator (aqueous solution of Na_2CO_3) in the samples, affected the nanogel response towards temperature change. The phase transition for the nanogel was reduced, as the concentration of the pH regulator increased from a half-saturated solution to a saturated solution. The endothermic peak was narrow and apparent for the sample containing no Na_2CO_3 , but then became small and broad for the sample containing half-saturated Na_2CO_3 , and essentially disappeared in the presence of saturated Na_2CO_3 . This phenomenon may be due to Na_2CO_3 , which was essentially an impurity in the samples and thus causing a reduction in the transition temperature. For the saturated Na_2CO_3 sample, it is possible that the transition shifted to below the experiment starting temperature (4°C). This is suggested by the dip at the lower end of the temperature range.

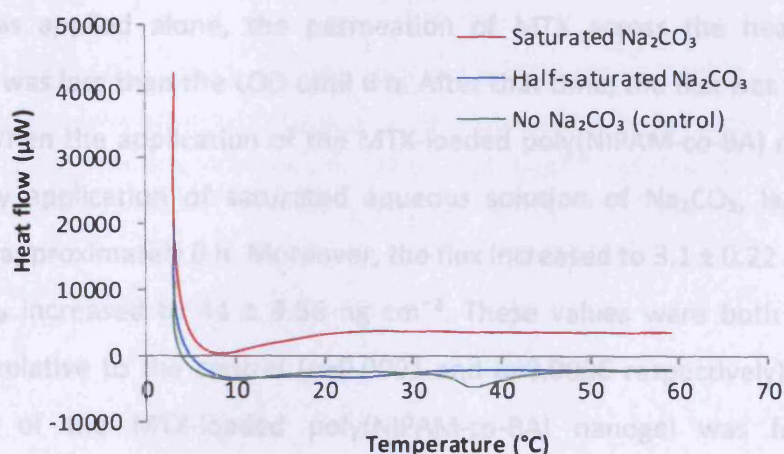


Figure 3-9: MC-DSC thermograms for aqueous dispersions of poly(NIPAM-co-BA) nanogel in the presence of saturated and half-saturated aqueous solutions of Na_2CO_3 . Aqueous dispersion of Na_2CO_3 -free poly(NIPAM-co-BA) nanogel served as control.

Table 3-3: Phase transitions of aqueous dispersions of poly(NIPAM-co-BA) nanogel in the presence of saturated and half-saturated aqueous solutions of Na₂CO₃ measured by MC-DSC; Aqueous dispersion of Na₂CO₃-free poly(NIPAM-co-BA) served as control (n=3 ± SD).

Sample	LCST (°C)
Poly(NIPAM-co-BA) , followed by saturated aqueous solution of Na ₂ CO ₃	<4°C
Poly(NIPAM-co-BA), followed by half-saturated aqueous solution of Na ₂ CO ₃	23 ± 1 x 10 ⁻⁵
Poly(NIPAM-co-BA) (control) – absence of Na ₂ CO ₃	36 ± 2

3.3.2 Permeation of MTX across Test Membranes

3.3.2.1 Silastic® Membrane

No MTX was detected in the receptor phases over the 12 h period, regardless of the absence or presence of Na₂CO₃ solution in the treatment regimens.

3.3.2.2 Heat-separated Porcine Epidermal Membrane

Figure 3-10 and **Table 3-4** show that, when the MTX-loaded poly(NIPAM-co-BA) nanogel was applied alone, the permeation of MTX across the heat-separated membrane was less than the LOD until 6 h. After that time, the flux was 1.4 ± 0.3 ng cm⁻² h⁻¹. When the application of the MTX-loaded poly(NIPAM-co-BA) nanogel was followed by application of saturated aqueous solution of Na₂CO₃, lag time was reduced to approximately 0 h. Moreover, the flux increased to 3.1 ± 0.22 ng cm⁻² h⁻¹, and the Q₂ increased to 44 ± 9.56 ng cm⁻². These values were both statistically significant relative to the control (p=0.0001 and p=0.0006 respectively). When the application of the MTX-loaded poly(NIPAM-co-BA) nanogel was followed by application of half-saturated aqueous solution of Na₂CO₃, lag time was again reduced to approaching 0 h. The flux was 2.6 ± 0.22 ng cm⁻² h⁻¹, and the Q₂ was 37 ± 2.14 ng cm⁻². Again, both values were statistically different to the control (p=0.007 and

$p=0.0001$ respectively), although statistically no difference in comparison to the fully saturated Na_2CO_3 .

The MTX-loaded poly(NIPAM-co-BA) nanogel alone was capable of delivering the drug, albeit with a relatively long lag/breakthrough time. However, for many therapeutic indications, a low lag time value is desirable in order to accelerate the onset of therapeutic activity. This was achieved by the co-administration of Na_2CO_3 , which both increased flux and virtually eliminated breakthrough/lag time. As half- and fully saturated Na_2CO_3 both gave the same results, the enhancement process appears to be saturable.

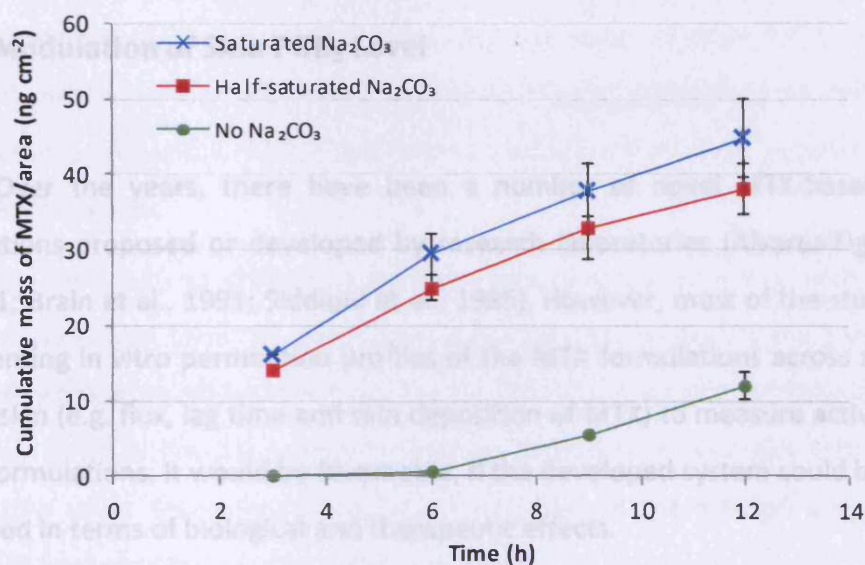


Figure 3-10: Permeation profiles of MTX from loaded poly(NIPAM-co-BA) nanogel across heat-separated porcine epidermis: No Na_2CO_3 – no added Na_2CO_3 ; saturated Na_2CO_3 – skin dosed with 25 μL saturated aqueous solution of Na_2CO_3 ; and half-saturated Na_2CO_3 – skin dosed with 25 μL half-saturated aqueous solution of Na_2CO_3 ($n \geq 3$, \pm SD).

Table 3-4: Lag time, steady state flux (J_{ss}) and cumulative permeation after 12 h (Q_{12}) data for MTX across heat-separated porcine epidermal membranes ($n \geq 3$, \pm SD).

Dosing Regimen	Lag Time (h)	J_{ss} ($\text{ng cm}^{-2} \text{h}^{-1}$)	Q_{12} (ng cm^{-2})
MTX-loaded poly(NIPAM-co-BA) nanogel	6	1.4 ± 0.30	12.0 ± 1.60
MTX-loaded poly(NIPAM-co-BA) nanogel, followed by 25 μL saturated aqueous solution of Na_2CO_3	~ 0	3.1 ± 0.22	44.0 ± 9.56
MTX-loaded poly(NIPAM-co-BA) nanogel, followed by 25 μL half-saturated aqueous solution of Na_2CO_3	~ 0	2.6 ± 0.22	37.0 ± 2.14

3.3.3 Modulation of Skin PGE_2 Level

Over the years, there have been a number of novel MTX-based topical formulations proposed or developed by research laboratories (Alvarez-Figueroa et al., 2001; Brain et al., 1991; Siddiqui et al., 1985). However, most of the studies only documenting in vitro permeation profiles of the MTX formulations across animal or human skin (e.g. flux, lag time and skin deposition of MTX) to measure activity levels of the formulations. It would be favourable, if the developed system could be further translated in terms of biological and therapeutic effects.

To probe the efficacy of nanogel-mediated dermal delivery of MTX in the absence and presence of a base (Na_2CO_3); it was decided to examine levels of the inflammation marker PGE_2 . Enhanced delivery of MTX to skin would be expected to be reflected in suppressed prostaglandin levels due to down-regulation of COX-2. Although principally a dihydrofolate reductase inhibitor (MTX) has anti-inflammatory properties, in the current model, enhanced bioavailability in the viable epidermis would be expected to lead to increased uptake by keratinocytes and thus, reduced production of PGE_2 .

Figure 3-11 shows that when dosed with a saturated solution of Na_2CO_3 , the amount of PGE_2 found in the skin was 3.93 ng – virtually the same level (3.90 ng) was

found following the application of water. This was very encouraging, as it demonstrated that Na_2CO_3 does not exert a pro-inflammatory effect. When the skin was dosed with MTX-loaded poly(NIPAM-co-BA) nanogel, a significant reduction (33%) in PGE_2 was observed ($p=0.0154$). Furthermore, when the skin was dosed with MTX-loaded poly(NIPAM-co-BA) nanogel and followed by Na_2CO_3 solution, the reduction was even greater, by 60% relative to the water control ($p=0.0012$). The effect on the PGE_2 levels of the added Na_2CO_3 compared to none was also significant (-57%) ($p=0.0052$).

Figure 3-11(A) supports the delivery data in Section 3.3.2.2 and demonstrates that the MTX-loaded poly(NIPAM-co-BA) nanogel was able to deliver the drug to the keratinocytes of the viable epidermis, as evidenced by the large reduction in PGE_2 present relative to the controls. However, the even greater (60%) reduction observed when Na_2CO_3 was co-administered [**Figure 3-11(B)**] again reflects the transport data of Section 3.3.2.2, but with the additional proof of enhanced uptake by the keratinocytes.

As there was no difference between skin membranes dosed with water of saturated Na_2CO_3 in terms of PGE_2 levels, it can be concluded that this solution had no pro-inflammatory effect when applied to skin. The probable explanation is that the highly polar of Na_2CO_3 molecules did not penetrate appreciably into the skin. This further infers that whatever effect Na_2CO_3 had on the nanogel and MTX, the process did not occur within the viable epidermis.

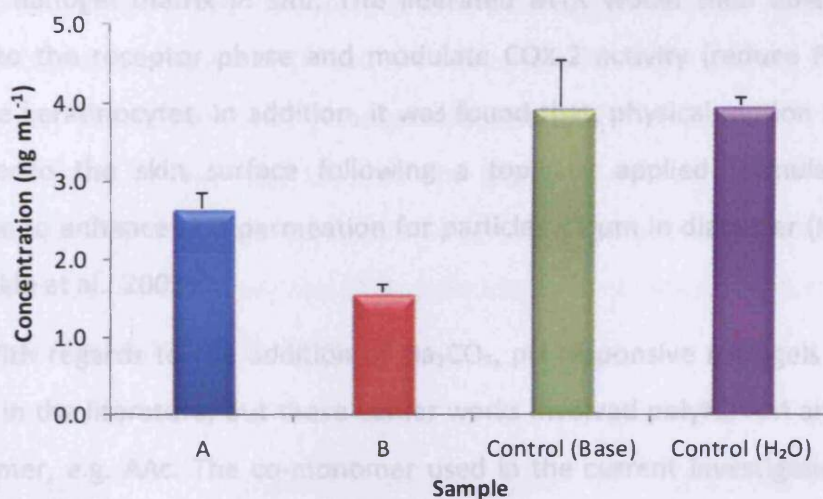


Figure 3-11: Bar chart comparing concentrations of PGE₂ (ng mL⁻¹) from different treatment groups, (n=3, ± SD). Skin dosed with: A – MTX-loaded poly(NIPAM-co-BA) nanogel alone; B – MTX-loaded poly(NIPAM-co-BA) nanogel, followed by 25 μL saturated aqueous solution of Na₂CO₃; control (base) – 25 μL saturated aqueous solution of Na₂CO₃ alone; and control (H₂O) – de-ionised water alone. $p < 0.0001$ between treatments

3.3.4 Proposed Mechanism

In establishing the delivery mechanism behind the observed data, there are two key facts. Firstly, the delivery and biological activity of MTX were both enhanced following the addition of Na₂CO₃ solution. Secondly, permeation of MTX and reduction of PGE₂ was observed even without the addition of Na₂CO₃.

Dealing with the second point first, nanogel particles might possibly migrate into skin as discussed in CHAPTER 5, hence their use in the current work. By use of a glass rod, the nanogels were massaged into the skin and, assuming the migration process was rapid, the nanogel would have experienced a significant increase in temperature once within the skin (RT → 32°C). As we know from **Figure 2-11**, this would have been accompanied by a 7% decreased in particle diameter. Further reduction would be expected while the particles possibly migrate through the skin, as 32°C represents only the skin surface temperature not the interior region. The temperature is expected to rise, as we advance from the skin surface to the interior part of the human body (32°C < T ≤ 37°C). Such de-swelling would act to expel MTX

from the nanogel matrix *in situ*. The liberated MTX would then be able to diffuse through to the receptor phase and modulate COX-2 activity (reduce PGE₂ levels) within the keratinocytes. In addition, it was found that, physical motion as massage applied onto the skin surface following a topically applied formulation could contribute to enhance skin permeation for particles <1 µm in diameter (Knorr et al., 2009; Tinkle et al., 2003).

With regards to the addition of Na₂CO₃, pH responsive nanogels have been reported in the literature, but these earlier works involved polyNIPAM and the ionic co-monomer, e.g. AAc. The co-monomer used in the current investigation was BA, and the resulting nanogel demonstrated a lack of pH sensitivity, therefore the enhancement observed following the addition of the Na₂CO₃ could not have involved pH-mediated particle size modulation. One potential explanation is that the increased pH, due to the addition of Na₂CO₃, facilitated the *in situ* solubilisation of the MTX (Section 3.2.2.1) and dissolution from within the nanoparticles already deposited within the skin. This would indicate localisation beyond the SC, i.e. within the more hydrophilic viable epidermis. As a result, MTX molecules were able to diffuse more freely from the nanogel matrix, further increasing the concentration gradient, hence also increasing flux and biological activity.

Silastic® membrane is a relatively simple matrix, lacking the complex architecture and biological activity of skin (Galaev and Mattiasson, 2007). Undetectable levels of permeated MTX could reflect low permeability of the drug across this membrane. Alternatively, it could have been due to MTX nanoparticles failing to penetrate into the membrane, unlike skin where MTX was released *in situ*. Overall, the proposed mechanism can be summarised as in [Figure 3-12](#). Solubilisation of MTX by the Na₂CO₃ and release from the nanogel particles must have involved ionisation of carboxylic acid groups. The fluxes of ionised compounds are generally known to be low through the SC due to its lipophilic nature, which suggests that the nanogel particles possibly migrated as far as the viable epidermis, which has a far more polar nature and therefore more conducive to the diffusion of ionised MTX. According to one of our studies (CHAPTER 5), it was shown that polyNIPAM-based nanoparticles are possibly able to penetrate the skin and migrate across the

epidermis following dosing. The poly(NIPAM-co-BA) particles were found to have a mean hydrodynamic diameter of 432 ± 4 nm at ambient temperature, which were comparatively smaller than the nanogels utilised in the study (550 – 650 nm in diameters). Thus, it may suggest that the particles of poly(NIPAM-co-BA) had possibly permeated the SC to liberate its effect. The notion is further supported by both the current MTX delivery and PGE₂ modulation data. However, further studies are required to support the findings.

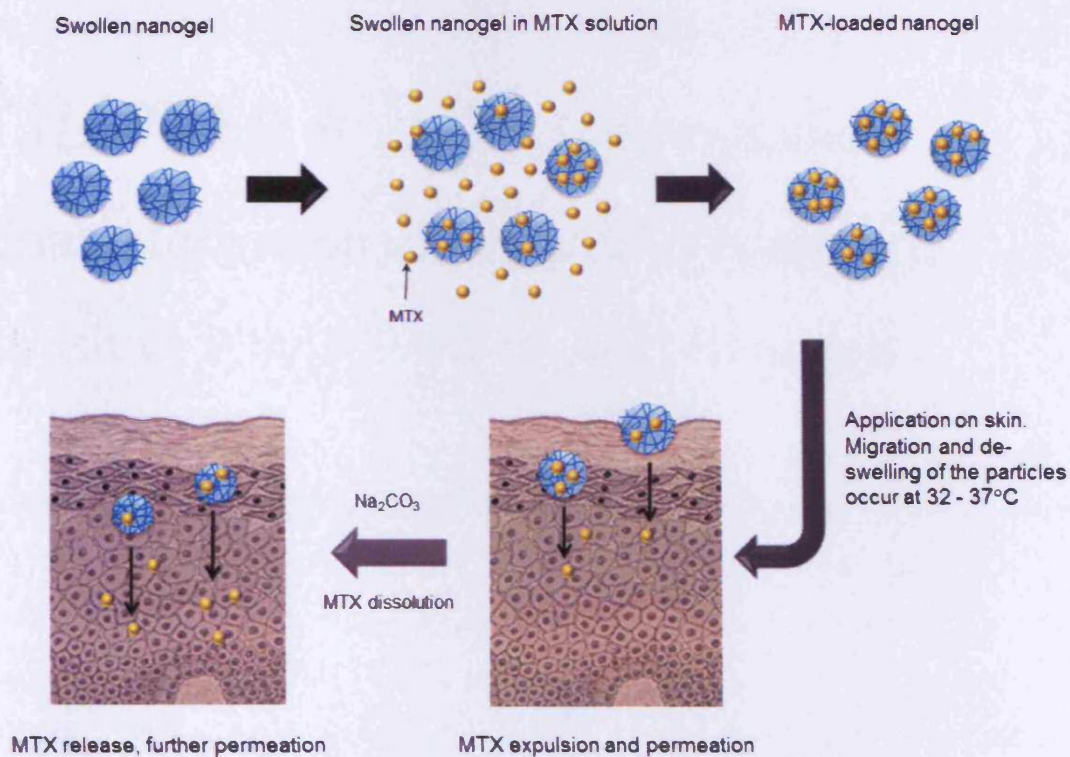


Figure 3-12: Schematic representation of MTX-loaded poly(NIPAM-co-BA) preparation for topical drug delivery and a proposed enhanced drug delivery mechanism by the nanogel as a carrier in the presence of a base (Na₂CO₃).

3.4 CONCLUSION

A drug delivery system with a unique mechanism for topically applied MTX is proposed, comprised of a poly(NIPAM-co-BA) nanogel loaded with MTX that is capable of delivering the drug across the epidermis in levels that significantly reduce

the biosynthesis of PGE₂, a key inflammatory mediator. Both delivery and biological activity are significantly enhanced by the addition of Na₂CO₃, which was found not to be pro-inflammatory. In a therapeutic context, this MTX nanogel delivery system is potentially useful for the topical delivery of a drug that has presented significant challenges hitherto.

CHAPTER 4 | Synthesis and
Characterisation of pH- and Temperature-
sensitive Poly(NIPAM-*co*-AAc) Nanogels

4.1 INTRODUCTION

PolyNIPAM-based nanogels were synthesised and investigated as potential carriers for use in topical drug delivery. The cross-linked polyNIPAM exhibits a conformational transition in the form of volume collapse in the range of 32 – 34°C in aqueous solution, below which the polymer particles are hydrophilic and above which they become hydrophobic (Galaev and Mattiasson, 2007). From the point of view of potential applications, the nanogels would be useful as drug carriers if they could respond to multiple stimuli simultaneously. PolyNIPAM cross-linked with MBA, has a hydrophilic amide group and a hydrophobic isopropyl group in its network. It is possible to increase the functionality of the nanogel particles (i.e. the structure and physical properties) by introducing monomers during synthesis that are responsive to other stimuli or tuned to a desired temperature range by copolymerisation with a more hydrophilic (which raises the LCST) or a hydrophobic (which lowers the LCST) co-monomer than the primary monomer, polyNIPAM.

For the polyNIPAM nanogel, it is suggested that the balance between polymer elasticity and osmotic pressure determines its dimension under equilibrium conditions (Galaev and Mattiasson, 2007). However, the introduction of ionic monomers into the gel network contributes an additional osmotic force to the nanogel. For low charge density, this effect can be explained by the ‘Donnan potential’ of the mobile counter ions within the nanogel network, which will be discussed in detail later. Overall, the swelling behaviour of an ionic polymer in a particular solvent depends on the nature of monomer, monomer concentration, cross-link density, degree of ionisation of a functional co-monomer and nature of the solvent (e.g. pH, temperature and ionic strength).

In the work described here, a hydrophilic monomer, AAc, was copolymerised into the polyNIPAM to obtain poly(NIPAM-co-AAc), a nanogel that is responsive to both, external pH and temperature stimuli. The main monomer, NIPAM, imparts temperature responsiveness to the nanoparticles, while the co-monomer, AAc, imparts pH-sensitivity and a negative charge (Zhang et al., 2004). A lower level of

MBA cross-linker (2.5% w/w) was used for the poly(NIPAM-co-AAc) synthesis compared to the nanogels prepared in CHAPTER 2. According to several publications, the swelling ratio of polyNIPAM-based gels with less cross-linker content is much more pronounced (Crowther and Vincent, 1998; Senff and Richtering, 2000; Woodward et al., 2003) and the swelling response could be attained faster (Bradley et al., 2005). This may be attributed to the lower cross-linking density, resulting in more water uptake into a more flexible gel network (Peppas et al., 2000; Senff and Richtering, 2000; Wang et al., 2008).

The primary aim of this study was to investigate the properties of poly(NIPAM-co-AAc) nanogels in aqueous solution and to determine the most suitable nanogel for the composite system as described in CHAPTER 1. To that end, nanogels were prepared by copolymerising polyNIPAM with varying amounts of AAc (0%, 2% and 5% w/v). The thermal and pH-responsive properties, heat capacity, swelling behaviour of the nanogels in aqueous solution and morphology were investigated.

4.2 MATERIALS AND METHODS

4.2.1 Materials

NIPAM (99%), KPS (99.9%), HCl, sodium chloride (NaCl), glass wool and HPLC-grade solvents were purchased from Fisher Scientific (Loughborough, UK). AAc (99%), CA anhydrous (99.5%), MBA, NaOH and Whatman® qualitative filter paper Grade 4 were all supplied by Sigma-Aldrich Company Ltd. (Poole, UK). Pioloform® and uranyl acetate (UA) were purchased from Agar Scientific Ltd. (Stansted, UK). All chemicals used were analytical grade and were used as received.

4.2.2 Methods

4.2.2.1 Synthesis of Poly(NIPAM-co-AAc) Nanogels

Copolymers of polyNIPAM with varying content of AAc monomer (% w/v) as listed in **Table 4-1**, were synthesised according to the method described in Section 2.2.2.1.1. AAc monomer was added to the mixture of the base monomer NIPAM and cross-linking agent MBA, 15 min prior to the addition of the persulfate initiator. A proposed scheme depicting the synthesis of poly(NIPAM-co-AAc) is shown in **Figure 4-1**. A lower amount of MBA was utilised in comparison to the synthesis of poly(NIPAM-co-BA) nanogel (CHAPTER 2), as a higher concentration of cross-linking agent may decrease the swelling capacity of the synthesised particles, due to the increase amount of covalent bonding between the polymer chains (Lee et al., 2008). A control nanogel, polyNIPAM containing no AAc (0% AAc) was synthesised and purified based on the same technique as the poly(NIPAM-co-AAc) nanogels.

Table 4-1: Poly(NIPAM-co-AAc) nanogels made-up to a total preparation volume of 250 mL with de-ionised water (da Silva and Ganzarolli de Oliveira, 2007; Kratz et al., 2000; Pelton and Chibante, 1986).

Nanogel/ Abbreviation	Components				Stirring Rate (rpm)
	NIPAM (mol)	AAc (mol)	MBA (mol)	KPS (mol)	
Poly(NIPAM-co-AAc)(2%)	0.02	0.001	0.0004	0.0002	300
Poly(NIPAM-co-AAc)(5%)	0.02	0.002	0.0004	0.0002	300
PolyNIPAM (0%) - control	0.02	–	0.0004	0.0002	300

Note: Poly(NIPAM-co-AAc) nanogel coded as poly(NIPAM-co-AAc)(x%), where x is percentage by weight (% w/v) of AAc = 0, 2 or 5 incorporated during nanogel synthesis.

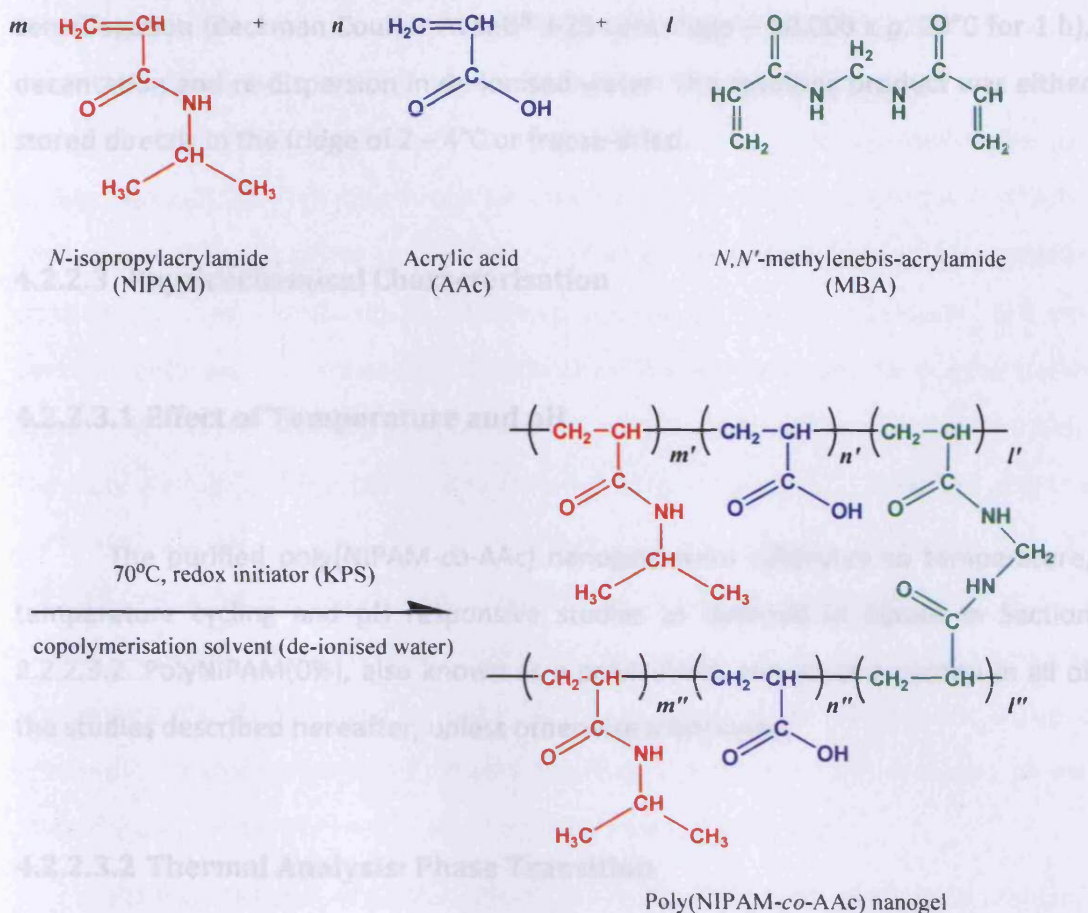


Figure 4-1: Proposed synthetic scheme for poly(NIPAM-co-AAc) nanogel by SFEP technique using MBA as cross-linker and KPS as initiator at 70°C .

4.2.2.2 Nanogel Purification

The poly(NIPAM-co-AAc) nanogels were purified according to the method in Section 2.2.2.2. However, under identical conditions, the ionic nanogels would not centrifuge out and only a very small amount of particles settled to form a pellet at the bottom of the tube. This suggests that the particles have a density very similar to that of the dispersant solvent, i.e. de-ionised water. The particles were thus highly swollen with water, most probably due to the added hydrophilic property to the nanogel by the AAc co-monomer.

The suspensions were purified at a higher centrifugation speed compared to the nanogels prepared in CHAPTER 2. They were purified via repeated steps of

centrifugation (Beckman Coulter Avanti® J-25 centrifuge – 50,000 x *g*, 20°C for 1 h), decantation and re-dispersion in de-ionised water. The resulting product was either stored directly in the fridge of 2 – 4°C or freeze-dried.

4.2.2.3 Physicochemical Characterisation

4.2.2.3.1 Effect of Temperature and pH

The purified poly(NIPAM-co-AAc) nanogels were subjected to temperature, temperature cycling and pH responsive studies as outlined in details in Section 2.2.2.3.2. PolyNIPAM(0%), also known as a polyNIPAM, served as a control in all of the studies described hereafter, unless otherwise mentioned.

4.2.2.3.2 Thermal Analysis: Phase Transition

The phase transitions of poly(NIPAM-co-AAc)(2%), poly(NIPAM-co-AAc)(5%) and polyNIPAM (control) nanogels prepared in de-ionised water (50% w/v) were investigated by the MC-DSC instrument. Each sample was prepared in triplicate (n=3) and de-ionised water was used as a reference. The general method of sample preparation and parameters applied during analysis were described in Section 2.2.2.3.3.

4.2.2.3.3 Swelling Behaviour: Measurement of Swelling Ratio (SR)

One of the most important properties of nanogel particles is their swelling behaviour. The dynamic and equilibrium swelling study was carried out as a function of temperature and ionic strength of a solvent. The nanogels were synthesised as potential carriers for topical drug delivery; therefore the pH of the buffer solution

should ideally be close to the pH of the skin surface. Variable skin surface pH values have been reported, although all in the acidic broad range from pH 4.0 – 7.0 (Lambers et al., 2006). Additionally, the pH of the solution should be above the pK_a of AAc residues ($pK_a = 4.25$) to ensure ionisation of the carboxyl groups ($-\text{COOH}$) takes place. The ionisation causes the particles to be in an extended and swollen state which may contribute to enhanced uptake of solvent molecules into the nanogel (detailed mechanism described in CHAPTER 1). As a result, an acetate buffer (0.01 M, pH 5) was used to simulate the pH of skin surface (Lambers et al., 2006). The ionic strength of the buffer was varied over a range of 1.0 to 0.01 M and the study was carried out at a constant temperature of either 4°C (cold room) or RT (~25°C). These temperatures were selected in order to investigate loading capacity of the nanogels, as it was expected to be higher at a lower temperature. Measurements of the swelling ratio of the nanogels were carried out using a gravimetric method (Swarbrick, 2004). Swelling behaviour of the nanogels in de-ionised water, in the absence of electrolyte was also investigated.

Poly(NIPAM-co-AAc)(2%), poly(NIPAM-co-AAc)(5%) and polyNIPAM (control) nanogels were subjected to the swelling ratio study. A fixed volume (1 mL) of the acetate buffer (0.01 M, pH 5) varies with ionic strengths (1.0, 0.5, 0.1, 0.05 and 0.01 M) was added into centrifuge tubes containing pre-weighted freeze-dried nanogels (W_0). The ionic strengths were attained by the addition of NaCl. The samples were continuously mixed on Stuart® Flask Shaker-SF1 for 30 min prior to storage either in a cold room (4°C) or on the bench (25°C). Four replicates were prepared for each nanogel sample ($n=4$). At predetermined timepoints, the swollen samples were concentrated by centrifugation in the Beckman Coulter Avanti® J-25 centrifuge (50,000 $\times g$, either at 4°C or 25°C for 1 h). The supernatants were removed and the swollen samples weighed (W_s) immediately after blotting off the excess surface water with a moistened filter paper. Later on, the same volume of fresh solvent was added to the swollen samples and the swelling, centrifugation and weighing processes were repeated until the weight of each sample was constant, indicating that equilibrium swelling had been attained. A similar procedure was repeated using

de-ionised water without the addition of NaCl. The swelling ratio (SR) was calculated from the following equation, Equation 4-1 (Swarbrick, 2004):

$$SR \text{ (g/g)} = \frac{W_S - W_D}{W_D}$$

Equation 4-1

4.2.2.3.4 Morphology Determination by SEM and TEM

TEM was used to determine the shape and size of the nanogel particles. Their morphology was also characterised by SEM.

4.2.2.3.4.1 SEM

Samples of poly(NIPAM-co-AAc)(2%) and poly(NIPAM-co-AAc)(5%) for SEM imaging were prepared as described in Section 2.2.2.3.4.1.

4.2.2.3.4.2 TEM

4.2.2.3.4.2.1 Ionic Functional Groups Distribution: Droplet Negative-staining

The distribution of AAc functional groups (i.e. —COOH) within the nanogels' network plays a critical role in controlling their swelling and de-swelling behaviour. A negative staining technique with uranyl acetate (UA) was carried out in order to visualise the distribution of carboxylic acid. Theoretically, uranyl ions bind to the negatively charged carboxyl side chains of the AAc residues (Hayat, 2000; Hoare and McLean, 2006; Hoare and Pelton, 2008a), resulting in the enhanced image contrast

as well as imparting a fine grain to the image, which is particularly useful for smaller particulate samples (Hayat, 2000). The sample preparation steps involved are illustrated in **Figure 4-2**. For the purpose of this study, poly(NIPAM-co-AAc)(10%) served as a positive control, as it was expected to exhibit maximal UA staining, caring maximal carboxylate functionality. On the other hand, the polyNIPAM was assumed lacked of anionic functionality, due to the absence of AAac moieties, and served as a negative control.

A single droplet procedure was used, whereby about 20 μL of de-ionised water and aqueous solution of UA (2% w/v) were placed separately onto a Parafilm[®] strip with a pipette. Then, 10 μL (a drop) of each diluted nanogel solution (0.1% w/v) was pipetted out onto a Pioloform[®]-coated copper grid. After 1 min, any remaining fluid on the grid was removed by carefully touching the edge of the grid to a filter paper. Following that, the sample was gently rinsed with one or more droplets of distilled water. Next, the sample was stained by floating the grid (the side with the sample facing down) on a drop of aqueous UA (2% w/v) for 30 min as shown in **Figure 4-2(C)**. The stained sample was rinsed twice with distilled water to remove any excess UA [**Figure 4-2(D)**]. The grid was then allowed to air-dry at ambient temperature prior to TEM imaging using a Phillips EM 208 TEM, operated at 80 kV accelerated voltage. At least three replicates were prepared for each sample ($n \geq 3$). The mean particle diameter of each nanogel sample was determined by measuring 150 individual particles and taking a mean value ($n=150$).

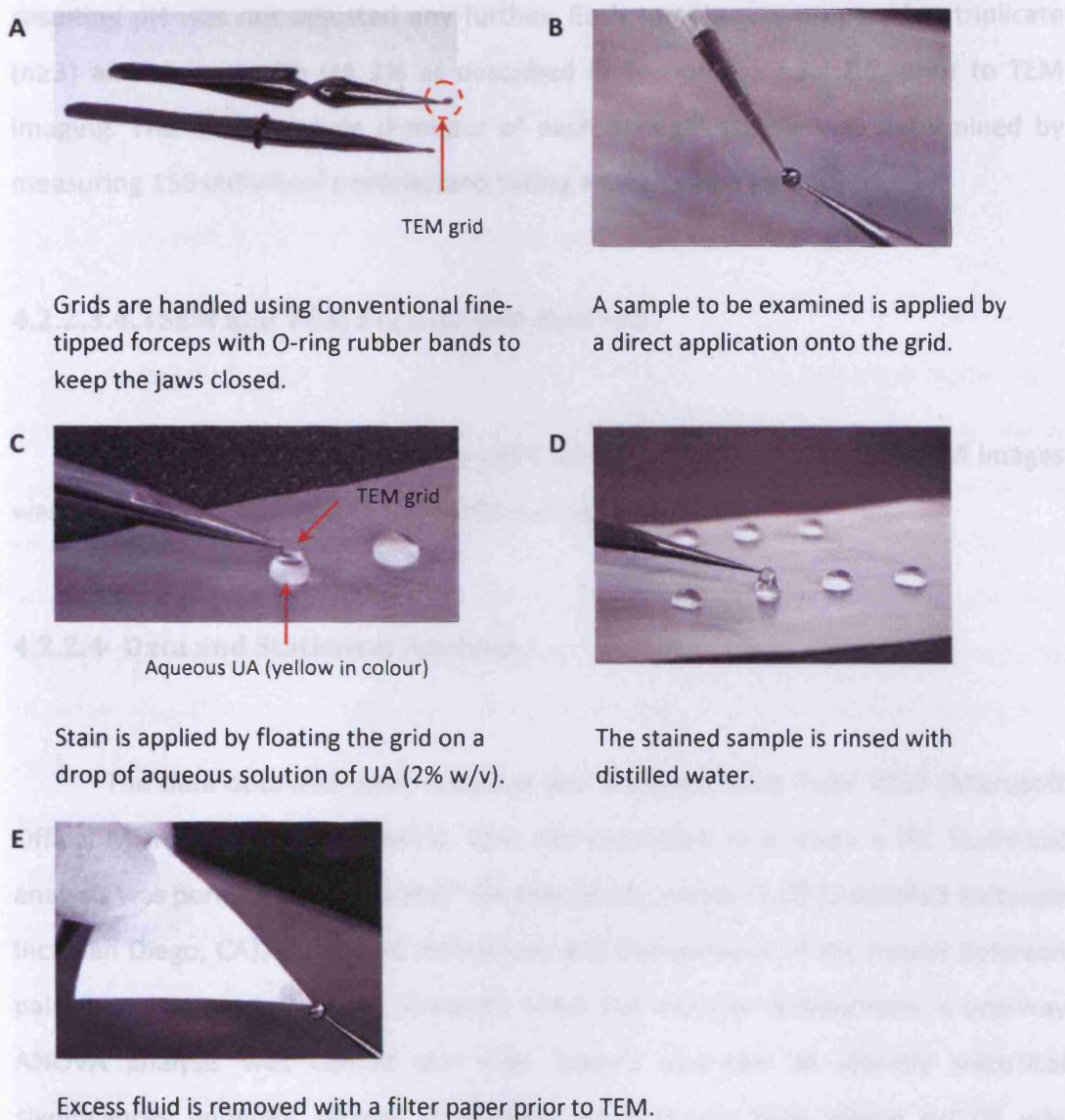


Figure 4-2: UA droplet negative-staining procedure for TEM.

4.2.2.3.4.2.2 Effect of pH

The effect of pH on the nanogels was also investigated by TEM. The solutions of ~pH 2 (the most acidic condition), ~pH 5 (close to the pH of the skin) and ~pH 10 (the most alkaline condition) were prepared by adjusting de-ionised water to the required pH with the drop-wise addition of either HCl (0.1 M) or NaOH (0.1 M). Subsequently, the freeze-dried nanogels were added into the solutions and mixed at

ambient temperature for about 30 min on Stuart® Flask Shaker-SF1. Once mixed, the resulting pH was not adjusted any further. Each sample was prepared in triplicate ($n \geq 3$) and stained with UA 2% as described in Section 4.2.2.3.4.2.1, prior to TEM imaging. The mean particle diameter of each nanogel sample was determined by measuring 150 individual particles and taking a mean value ($n=150$).

4.2.2.3.4.3 SEM and TEM Particle Size Analysis

Particle diameter of each nanogel obtained from the SEM and TEM images was determined according to the method in Section 2.2.2.3.4.3.

4.2.2.4 Data and Statistical Analysis

The data obtained were recorded and analysed using Excel 2007 (Microsoft Office, Microsoft Corp., Redmond, WA) and expressed as a mean \pm SD. Statistical analysis was performed with InStat® for Macintosh, version 3.00 (GraphPad Software Inc., San Diego, CA). Significant differences and comparisons of the means between paired data were made using Student's *t*-test. For multiple comparisons, a one-way ANOVA analysis was carried out with Tukey's post-test to identify statistical significances between groups. Confidence interval was 95% where $p < 0.05$ was considered to be significant.

4.3 RESULTS AND DISCUSSION

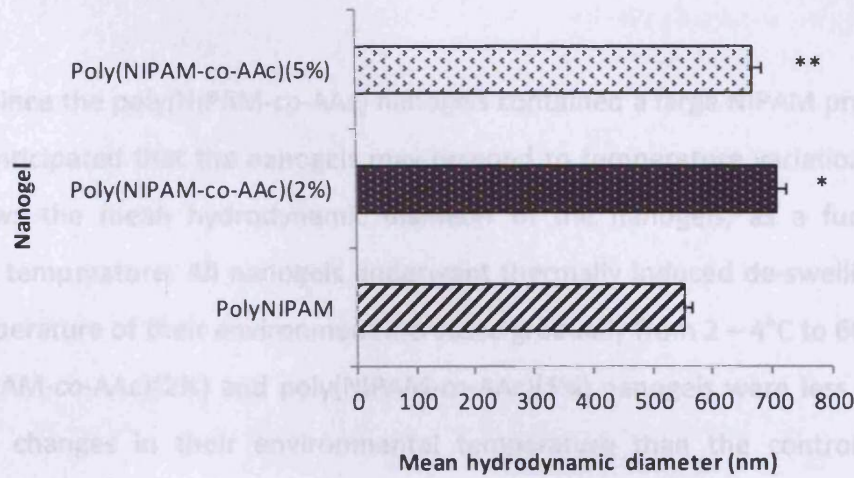
4.3.1 Physicochemical Characterisation

4.3.1.1 Particle Size and Size Distribution

A series of gels with particle diameters range in the nanosize scale were synthesised with variable AAc concentrations (0, 2, and 5% w/v). The mean hydrodynamic diameters for the poly(NIPAM-co-AAc)(2%), poly(NIPAM-co-AAc)(5%) and polyNIPAM (control) were found to be, 705 ± 14 nm, 664 ± 17 nm and 551 ± 10 nm, respectively (**Figure 4-3**). The further expansion of the poly(NIPAM-co-AAc) nanogel matrices in comparison to the control can be explained by increased uptake of water due to the incorporation of the hydrophilic AAc co-monomer (Lee et al., 2008; Peppas et al., 2000). Surprisingly, the mean hydrodynamic diameter of the poly(NIPAM-co-AAc)(2%) particles was found to be significantly larger than the poly(NIPAM-co-AAc)(5%), even though it contained less of the AAc co-monomer ($p=0.0314$). It was reported that a copolymer of NIPAM and AAc, with a low amount of cross-linker, exhibited an increase in size upon increasing the AAc content (Makino et al., 2001). Although we do not have a clear explanation for the contrasting results that we obtained, further investigations regarding the issue will be discussed in the following Section 4.3.1.2.

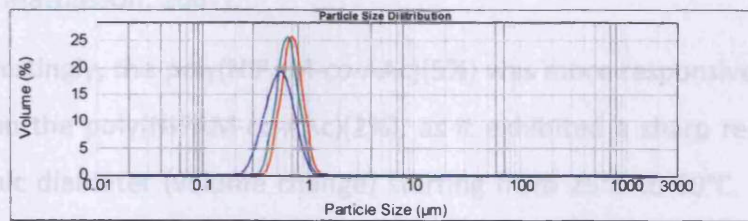
There were minimum variations in the particle size of the assessed nanogels, based on the low values of the measured span and uniformity (**Figure 4-3**). **Figure 4-4** shows the characteristic size distribution curves for the nanogels. In all cases, the nanogels demonstrated a fairly narrow and a unimodal particle size distribution.

4.3.1.2 Temperature-responsive Effect



Nanogel	Particle Diameter (μm)		Span	Uniformity
	Minimum	Maximum		
Poly(NIPAM-co-AAc)(2%)	513 ± 8	928 ± 19	0.60 ± 0.004	0.19 ± 0.004
Poly(NIPAM-co-AAc)(5%)	461 ± 12	842 ± 22	0.61 ± 0.002	0.20 ± 0.01
PolyNIPAM (control)	340 ± 12	796 ± 27	0.84 ± 0.06	0.27 ± 0.02

Figure 4-3: Particle size profiles of poly(NIPAM-co-AAc)(2%) and poly(NIPAM-co-AAc)(5%) nanogels in de-ionised water, determined at RT by a laser light diffraction analyser; polyNIPAM served as control; polydispersity of each sample represents by span and uniformity values ($n=3$, \pm SD). * $p=0.0001$, vs. control; ** $p=0.0006$, vs. control; and *** $p<0.0314$ between nanogels



— Poly(NIPAM-co-AAc)(2%) — Poly(NIPAM-co-AAc)(5%) — PolyNIPAM (control)

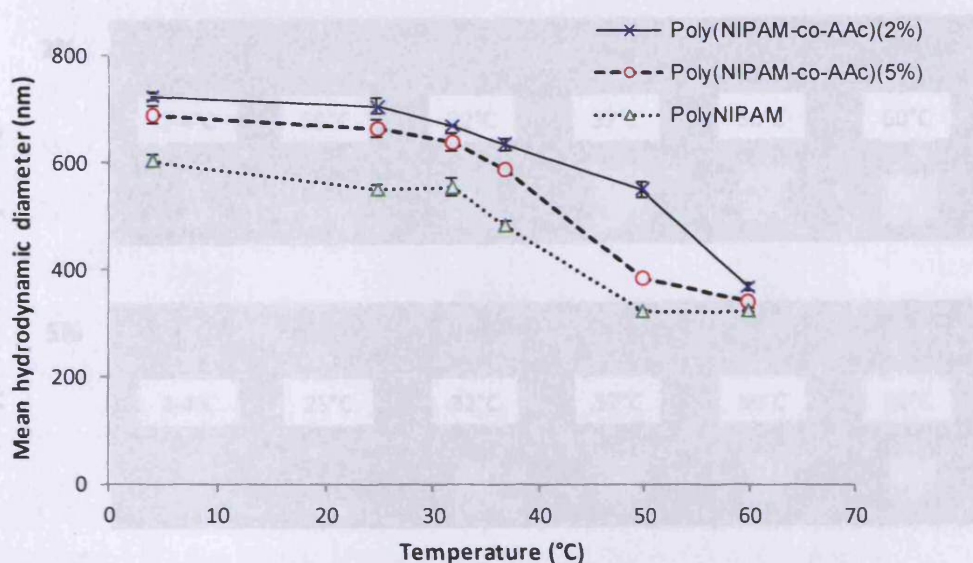
Figure 4-4: Particle size distribution curves for poly(NIPAM-co-AAc)(2%) and poly(NIPAM-co-AAc)(5%) nanogels in de-ionised water, measured at RT using a laser light diffraction analyser. PolyNIPAM served as control.

4.3.1.2 Temperature-responsive Effect

Since the poly(NIPAM-co-AAc) nanogels contained a large NIPAM proportion, it was anticipated that the nanogels may respond to temperature variations. **Figure 4-5** shows the mean hydrodynamic diameter of the nanogels, as a function of solution temperature. All nanogels underwent thermally induced de-swelling when the temperature of their environment increased gradually from 2 – 4°C to 60°C. Both poly(NIPAM-co-AAc)(2%) and poly(NIPAM-co-AAc)(5%) nanogels were less sensitive towards changes in their environmental temperature than the control. It was reported that the presence of hydrophilic AAc monomer in the copolymer network could diminish or even eliminate the temperature-dependence of the hydrodynamic diameter of the particles, compared to the control due to alteration in their hydrophilic-hydrophobic balance (Lee et al., 2008; Zhang et al., 2002).

The de-swelling process was accompanied by a change in turbidity of the samples, from transparent milky white in the swollen state to absolute milky white in the collapsed state, as observed in **Figure 4-6**. Initially, the particles were in an extended conformation, swollen with solvent and therefore had an almost clear appearance. This is due to the refractive index of the swollen particles being closely matched to the continuous solvent medium, i.e. de-ionised water. As the temperature increased, the turbidity phenomenon occurred due to water being expelled from the nanogels' network, leading to formation of the insoluble aggregates (Galaev and Mattiasson, 2007).

Interestingly, the poly(NIPAM-co-AAc)(5%) was more responsive to a thermal stimulus than the poly(NIPAM-co-AAc)(2%), as it exhibited a sharp reduction of its hydrodynamic diameter (volume change) starting from 25°C to 60°C. Furthermore, the visual inspection of the nanogel demonstrated noticeable milky white appearance (i.e. phase separation) around 32°C, in contrast to the poly(NIPAM-co-AAc)(2%) at 37°C. This further supports the idea that the VPTT of the poly(NIPAM-co-AAc)(5%) was roughly around 32°C, lower than the poly(NIPAM-co-AAc)(2%).



Temperature (°C)	Poly(NIPAM-co-AAc)(2%)		Poly(NIPAM-co-AAc)(5%)		PolyNIPAM (control)	
	Span	Uniformity	Span	Uniformity	Span	Uniformity
2-4	0.62 ± 0.001	0.19 ± 0.004	0.61 ± 0.01	0.19 ± 0.004	0.80 ± 0.04	0.25 ± 0.01
25	0.60 ± 0.004	0.19 ± 0.004	0.64 ± 0.03	0.20 ± 0.01	0.84 ± 0.06	0.27 ± 0.02
32	0.61 ± 0.04	0.20 ± 0.01	0.61 ± 0.002	0.20 ± 0.001	0.79 ± 0.003	0.25 ± 0.003
37	0.65 ± 0.001	0.20 ± 0.01	0.62 ± 0.02	0.27 ± 0.02	0.83 ± 0.04	0.26 ± 0.01
50	0.65 ± 0.10	0.21 ± 0.03	0.73 ± 0.04	0.23 ± 0.02	0.57 ± 0.002	0.18 ± 0.001
60	0.77 ± 0.10	0.24 ± 0.03	0.59 ± 0.001	0.18 ± 0.001	0.57 ± 0.004	0.18 ± 0.002

Figure 4-5: Mean hydrodynamic particle diameter, as a function of temperature for poly(NIPAM-co-AAc)(2%) and poly(NIPAM-co-AAc)(5%) nanogels in de-ionised water, measured by a laser light diffraction analyser; polyNIPAM acted as a control nanogel; span and uniformity values represent polydispersity ($n=3$, \pm SD).

($p=0.0032$). While for the polyNIPAM, volume $\text{vol.} = 19.9\%$ ($504 \pm 11 \text{ nm} \rightarrow 493 \pm 3 \text{ nm}$), higher than the poly(NIPAM-co-AAc)(2%) nanogel but lower than the poly(NIPAM-co-AAc)(5%). Overall, the poly(NIPAM-co-AAc)(5%) was found to be the most temperature-responsive among the nanogels due to the hydrophilic nature of the AAc introduced into the polymer network, which in turn led to the higher water uptake.

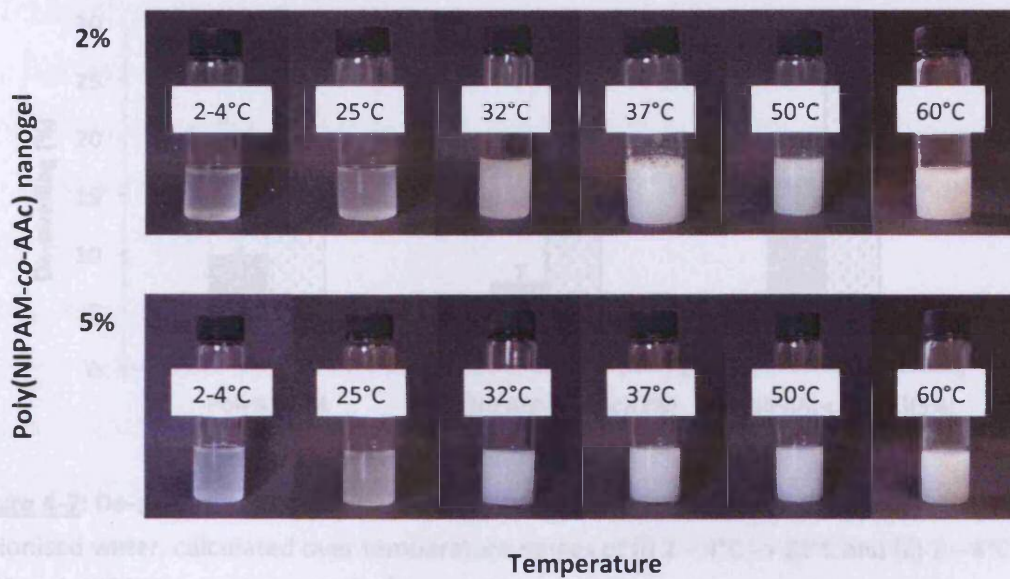


Figure 4-6: Images of aqueous dispersions of poly(NIPAM-co-AAc)(2%) and poly(NIPAM-co-AAc)(5%) taken after 30 min of storage at designated temperatures, 2 – 4°C → 60°C.

Figure 4-7 presents de-swelling (%) of the nanogel particles calculated based on their hydrodynamic diameter in temperature intervals of (i) 2 – 4°C → 32°C and (ii) 2 – 4°C → 37°C using Equation 2-3. As outlined in CHAPTER 2, these temperature ranges are significant from a topical delivery perspective. Over the range, the poly(NIPAM-co-AAc)(5%) demonstrated a very significant de-swelling by 24.9% ($689 \pm 16 \text{ nm} \rightarrow 532 \pm 21 \text{ nm}$) ($p=0.0005$). As for the poly(NIPAM-co-AAc)(2%), the nanogel demonstrated only 13.6% ($725 \pm 6 \text{ nm} \rightarrow 635 \pm 11 \text{ nm}$) de-swelling which was considered significantly low in comparison to the poly(NIPAM-co-AAc)(5%) ($p=0.0052$). While for the polyNIPAM, volume loss was 19.9% ($604 \pm 11 \text{ nm} \rightarrow 483 \pm 8 \text{ nm}$), higher than the poly(NIPAM-co-AAc)(2%) nanogel but lower than the poly(NIPAM-co-AAc)(5%). Overall, the poly(NIPAM-co-AAc)(5%) was found to be the most temperature-responsive among the nanogels due to the hydrophilic nature of the AAc introduced into the polymer network, which in turn led to the higher water uptake.

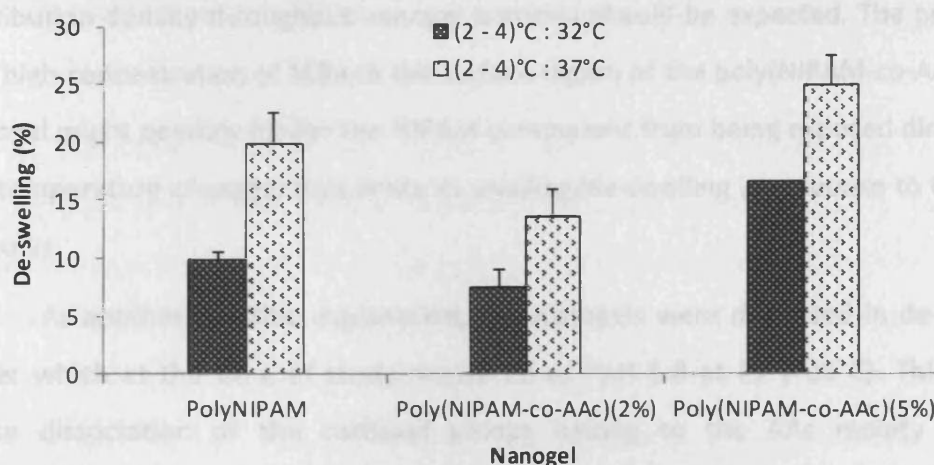


Figure 4-7: De-swelling of poly(NIPAM-co-AAc)(2%) and poly(NIPAM-co-AAc)(5%) nanogels in de-ionised water, calculated over temperature ranges of (i) 2 – 4°C → 32°C and (ii) 2 – 4°C → 37°C; polyNIPAM served as a control nanogel ($n=3$, \pm SD).

While several experiments suggested that the LCST of polyNIPAM-based polymers (32 – 34°C) would be raised to a higher temperature and had a wider transition temperature range with increasing amount of hydrophilic co-monomer (Hoffman, 1995; Kratz et al., 2000; Lee et al., 2008; Lin et al., 2006), the current data leads to the opposite conclusion. The poly(NIPAM-co-AAc)(5%) nanogel exhibited higher thermal sensitivity than the poly(NIPAM-co-AAc)(2%), despite containing a higher AAc level. The poly(NIPAM-co-AAc)(5%) nanogel experienced pronounced de-swelling in comparison to the poly(NIPAM-co-AAc)(2%) at the same temperature point.

Although there is no clear explanation for this discrepancy, the following may be relevant. The swelling/de-swelling measurements have been traditionally used to characterise cross-linking density. The distribution of NIPAM (primary monomer), AAc (hydrophilic co-monomer) and MBA (cross-linker) in the nanogels might affect the kinetic behaviour of these gels towards their environment. MBA is proven to be consumed faster during polymerisation than NIPAM leading to its localisation in the core region of each of the functionalised nanogel particle (Hoare and McLean, 2006; Wu et al., 1994). Nonetheless, the addition of functional monomer during nanogel synthesis may affect the MBA reactivity. MBA is consumed progressively slower relative to NIPAM, as the polymerisation proceeds; thus variation in the MBA

distribution density throughout nanogel particles should be expected. The presence of a high concentration of MBA in the surface region of the poly(NIPAM-co-AAc)(2%) nanogel might possibly hinder the NIPAM component from being exposed directly to the temperature changes; thus limits its swelling/de-swelling in response to thermal stimulus.

As another possible explanation, the nanogels were dispersed in de-ionised water which at the time of study measured as \sim pH 5.8 at RT (\sim 25°C). This might cause dissociation of the carboxyl groups belong to the AAc moiety of the poly(NIPAM-co-AAc) nanogels, which further influenced the extent of swelling/de-swelling experienced by the nanogel particles. The pH-responsive property possessed by the poly(NIPAM-co-AAc)(5%) might have contributed to further de-swelling of the nanogel in comparison to the control.

Both poly(NIPAM-co-AAc)(2%) and poly(NIPAM-co-AAc)(5%) exhibited reversible volumetric swelling response to temperature changes (Figure 4-8). When cooling the nanogel suspensions from high temperature of 60°C to RT (25°C), the mean hydrodynamic diameter demonstrated similar temperature dependence. The distribution during both heating and cooling processes overlapped, indicating the temperature sensitivities of these nanogels were reversible.

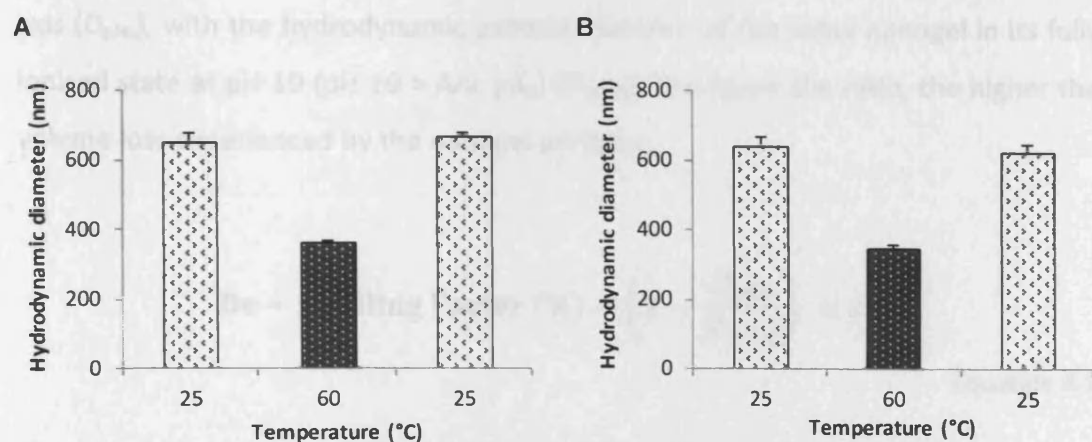


Figure 4-8: Reversibility of hydrodynamic diameter (A) poly(NIPAM-co-AAc)(2%) and (B) poly(NIPAM-co-AAc)(5%) in de-ionised water, as a function of alternating temperatures (25°C \rightarrow 60°C \rightarrow 25°C). $p < 0.0001$ between treatments

4.3.1.3 pH-responsive Effect

The incorporation of a co-monomer containing acidic functionality (AAc) into the polyNIPAM nanogel yielded poly(NIPAM-co-AAc) particles with a pH-driven swelling property. As shown in [Figure 4-9](#), the hydrodynamic diameters of both poly(NIPAM-co-AAc)(2%) and poly(NIPAM-co-AAc)(5%) particles increased, as the pH of their external medium increased ($\text{pH} > \text{p}K_a$). At the pH above the $\text{p}K_a$ of AAc moieties ($\text{p}K_a$ at $25^\circ\text{C} = 4.25$), the carboxyl groups of the AAc became ionised ($-\text{COOH} \rightarrow -\text{COO}^- + \text{H}^+$), creating strong electrostatic repulsive forces between the adjacent carboxylate anions ($-\text{COO}^-$) within the network (Beltran et al., 1991; Khare and Peppas, 1995; Peppas et al., 2000). This, in turn, resulted in an increased hydrophilicity of the network, causing the nanogel particles to exhibit a more extended conformation i.e. swollen form. On the contrary, at a pH below the $\text{p}K_a$, the carboxyl groups of the AAc were protonated ($-\text{COO}^- + \text{H}^+ \rightarrow -\text{COOH}$), no charge repulsion occurred within the network and therefore the particles had a compact conformation i.e. de-swollen form (Peppas et al., 2000).

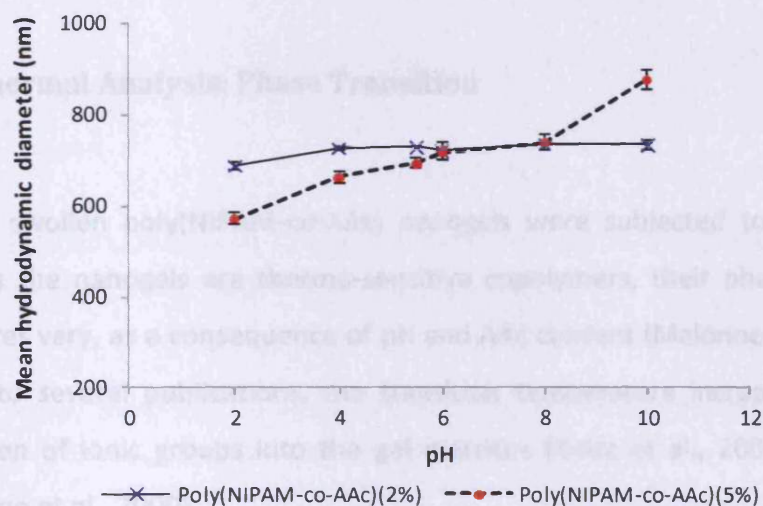
The hydrodynamic diameter data were further simplified and reported as a de-swelling factor in [Figure 4-10](#). The factor was calculated according to Equation 4-2, by dividing the measured hydrodynamic particle diameter at the pH given on the x-axis ($D_{\text{pH}x}$), with the hydrodynamic particle diameter of the same nanogel in its fully ionised state at pH 10 ($\text{pH} 10 > \text{AAc } \text{p}K_a$) ($D_{\text{pH}10}$). The lower the ratio, the higher the volume loss experienced by the nanogel particles:

$$\text{De - swelling Factor (\%)} = \left(1 - \frac{D_{\text{pH}x}}{D_{\text{pH}10}} \right) \times 100$$

Equation 4-2

As seen in [Figure 4-10](#), the poly(NIPAM-co-AAc)(5%) particles had a mean hydrodynamic diameter of 877 ± 23 nm at pH 10, and declined to 573 ± 11 nm at pH 2. Thus, the particles underwent de-swelling by 35% which was considered

extremely significant ($p=0.0001$). Over the same pH range, the poly(NIPAM-co-AAc)(2%) underwent significant reduction of its hydrodynamic diameter, although only by 6% ($734 \pm 11 \text{ nm} \rightarrow 688 \pm 9 \text{ nm}$) ($p=0.0049$). Therefore, the poly(NIPAM-co-AAc)(5%) nanogel was found to be significantly more responsive towards a pH variation with the lowest de-swelling factor in comparison to the poly(NIPAM-co-AAc)(2%) at pH 2, where the particles were in their fully unionised form ($p=0.0012$). Its profound pH-sensitivity might be contributed by the higher level of AAc incorporated within the nanogel network. For this study, no control nanogel (polyNIPAM) was studied due to the fact that it lacked pH-sensitivity as proven in Section 2.3.1.3.



pH	Poly(NIPAM-co-AAc)(2%)		Poly(NIPAM-co-AAc)(5%)	
	Span	Uniformity	Span	Uniformity
2	0.85 ± 0.04	0.27 ± 0.01	1.07 ± 0.18	1.01 ± 0.71
4	0.62 ± 0.03	0.19 ± 0.01	0.79 ± 0.06	0.25 ± 0.03
5.5	0.63 ± 0.02	0.19 ± 0.01	0.64 ± 0.003	0.20 ± 0.001
6	0.62 ± 0.03	0.19 ± 0.01	0.70 ± 0.001	0.22 ± 0.001
8	0.60 ± 0.002	0.18 ± 0.001	0.78 ± 0.02	0.26 ± 0.01
10	0.60 ± 0.001	0.18 ± 0.004	0.56 ± 0.02	0.18 ± 0.001

Figure 4-9: Mean hydrodynamic particle diameter, as a function of pH for poly(NIPAM-co-AAc) nanogels measured at RT using a laser light diffraction analyser; solutions of varied pH were prepared in the absence of NaCl as ionic strength contributor; span and uniformity represent polydispersity of the particles ($n=3, \pm \text{SD}$).

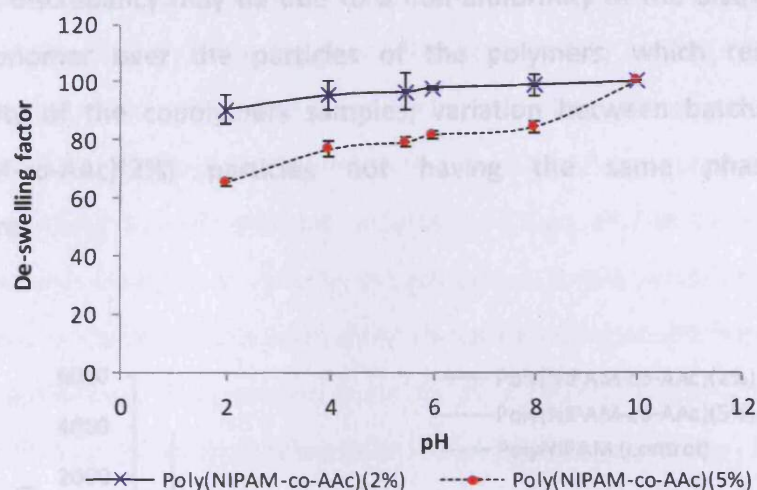


Figure 4-10: De-swelling factor, as a function of pH for poly(NIPAM-co-AAc)(2%) and poly(NIPAM-co-AAc)(5%) nanogels ($n=3$, \pm SD).

4.3.1.4 Thermal Analysis: Phase Transition

The swollen poly(NIPAM-co-AAc) nanogels were subjected to calorimetric analysis. As the nanogels are thermo-sensitive copolymers, their phase transition temperatures vary, as a consequence of pH and AAc content (Malonne et al., 2005). According to several publications, the transition temperature increases with the incorporation of ionic groups into the gel matrices (Kratz et al., 2000; Lee et al., 2008; Makino et al., 2000).

Figure 4-11 shows the MC-DSC thermograms for poly(NIPAM-co-AAc) nanogels. The results show that the increase of AAc content in the polymer chains lead to greater changes in the shapes of the DSC curves in terms of their height and broadness (temperature range). **Table 4-2** presents the thermal analysis data obtained from the thermograms of the samples. The lowest LCST was exhibited by the poly(NIPAM-co-AAc)(2%) followed by the polyNIPAM and poly(NIPAM-co-AAc)(5%) with the LCST of 33°C, 35°C and 37°C, respectively. These unexpected results are in contrast with the experimental data of laser light diffraction in Section 4.3.1.2, where the poly(NIPAM-co-AAc)(2%) is shown to be the least responsive to temperature changes.

The discrepancy may be due to a non-uniformity of the distribution of the AAc co-monomer over the particles of the polymers, which results in non-homogeneity of the copolymers samples; variation between batches. Thus, the poly(NIPAM-co-AAc)(2%) particles not having the same phase transition temperature.

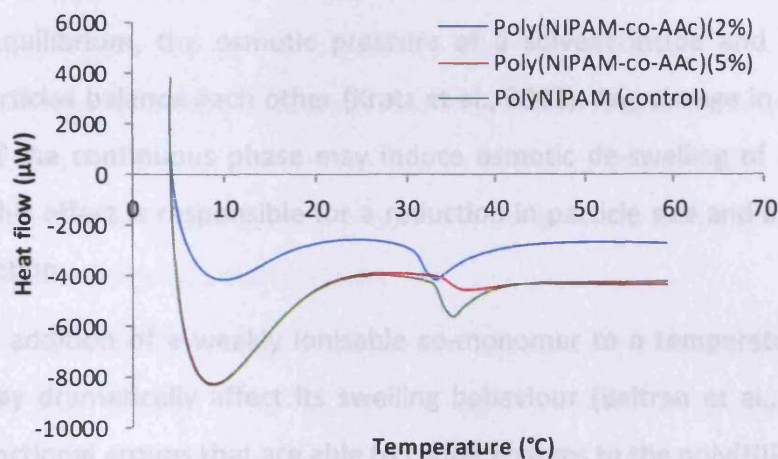


Figure 4-11: MC-DSC thermograms of poly(NIPAM-co-AAc)(2%) and poly(NIPAM-co-AAc)(5%) nanogel in de-ionised water. PolyNIPAM served as control.

Table 4-2: Phase transitions of poly(NIPAM-co-AAc)(2%) and poly(NIPAM-co-AAc)(5%) nanogels in de-ionised water measured by MC-DSC; polyNIPAM served as control (n=3 ± SD).

Sample	LCST (°C)
Poly(NIPAM-co-AAc)(2%)	33 ± 2
Poly(NIPAM-co-AAc)(5%)	37 ± 6 × 10 ⁻⁵
PolyNIPAM (control)	35 ± 4 × 10 ⁻⁵

4.3.1.5 Swelling Behaviour: Effect of Temperature and Ionic Strength

The aim of this study was to investigate the simultaneous effects of salt concentration and temperature over swelling behaviour of the nanogels, which is important in order to determine a suitable and optimal condition for drug loading.

The average SR value was calculated based on Equation 4-1 which represents the aqueous uptake capacity of a dry nanogel in a particular solvent. **Figure 4-12** and **Figure 4-13** present the swelling ratio (g/g) of the copolymer nanogels in an acetate buffer (~pH 5), at specified ionic strength (0.01 – 1.00 M) maintained at a constant temperature, either 2 – 4°C or RT over a period of 5 days. Equilibrium is reached only after the nanogel adjusted its volume and requires a certain period of time to attain it. All nanogels prepared in this work attained their swelling equilibrium at a period \geq 24 h. At equilibrium, the osmotic pressure of a solvent inside and outside the nanogel particles balance each other (Kratz et al., 2001). Any change in the osmotic pressure of the continuous phase may induce osmotic de-swelling of the nanogel particles. This effect is responsible for a reduction in particle size and a decrease in volume fraction.

The addition of a weakly ionisable co-monomer to a temperature-sensitive nanogel may dramatically affect its swelling behaviour (Beltran et al., 1991). Two types of functional groups that are able to confer charges to the poly(NIPAM-co-AAc) are:

- (i) Sulfate groups originating from the persulfate initiator, located at the periphery of the particles, and
- (ii) The constituent monomer, AAc, located within the particles (Peppas et al., 2000; Snowden et al., 1996).

Under the experimental conditions (~pH 5), the carboxylate groups within the nanogel particles were ionised, seeing that the pK_a of AAc residues is around 4.25 (Peppas et al., 2000). The ionisation caused the nanogel to adapt to an extended conformation due to electrostatic repulsion between the like charges within the nanogel network, as discussed in Section 4.3.1.3. On the other hand, the sulfate groups were expected to have insignificant contribution to the swelling of the particles, due to the absence of internal surface charges in the polyNIPAM network (Christensen and Keiding, 2005).

It was observed that the mass uptake of the buffer solution declined with the increasing concentration of NaCl at both 2 – 4°C and RT, believed to be as a result of

an 'electrolyte screening' effect (Khare and Peppas, 1995). This could be explained according to the Donnan equilibrium (Kokufuta et al., 1998). The equilibrium characterised by an unequal distribution of diffusible ions between two compartments separated by a semi-permeable membrane. By applying the concept onto a nanogel system – at a constant pH above the pK_a , the ionic strength increased as the ionisation of the carboxyl groups increased. This event led to a higher equilibrium water uptake. After the gel ionisation was completed, a further increase in the ionic strength created the 'screening effect' of the counter ions (NaCl), in which the counter ions were excluded from further entering into the gel. Thus, the concentration differential of counter ions between the gel and swelling medium was reduced, causing a decrease to ion osmotic swelling pressure which further resulted in a decrease in equilibrium water uptake.

It can be seen that, in the absence of added electrolyte (de-ionised water with pH of 5.83 ± 0.01 at 25°C), the nanogel particles were greatly swollen particularly for the samples kept at $2 - 4^\circ\text{C}$ in de-ionised water ([Figure 4-14](#)). A better view can be observed in [Figure 4-15](#) which shows the SR values calculated for a 72 h period of incubation. The ionic nanogels, particularly poly(NIPAM-co-AAc)(5%), demonstrated almost 2-fold bigger SR values in the absence of NaCl. Temperature change did affect the gel swelling behaviour and this is demonstrated, as a higher SR was attained at $2 - 4^\circ\text{C}$ in comparison to the samples of the same batch maintained at RT. This could be attributed to the fact that the nanogels were greatly swollen at lower temperature as shown in [Figure 4-5](#).

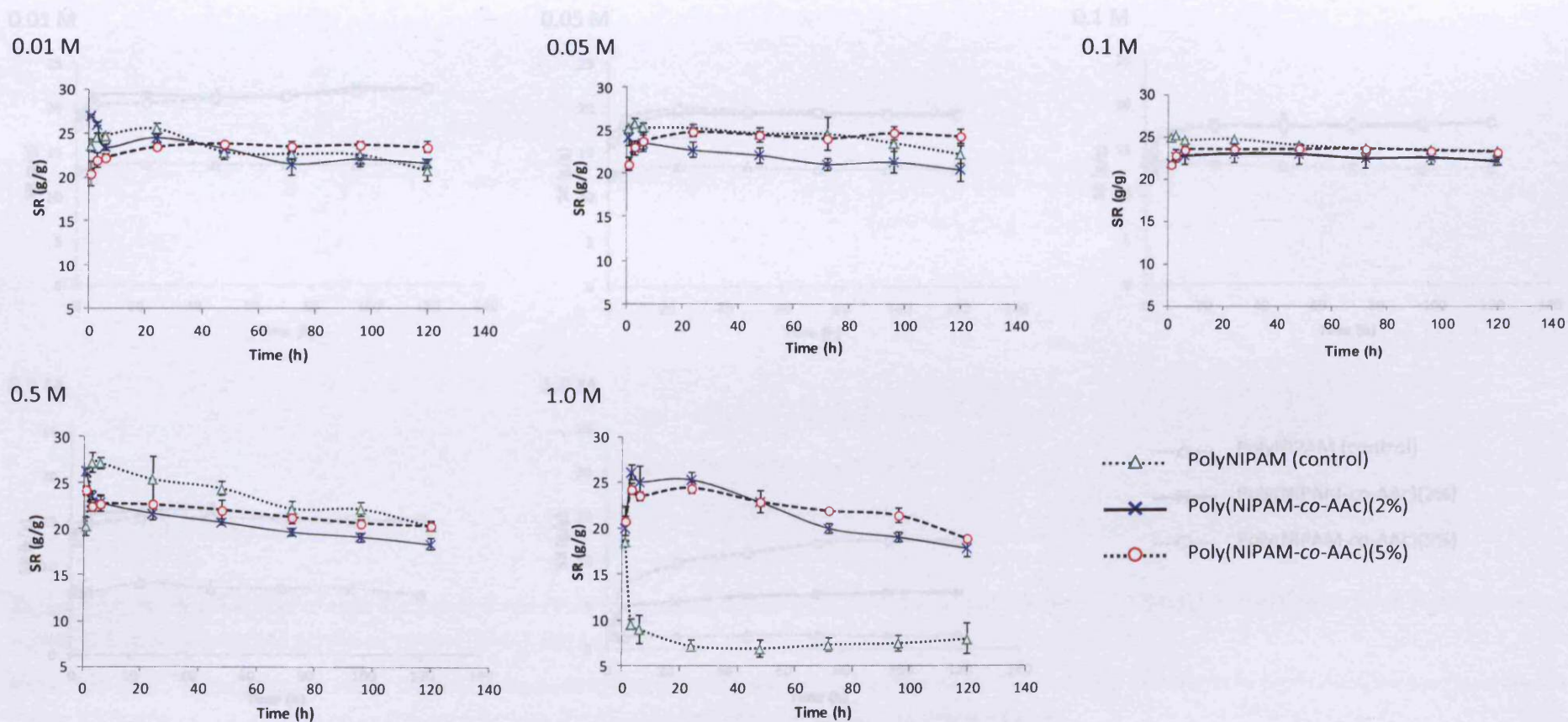


Figure 4-12: SR as a function of time for poly(NIPAM-co-AAc) nanogels dispersed in pH 5 acetate buffer, maintained at 2 – 4°C over a period of 5 days; polyNIPAM served as control and NaCl (0.01 – 1.00 M) used as the background electrolyte in all measurements (n=4, ± SD).

Note: The mass uptake of the acetate buffer solution declined with increasing concentrations of NaCl (0.01 → 1.0 M).

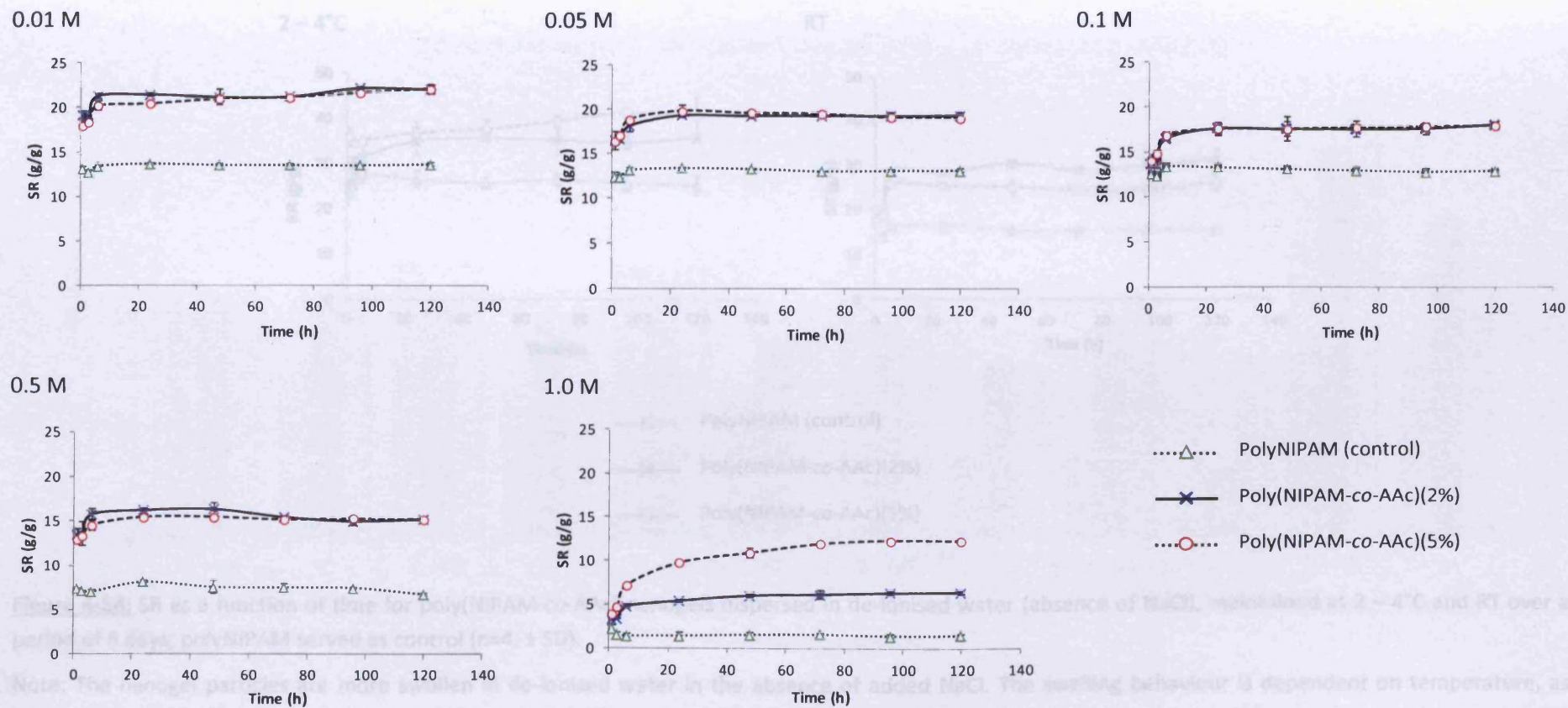


Figure 4-13: SR as a function of time for poly(NIPAM-co-AAc) nanogels dispersed in pH 5 acetate buffer, maintained at RT over a period of 5 days; polyNIPAM served as control and NaCl (0.01 – 1.00 M) used as the background electrolyte in all measurements (n=4, ± SD).

Note: The mass uptake of the acetate buffer solution declined with increasing concentrations of NaCl (0.01 – 1.0 M).

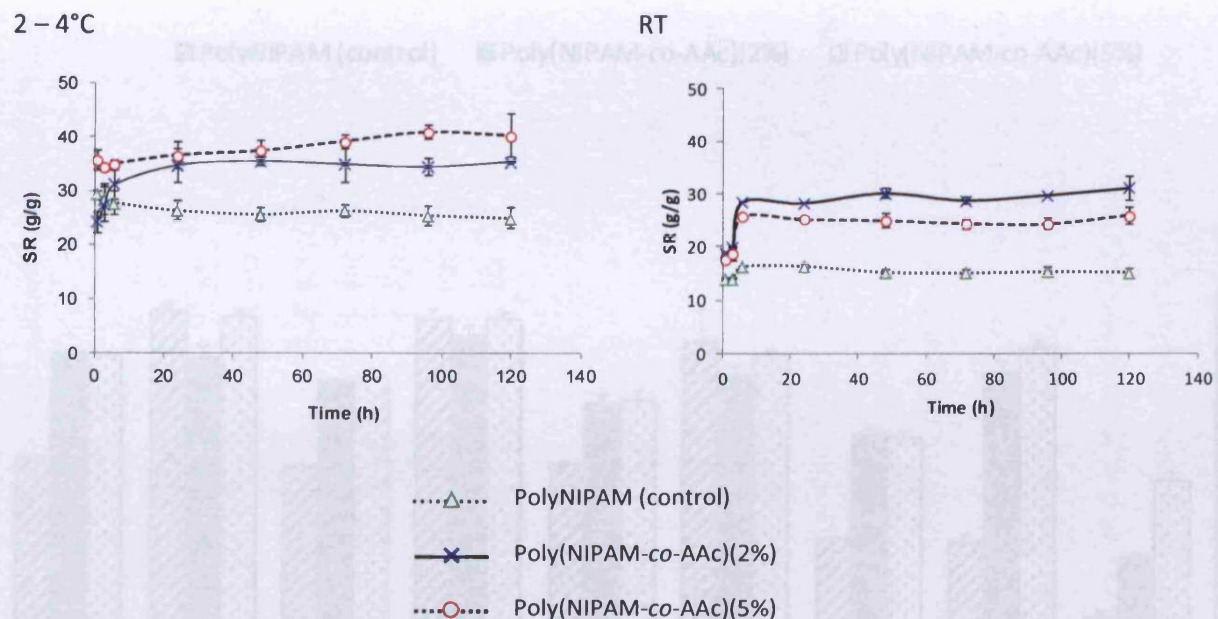


Figure 4-14: SR as a function of time for poly(NIPAM-co-AAc) nanogels dispersed in de-ionised water (absence of NaCl), maintained at 2 – 4°C and RT over a period of 5 days; polyNIPAM served as control (n=4, ± SD).

Note: The nanogel particles are more swollen in de-ionised water in the absence of added NaCl. The swelling behaviour is dependent on temperature, as higher SR values are attained at lower temperature (2 – 4°C) in comparison to the samples maintained at RT.

Note: Poly(NIPAM-co-AAc)(5%) exhibits the highest SR among the studied nanogels. The nanogel particles are more swollen in de-ionised water in the absence of added NaCl. Furthermore, the highest SR values are achieved for the samples maintained at 2 – 4°C.

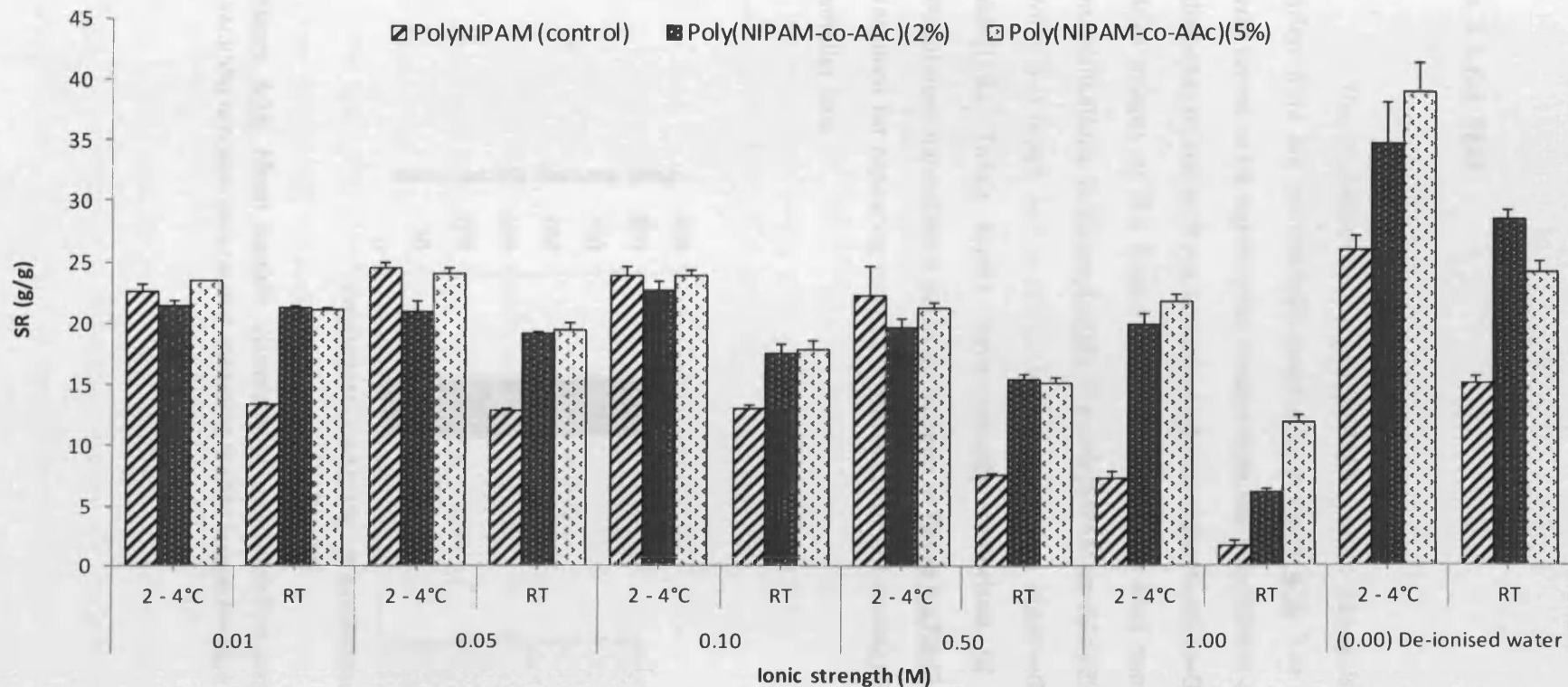


Figure 4-15: SR as a function of ionic strength for poly(NIPAM-co-AAc) nanogels in pH 5 acetate buffer, maintained at 2 – 4°C and RT for 3 days; polyNIPAM served as control and NaCl (0.01 – 1.00 M) used as the background electrolyte for the acetate buffer (n=4, ± SD).

Note: Poly(NIPAM-co-AAc)(5%) exhibits the highest SR among the studied nanogels. The nanogel particles are more swollen in de-ionised water in the absence of added NaCl. Furthermore, the highest SR values are achieved for the samples maintained at 2 – 4°C.

4.3.1.6 Size and Morphology

4.3.1.6.1 SEM

The diameter of the poly(NIPAM-co-AAc) nanogels as determined in their dried state are summarised graphically in [Figure 4-16](#). The poly(NIPAM-co-AAc)(5%) was found to be significantly smaller than the poly(NIPAM-co-AAc)(2%) with a mean diameter of 302 ± 13 nm and 311 ± 18 nm, respectively ($p=0.0342$). [Figure 4-17](#) shows SEM images of the freeze-dried poly(NIPAM-co-AAc) nanogels taken at different magnifications. In [Figure 4-17\(A\)](#), the poly(NIPAM-co-AAc)(2%) particles assembled to form 3-D layers and a similar arrangement was observed for the poly(NIPAM-co-AAc)(5%). Those layers were actually comprised of close-packed, narrowly distributed nanosphere particles as seen in [Figure 4-17\(B-C\)](#). A higher resolution was required for capturing images of the poly(NIPAM-co-AAc)(5%) particles due to their smaller size.

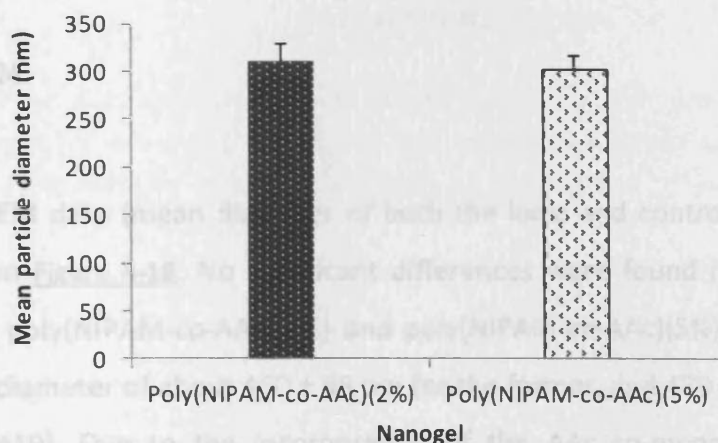


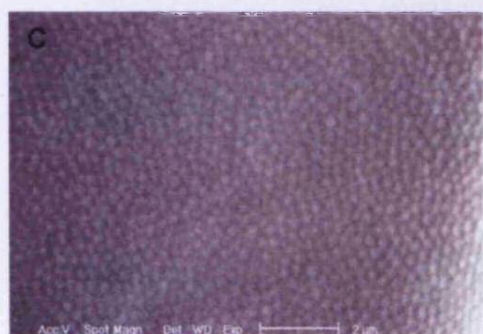
Figure 4-16: Mean particle diameters of poly(NIPAM-co-AAc)(2%) and poly(NIPAM-co-AAc)(5%) nanogels determined according to SEM images ($n=30$, \pm SD). $p=0.0342$



Scale bar: 50 μm (Magn: 1000x)



Scale bar: 5 μm (Magn: 10Kx)



Scale bar: 2 μm (Magn: 20Kx)

Figure 4-17: SEM images of freeze-dried nanogels – (A & B) poly(NIPAM-co-AAc)(2%) and (C) poly(NIPAM-co-AAc)(5%) particles.

4.3.1.6.2 TEM

The TEM data (mean diameter of both the ionic and control nanogels) are summarised in **Figure 4-18**. No significant differences were found in terms of size between the poly(NIPAM-co-AAc)(2%) and poly(NIPAM-co-AAc)(5%) in dried state, with a mean diameter of about 460 ± 98 nm for the former, and 470 ± 36 nm for the latter ($p=0.2419$). Due to the incorporation of the AAc co-monomer, the ionic nanogels were relatively larger as compared to the control nanogel (421 ± 63 nm). The diameter of poly(NIPAM-co-AAc)(5%) determined by TEM was found to be about 33% smaller than its hydrodynamic diameter, which was measured at its hydrated state by a laser light diffraction system at ambient temperature. As for the poly(NIPAM-co-AAc)(2%), the nanogel demonstrated only 20% diameter reduction.

The smaller particle diameter generated by TEM could be due to water evaporation on the TEM grid during the sample preparation.

TEM images of **Figure 4-19** confirmed that the poly(NIPAM-co-AAc) and control nanogels were successfully prepared as monodisperse nanospheres, in agreement with the SEM findings (Section 4.3.1.6.1). Furthermore, the nucleation process during synthesis was successful as shown by the presence of spherical structures in the images.

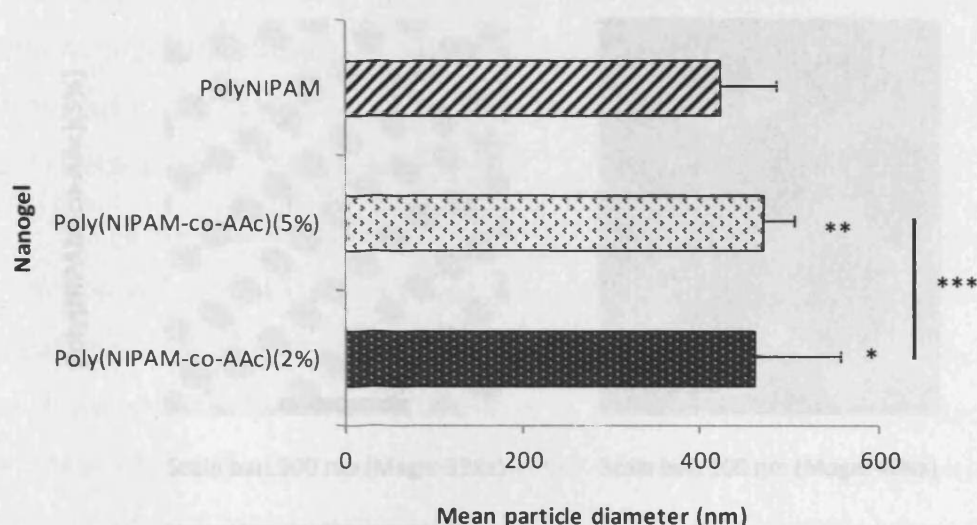


Figure 4-18: Mean particle diameters of poly(NIPAM-co-AAc)(2%) and poly(NIPAM-co-AAc)(5%) nanogels determined according to TEM images; polyNIPAM served as control (n=150, \pm SD). * $p=0.0001$, vs. control; ** $p=0.0001$, vs. control; and *** $p=0.2419$ between nanogels.

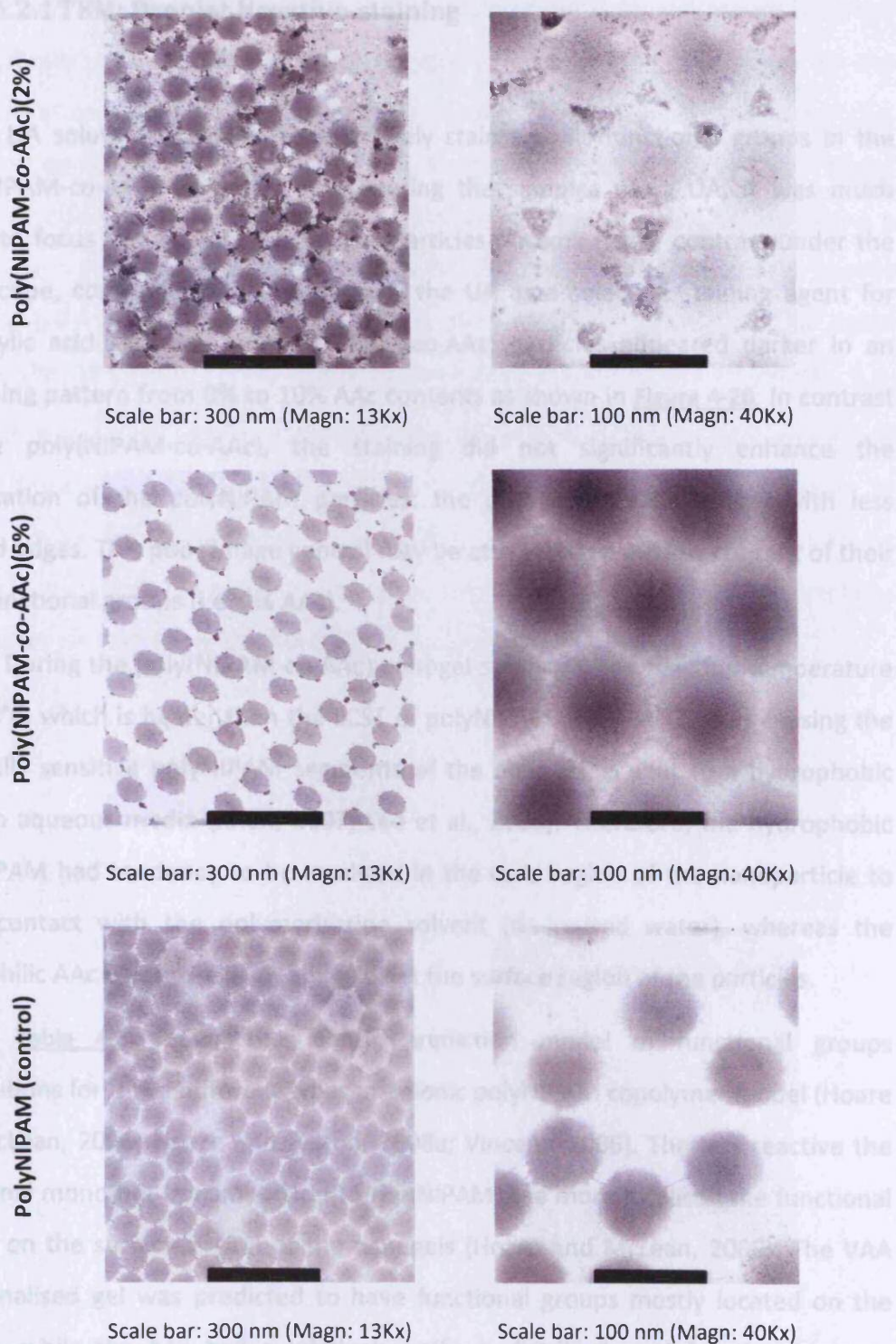


Figure 4-19: TEM images of poly(NIPAM-co-AAc)(2%) and poly(NIPAM-co-AAc)(5%) particles; polyNIPAM served as control.

4.3.1.6.2.1 TEM: Droplet Negative-staining

UA solution was used to selectively stain anionic functional groups in the poly(NIPAM-co-AAc) nanogels. By preparing the samples using UA, it was much easier to focus the nanospheres as the particles became highly contrast under the microscope, confirming the suitability of the UA as a selective staining agent for carboxylic acid groups. The poly(NIPAM-co-AAc) particles appeared darker in an increasing pattern from 0% to 10% AAc contents as shown in [Figure 4-20](#). In contrast to the poly(NIPAM-co-AAc), the staining did not significantly enhance the visualisation of the polyNIPAM particles: the particles appeared hazy with less defined edges. This poor image control may be attributed to the low content of their ionic functional groups (i.e. 0% AAc).

During the poly(NIPAM-co-AAc) nanogel synthesis, the reaction temperature was 70°C, which is higher than the LCST of polyNIPAM (32 – 34°C), thus causing the thermally sensitive polyNIPAM segments of the nanogel to shift to a hydrophobic state in aqueous media (Khan, 2007; Lee et al., 2008). Therefore, the hydrophobic polyNIPAM had tendency to be localised in the core region of the nanoparticle to avoid contact with the polymerisation solvent (de-ionised water), whereas the hydrophilic AAc was more likely to reside at the surface region of the particles.

[Table 4-3](#) shows the kinetic prediction model of functional groups distributions for three different types of anionic polyNIPAM copolymer model (Hoare and McLean, 2006; Hoare and Pelton, 2008a; Vincent, 2006). The less reactive the functional monomer in comparison to the NIPAM, the more localised the functional groups on the surface region of the nanogels (Hoare and McLean, 2006). The VAA functionalised gel was predicted to have functional groups mostly located on the surface, while the AAc had a relatively uniform distribution of functional groups throughout the gel (Hoare and Pelton, 2008b). MAA on the other hand, was found to have functional groups within the core of the gel. The cross-linker distribution was also predicted to be core-localised. According to the kinetic prediction model in [Table 4-3](#), NIPAM and AAc have reactivity ratio (r) for polymerisation of 0.57 and 0.32

respectively, which are almost similar. Thus, each of the monomer would have the same affinity to be localised in the core region of each particle. This is true for the poly(NIPAM-co-AAc)(5%) and poly(NIPAM-co-AAc)(10%), where their particles exhibited no distinct core-shell structure as shown in **Figure 4-20(E-F)** and **Figure 4-20(G-H)**, respectively. On the contrary, the poly(NIPAM-co-AAc)(2%) exhibited a somewhat reverse core-shell structure with the stained carboxylic acid groups localised more towards the core nanogel particles [**Figure 4-20(C-D)**]. This could explain why the nanogel lacked responsiveness towards thermal and pH stimuli.

It is worth noting that UA might stain the anionic sulfate initiator end group as well (Hoare and McLean, 2006; Vincent, 2006). Even though the presence of sulfate groups originated from the persulfate initiator is usually assumed to be negligible, its minor contribution should be taken into consideration. This explains the lightly pale staining of the polyNIPAM images [**Figure 4-20(A & B)**].

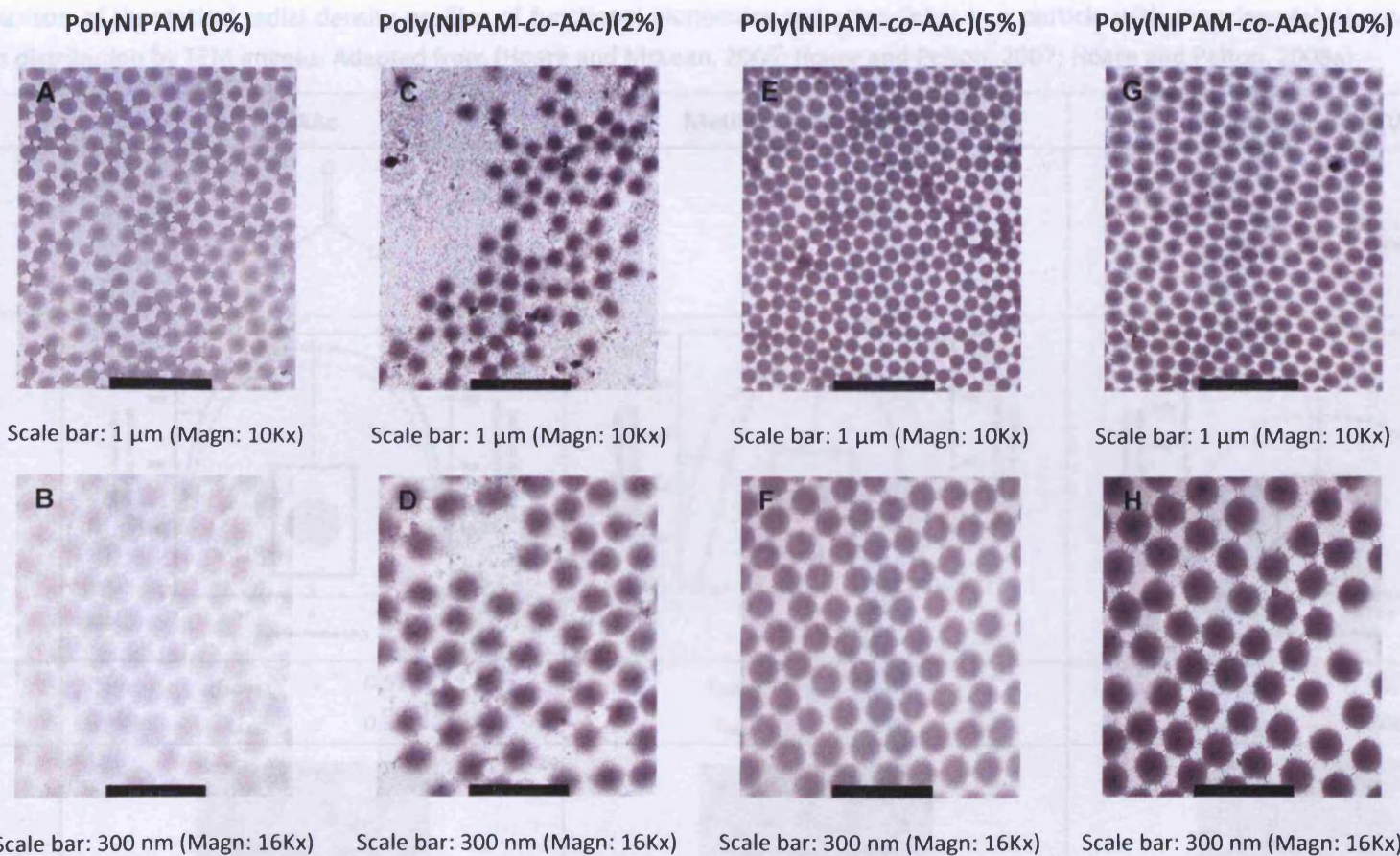


Figure 4-20: TEM images of poly(NIPAM-co-AAc) nanogels of varied AAc content (2, 5 and 10%), negatively stained with aqueous UA 2%; polyNIPAM served as control.

From the images it can be seen that there is enhanced intensity of image contrast and defined edges of nanospheres, from 0 → 10% of AAc content.

Table 4-3: Comparison of theoretical radial density profiles of functional monomers and cross-linker in a particle with experimental observation of a radial functional groups distribution by TEM images. Adapted from (Hoare and McLean, 2006; Hoare and Pelton, 2007; Hoare and Pelton, 2008a).

	AAc	Methacrylic acid (MAA)	Vinylacetic acid (VAA)
Co-monomer			
Radial Profile			
	r_{NIPAM} : 0.57 r_{AAc} : 0.32	r_{NIPAM} : 0.20 r_{MAA} : 2.8	r_{NIPAM} : 16.7 r_{VAA} : 0.002
TEM Image			

4.3.1.6.2 pH-responsive Effect

The mean diameter of the poly(NIPAM-co-AAc)(2%), poly(NIPAM-co-AAc)(5%) and control nanogels are summarised graphically in [Figure 4-21](#). The control nanogel contained only NIPAM monomer and was therefore expected not to respond significantly to any pH changes. This later proved to be true, as the diameter of its particles hardly changed between different pH environments. In general, the mean diameter of the poly(NIPAM-co-AAc) nanogels increased with the increasing pH, as a result of developing a bulk of negative charges originating from the carboxylic acid groups ionisation. For example, between pH 10 and pH 2, the diameter of poly(NIPAM-co-AAc)(5%) particles decreased by a factor of about 1.6.

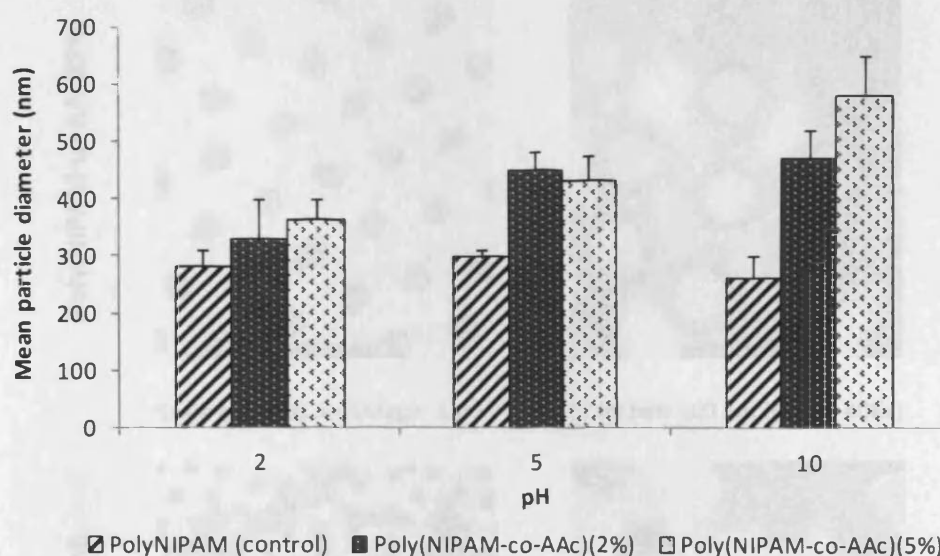


Figure 4-21: Mean particle diameter, as a function of pH for poly(NIPAM-co-AAc)(2%) and poly(NIPAM-co-AAc)(5%) nanogels determined according to TEM images; polyNIPAM served as control ($n=150, \pm$ SD).

[Figure 4-22](#), [Figure 4-23](#) and [Figure 4-24](#) present TEM images of the poly(NIPAM-co-AAc) nanogels dispersed in solutions of pH 2, 5 and 10 accordingly. The particles of each sample retained their spherical shape despite being in different environments, where they had either gained or lost volume. It can be seen that, the poly(NIPAM-co-AAc)(5%) particles exhibited the most pronounced swelling

conformation at pH 10, and this finding was consistent with the investigation carried out in Section 4.3.1.3.

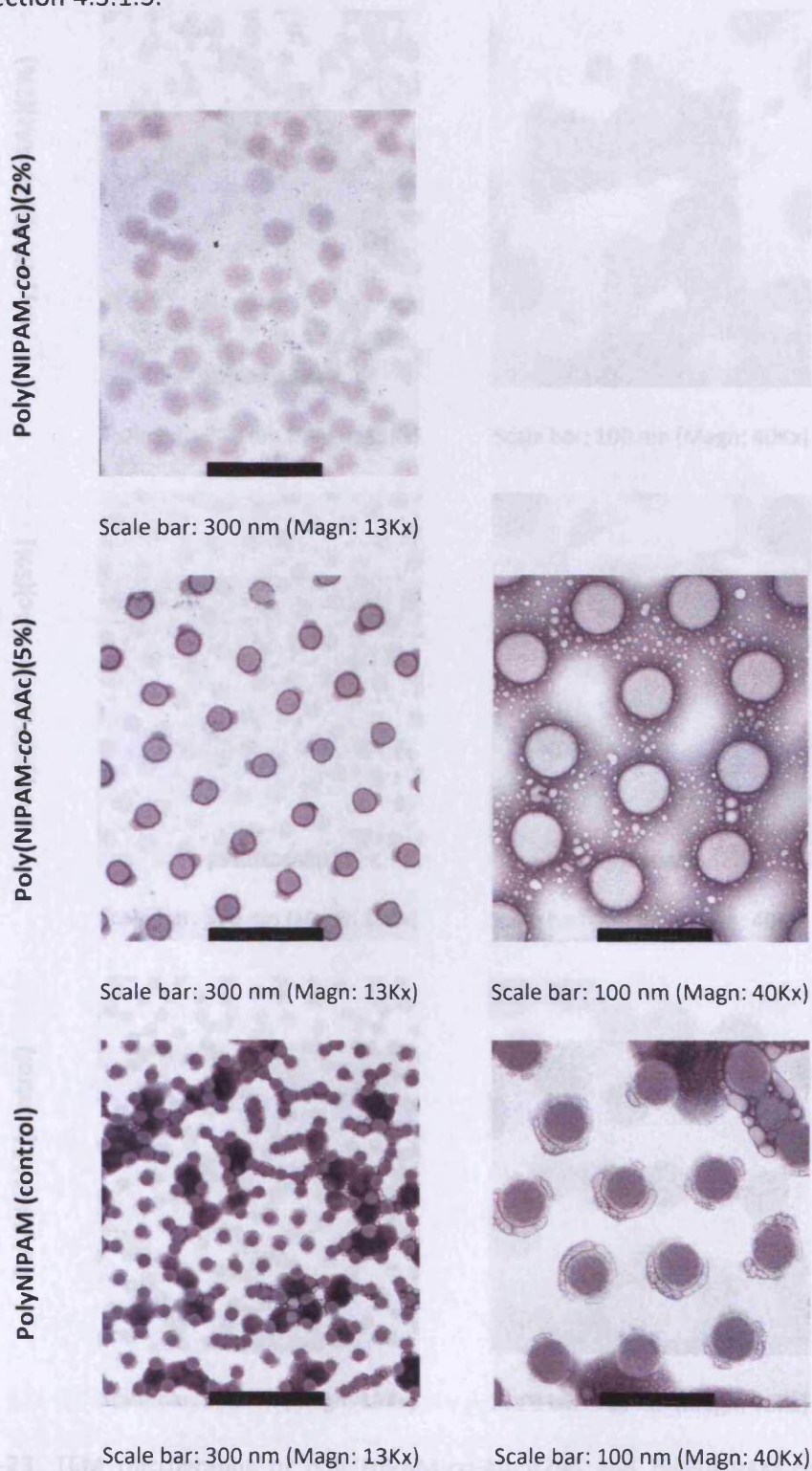


Figure 4-22: TEM micrographs of poly(NIPAM-co-AAc)(2%) and poly(NIPAM-co-AAc)(5%) nanogels in a buffer solution of pH 2, negatively-stained with aqueous UA 2%; polyNIPAM served as control.

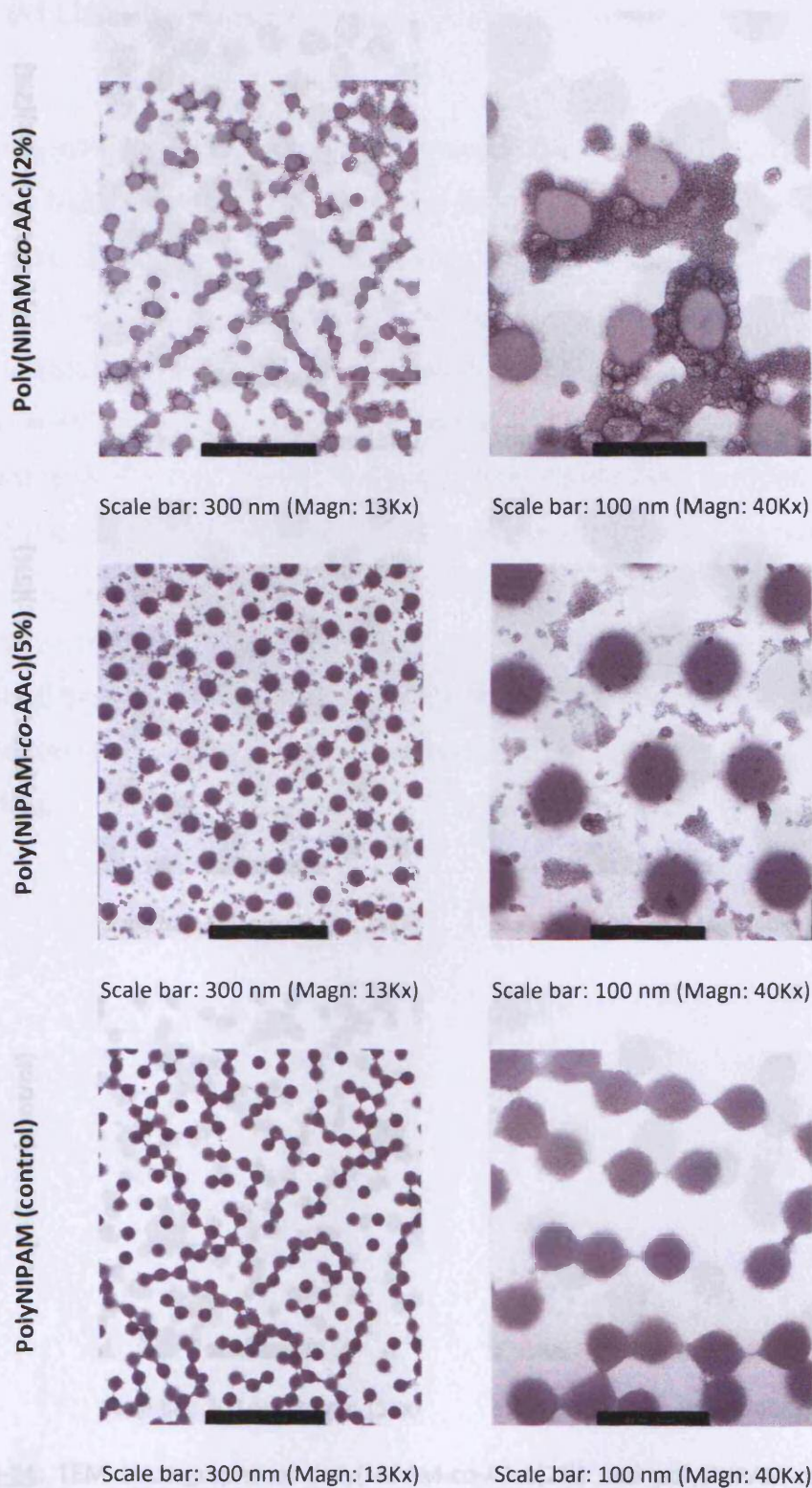


Figure 4-23: TEM micrographs of poly(NIPAM-co-AAc)(2%) and poly(NIPAM-co-AAc)(5%) nanogels in a buffer solution of pH 5, negatively-stained with aqueous UA 2%; polyNIPAM served as control.

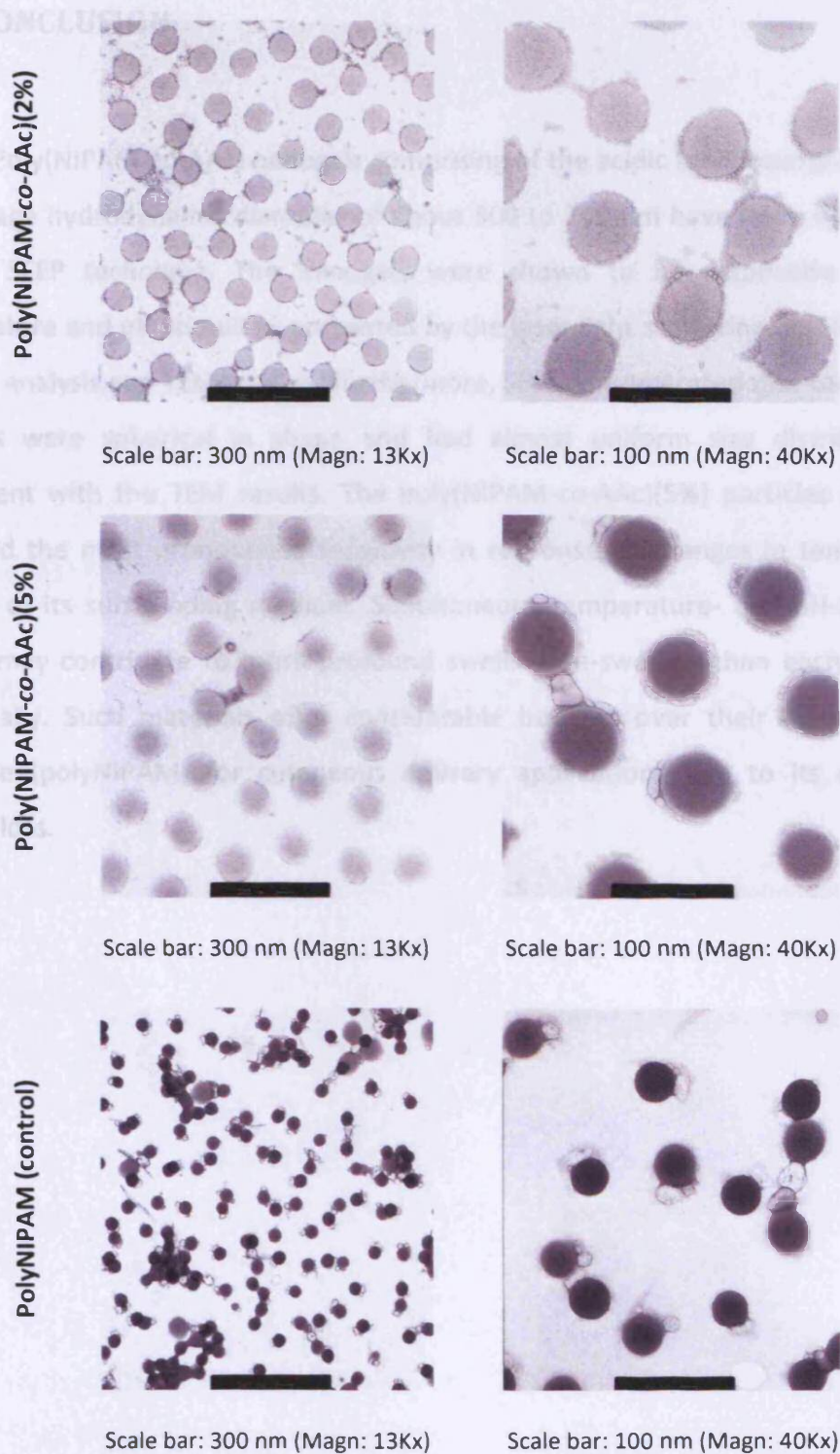


Figure 4-24: TEM micrographs of poly(NIPAM-co-AAc)(2%) and poly(NIPAM-co-AAc)(5%) nanogels in a buffer solution of pH 10, negatively-stained with aqueous UA 2%; polyNIPAM served as control.

4.4 CONCLUSION

Poly(NIPAM-co-AAc) nanogels comprising of the acidic functional groups with an average hydrodynamic diameter of about 500 to 700 nm have been synthesised by the SFEP technique. The nanogels were shown to be responsive towards temperature and pH stimuli as presented by the laser light scattering, swelling ratio, thermal analysis and TEM studies. Furthermore, SEM demonstrated that the nanogel particles were spherical in shape and had almost uniform size distribution in agreement with the TEM results. The poly(NIPAM-co-AAc)(5%) particles in water, exhibited the most pronounced sensitivity in response to changes in temperature and pH of its surrounding medium. Simultaneous temperature- and pH-triggering effects may contribute to more profound swelling/de-swelling than each stimulus individually. Such materials offer considerable benefits over their homopolymer analogue (polyNIPAM) for cutaneous delivery applications due to its enhanced volume loss.

CHAPTER 5 | Probing the Uptake
and Migration of Nanogel Particulates across
Skin

5.1 INTRODUCTION

Despite the growing body of evidence demonstrating the efficacy of nanoparticles in topical drug delivery, a mechanism remains to be established, as does any definitive evidence that such particles either penetrate or permeate the skin. Several methods have been proposed and established to investigate percutaneous penetration enhancement of a topically applied compound and its quantification:

- (i) *in vitro* diffusion study (flux measurement) (Williams, 2003) – quantifies the amount and the rate of permeation of the model compound.
- (ii) *in vitro* penetration study (tape stripping) (Moser et al., 2001) – investigates the amount and depth of penetration for the compound.
- (iii) microscopy visualisations (e.g. TEM and confocal laser scanning microscopy, CLSM) (Alvarez-Román et al., 2004b) – provide detailed information about the structure and physiological effects of the compound on the skin.

To date, investigations carried out on nanoparticles intended as carriers for topical drug delivery, centre on the use of biophysical techniques to image nanoparticles loaded with fluorescent probe within the skin, e.g. CLSM, and these have so far been of limited success. CLSM provides information about the localisation and the permeation pathway of a fluorescent model compound in the skin tissues based on intensity of the fluorescence signal. A study was conducted using CLSM to visualise the distribution of nanoparticles containing Nile red, a lipophilic and fluorescent probe in porcine ear skin, *in vitro* (Alvarez-Román et al., 2004b). It was found that the nanoparticulate encapsulation increased fluorescence intensity across the SC. However, this study could not determine whether the fluorescence observed in the CLSM images, originated from the intact particles (fluorophore associated with the particles) and/or from the free fluorophore

(released from the particles). The same problem would rise with the penetration studies involving fluorophore-loaded nanoparticles.

Markers can be chemically bound to carrier particles to ensure that the fluorescence detected by CLSM originated from the nanoparticles, such as non-biodegradable polystyrene nanoparticles containing covalently bound fluorophore (Alvarez-Román et al., 2004c). However, the attachment of these markers may influence the permeability behaviour of the particles (e.g. rate, extent and route of penetration). Also, only a limited range of fluorophores are available for specific purpose of imaging (Alvarez-Román et al., 2004a).

Following the synthesis of pH- and temperature-responsive nanogels in CHAPTER 4, the current work focussed on the polyNIPAM and its copolymer poly(NIPAM-*co*-AAc) nanogel. It was demonstrated in [Figure 4-9](#) that lowering the pH of a solution to less than the pK_a of AAc residues ($pK_a = 4.25$), caused the poly(NIPAM-*co*-AAc)(5%) nanogel particles to collapse, reflected by the reduction in their mean particle diameter. By inference, this would lead to release of their content to the surrounding medium. In addition, it is known that polyNIPAM copolymers that form hydrogen-bonded complexes involving carboxylic acid groups ($-\text{COOH}$) may exhibit temperature sensitivity upon increased temperature, but this usually disappears when the pH of their environment is raised above the pK_a of the acid groups, ionising them to carboxylate ($-\text{COO}^-$) (Kokufuta et al., 1998). Although the nanogel particles gradually collapsed as temperature was raised, the temperature sensitivity would not occur, as the particles were swollen owing to the ionisation of the carboxyl groups and the consequent disruption of the complex.

CA as illustrated in [Figure 5-1](#) was utilised as a model pH modulator. It is categorised as a α -hydroxy acid (AHA), a group of water soluble acids with a hydroxyl group ($-\text{OH}$) in the alpha position (Baumann and Saghari, 2009; Draelos, 2002). It can be extracted from citrus fruits (e.g. lemon)(Baumann and Saghari, 2009) or prepared synthetically by fermentation (US Food & Drug Administration, 1994). In consumer products particularly cosmetics and personal care, CA has a wide variety of functions including as chelating agents or pH adjusters (Mayer et al., 1993). The CIR panel concluded that CA is safe for use as it is on the list of direct food substances affirmed

as Generally Recognised as Safe (GRAS) by the FDA (US Food & Drug Administration, 1994).

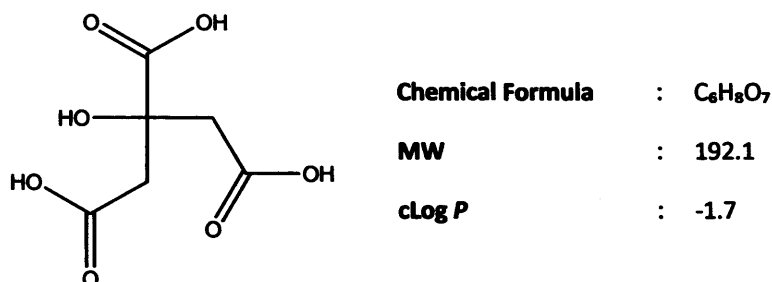


Figure 5-1: Chemical structure and physicochemical data for CA.

In the current work, we took the view that if nanogel particles indeed penetrate into the SC or appendages, then ultimately they could be expected to migrate all the way across the skin. In an *in vitro* setting using heat-separated epidermal as a model membrane, it should therefore be possible to locate them within the receptor phases of diffusion cells. The aim of this work was to probe the potential of polyNIPAM nanogel particles in the presence and absence of an ionic comonomer (AAc), with diameters <1 μm to serve as carriers in drug delivery by TEM imaging. Two types of unloaded nanogels were investigated:

- (i) Poly(NIPAM-*co*-AAc)(5%) – temperature-sensitive polyNIPAM modified using AAc to yield particles with pH-responsive swelling properties. Since the nanogel exhibited the most pronounced response towards changes in its environment of all the prepared nanogels in CHAPTER 4, it was selected for further investigation, and
- (ii) Temperature-sensitive polyNIPAM served as a control nanogel.

Effect of an external pH modulator of acidic functionality (i.e. CA molecules) on migration of the unloaded poly(NIPAM-*co*-AAc)(5%) particles was also investigated. As the VPTT of poly(NIPAM-*co*-AAc)(5%) may be influenced by acidic and basic environments, an additional investigation was carried out involving the environment created by the pH modulator.

5.2 MATERIALS AND METHODS

5.2.1 Materials

CA anhydrous (99.5%), Hanks' balanced salt buffer, and PBS (pH 7.4) were all purchased from Sigma-Aldrich Company Ltd. (Poole, UK). HPLC-grade solvents were purchased from Fisher Scientific (Loughborough, UK). MTX was obtained from Heumann PCS GmbH (Feucht, Germany). Pioloform[®] and UA were purchased from Agar Scientific Ltd. (Stansted, UK). Freshly excised porcine ears were obtained from a local abattoir prior to steam cleaning and immersed in iced Hanks' buffer upon excision. Poly(NIPAM-co-AAc)(5%) and polyNIPAM nanogels were synthesised as detailed in Section 4.2.2.1.

5.2.2 Methods

Figure 5-2, briefly depicts the main approach of the work in this chapter. The first phase involves the application of swollen nanogel particles onto heat-separated porcine epidermal membranes installed in glass Franz diffusion cells. After 24 h, the receptor phases were retrieved and analysed by TEM imaging. The second part of the investigation was carried out with the aim of validating the integrity of the epidermal membranes post-treatment with the nanogels. To this end, the membranes were re-used and the permeation of a model compound (MTX) determined under several conditions.

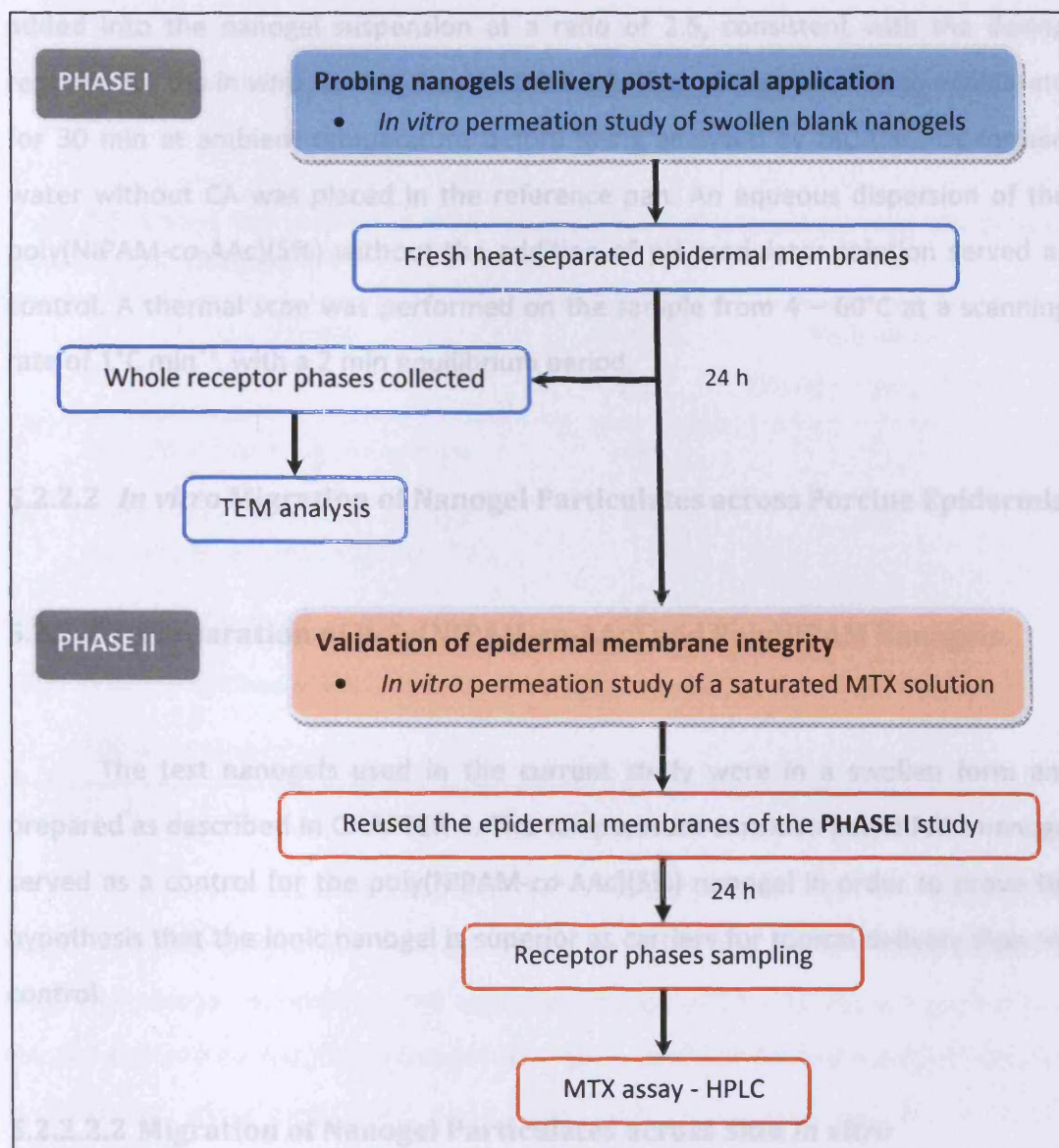


Figure 5-2: Schematic diagram of the experimental design.

5.2.2.1 Thermal Analysis: Phase Transition in the Presence of pH Modulator (CA)

DSC analysis was performed using the MC-DSC instrument according to the protocol detailed in Section 2.2.2.3.3. However, the samples were prepared by the addition of a pH modulator, aqueous solution of CA. Briefly, a stock nanogel suspension was prepared by dispersing the swollen poly(NIPAM-co-AAc)(5%) in de-ionised water, at a concentration of 50% w/v. Aqueous solution of CA (5% w/v) was

added into the nanogel suspension at a ratio of 2:5, consistent with the dosing regimen for the *in vitro* work in Section 5.2.2.2.2. The mixture was left to equilibrate for 30 min at ambient temperature before being analysed by MC-DSC. De-ionised water without CA was placed in the reference pan. An aqueous dispersion of the poly(NIPAM-*co*-AAc)(5%) without the addition of pH modulator solution served as control. A thermal scan was performed on the sample from 4 – 60°C at a scanning rate of 1°C min⁻¹, with a 2 min equilibrium period.

5.2.2.2 *In vitro* Migration of Nanogel Particulates across Porcine Epidermis

5.2.2.2.1 Preparation of Poly(NIPAM-*co*-AAc) and PolyNIPAM Nanogels

The test nanogels used in the current study were in a swollen form and prepared as described in CHAPTER 4. The temperature-sensitive polyNIPAM nanogel served as a control for the poly(NIPAM-*co*-AAc)(5%) nanogel in order to prove the hypothesis that the ionic nanogel is superior as carriers for topical delivery than the control.

5.2.2.2.2 Migration of Nanogel Particulates across Skin *In vitro*

Heat-separated porcine epidermal membranes were prepared according to the technique described in Section 3.2.2.4. *In vitro* migration study was carried out according to the protocol described in Section 3.2.2.5. **Figure 5-3** illustrates the cells set up for this experiment. Briefly, the epidermal membrane sections were installed in the glass Franz diffusion cells and the receptor compartments filled with temperature-equilibrated (~32°C), degassed de-ionised water (receptor phase) using a syringe. De-ionised water was used as the receptor phase, in order to exclude any salt or ionic environment which might influence behaviour of the nanogels. After 15 min, samples were applied to the surface of the skin using a pipette and then a blunt

glass rod was used to gently massage (20 circular motions) the samples onto the membranes. Five dosing procedures as listed in **Table 5-1** were used.

Table 5-1: Dosing regimens for *in vitro* migration study of nanogel particles across heat-separated porcine epidermis.

	Sample	Nanogel (μL)	Aqueous CA (5% w/v, $\sim\text{pH 1.9}$) (μL)
(i)	Poly(NIPAM-co-AAc)(5%) nanogel	500	–
(ii)	Poly(NIPAM-co-AAc)(5%) nanogel, followed by aqueous solution of CA	500	200
(iii)	PolyNIPAM nanogel	500	–
(iv)	Aqueous solution of CA	–	200
(v)	500 μL de-ionised water	–	–

Three replicates were prepared for each test sample ($n=3$). The membranes dosed with the polyNIPAM nanogel served as a control for the poly(NIPAM-co-AAc)(5%) nanogel. In addition, the aqueous solution of CA was added together with the poly(NIPAM-co-AAc)(5%) nanogel, as a pH modulator for the nanogel particles. Furthermore, some membranes were dosed with the aqueous solution of CA (5% w/v) alone, in order to determine whether the pH modulator could cause any damage to the skin barrier. Membranes treated with de-ionised water were used as an overall control. After 24 h, the receptor phases were retrieved using individual Pasteur pipettes to avoid cross-contamination and immediately analysed by TEM. The membranes were also retrieved for validation of membrane integrity.

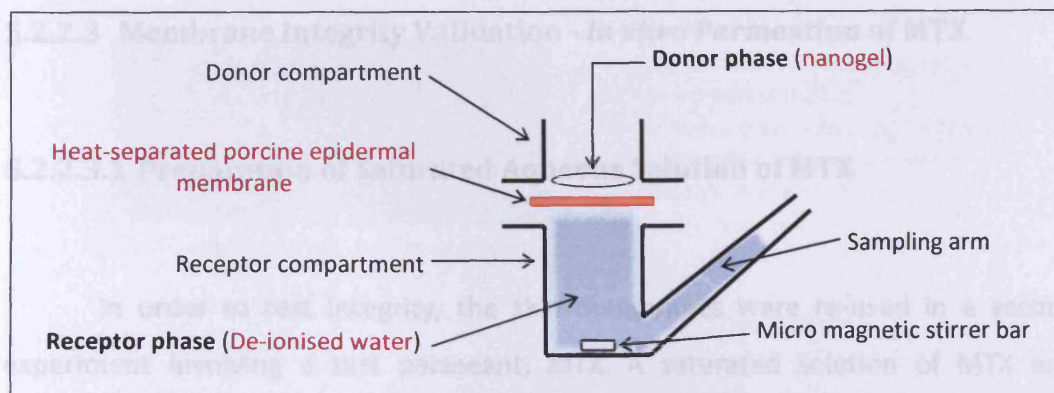


Figure 5-3: Sketch of a Franz diffusion cell set up for *in vitro* investigation of poly(NIPAM-co-AAc)(5%) particulate migration across heat-separated porcine epidermis. PolyNIPAM nanogel served as control.

5.2.2.2.3 TEM Analysis

Receptor phases were scrutinised for the presence of nanogel particles using a Phillips EM 208 instrument operated at 80 kV accelerated voltage. Approximately 10 μL of each receptor phase sample was transferred using a pipette onto a 200-mesh size Pioloform[®]-coated copper grid. The sample was stained with UA (2% w/v) according to the negative-stained technique (Section 4.2.2.3.4.2.1). In order to minimise any loss of particles on the grid, the sample was not washed with distilled water. The magnification selected was sufficient to examine the general morphology of the sample under study. At least five micrographs were taken for each sample ($n=5$). Quantitative measurements of the TEM micrographs were laboriously performed using a digital image processing ImageJ, version 1.43f (National Institute of Health, Bethesda, MD).

5.2.2.3 Membrane Integrity Validation - *In vitro* Permeation of MTX

5.2.2.3.1 Preparation of Saturated Aqueous Solution of MTX

In order to test integrity, the skin membranes were re-used in a second experiment involving a test permeant, MTX. A saturated solution of MTX was prepared by adding excess drug into 15 mL of de-ionised water in an amber glass bottle until no further dissolution was observed visually. The mixture was left to equilibrate for 24 h at ambient temperature on a SB1 Stuart® blood tube rotator, before being spun in a Beckman Coulter Avanti® J-25 centrifuge at 5,000 x g, 25°C for 1 h. The supernatant was sampled and used immediately.

5.2.2.3.2 *In vitro* Skin Permeation of MTX

In vitro skin permeation was generally carried out according to the method outlined in Section 3.2.2.5. The membranes were carefully recovered from the nanogel migration test, rinsed with de-ionised water and gently blotted with soft tissues before being examined by a magnifying lens to check for any physical damage after being exposed to the nanogels. The membranes were re-mounted in the glass Franz diffusion cells as shown in [Figure 5-4](#). A receptor phase of PBS was used to provide a good sink condition for MTX. Each membrane was dosed with 500 µL of the aqueous saturated solution of MTX ($0.17 \pm 0.001 \text{ mg mL}^{-1}$, ~pH 4.6) using a pipette and rubbed gently using a glass rod (20 times). After 24 h, the receptor phases were collected and immediately assayed for MTX by HPLC.

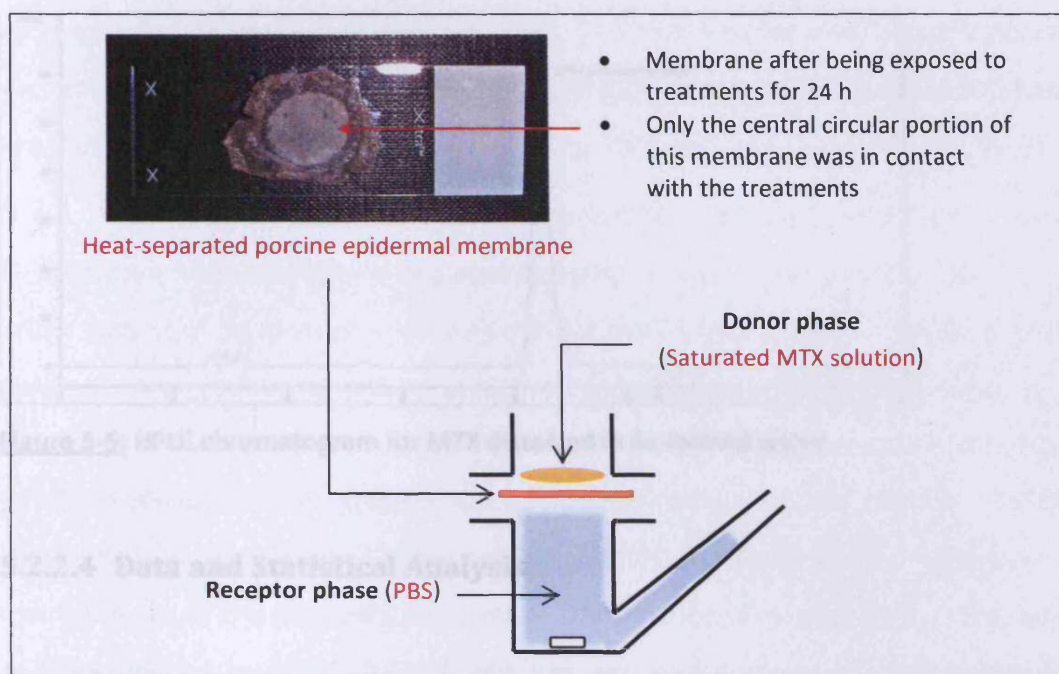


Figure 5-4: Sketch of a Franz diffusion cell set up to determine *in vitro* permeation of MTX across the same skin membranes used in Section 5.2.2.2.2.

5.2.2.3.3 Quantitative Analysis

Samples were analysed for MTX by reverse-phase liquid chromatography using an Agilent 1100 series automated system with Agilent ChemStation software. The HPLC method was developed in-house: A Gemini-NX C₁₈ ODS 250 x 4.6 mm, 5 μm column (Phenomenex Inc., Macclesfield, UK), fitted with a Phenomenex SecurityGuard guard column. The mobile phase was 3:1 potassium phosphate buffer (0.1 M, pH 6.5) and methanol, with flow rate set at 1 mL min⁻¹. Sample injection volume was 20 μL , detection was by UV at $\lambda = 305 \text{ nm}$ and the runtime was 15 min. For calibration, a stock solution of MTX was prepared in de-ionised water and a standard calibration curve obtained over the range of 0.8 – 200 $\mu\text{g mL}^{-1}$. Excellent linearity was achieved, as evidenced by R^2 of 0.99, with the LOD of 8.3 $\mu\text{g mL}^{-1}$. MTX was found to elute at $\sim 8 \text{ min}$, as shown in [Figure 5-5](#). The peak areas of samples were calculated and the concentrations of MTX in samples were extrapolated using the calibration coefficient. For quantitation of MTX in PBS (the receptor phase of the permeation test), the protocol is outlined in Section 3.2.2.5.1.

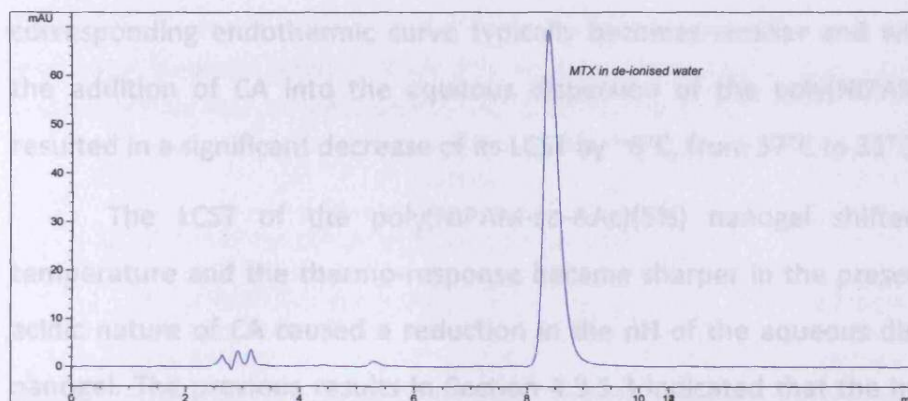


Figure 5-5: HPLC chromatogram for MTX dissolved in de-ionised water.

5.2.2.4 Data and Statistical Analysis

Data analysis was performed using Excel 2007 (Microsoft Office, Microsoft Corp., Redmond, WA) and expressed as a mean \pm SD. Statistical tests were performed with InStat[®] for Macintosh, version 3.00 (GraphPad Software Inc., San Diego, CA). Significant differences and comparisons of the means between paired data were made using Student's *t*-test. For multiple comparisons, a one-way ANOVA analysis was carried out with Tukey's post-test to identify statistical significances between groups. Confidence interval was 95% with $p < 0.05$ considered as significant.

5.3 RESULTS AND DISCUSSION

5.3.1 Thermal Analysis: Phase Transition

Figure 5-6 shows the MC-DSC thermograms of poly(NIPAM-*co*-AAc)(5%) nanogel in the presence of the pH modulator (CA), whereas **Table 5-2** presents the LCST data of the nanogel. The LCST of the aqueous dispersion of poly(NIPAM-*co*-AAc)(5%) nanogel was found to be around 37°C in comparison to the homopolymer polyNIPAM, ~35°C. As discussed in CHAPTER 4, the addition of a hydrophilic comonomer, i.e. AAc, is usually accompanied by an increase in the LCST and the

corresponding endothermic curve typically becomes smaller and wider. However, the addition of CA into the aqueous dispersion of the poly(NIPAM-co-AAc)(5%), resulted in a significant decrease of its LCST by $\sim 6^{\circ}\text{C}$, from 37°C to 31°C ($p < 0.0001$).

The LCST of the poly(NIPAM-co-AAc)(5%) nanogel shifted to a lower temperature and the thermo-response became sharper in the presence of CA. The acidic nature of CA caused a reduction in the pH of the aqueous dispersion of the nanogel. The previous results in Section 4.3.1.3 indicated that the hydrophilicity of the nanogel decreased with a decrease in pH. This is probably because the acidic environment led to the protonation of carboxyl groups of the nanogel particles (Mizoguchi et al., 2010; Peppas et al., 2000) resulting in the reduction of hydrophilicity of the nanogels. Another possible reason was suggested, is that inter- or intra-polymer hydrogen interactions between amide group of NIPAM chain and carboxyl group in AAc segment or between two carboxyl groups may also have contributed to the decrease in hydrophilicity of the poly(NIPAM-co-AAc)(5%) at lower pH (Mizoguchi et al., 2010).

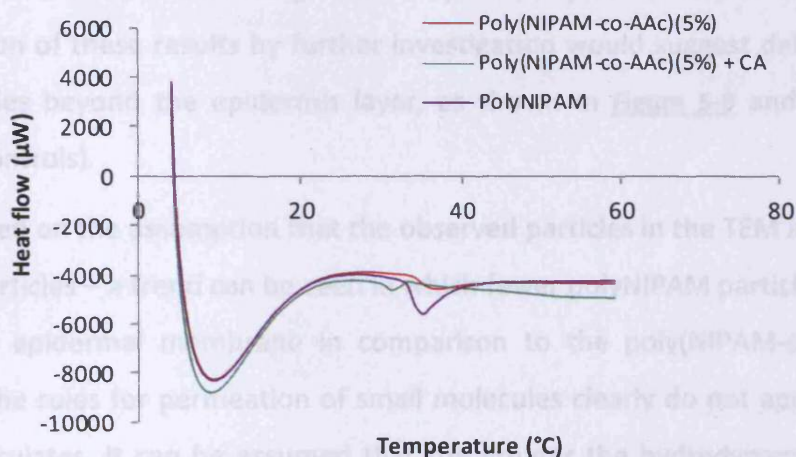


Figure 5-6: MC-DSC thermogram of an aqueous dispersion of poly(NIPAM-co-AAc)(5%) in the presence of a pH modulator (aqueous solution of CA, 5%); aqueous dispersions of pH modulator-free poly(NIPAM-co-AAc)(5%) and polyNIPAM served as control.

Table 5-2: Phase transition of poly(NIPAM-co-AAc)(5%) nanogel in the presence of a pH modulator (aqueous solution of CA, 5%); aqueous dispersions of poly(NIPAM-co-AAc)(5%)- and polyNIPAM-free pH modulator served as control (n=3 ± SD).

Sample	LCST (°C)
Poly(NIPAM-co-AAc)(5%) in aqueous solution of CA	31 ± 1 × 10 ⁻⁴
Poly(NIPAM-co-AAc)(5%)	37 ± 6 × 10 ⁻⁵
PolyNIPAM	35 ± 4 × 10 ⁻⁵

5.3.2 Evidence of Nanogel Particulates in Receptor Phase

For the TEM analysis, the content of each receptor phase was considered to be uniformly distributed across the grid during the sample preparation. The grid was assumed to have an equal size of squares (200 squares per grid), thus no specific unit was assigned for each square. Nanoparticles were observed in the receptor samples following the application of the nanogels as shown in [Figure 5-7](#) and [Figure 5-8](#). The particles were identified as poly(NIPAM-co-AAc)(5%) and polyNIPAM nanogels based on comparison to the TEM images of the particles prior to the *in vitro* studies. Confirmation of these results by further investigation would suggest delivery of the nanoparticles beyond the epidermis layer, as shown in [Figure 5-9](#) and [Figure 5-10](#) (positive controls).

Based on the assumption that the observed particles in the TEM images were nanogel particles – a trend can be seen in which fewer polyNIPAM particles migrated across the epidermal membrane in comparison to the poly(NIPAM-co-AAc)(5%). Although the rules for permeation of small molecules clearly do not apply to nano-sized particulates, it can be assumed that the greater the hydrodynamic diameter the more arduous migration process. [Figure 5-11](#) presents the TEM images of the receptor phases, 24 h following the application of the aqueous solution of CA [[Figure 5-11\(A & B\)](#)] and de-ionised water [[Figure 5-11\(C & D\)](#)] in the absence of nanogels on the porcine epidermal membranes (negative controls); only skin debris (filamentous-like structures) and lipid vesicles (lamellar structures) present in the receptor phases are observed.

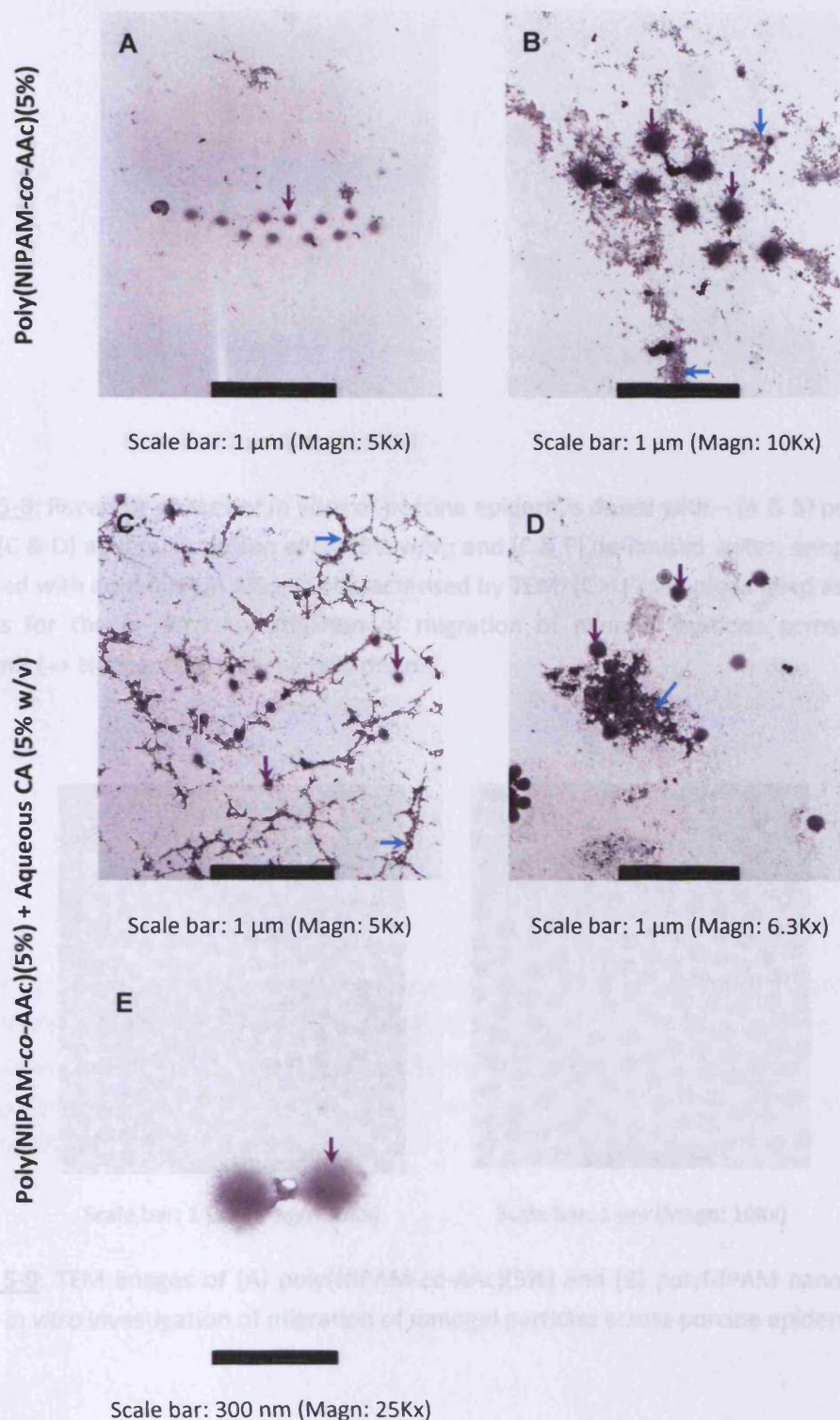


Figure 5-7: Receptor phases of *in vitro* of porcine epidermis dosed with – (A & B) poly(NIPAM-co-AAc)(5%) and (C – E) poly(NIPAM-co-AAc)(5%), followed by aqueous solution of CA (5% w/v), sampled at 24 h, stained with aqueous UA 2% and characterised by TEM; (→ Nanogel particle; → Skin debris).

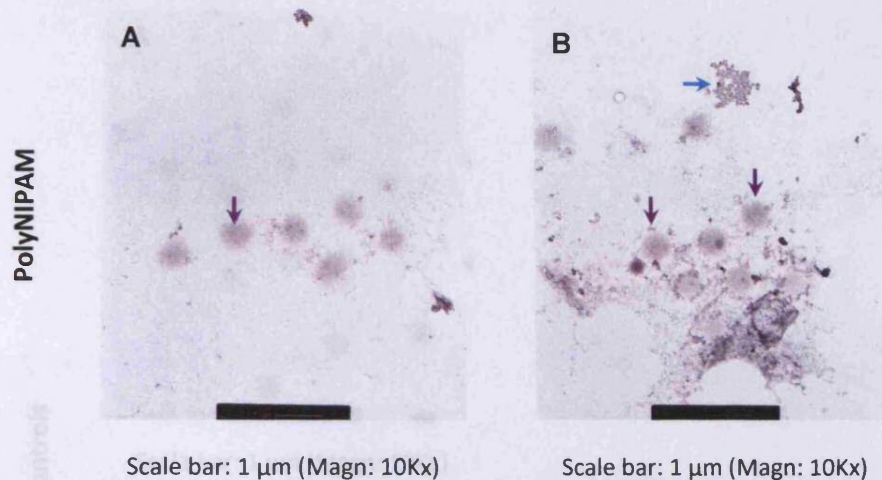


Figure 5-8: Receptor phases of *in vitro* of porcine epidermis dosed with – (A & B) polyNIPAM alone; (C & D) aqueous solution of CA (5% w/v); and (E & F) de-ionised water, sampled at 24 h, stained with aqueous UA 2% and characterised by TEM; (C – F) samples served as negative controls for the *in vitro* investigation of migration of nanogel particles across porcine epidermis (→ Nanogel particle; → Skin debris).

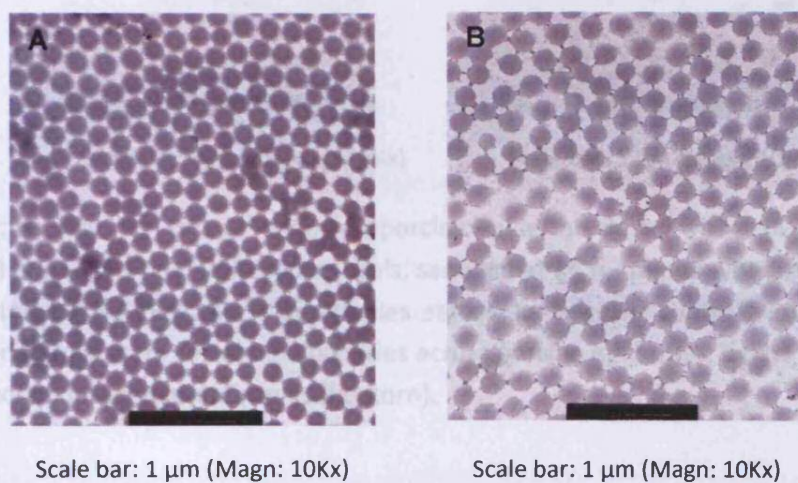


Figure 5-9: TEM images of (A) poly(NIPAM-co-AAc)(5%) and (B) polyNIPAM nanogels used for the *in vitro* investigation of migration of nanogel particles across porcine epidermis.

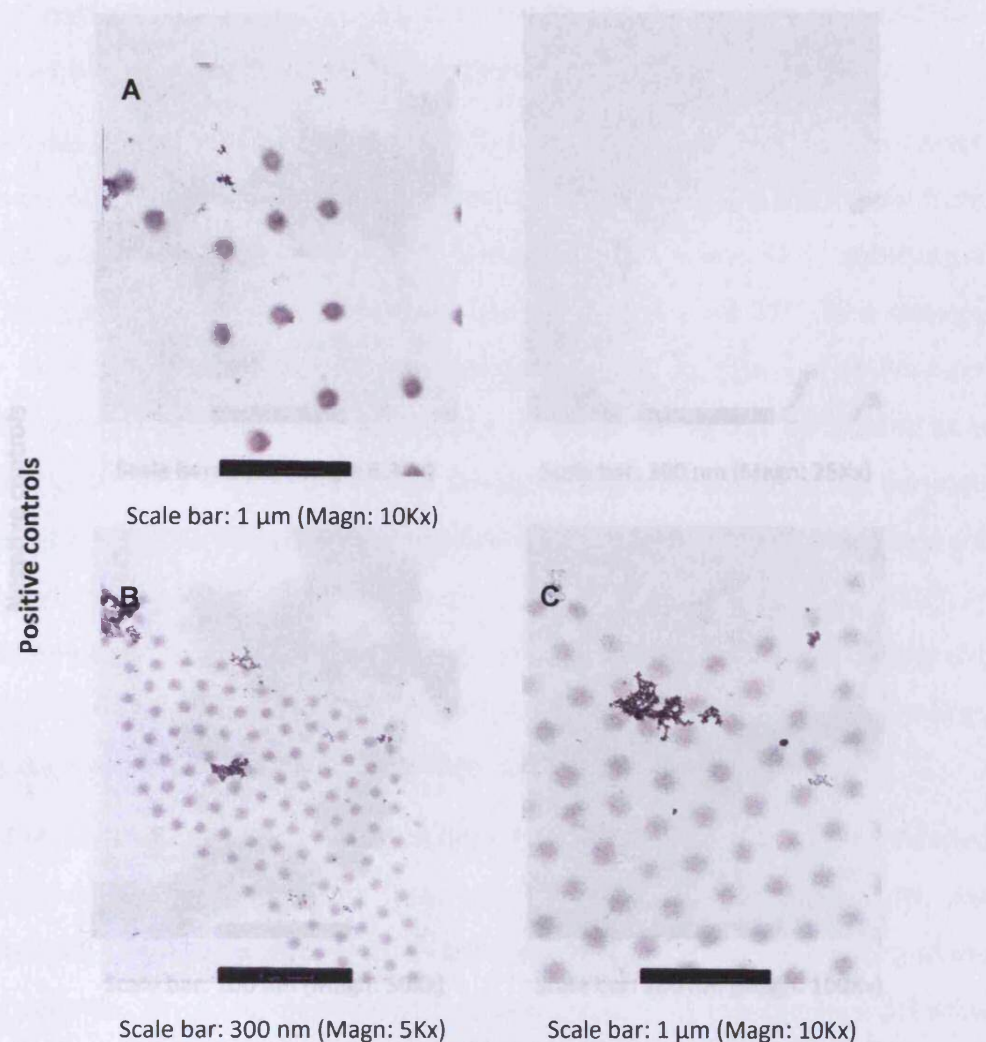


Figure 5-10: Receptor phases of *in vitro* of porcine epidermis dosed with – (A & B) aqueous

Figure 5-10: Receptor phases of *in vitro* of porcine epidermis dosed with – (A) poly(NIPAM-co-AAc)(5%) and (B & C) polyNIPAM nanogels, sampled at 24 h, stained with aqueous UA 2% and characterised by TEM; (A – C) samples served as positive controls for the *in vitro* investigation of migration of nanogel particles across porcine epidermis, where the nanogels were applied on defected membranes (i.e. torn).

Figure 5-12 shows the relative quantities of particles detected in the receptor phases after 24 h. There was a significant difference in levels of particle migration between the polyNIPAM and poly(NIPAM-co-AAc)(5%) ($p=0.0434$). The trend may be explained as the polyNIPAM particles only being responsive towards a thermal stimulus (32°C, average skin surface temperature), whereas the poly(NIPAM-co-AAc)(5%) particles were responsive towards both thermal and pH stimuli (skin surface temperature and pH) as previously discussed (sections 4.3.1.2 and 4.3.1.3). The responsiveness of the nanogel particles towards a particular stimulus was

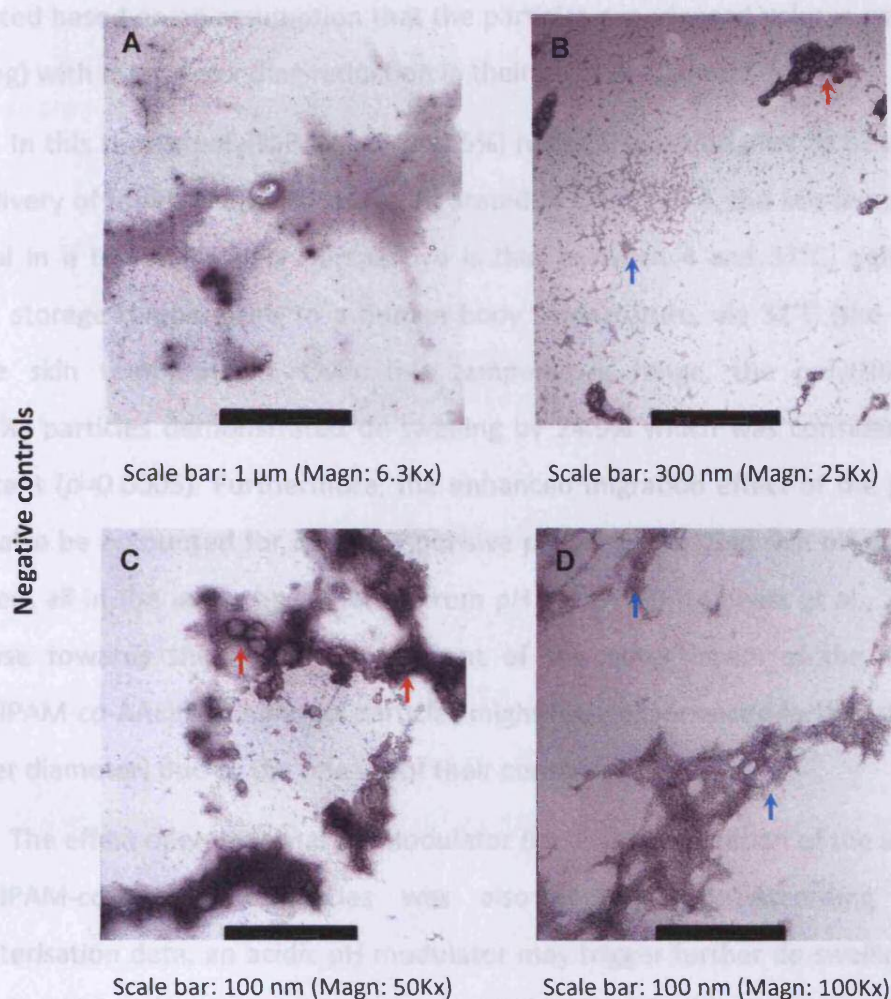


Figure 5-11: Receptor phases of *in vitro* of porcine epidermis dosed with – (A & B) aqueous solution of CA (5% w/v); and (C & D) de-ionised water, sampled at 24 h, stained with aqueous UA 2% and characterised by TEM; (A – D) samples served as negative controls for the *in vitro* investigation of migration of nanogel particles across porcine epidermis (→ Skin debris; → Lipid).

Figure 5-12 shows the relative quantities of particles detected in the receptor phases after 24 h. There was a significant difference in levels of particle migration between the polyNIPAM and poly(NIPAM-co-AAc)(5%) ($p=0.0434$). The trend may be explained as the polyNIPAM particles only being responsive towards a thermal stimulus (32°C, average skin surface temperature), whereas the poly(NIPAM-co-AAc)(5%) particles were responsive towards both thermal and pH stimuli (skin surface temperature and pH) as previously discussed (Sections 4.3.1.2 and 4.3.1.3). The responsiveness of the nanogel particles towards a particular stimulus was

evaluated based on an assumption that the particles experienced volume expel (de-swelling) with a corresponding reduction in their particle diameter.

In this thesis, poly(NIPAM-co-AAc)(5%) nanogel was designed to be a carrier for delivery of topically applied drugs. As stated in CHAPTER 4, the key temperature interval in a topical delivery perspective is that between 4 and 37°C, signifying a typical storage temperature to a human body temperature, via 32°C (the average surface skin temperature). Over this temperature range, the poly(NIPAM-co-AAc)(5%) particles demonstrated de-swelling by 24.9% which was considered very significant ($p=0.0005$). Furthermore, the enhanced migration effect of the particles might also be accounted for its pH-responsive property. Variable skin pH values are reported, all in the acidic broad range from pH 4.0 to 7.0 (Lambers et al., 2006). In response towards the acidic environment of the outer layers of the skin, the poly(NIPAM-co-AAc)(5%) nanogel particles might have experienced further shrinkage (smaller diameter) due to the release of their content.

The effect of an external pH modulator (i.e. CA) on migration of the unloaded poly(NIPAM-co-AAc)(5%) particles was also investigated. According to the characterisation data, an acidic pH modulator may trigger further de-swelling of the nanogel particles. Since the pH modulator solution used in this study had a pH value around 1.9, and the nanogel was prepared in de-ionised water of pH 5.8, the particles were expected to exhibit a very significant size reduction of about 17.3% over this range ($p=0.0002$) as shown in [Figure 4-10](#). However, application of CA onto the poly(NIPAM-co-AAc)(5%) nanogel contributed only a minor effect on the migration of the ionic nanogel particles, as there was no significance difference reported with or without the addition of the pH modulator, aqueous solution of CA ($p=0.3659$).

It should be noted that this study has several limitations. Even though the particles observed were physically similar in appearance with the nanogel particles, the identification was inconclusive. No further analytical identification was carried out to validate the particles as they could be particles made of other constituents.

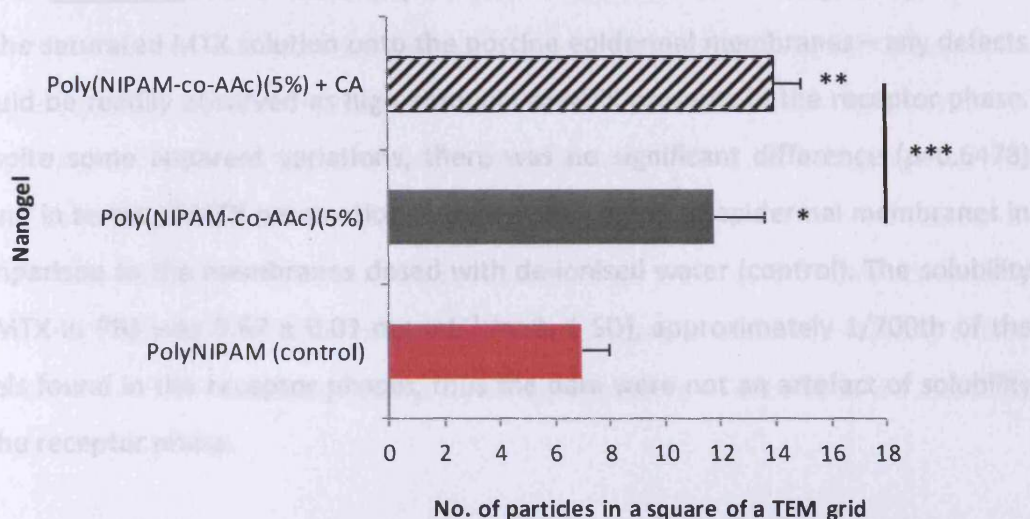


Figure 5-12: Nanogel particles observed in receptor phase by TEM, 24 h post-*in vitro* permeation study (n=3, \pm SD); polyNIPAM served as a control nanogel. * $p=0.0434$, vs. control; ** $p=0.0004$, vs. control; and *** $p=0.3659$

5.3.3 Validation of Skin Membrane Integrity Post-application of Nanogels

As nanogels have such a low hydrodynamic diameter, any breaches or defects in the membrane would be liable to yield false positives in terms of nanoparticles appearing in the receptor phase, not having migrated through the intact barrier function of the skin. The purpose of this experiment was therefore to validate the integrity of the membranes by determining the permeation of the model permeant, MTX across the membranes used earlier. Although this is conventionally achieved by determining the flux of tritium (^3H) or electrical resistance of the skin by means of conductometer (Fasano et al., 2002), membrane integrity can also be indicated by demonstrating equal fluxes across a range of treatments *in vitro* (Williams, 2003). MTX, which is hydrophilic in nature, was selected as a model permeant due to its low passive percutaneous permeation (McCullough et al., 1976) and defects would be obvious by high levels permeated. To this end, the *in vitro* skin permeation of MTX was probed to validate the integrity of the epidermal membranes post-application of the nanogels, aqueous solution of CA and de-ionised water.

Figure 5-13 shows the total permeation of MTX after 24 h topical application of the saturated MTX solution onto the porcine epidermal membranes – any defects would be readily observed as high amounts of MTX presents in the receptor phase. Despite some apparent variations, there was no significant difference ($p=0.6478$) found in terms of MTX permeation between each group of epidermal membranes in comparison to the membranes dosed with de-ionised water (control). The solubility of MTX in PBS was $0.67 \pm 0.01 \text{ mg mL}^{-1}$ ($n=3, \pm \text{SD}$), approximately 1/700th of the levels found in the receptor phases, thus the data were not an artefact of solubility in the receptor phase.

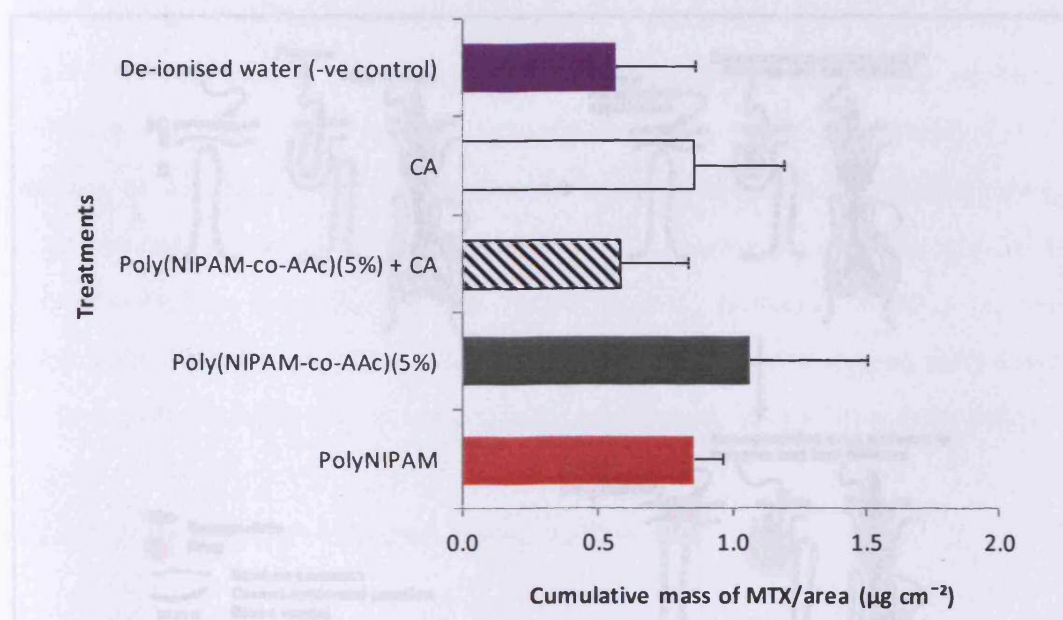


Figure 5-13: Total mass of MTX ($\mu\text{g cm}^{-2}$) recovered in receptor phase after 24 h ($n=3, \pm \text{SD}$) *in vitro* permeation across porcine epidermis. Membranes were previously treated with polyNIPAM nanogel alone; poly(NIPAM-co-AAc)(5%) nanogel alone; poly(NIPAM-co-AAc)(5%) nanogel and aqueous solution of CA (5% w/v); aqueous solution of CA (5% w/v) alone; and de-ionised water alone. $p=0.6478$ between treatments.

5.3.4 Proposed Mechanism: Penetration of Nanogel Particulates

Figure 5-14 shows the potential sites in skin for nanoparticle migration including the SC, furrows and hair follicles. The migration of nanoparticulates across skin seems counter-intuitive, given the barrier function of the skin, as detailed in

CHAPTER 1, and the size of the particulates in **Figure 4-3**. However, the TEM images show that this migration could possibly occur, and the model drug, MTX shows that physical damage is not responsible (Section 5.3.3). In seeking a rationalisation of these data, it should be borne in mind that other types of macromolecular materials have been found to penetrate skin, e.g. transfersomes (a form of elastic or deformable vesicles), with no explanation obtained (Cevc et al., 1995). However, there are two factors that possibly contribute to the penetration of nanogel particles into skin – mechanical massage and/or geared-pump mechanism via follicular routes.

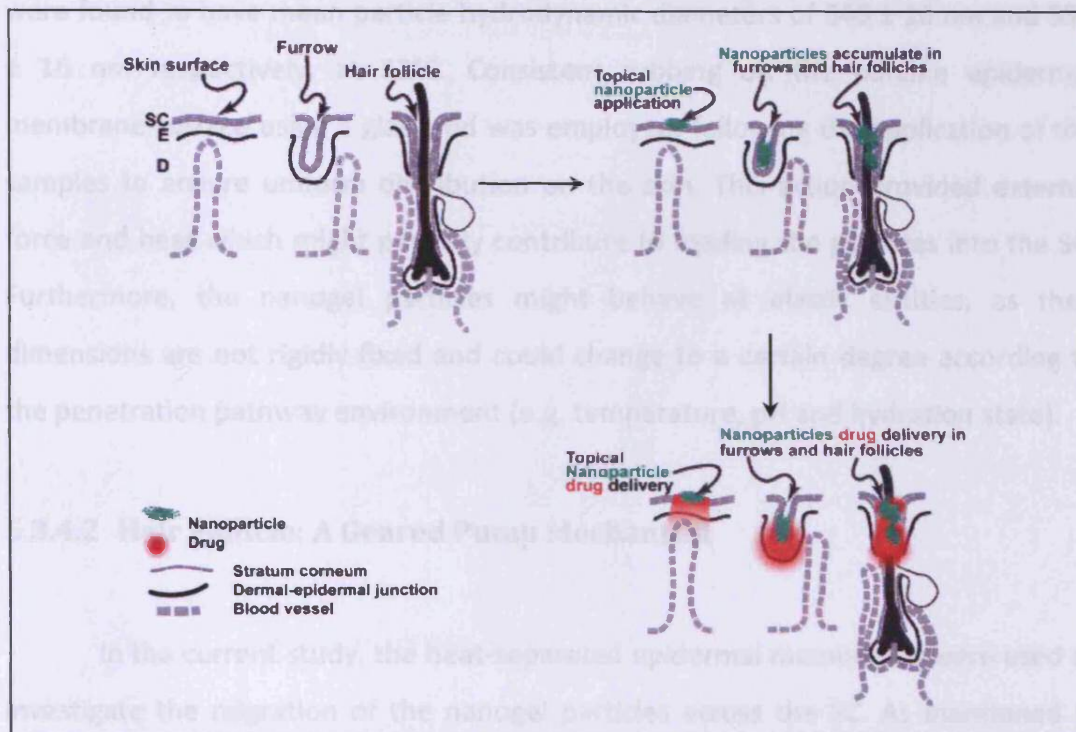


Figure 5-14: Nanoparticle migration via skin surface (SC), furrows and hair follicle infundibulum. Adapted from (Prow et al., 2011).

5.3.4.1 Mechanical Massage

It was reported that topically applied particles with a diameter $<1 \mu\text{m}$ could penetrate the SC and may reach the epidermis and occasionally the dermis, if a motion mimicking a skin massage was applied on the skin surface (Tinkle et al., 2007).

2003). It was postulated that the particles could enter the epidermis through channels formed by the lipids surrounding corneocytes of the SC, i.e. intercellular pathway. These lipid channels provide a continuous pathway from the surface of the skin into the epidermis and would be considerably flexible to allow the particles in conjunction with external force (motion) entering the epidermis. Once the particles managed to enter into the channels, they could move into the skin over time. These findings are consistent with several studies where mechanical motions such as massage and flexing were found to significantly increase the penetration of the investigated particulates (Lademann et al., 2007; Toll et al., 2003).

In the current work, the poly(NIPAM-co-AAc)(5%) and polyNIPAM nanogels were found to have mean particle hydrodynamic diameters of 640 ± 16 nm and 551 ± 16 nm respectively, at 32°C. Consistent rubbing on the porcine epidermal membrane surface using a glass rod was employed, following the application of the samples to ensure uniform distribution on the skin. This action provided external force and heat which might partially contribute to loading the particles into the SC. Furthermore, the nanogel particles might behave as elastic entities, as their dimensions are not rigidly fixed and could change to a certain degree according to the penetration pathway environment (e.g. temperature, pH and hydration state).

5.3.4.2 Hair Follicle: A Geared Pump Mechanism

In the current study, the heat-separated epidermal membranes were used to investigate the migration of the nanogel particles across the SC. As mentioned in CHAPTER 3, the heat-separation technique could possibly cause loss of hair follicles which may have provided a route of penetration to the applied nanogel particles across the SC. However, to the best of our knowledge, following microscopic evaluation, almost all the hairs remained associated with the epidermal membranes. Thus, the geared pump mechanism may be applicable as one of the possible mechanisms for nanogel particle migration.

Perhaps a more obvious route involves the particles traversing the skin via pores of pilosebaceous units (PSU, [Figure 5-15](#)) and/or through sweat gland pores,

which were reported to have diameters in the ranges of 10 – 70 μm (Lauer et al., 1996) and 60 – 80 μm (Sato et al., 1989) respectively. These openings are usually regarded to have a minor role in percutaneous transport as they only occupy 0.1% of the total skin surface (Lauer et al., 1996; Otberg et al., 2004; Williams, 2003). However, the assumption was later found to be valid only for the forearm. The skin area with a higher follicle density for example the forehead region, exhibited a much greater area, about 13.7% (Otberg et al., 2004).

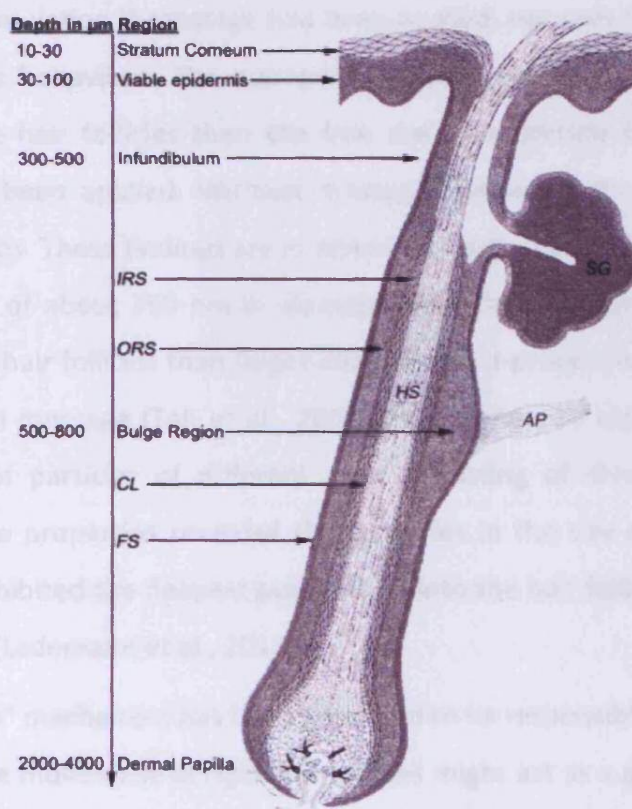


Figure 5-15: Structures of terminal hair follicle – ORS (outer root sheath); IRS (inner root sheath); CL (companion layer); FS (fibrous sheath); SG (sebaceous gland); and AP (arrector pili).

Reprinted from, J. Investig. Dermatol., 123, Toll, R., Jacobi, U., Richter, H., Lademann, J., Schaefer, H., Blume-Peytavi, U., Penetration profile of microspheres in follicular targeting of terminal hair follicles, 168-176, Copyright (2011), with permission from Elsevier [OR APPLICABLE SOCIETY COPYRIGHT OWNER].

It was suggested that if the size of the particles is $>5 \mu\text{m}$, they do not permeate into the lipid layers of the SC, instead only into the infundibula of the hair

follicles (i.e. the upper portion of the hair follicle above the entry of the sebaceous duct) (Lademann et al., 2007). Particles ranging in diameters between 20 nm and 7 μm were found in the hair follicle infundibulum and below (Lauer et al., 1996; Rolland et al., 1993; Toll et al., 2003).

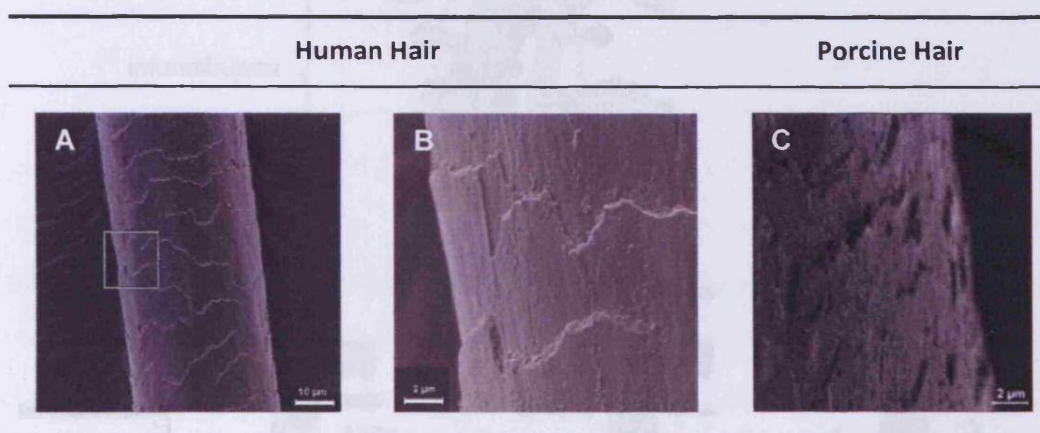
A study was conducted to compare the penetration and storage efficacy of a permeant in particle (320 nm in diameter) and non-particle form (free form) into hair follicles using a fluorescent dye sodium fluorescein on porcine ear skin, *in vitro* (Lademann et al., 2007). It was found that the particle formulation is superior to the non-particle formulation if massage had been applied, not only for penetration but also for storage behaviour. The nanoparticles were reported to penetrate much deeper into the hair follicles than the free dye (non-particle form – solution), if massaging had been applied. Without massage similar results were obtained for both formulations. These findings are in agreement with the results in another study, where particles of about 750 nm in diameter were found to penetrate better and deeper into the hair follicles than larger ones (6 μm), a process which was enhanced by a mechanical massage (Toll et al., 2003). Furthermore, a recent study analysed various types of particles of different sizes consisting of diverse materials with different surface properties revealed that particles in the size range between 300 and 600 nm, exhibited the deepest penetration into the hair follicles than smaller or larger particles (Lademann et al., 2011).

A “pump” mechanism has been proposed to be responsible for particle-based penetration. The movement of rigid hair follicles might act as a geared pump due to the zigzag structure of the cuticular layers along the hair shaft (**Table 5-3**), where particles of a similar size to hair cuticles (~530 nm in the case of human hairs and ~320 nm in the case of porcine skin, determined by the thickness of the keratin cells) are pushed deep into the follicles (Lademann et al., 2009). Once penetrated, the particles are entrapped within the follicle structures and only expelled following the slow processes of sebum secretion and hair growth. *In vitro*, the movement can be simulated by massage or flexing motion, while under *in vivo* conditions, a continuous body movement is likely responsible. The movement is assumed to be less than in the case of massage, but it occurs continuously.

Table 5-3: Surface structure of a (A & B) human and (C) porcine hair follicle with a zigzag formation of the cuticular layers along the hair shaft which serves as a basis for a geared pump delivery; image (B) is the magnified version of the image (A).

(A & B) reprinted from *Eur. J. Pharm. Biopharm.*, 77, Lademann, J., Richter, H., Schanzer, S., Knorr, F., Meinke, M., Sterry, W., Patzelt, A., Penetration and storage of particles in human skin: perspectives and safety aspects, 465-468, Copyright (2011), with permission from Elsevier [OR APPLICABLE SOCIETY COPYRIGHT OWNER].

(C) reprinted from *Adv. Drug Delivery Rev.*, 63, Prow, T.W., Grice, J.E., Lin, L.L., Faye, R., Butler, M., Becker, W., Wurm, E.M.T., Yoong, C., Robertson, T.A., Soyer, H.P., Roberts, M.S., Nanoparticles and microparticles for skin drug delivery, 470-491, Copyright (2011), with permission from Elsevier [OR APPLICABLE SOCIETY COPYRIGHT OWNER].



In addition to the above theory, it was also suggested the better delivery obtained with massage could be due to a “dislocation” of the follicular cast (a “plug” or barrier) in the follicular orifice or infundibulum caused by the mechanical massage (Prow et al., 2011; Toll et al., 2003).

However, even if such pumping action occurs, there remains the question of how the nanoparticulates are then able to migrate from across the PSU and beyond. Although there is no clear explanation for the mechanism, the following may be relevant. The hair follicle infundibulum which serves as a key reservoir for penetration processes by nanoparticles, may provide an interface for interaction between the topically applied nanoparticles with hair follicle-associated cell populations (Knorr et al., 2009). The superficial part of the hair follicle infundibulum, i.e. acro-infundibulum, is lined by an intact and impermeable epidermis including a well-developed SC and a stratum granulosum. However, the barrier is interrupted in

the lower follicular infundibulum, where the corneocytes of this area appear smaller and only few to little differentiated corneocytes present, suggesting that the skin barrier is incomplete and permeable (Knorr et al., 2009; Patzelt et al., 2011; Vogt et al., 2005). Due to the increased permeability condition, epithelial cells and associated-cell populations (APC) are accessible (Vogt et al., 2005) by the topically applied compounds as shown in **Figure 5-16(A)**.

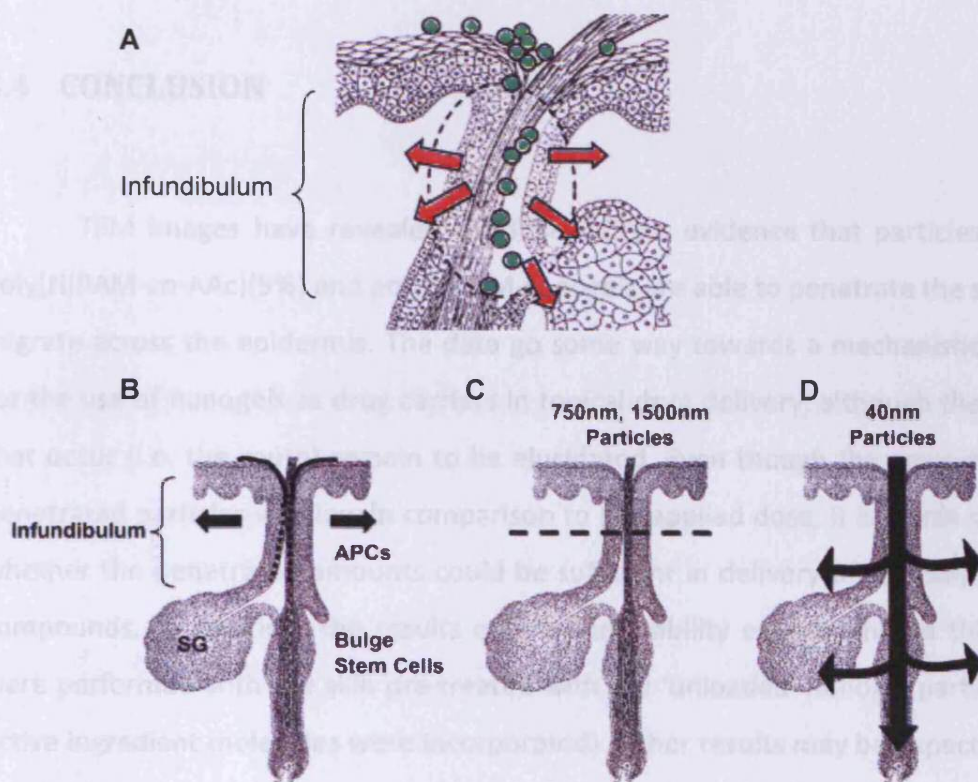


Figure 5-16: Penetration depth and capacity in relation to particle size within hair follicles; APC (antigen-presenting cells).

(A) adapted from (Vogt et al., 2005).

(B – D) reprinted from Eur. J. Pharm. Biopharm., 71, Knorr, F., Lademann, J., Patzelt, A., Sterry, W., Blume-Peytavi, U., Vogt, A., Follicular transport route - research progress and future perspectives, 173-180, Copyright (2011), with permission from Elsevier [OR APPLICABLE SOCIETY COPYRIGHT OWNER].

Figure 5-16(B & D) illustrates the penetration depths for micro- and nano-particles to the epithelium depend on the particle size – larger particles may deposit high concentration of permeants in the follicular duct, where they can be released

and penetrate independently, whereas small particles (40 nm) may be used to directly deliver particle-bound permeants to specific cell populations (Knorr et al., 2009). However, in the current chapter the opposite was found, where the particles in the diameter range of 550 – 650 nm were capable of traversing across the SC and observed in the receptor phase of *in vitro* migration study. The routes offered by these appendages might possibly play a significant role in delivering the nanogel particles into the skin.

5.4 CONCLUSION

TEM images have revealed the first indirect evidence that particles of the poly(NIPAM-*co*-AAc)(5%) and polyNIPAM nanogels are able to penetrate the skin and migrate across the epidermis. The data go some way towards a mechanistic insight for the use of nanogels as drug carriers in topical drug delivery, although the events that occur (i.e. the route) remain to be elucidated. Even though the amount of the penetrated particles was low in comparison to the applied dose, it is worth studying whether the penetrated amounts could be sufficient in delivery of topically-applied compounds. In addition, the results of the permeability experiments in this study were performed with the skin pre-treated with the ‘unloaded’ nanogel particles (no active ingredient molecules were incorporated). Other results may be expected with the loaded particles. More experiments are needed to completely understand the mechanism of the nanogel particles penetration through epidermis such as attenuated total reflectance Fourier transform infrared (ATR - FTIR) spectroscopy to show possible changes in the lipid structures of epidermal membrane. Furthermore, the safety of nanoparticulates potentially entering the systemic circulation via the topical route needs further study (Warheit et al., 2008), although on the basis of the evidence in this chapter, migration may be regulated to a certain extent by modifying the chemistry of the nanogel particulates.

CHAPTER 6 | Delivery of Model
Permeants Using a Temperature- and pH-
sensitive poly(NIPAM-co-AAc) Nanogel

6.1 INTRODUCTION

Multiple responsive polymers, such as those composed of polyNIPAM have led to them becoming the source of considerable interest in the area of drug delivery. They are recognised as “smart” polymers due to their conformational changes in response to changes in environmental conditions such as temperature and pH (Samah et al., 2010). Despite growing interest in the field of smart polymers for pharmaceutical applications, there is less attention in relation to their use in topical delivery systems. One of the few published studies concerned the copolymer of polyNIPAM co-BA co-methacrylic acid (NIPAM/BA/MAA)(85/10/5), which was investigated as a potential pH and temperature sensitive carrier for either dermal or transdermal delivery (Lopez et al., 2005). The authors concluded that the polymer had potential in drug release to the skin, and the incorporation of compounds into the polymer and the subsequent release depends on the octanol/water partition coefficient and solubility of the respective compounds.

In CHAPTER 4, particles of poly(NIPAM-co-AAc)(5%) nanogel were found to be able to undergo reversible volume change in response to changes in their environmental pH and temperature. In this study, the nanogel was investigated as a potential carrier for the delivery of dermatological and cosmetic agents through skin.

6.1.1 Loading of Model Compounds into Poly(NIPAM-co-AAc)(5%)

There are two commonly used techniques for loading compounds into a nanogel as a drug carrier. In the first technique, a compound to be loaded is added during the initial stage of polymerisation process, known as polymerisation encapsulation (Gehrke et al., 1998). It involves mixing the compound with an appropriate nanogel monomer, a cross-linking agent and an initiator solution, allowing them to polymerise and entrapping the compound within the formed matrix as illustrated in [Figure 6-1\(A\)](#). This method is preferable for hydrophobic compounds, as they can easily attach to the collapsed precursor particles during the

polymerisation, thus entrapped inside the nanogel particles (Nayak and Lyon, 2005). However, this technique has some limitations:

- (i) It is essential for the compound to be stable at high temperatures (Nayak and Lyon, 2005). In the SFEP technique utilised to synthesise the poly(NIPAM-co-AAc) nanogel, the reaction must take place at temperatures $\geq 70^{\circ}\text{C}$ to ensure successful polymerisation process. Thus, it is unsuitable for incorporation of biological materials such as peptides or proteins, as they are usually sensitive to high temperatures.
- (ii) The compound may suffer possible deleterious effects on their properties due to side reactions between the gel and the compound (Bromberg and Ron, 1998; Kim et al., 1992; Zhang et al., 2005).
- (iii) The difficulties in end-product purification due to inability to extract impurities and by-products without as well removing the compound (Bromberg and Ron, 1998; Gehrke et al., 1998; Kim et al., 1992).

In the second technique as illustrated in **Figure 6-1(B)**, a preformed purified nanogel is allowed to swell to equilibrium in a suitable drug solution, known as a post-fabrication encapsulation technique or a 'breathing-in' technique (Gehrke et al., 1998; Nolan, 2005; Nolan et al., 2004; Zhang et al., 2005). Even though this method is mostly preferred in view of the above, it does suffer size exclusion of large molecules for example proteins from the gel mesh network and due to that, it usually offers low loading levels (Zhang et al., 2005). The loading can be calculated with assumptions (Dong and Hoffman, 1991):

- (i) The compound is dissolved in the dispersant (de-ionised water) presents in the nanogel particles.
- (ii) The compound concentration in the dispersant inside the nanogel particles is equal to that in the external solution.
- (iii) No interaction occurs between the compound and the polymer matrix.

The swelling capacity of the nanogel particles in de-ionised water and the concentration of the drug are the key factors determining the amount loaded (Bromberg and Ron, 1998).

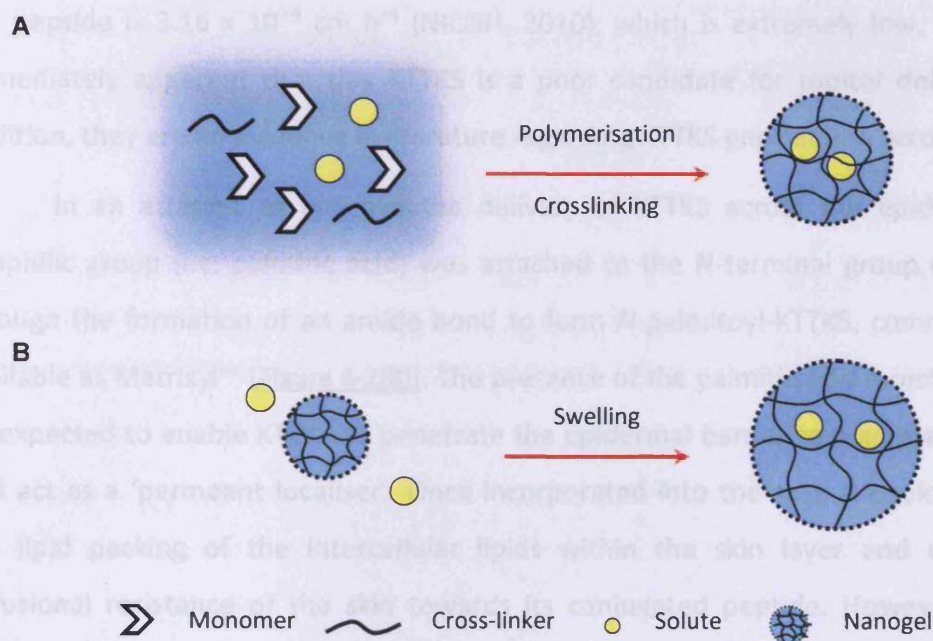


Figure 6-1: Summary of techniques available for nanogel loading – (A) polymerisation encapsulation and (B) post-fabrication.

6.1.2 Model Compounds

Three compounds currently used for cosmetic purposes were selected for the purpose of this study – a pentapeptide with a sequence of lysine-threonine-threonine-lysine-serine (termed as KTTKS), a fatty acid-conjugated KTTKS, i.e. palmitoyl-KTTKS and caffeine. Their physicochemical properties are listed in **Table 6-1**.

The most widely promoted peptide for topical application is KTTKS [**Figure 6-2(A)**] (Abu Samah and Heard, 2011). Comprises of five amino acid residues, KTTKS is regarded as a ‘signal peptide’ – a short amino acid sequence that possesses the ability to enhance dermal remodelling by triggering cellular processes, such as inhibiting collagenases activities and increasing extracellular matrix (ECM) production (Lupo and Cole, 2007). Peptides generally have high to very high molecular weights and they are typically charged at physiological pH which making them hydrophilic, thus contributing to their poor passive skin permeation (Benson et

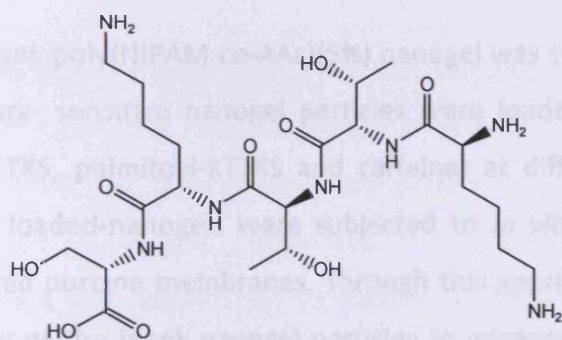
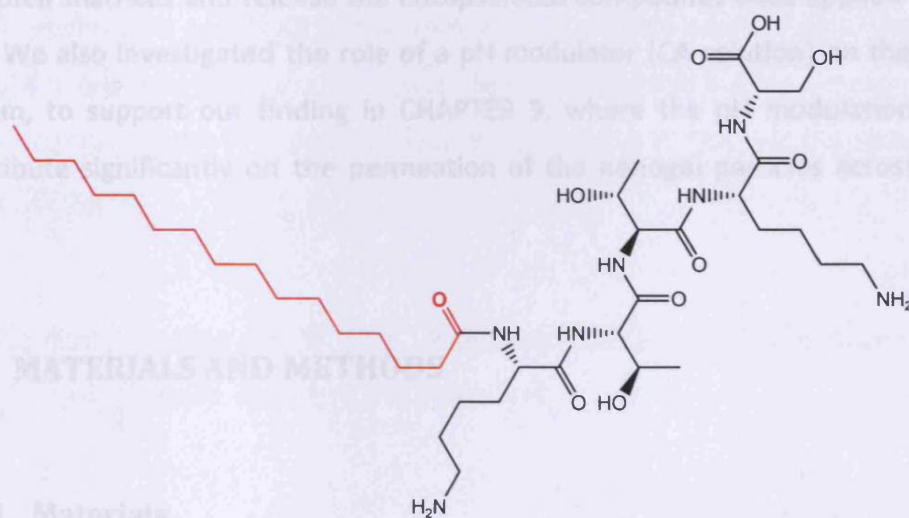
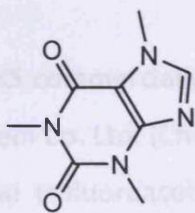
al., 2003; Williams, 2003). The calculated value for permeability coefficient (K_p) of the peptide is $3.16 \times 10^{-9} \text{ cm h}^{-1}$ (NIOSH, 2010), which is extremely low, and it is immediately apparent that this KTTKS is a poor candidate for topical delivery. In addition, there is no evidence in literature regarding KTTKS permeation across skin.

In an attempt to improve the delivery of KTTKS across the epidermis, a lipophilic group (i.e. palmitic acid) was attached to the N-terminal group of lysine through the formation of an amide bond to form *N*-palmitoyl-KTTKS, commercially available as Matrixyl™ [Figure 6-2(B)]. The presence of the palmitic acid moiety would be expected to enable KTTKS to penetrate the epidermal barrier to a greater extent and act as a 'permeant localiser'. Once incorporated into the skin, it could disrupt the lipid packing of the intercellular lipids within the skin layer and decrease diffusional resistance of the skin towards its conjugated peptide. However, even using saturated solutions and penetration enhancers (i.e. isopropyl myristate and polyethylene glycol-400) have yielded no detectable permeation across excised skin according to our initial work. Lintner (2002), however, claims to have confirmed penetration of the peptide into the skin but not through it, although no data were presented (Lintner and Peschard, 2000).

Caffeine [Figure 6-2(C)] can be found naturally in the leaves, seeds, or fruit in several plants such as tea and coffee beans. Caffeine and its derivatives are used in a number of commercial anti-cellulite creams, as an additive ingredient although there are limited direct evidences to support its role in cellulite reduction (Egger et al., 2003). It was claimed able to improve the appearance of cellulite when applied topically on skin, owing to its dehydration effect and lipolytic activity on fatty cells (Velasco et al., 2008). Caffeine is chosen as a model permeant because of its well characterised skin permeation properties and widely incorporated in cosmetic-related products intended for skin.

Table 6-1: Physicochemical properties of KTTKS, palmitoyl-KTTKS and caffeine.

	KTTKS	Palmitoyl-KTTKS	Caffeine
Chemical Formula	$C_{23}H_{45}N_7O_9$	$C_{39}H_{75}N_7O_{10}$	$C_8H_{10}N_4O_2$
MW	563.64	802.05	194.19
cLog P	-3.27	3.32	-0.131
pK_a	Most acidic : 3.23 Most basic: 10.47	Most acidic : 3.23 Most basic: 10.43	-0.130 – 1.22

A**B****C****Figure 6-2:** Chemical structures of (A) KTTKS; (B) palmitoyl-KTTKS; and (C) caffeine.

The main concept of the post-fabrication technique – if a substance is loaded at lower temperatures ($T < LCST$), it can be squeezed out above its LCST due to the pressure generated during the gel collapse (Hoffman, 1995). We applied the above concept for this experimental work in order to illustrate the potential of poly(NIPAM-co-AAc)(5%) nanogel particles, as alternative carriers of enhancing penetration of compounds intended for cutaneous applications. The LCST of poly(NIPAM-co-AAc)(5%) dispersed in de-ionised water was found to be 37°C, as stated in Section 4.3.1.4., which is close to the human physiological temperature. Thus, the nanogel is a suitable candidate for the current study.

Initially, a blank poly(NIPAM-co-AAc)(5%) nanogel was synthesised. Next, the pH- and temperature- sensitive nanogel particles were loaded with three model compounds (i.e. KTTKS, palmitoyl-KTTKS and caffeine) at different environments. Following this, the loaded-nanogels were subjected to *in vitro* permeation study across heat-separated porcine membranes. Through this approach, we intended to assess the efficiency of the blank nanogel particles to encapsulate the compounds into their matrices and release the encapsulated compounds once applied onto the skin. We also investigated the role of a pH modulator (CA solution) on the nanogel system, to support our finding in CHAPTER 5, where the pH modulation did not contribute significantly on the permeation of the nanogel particles across porcine skin.

6.2 MATERIALS AND METHODS

6.2.1 Materials

KTTKS and palmitoyl-KTTKS commercially known as Matrixyl® (97.73%) were supplied from Chengdu CP Biochem Co. Ltd. (Chengdu, China). Caffeine anhydrous ($\geq 99\%$), CA anhydrous (99.5%) and trifluoroacetic acid (TFA, 99%) were purchased from Sigma-Aldrich Company Ltd. (Poole, UK). All solvents used were HPLC-grade or equivalent and were supplied by Fisher Chemicals (Loughborough, UK). Freshly

excised porcine ears were obtained from a local abattoir prior to steam cleaning. Poly(NIPAM-co-AAc)(5%) and polyNIPAM nanogels were synthesised as detailed in Section 4.2.2.1.

6.2.2 Methods

6.2.2.1 Preparation of KTTKS, Palmitoyl-KTTKS and Caffeine Solutions

Saturated solutions of palmitoyl-KTTKS and caffeine were prepared in de-ionised water according to the method outline in Section 3.2.2.2. For palmitoyl-KTTKS, despite its slightly soluble property in de-ionised water due to the presence of a long hydrocarbon chain (C16), originated from the palmitoyl segment, the saturated solution was still prepared in de-ionised water, as the poly(NIPAM-co-AAc)(5%) particles exhibited the highest degree of swelling in the solvent.

In the case of KTTKS – it is a very water soluble peptide and thus, a large amount is required to attain saturation. Since the peptide is very expensive, only a known concentration of a peptide solution-containing KTTKS was prepared for this study (15 mg mL⁻¹).

6.2.2.2 Preparation of KTTKS, Palmitoyl-KTTKS and Caffeine Loaded-Poly(NIPAM-co-AAc)(5%) Nanogel

A post-fabrication technique was employed to load the model compounds into the poly(NIPAM-co-AAc)(5%) nanogel particles. It was performed by equilibrating and hydrating the freeze-dried nanogel with solutions made up of a known concentration of each compound. In all conditions, the polyNIPAM nanogel was used as a control nanogel and treated in a similar manner as the poly(NIPAM-co-AAc)(5%).

6.2.2.2.1 Peptides (KTTKS and Palmitoyl-KTTKS)

The post-fabrication technique can avoid many classic problems experienced with the *in situ* encapsulation particularly on peptide or protein molecules (Section 6.1.1), thus justifying the use of this technique in our loading studies.

KTTKS was loaded into freeze-dried poly(NIPAM-co-AAc)(5%) nanogel (15 – 20 mg) by immersing the latter with 5 mL of the peptide solution (15 mg mL⁻¹) in amber coloured bottles equipped with micromagnetic stirrer bars. The large excess of the solution was to ensure that the loading solution concentration did not change significantly upon swelling of the nanogel particles. The resulting mixture was ultrasonicated for about 10 min and placed on a submersible magnetic stirring plate, set up in a cold room of 4°C environment (the nanogel particles swollen the most at 2 – 4°C, which may enhance the loading of compound into the nanogel network, Section 0). Four replicates were prepared (n=4) and the loading process was allowed to proceed for ~72 h, under continuous stirring. The period of incubation was determined based on the result obtained in Section 0, where the nanogel dispersed in de-ionised water required ≥ 24 h to attain equilibrium swelling.

The loading of palmitoyl-KTTKS was performed using the same procedure for KTTKS, but the loading solution was saturated (0.85 ± 0.01 mg mL⁻¹). The saturated solution would provide maximum concentration of the compound to be loaded into the nanogel particles which might further enhance the loading capacity.

6.2.2.2.2 Caffeine

Caffeine was loaded into the poly(NIPAM-co-AAc)(5%) nanogel by mixing the saturated solution of caffeine (15.8 ± 0.09 mg mL⁻¹) with the freeze-dried nanogel, according to the above method (Section 6.2.2.2.1), but with a slight modification. The mixture was prepared in two identical sets of four replicates (n=4), and each set was placed either at: (i) 4°C – cold room or (ii) RT (~25°C) – on a laboratory bench.

Since caffeine is stable at RT environment, the loading was also conducted at RT to investigate whether the loading process was dependant on temperature.

6.2.2.3 Determination of EE

Loading levels of the model permeants into the nanogel were determined by reverse-phase HPLC. To determine the actual loading and not just adsorption, the mixtures were washed via centrifugation at 50,000 x *g* for 90 min, either at 4°C or 25°C using the Beckman Coulter Avanti® J-25 centrifuge. After each centrifugation cycle, the supernatant was sampled for HPLC analysis and the loaded-nanogel pellet was then re-dispersed in de-ionised water. The supernatant solution was monitored until no free compound was seen on HPLC chromatograms, and this occurred after three cycles of centrifugation. The total mass of compound removed over the centrifugation process could then be subtracted from the total mass of compound initially added to the freeze-dried nanogel, to obtain the mass of compound loaded into the nanogel. The obtained value was used to calculate EE (%) according to Equation 3-1. All measurements were performed in triplicates (n=3).

6.2.2.4 Quantitative Analysis

All samples were analysed using Agilent series 1100 HPLC system automated with Chemstation software, fitted with a reverse-phase Gemini-NX C₁₈ ODS 250 x 4.6 mm, 5 µm column (Phenomenex Inc., Macclesfield, UK) and a Phenomenex SecurityGuard guard column. Detection was done by UV and analysed accordingly as listed below:

6.2.2.4.1 KTTKS

KTTKS was analysed using a gradient elution established based on two reagents as listed in [Table 6-2](#). The elution was set to run for 30 min with a flow rate of 1 mL min⁻¹, followed by 5 min post-run for washing and column re-equilibration

prior to the next analysis. Sample injection volume was 20 μL and detection was by UV at $\lambda = 220 \text{ nm}$, with a resultant retention time of $\sim 5 \text{ min}$ as shown in **Figure 6-3**. For calibration, a stock solution of KTTKS in de-ionised water (i.e. receptor phase) was prepared, and a standard calibration curve obtained over the range of 20 – 600 $\mu\text{g mL}^{-1}$. Excellent linearity was achieved as evidenced by R^2 of 0.99, with the LOD of 8.27 ng mL^{-1} .

Table 6-2: Gradient elution for HPLC analysis of KTTKS.

Time (min)	Mobile Phase	
	0.1% TFA in De-ionised Water	0.1% TFA in Acetonitrile
0	90	10
30	68	32
35 (post-wash)	90	10

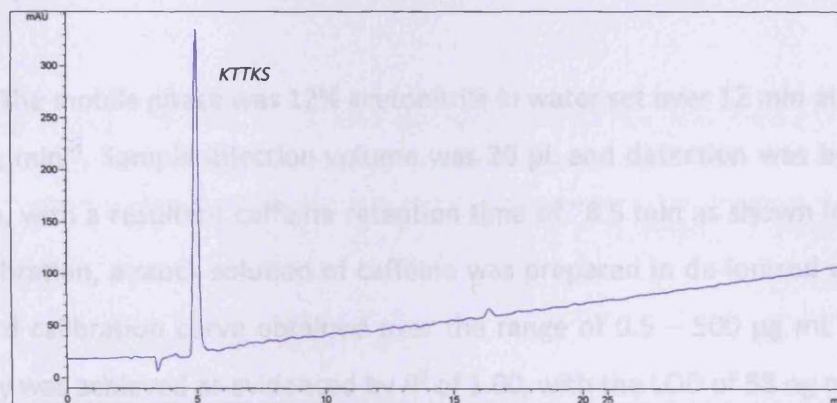


Figure 6-3: HPLC chromatogram for KTTKS dissolved in de-ionised water.

6.2.2.4.2 Palmitoyl-KTTKS

An isocratic mobile phase system was used which comprised of acetonitrile and deionised water, 55:45 (v/v), with 0.1% TFA for pH adjustment. The UV detection was set at $\lambda = 220 \text{ nm}$. The injection volume was 20 μL and the flow rate was 1.0 mL min^{-1} . Under these conditions, a retention time of about 6 min was obtained (**Figure 6-4**). For calibration, a stock solution was prepared in de-ionised

water and a standard calibration curve obtained over the range of 5 – 1300 $\mu\text{g mL}^{-1}$. Excellent linearity was achieved as evidenced by R^2 value of ≥ 0.99 , with the LOD of 92 ng mL^{-1} .

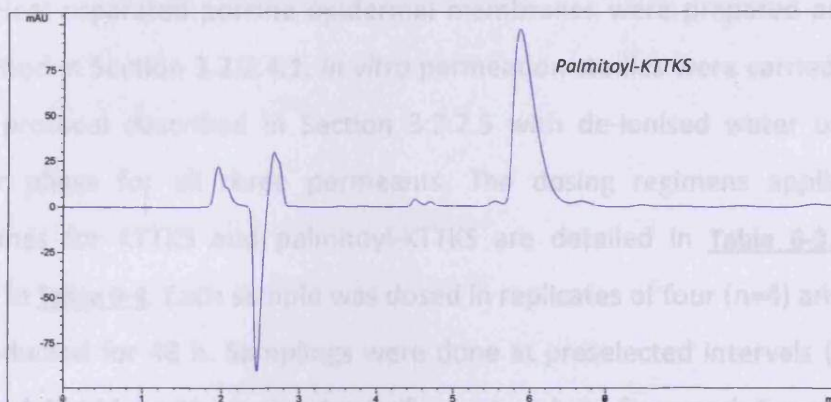


Figure 6-4: HPLC chromatogram for palmitoyl-KTTKS dissolved in de-ionised water.

6.2.2.4.3 Caffeine

The mobile phase was 12% acetonitrile in water set over 12 min at a flow rate of 1 mL min^{-1} . Sample injection volume was 20 μL and detection was by UV at $\lambda = 273 \text{ nm}$, with a resultant caffeine retention time of $\sim 8.5 \text{ min}$ as shown in **Figure 6-5**. For calibration, a stock solution of caffeine was prepared in de-ionised water and a standard calibration curve obtained over the range of 0.5 – 500 $\mu\text{g mL}^{-1}$. Excellent linearity was achieved as evidenced by R^2 of 1.00, with the LOD of 58 ng mL^{-1} .

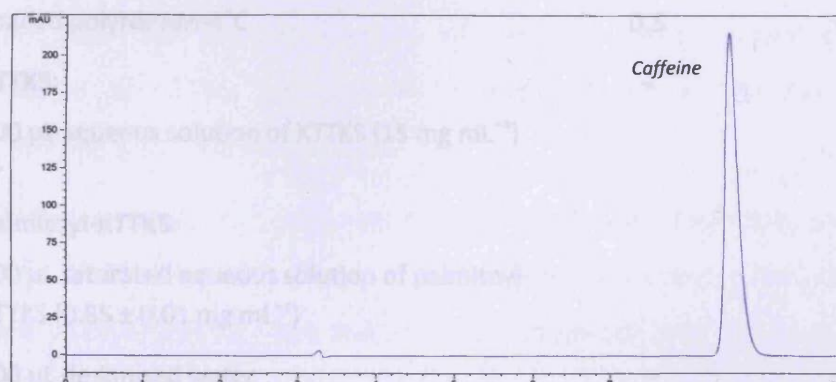


Figure 6-5: HPLC chromatogram for caffeine dissolved in de-ionised water.

6.2.2.5 *In vitro* Permeation of Permeants across Heat-separated Porcine Epidermal Membranes from Loaded-poly(NIPAM-co-AAc)(5%) Nanogel

Heat-separated porcine epidermal membranes were prepared according to the method in Section 3.2.2.4.1. *In vitro* permeation studies were carried out based on the protocol described in Section 3.2.2.5 with de-ionised water used as the receptor phase for all three permeants. The dosing regimens applied on the membranes for KTTKS and palmitoyl-KTTKS are detailed in **Table 6-3**, while for caffeine in **Table 6-4**. Each sample was dosed in replicates of four ($n=4$) and the study was conducted for 48 h. Samplings were done at preselected intervals (3, 6, 9, 12, 18, 24 and 48 h) by withdrawing 1 mL of receptor phase from each Franz cell using a dedicated pipette and transferred into a 1 mL amber HPLC auto-sampler vial. The collected samples were assayed for the model permeants by HPLC according to the protocol in Section 6.2.2.4.

Table 6-3: Dosing regimens for *in vitro* permeation of KTTKS- and palmitoyl-KTTKS from loaded nanogels across heat-separated porcine epidermis ($n=4$).

	Sample	Nanogel (g)	Aqueous CA (5% w/v) (μL)
(i)	Loaded poly(NIPAM-co-AAc)(5%)-4°C	0.5	–
(ii)	Loaded poly(NIPAM-co-AAc)(5%)-4°C, followed by aqueous solution of CA	0.5	200
(iii)	Loaded polyNIPAM-4°C	0.5	–
(iv)	KTTKS: 500 μL aqueous solution of KTTKS (15 mg mL^{-1}) or Palmitoyl-KTTKS: 500 μL saturated aqueous solution of palmitoyl-KTTKS ($0.85 \pm 0.01 \text{ mg mL}^{-1}$)	–	–
(v)	500 μL de-ionised water	–	–

Table 6-4: Dosing regimens for *in vitro* permeation of caffeine from loaded-nanogels across heat-separated porcine epidermis (n=4).

	Sample	Nanogel (g)	Aqueous CA (5% w/v) (μL)
(i)	Caffeine-loaded poly(NIPAM-co-AAc)(5%)-4°C	0.5	–
(ii)	Caffeine-loaded poly(NIPAM-co-AAc)(5%)-4°C, followed by aqueous solution of CA	0.5	200
(iii)	Caffeine-loaded polyNIPAM-4°C	0.5	–
(iv)	Caffeine-loaded poly(NIPAM-co-AAc)(5%)-RT	0.5	–
(v)	Caffeine-loaded poly(NIPAM-co-AAc)(5%)-RT, followed by aqueous solution of CA	0.5	200
(vi)	Caffeine-loaded polyNIPAM-RT	0.5	–
(vii)	500 μL saturated aqueous solution of caffeine (15.80 ± 0.09 mg mL ⁻¹)	–	–
(viii)	500 μL de-ionised water	–	–

6.2.2.6 Data and Statistical Analysis

All data were analysed using Excel 2007 ((Microsoft Office, Microsoft Corp., Redmond, WA) and presented in the text as a mean ± SD. Cumulative amounts of KTTKS, palmitoyl-KTTKS and caffeine permeated per unit area (mass cm⁻²) were plotted against time (h), with lag time and steady state flux (J_{SS}) were determined by standard methods. Cumulative permeation after 12 h (Q_{12}), 24 h (Q_{24}) and 48 h (Q_{48}) were also reported. The peak areas of samples were calculated and the concentrations of KTTKS, palmitoyl-KTTKS and caffeine in the samples were extrapolated using the standard curves.

Statistical tests were performed with InStat® for Macintosh, version 3.00 (GraphPad Software Inc., San Diego, CA). Significant differences and comparisons were made using Student's *t*-test and ANOVA. Confidence intervals were set at 95% and $p < 0.05$ was defined as statistically significant.

6.3 RESULTS AND DISCUSSION

The poly(NIPAM-co-AAc)(5%) nanogel used in this study has characteristic features of pH- and temperature-responsive, with high degree of swelling in aqueous solutions at low temperatures and at pH values greater than the pK_a of AAc groups, i.e. 4.25. A well establish polyNIPAM was selected to play a role, as a control nanogel in this experimental work due to its well-known ability to undergo conformational changes in response to its environmental temperature.

6.3.1 Loading of KTTKS, Palmitoyl-KTTKS and Caffeine into Poly(NIPAM-co-AAc)(5%) Nanogel

The loading of KTTKS and palmitoyl-KTTKS into the poly(NIPAM-co-AAc)(5%) nanogel was carried out only at a refrigerated condition of 4°C due to the unstable nature of the peptides at high temperatures. [Figure 6-6](#) and [Figure 6-7](#) represent EE (%) of KTTKS and palmitoyl-KTTKS, respectively. [Table 6-5](#) listed the loading level of each compound into the poly(NIPAM-co-AAc)(5%) and control nanogels. The poly(NIPAM-co-AAc)(5%) nanogel was shown to have quite satisfactory loading level of KTTKS and palmitoyl-KTTKS with 368 mg g⁻¹ dry gel for the former, and 85 mg g⁻¹ dry gel for the latter. Slightly higher loading was shown by the control polyNIPAM for both peptides.

For caffeine, since the compound was stable at RT, the loading was conducted both at 4°C and RT. [Figure 6-8](#) and [Table 6-5](#) show the EE (%) and loading level of caffeine into the poly(NIPAM-co-AAc)(5%) particles, accordingly. At 4°C, caffeine was loaded into the particles at a level of 334 mg g⁻¹ dry gel, whereas at RT, the level reduced almost by 20% to 267 mg g⁻¹ dry gel. As for the control nanogel, a similar pattern of loading level can be observed, with a higher loading at 4°C than at RT.

The loading level was found to depend on environmental temperatures and this is consistent with a previously published paper (Kawaguchi et al., 1992). A significant amount of caffeine was loaded into the nanogel particles at 4°C than at ambient temperature. The nanogel particles experienced a higher degree of swelling at 4°C and due this extended conformation, provided more space for the further loading of the caffeine molecules. In addition, loading of a compound also depends on factors such as solubility of the compound and octanol/water partition coefficient of the compound (Lopez et al., 2005). These factors were seen in the case of palmitoyl-KTTKS (cLog $P = 3.32$), where a considerably low level of the compound loaded into the nanogel compared to the other two hydrophilic compounds.

Furthermore, the hydrophilic balance of the gel also plays a role in the efficiency of the loading process (Kawaguchi et al., 1992; Nolan et al., 2004). At 4°C, the polymer was in a hydrophilic state, thus had higher tendency for hydrophilic compounds such as caffeine. However, at higher temperature (25°C), its surface becoming hydrophobic and thus, had more tendency for lipophilic palmitoyl-KTTKS, reflected by higher loading of this compound. This unique property facilitates the loading of the compounds into the nanogel particles, as well as the release of encapsulated compounds from the particles (Oh et al., 2008).

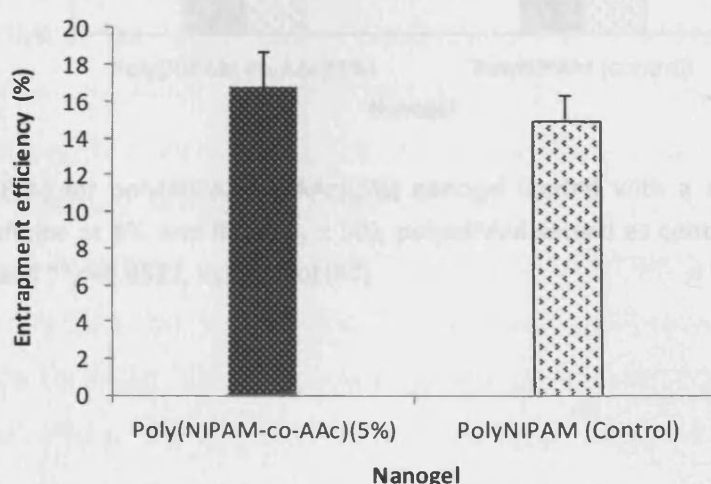


Figure 6-6: EE(%) for poly(NIPAM-co-AAc)(5%) nanogel loaded with an aqueous solution of KTTKS at 4°C ($n=4$, \pm SD); polyNIPAM served as control. $p=0.1757$

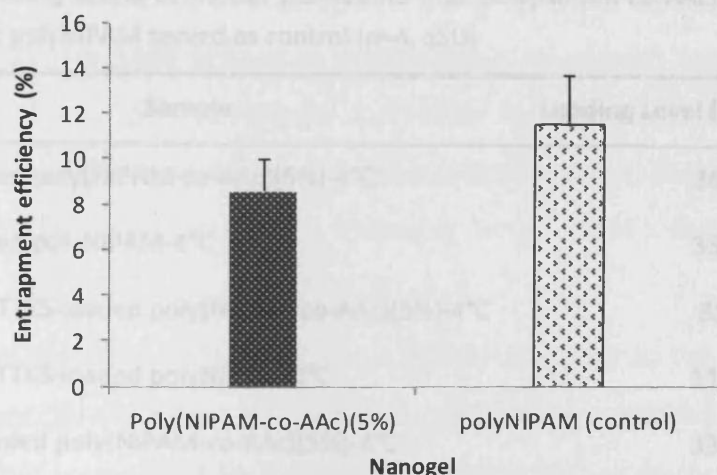


Figure 6-7: EE(%) for poly(NIPAM-co-AAc)(5%) nanogel loaded with a saturated aqueous solution of palmitoyl-KTTKS at 4°C (n=4, ± SD); polyNIPAM served as control. $p=0.0578$

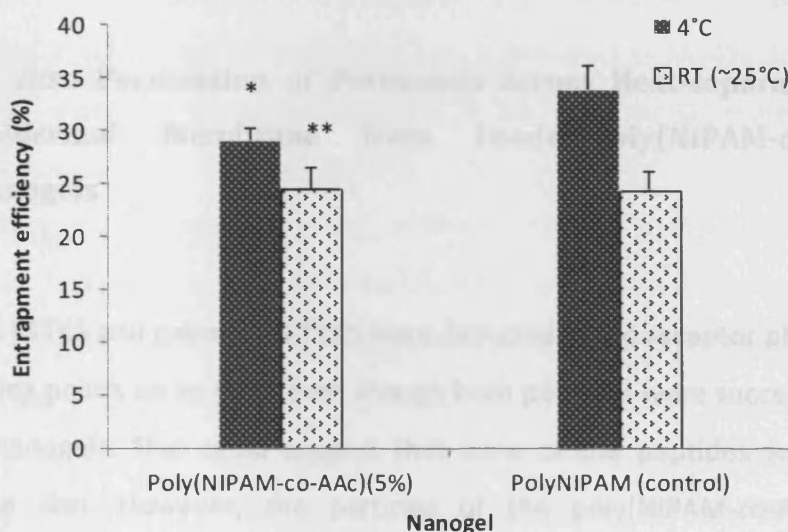


Figure 6-8: EE(%) for poly(NIPAM-co-AAc)(5%) nanogel loaded with a saturated aqueous solution of caffeine at 4°C and RT (n=4, ± SD); polyNIPAM served as control. $*p=0.0070$, vs. control (4°C) and $**p=0.8521$, vs. control (RT)

Table 6-5: Loading levels of model permeants into poly(NIPAM-co-AAc)(5%) at different temperatures; polyNIPAM served as control (n=4, \pm SD)

Sample	Loading Level (mg g ⁻¹ dry gel)
KTTKS-loaded poly(NIPAM-co-AAc)(5%)-4°C	368
KTTKS-loaded polyNIPAM-4°C	334
Palmitoyl-KTTKS-loaded poly(NIPAM-co-AAc)(5%)-4°C	85
Palmitoyl-KTTKS-loaded polyNIPAM-4°C	115
Caffeine-loaded poly(NIPAM-co-AAc)(5%)-4°C	334
Caffeine-loaded polyNIPAM-4°C	300
Caffeine-loaded poly(NIPAM-co-AAc)(5%)-RT	267
Caffeine-loaded polyNIPAM-RT	210

6.3.2 *In vitro* Permeation of Permeants across Heat-separated Porcine Epidermal Membrane from Loaded-poly(NIPAM-co-AAc)(5%) Nanogels

No KTTKS and palmitoyl-KTTKS were detected in the receptor phase at any of the sampling points up to 48 h, even though both peptides were successfully loaded into the nanogels. This could suggest that none of the peptides were delivered across the skin. However, the particles of the poly(NIPAM-co-AAc)(5%) and polyNIPAM nanogels were shown to be able to penetrate the skin and migrate across the epidermis, as discussed in CHAPTER 5. This lead to another possibility that the absence of detectable level of KTTKS and palmitoyl-KTTKS from the receptor solutions is more likely due to inability of the peptides to diffuse out of the nanogel network in the collapsed state, particularly for the palmitoyl-KTTKS due to its 'long carbon chain' effect. The palmitoyl chain (16-carbon long) of the fatty acids conjugated peptide might get entangled with the polymer network which further preventing the release of encapsulated palmitoyl-KTTKS.

Another explanation, it could be due to low detection sensitivity of palmitoyl-KTTKS by HPLC. This could happen as the detection wavelength used to assay both peptides is 220 nm. This wavelength is specific for the peptide bond detection (Marshak et al., 1995). However, it is too non-selective and insensitive to detect low nanomole concentration of peptide (Marshak et al., 1995) present in *in vitro* samples.

On the contrary, caffeine was successfully detected in the receptor phase samples. **Figure 6-9** and **Figure 6-10** show the permeation profiles for the caffeine-loaded nanogels prepared at 4°C and RT, respectively. Flux values for all the samples were calculated and listed in **Table 6-6**. The highest permeation was exhibited by the loaded-poly(NIPAM-co-AAc)(5%) prepared at 4°C, with the flux value of $16.89 \pm 2.46 \mu\text{g cm}^{-2} \text{ h}^{-1}$ and Q_{48} of $632.52 \pm 52.58 \mu\text{g cm}^{-2}$. However, the flux reduced by 2.5-fold when a pH modulator (aqueous solution of CA) was applied together with the nanogel ($p=0.0011$). A similar behaviour was shown by the loaded-poly(NIPAM-co-AAc)(5%)-RT, where in the presence of CA, its flux significantly reduced by almost 1.7-fold in comparison to the nanogel applied without the pH modulator ($p=0.0005$). This observation indicates that the addition of CA did not enhance caffeine permeation, instead seems to have suppressed the release of permeant from the nanogel particles. This result was unexpected, as we postulated the addition of CA would enhance the release of the compound out of the particles. Details of the nanogels with different swelling ratio at low pH environment were disclosed in characterisation section of CHAPTER 4. A possible explanation for such phenomenon – simultaneous application of CA and a thermal stimulus (skin, 32°C), triggered abrupt and greater collapse to the structure and reduced mesh size of the network instead of each stimulus individually. As a consequence, the caffeine molecules became entrapped inside of the particles, unable to diffuse out of the particles' network.

By comparing the loaded poly(NIPAM-co-AAc)(5%) prepared at 4°C and RT, a significantly higher flux and cumulative permeation of caffeine was seen with the poly(NIPAM-co-AAc)(5%)-4°C with a p value of 0.0267. This might be attributed to the higher level of caffeine available in its matrix. Apart than that, the nanogel

experienced a wide change of temperature once applied onto the surface of the skin ($4^{\circ}\text{C} \rightarrow 32^{\circ}\text{C}$), thus higher osmotic pressure would be created inside the nanogel particles, leading to a greater amount of caffeine being forced out of the particles' network. The nanogel also exhibited reduced lag time (~ 6 h) in comparison to the saturated solution of caffeine (~ 8 h). A low lag time value is desirable in order to accelerate the onset of therapeutic activity.

Interestingly, the nanogels loaded at RT exhibited higher lag times, almost by 2-fold compared to the nanogels prepared at 4°C . This could be due to a narrow temperature change experienced by the nanogels ($25^{\circ}\text{C} \rightarrow 32^{\circ}\text{C}$). Thus, a longer period of time was required for an adequate osmotic force to build up inside the particles and forcing out the caffeine molecules. Furthermore, at the end of the study, almost the same cumulative amount (Q_{48}) of caffeine was assayed in the samples supporting this hypothesis.

It worth noting, the loaded-polyNIPAM nanogel (control) prepared either at 4°C or RT, was superior to the saturated solution in delivering caffeine molecules across the epidermal membranes ($p=0.0280$ for polyNIPAM- 4°C and $p=0.0015$ for polyNIPAM-RT). The saturated solution of caffeine exhibited the lowest flux (4.87 ± 1.44) and cumulative permeation ($Q_{48} = 181.38 \pm 43.34 \mu\text{g cm}^{-2}$) among all the dosing regimens applied in the *in vitro* permeation study. The poly(NIPAM-co-AAc)(5%) nanogel successfully enhanced caffeine delivery by about 3.5-fold higher than the saturated solution, may prove our hypothesis that the nanogel particles capable to penetrate skin and subsequently deliver the loaded permeant.

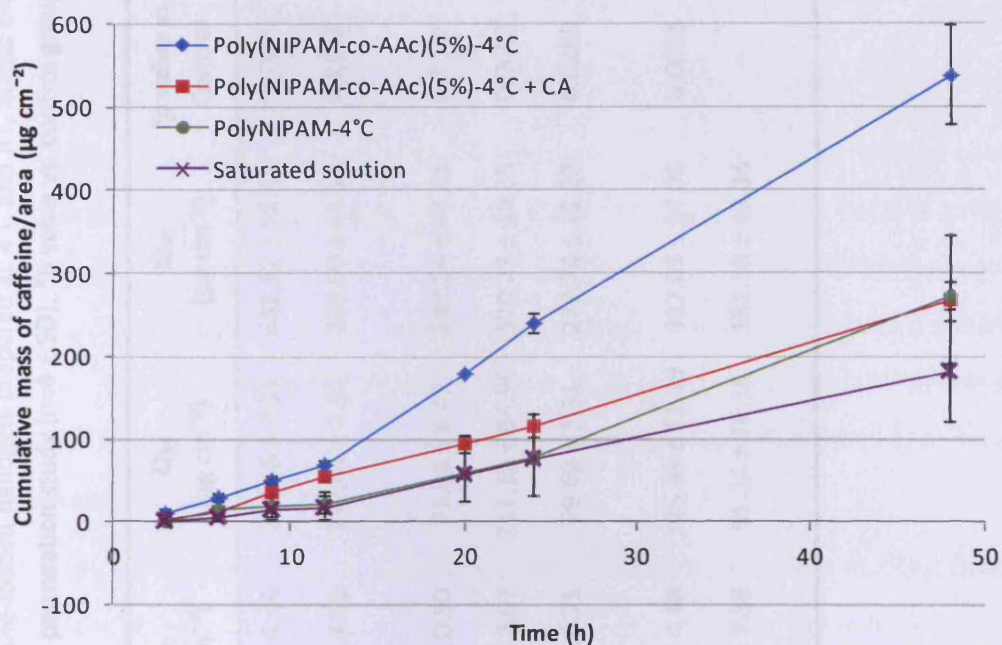


Figure 6-9: Cumulative permeation profiles for caffeine from loaded-poly(NIPAM-co-AAc)(5%) nanogel with and without the addition of CA solution (5% w/v); caffeine was loaded into the nanogel at 4°C environment; loaded-polyNIPAM nanogel and saturated solution of caffeine served as controls ($n=4$, \pm SD).

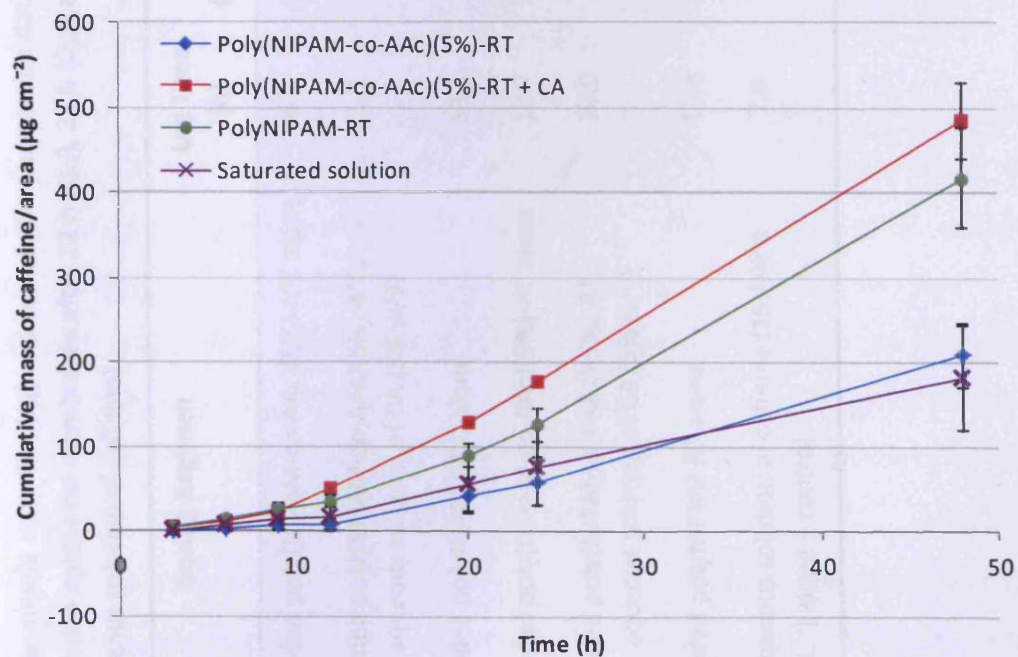


Figure 6-10: Cumulative permeation profiles for caffeine from loaded-poly(NIPAM-co-AAc)(5%) nanogel with and without the addition of CA solution (5% w/v); caffeine was loaded into the nanogel at RT environment; loaded-polyNIPAM nanogel and saturated solution of caffeine served as controls ($n=4$, \pm SD).

Table 6-6: Lag time, steady state flux (J_{SS}) and cumulative permeation data of caffeine from caffeine-loaded nanogels prepared at 4°C and RT, across the heat-separated porcine epidermal membranes after 12 h (Q_{12}), 24 h (Q_{24}), and 48 h (Q_{48}) of *in vitro* permeation study ($n=4 \pm SD$). * p value vs. control group (i.e. saturated aqueous solution of caffeine)

Dosing Regimen		Lag Time (h)	J_{SS} ($\mu\text{g cm}^{-2} \text{h}^{-1}$)	Q_{12} ($\mu\text{g cm}^{-2}$)	Q_{24} ($\mu\text{g cm}^{-2}$)	Q_{48} ($\mu\text{g cm}^{-2}$)	* p value vs. Control
(i)	Caffeine-loaded poly(NIPAM-co-AAc)(5%)-4°C alone	6.2	16.89 \pm 2.46	67.82 \pm 4.46	240.18 \pm 7.94	632.52 \pm 52.58	<0.0001
(ii)	Caffeine-loaded poly(NIPAM-co-AAc)(5%)-4°C, followed by aqueous solution of CA (5% w/v)	5.3	6.65 \pm 2.49	54.46 \pm 4.53	115.41 \pm 7.90	268.00 \pm 44.58	0.1293
(iii)	Caffeine-loaded polyNIPAM-4°C alone	13.1	7.19 \pm 2.59	13.83 \pm 0.50	71.48 \pm 6.49	249.14 \pm 43.81	0.2141
(iv)	Caffeine-loaded poly(NIPAM-co-AAc)(5%)-RT alone	13.7	12.87 \pm 1.23	51.86 \pm 2.67	211.10 \pm 34.96	520.23 \pm 40.35	0.0003
(v)	Caffeine-loaded poly(NIPAM-co-AAc)(5%)-RT, followed by aqueous solution of CA (5% w/v)	10.0	7.79 \pm 0.82	22.53 \pm 8.71	78.69 \pm 3.31	272.74 \pm 11.53	0.0280
(vi)	Caffeine-loaded polyNIPAM-RT alone	12.8	11.83 \pm 1.63	34.68 \pm 4.48	125.98 \pm 11.19	417.03 \pm 34.08	0.0015
(vii)	Saturated aqueous solution of caffeine (15.798 \pm 0.092 mg mL ⁻¹) alone – control	7.8	4.87 \pm 1.44	10.36 \pm 7.56	51.24 \pm 16.15	181.38 \pm 43.34	–

6.3.3 Proposed Mechanism

The proposed preparation and mechanism of the loaded-poly(NIPAM-co-AAc) is simplified and illustrated in [Figure 6-11](#). The *in vitro* permeation data of caffeine-loaded poly(NIPAM-co-AAc)(5%) showed that, the nanogel successfully enhanced the delivery of caffeine across the epidermal membrane, even relative to the saturated solution. The results are consistent with our finding in previous work, where MTX delivery into skin was significantly enhanced by the polyNIPAM-based nanogel served as a carrier (CHAPTER 3).

Based on its multiple stimuli-responsive natures, topically applied nanogel allows the release of its encapsulated material by collapsing in response to finite changes in its environmental conditions (i.e. temperature and pH) and subsequently expelling the aqueous compound solution. The application of CA as the pH modulator suppressed the release of encapsulated material due to the abrupt collapse of the structure, which may have impeded the release of the compound, as previously discussed. Thus, the thermal stimulus was the main controlling factor that affected the caffeine release behaviour of the nanogel.

In order to ensure high loading and subsequent release of the encapsulated compounds, the loading process should be performed at lower temperature, where the nanogel particles are highly swollen and in a hydrophilic state. In addition, a higher level of loading can be achieved with hydrophilic compounds due to their greater availability in the aqueous loading solution. Furthermore, by applying the water/octanol partition coefficient theory, at lower temperature ($T < LCST$), the hydrophilic materials would preferably partition into the hydrophilic particles leading to a higher loading level, in comparison to lipophilic compounds.

The following mechanism of drug delivery via the poly(NIPAM-co-AAc)(5%) nanogel is proposed. When a compound loaded into the poly(NIPAM-co-AAc)(5%) at lower temperature, it can be squeezed or expelled out once applied on the skin, as the thermal stimulus of 32°C originated from the skin would trigger the release of the loaded compound due to the pressure generated during the collapse of gel

structure. Additionally, pH of the skin which reportedly provides weak acid environment between pH 4 – 7 (Lambers et al., 2006) would also contribute to the collapse of the particles. The acidic environment creates by the skin would not be as strong as in the presence of the pH modulator. Thus, it should not cause sudden structure collapse, which might be the factor that entrapped the encapsulated material inside the nanogel network.

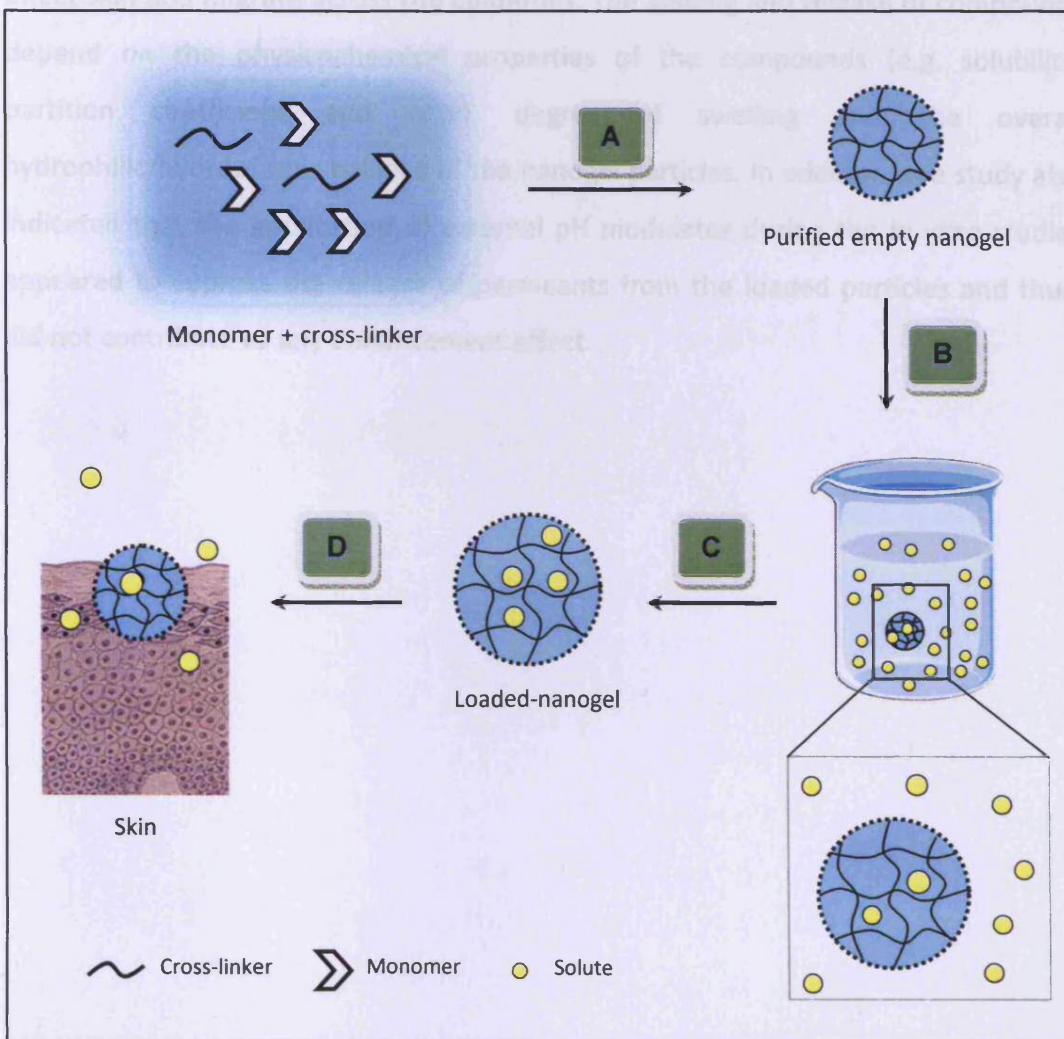


Figure 6-11: Schematic presentation of a post-fabrication loading of a model drug into nanogel particles, followed by its delivery or removal triggered by multiple stimuli.

(A) Empty nanogel particles are synthesised by the SFEP technique at 70°C; (B) loading is performed by hydrating a freeze-dried nanogel with a solution-containing dissolved solute at 2 – 4°C ($T < LCST$); (C) the mixture is purified to remove free solute molecules; and (D) once applied onto human skin (~32°C), the loaded solute molecules are squeezed out of the nanogel, due to the pressure generated during the structure collapsed at 32°C with respect to 2 – 4°C.

6.4 CONCLUSION

Poly(NIPAM-co-AAc)(5%) nanogel particles facilitate the skin permeation of loaded compounds and therefore have potential to act as carriers for topically applied compounds intended for topical delivery. In tandem with the migration results (CHAPTER 5), this demonstrates that the particles can possibly penetrate intact skin and migrate across the epidermis. The loading and release of compounds depend on the physicochemical properties of the compounds (e.g. solubility, partition coefficient and MW), degree of swelling and the overall hydrophilic/hydrophobic balance of the nanogel particles. In addition, the study also indicated that the application of external pH modulator during the *in vitro* studies appeared to suppress the release of permeants from the loaded particles and thus, did not contribute to any enhancement effect.

CHAPTER 7 | Probing the Effects of
Topically Applied PolyNIPAM-based Nanogels
on Skin Inflammation

7.1 INTRODUCTION

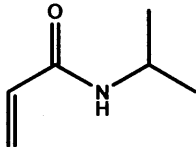
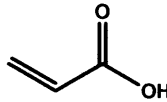
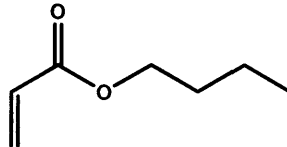
7.1.1 Biocompatibility of PolyNIPAM-based Polymers

The previous chapters (CHAPTERS 3, 5 and 6) demonstrated the potential of the poly(NIPAM-co-BA), poly(NIPAM-co-AAc)(5%) and polyNIPAM nanogels, as efficient carriers for drugs targeting skin as their site of action. It is necessary to justify the biocompatibility of the nanogels on the skin since they are directly in contact upon application. Several published works have reported the cytotoxicity profiles of polyNIPAM-based polymers and their corresponding monomers at cellular level (e.g. human keratinocytes, HaCaT), in addition to investigations using animal models such as mice and rats (Wadajkar et al., 2009).

7.1.1.1 Monomer and co-monomers: NIPAM, AAc and BA

NIPAM and co-monomers used to synthesise the poly(NIPAM-co-AAc)(5%) and poly(NIPAM-co-BA) are shown in [Table 7-1](#). A free NIPAM monomer (prior to polymerisation) may have some toxic effects at certain concentrations (Ankareddi et al., 2008; Wadajkar et al., 2009), a similar condition as AAc and BA co-monomers (Malonne et al., 2005). The simple acrylates have been shown to have some potential to cause skin irritancy to mucous membrane and skin, but have relatively low systemic mammalian toxicity (Dearman et al., 2007; deBethizy et al., 1987; Ghanayem et al., 1985). The toxicity effects caused by the free monomers are attributed by their small size and the participation of their double bond in interactions which may cause chemical modification to protein and nucleic acid molecules (Ankareddi et al., 2008; Ghanayem et al., 1985). They are reported capable to permeate cell membranes consequently affecting biological processes such as preventing cell division, elongation of cells, and inhibition of nucleic acid synthesis.

Table 7-1: Physicochemical properties of NIPAM, AAc and BA monomers.

	NIPAM	AAc	BA
Chemical Structure			
Chemical Formula	C ₆ H ₁₁ NO	C ₃ H ₄ O ₂	C ₇ H ₁₂ O ₂
MW	113.16	72.06	128.17
cLog P	0.28	0.31	2.36

Despite of the wide use of acrylates in consumer's products, there are few literature reports discussing their irritancy mechanism, particularly in triggering inflammatory reaction in cutaneous tissues. Most of the studies carried out concerned their systemic toxicity effects (Ghanayem et al., 1985; Hideji and Kazuo, 1982; Silver and Murphy, 1981).

7.1.1.2 PolyNIPAM-based Polymers

To date, studies indicate that the polyNIPAM-based polymers are biocompatible even exposed for longer durations (up to 96 h) (Naha et al., 2010a; Wadajkar et al., 2009). The polymers are widely used in gel electrophoresis and biomaterials such as soft contact lenses and tissue implants. The biocompatible properties of the polymers are suggested to be due to its large size and absence of any reactive groups for chemical reactions. Copolymers are comprised of several building blocks of monomers, i.e. a primary monomer and co-monomers, cross-linked by a cross-linker agent in a chemical reaction where the monomer should generally largely consumed by the reaction. However, it was reported that some unreacted monomers (residual) could possibly remain even after being purified, typically in the range of 10 – 1000 ppm for polymers used in cosmetic products (Zondlo, 2002). After thorough assessment, the CIR Expert Panel considered the levels as safe to be use in cosmetic formulations.

Exogenous compounds have the potential to induce inflammatory reaction in the skin tissue, although not necessarily caused toxicity. However, one of the characteristic features of toxicity is inflammation. Even though there are numerous toxicological studies for polyNIPAM-based polymers (Ankareddi et al., 2008; Malonne et al., 2005; Naha et al., 2010a; Wadajkar et al., 2009), to best of our knowledge, there is no published information about their inflammatory reaction particularly in skin. Clearly, if such materials caused adverse skin reactions, it would limit their applicability in a clinical setting.

7.1.2 Determining the Modulation of Skin Inflammation

The skin plays a critical role as a part of human body defence mechanism system. Beneath the cornified stratum corneum is the viable epidermis which is composed of living cells (keratinocytes) that can exhibit rapid characteristic tissue response to damage and irritation via inflammation as well as protective and repair processes (e.g. wound healing) when the irritants get through. The keratinocytes respond to skin irritation and injury by cytokine release and a rapid but transient activation of arachidonic acid metabolism along both the COX and lipoxygenase pathways (Marks et al., 1998). COX-1 and COX-2 are involved in the biosynthesis of prostaglandin E₂, a major prostaglandin involved in epidermal homeostasis and repair. COX-1 is thought to be involved in normal skin homeostasis, whereas COX-2 is important in various responses to insults to the skin either mechanical or chemical.

Cyclooxygenase (COX) is the key enzyme that is responsible for the conversion of arachidonic acid to prostaglandins, as shown in the pathway illustrated in **Figure 7-1**.

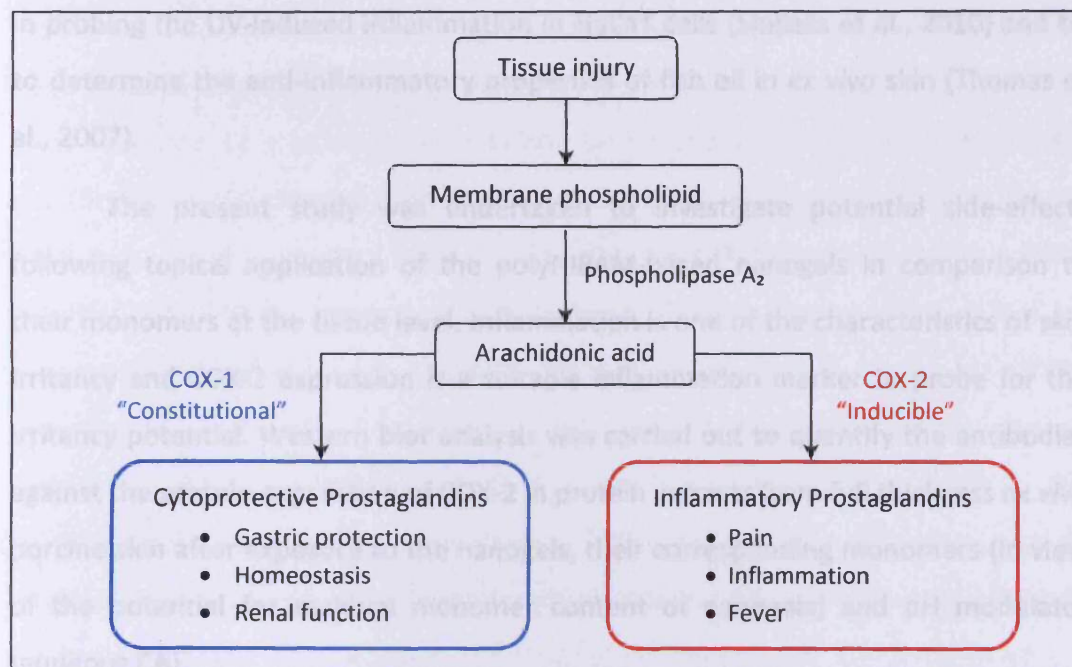


Figure 7-1: Schematic showing COX pathway – COX-1 and COX-2 enzymes. Adapted from (Maroon et al., 2006).

7.2 MATERIALS AND METHODS

Two main COX isoforms have been identified and are recognised as COX-1 and COX-2. COX-1, thought to be a “housekeeping enzyme”, is expressed constitutively in most cell types including keratinocytes, and is responsible for maintaining physiological prostaglandins concentrations that maintain cellular homeostasis, platelet aggregation (Rajakariar et al., 2006) and protection of the gastric mucosa (Futagami et al., 2002). COX-2, a 74 kiloDalton (kDa) protein, occurs in fewer cells, such as the epidermis and vascular endothelium, but its expression is induced in many tissues following injury or inflammation (Crofford, 1997). It is also induced in inflammatory diseases (e.g. psoriasis) (Hernández et al., 2001; Stark et al., 2006) and therapeutic anti-inflammatory drugs, such as naproxen, target this enzyme. It has been reported that COX-2 is also associated with differentiation and transformation of keratinocytes (Leong et al., 1996) for example during wound healing (Futagami et al., 2002).

COX-2 has a short half-life and so the relative levels of its expression can be directly related to the level of pro- or anti-inflammatory stimulus at a particular time point, given that the cells or skin tissue remains viable. This approach has been used

in probing the UV-induced inflammation in HaCaT cells (Shibata et al., 2010) and by to determine the anti-inflammatory properties of fish oil in *ex vivo* skin (Thomas et al., 2007).

The present study was undertaken to investigate potential side-effects following topical application of the polyNIPAM-based nanogels in comparison to their monomers at the tissue level. Inflammation is one of the characteristics of skin irritancy and COX-2 expression is a suitable inflammation marker to probe for the irritancy potential. Western blot analysis was carried out to quantify the antibodies against the protein expression of COX-2 in protein extracts from full thickness *ex vivo* porcine skin after exposure to the nanogels, their corresponding monomers (in view of the potential for residual monomer content of nanogels) and pH modulator (aqueous CA).

7.2 MATERIALS AND METHODS

7.2.1 Materials

The materials used for synthesis of polyNIPAM-based nanogels were outlined in Sections 2.2.1 and 4.2.1. Acrylamide/bis-acrylamide (30% solution v/v), ammonium persulfate (APS, ≥98%), aprotinin (≥98%), dithiothreitol (DTT, 1 M in water), ethylene diamine tetraacetic acid (EDTA, 98%), Hanks' balanced salt buffer, leupeptin hydrochloride (≥70%), Monoclonal Anti-β-Actin antibody produced in mouse (clone AC-74, ascites fluid, A 5316), HEPES (≥99.5%), phenylmethylsulphonyl fluoride (PMSF, ≥99%), PBS (pH 7.4), polyoxyethylene-sorbitan monolaurate (Tween® 20), ponceau S and RIPA Buffer were purchased from Sigma-Aldrich (Poole, UK). Cyclooxygenase-2 antibody (COX-2, #4842), anti-rabbit immunoglobulins (IgG) horseradish-peroxidase (HRP)-linked antibodies and positive controls for COX-2 (RAW 264.7 cells lysate, untreated or LPS treated) by Cell Signaling Technology, purchased from New England BioLabs Ltd., (Hitchin, UK). Full range Rainbow® recombinant protein molecular weight marker (12 – 225 kDa) was purchased from

GE Healthcare Life Sciences (Little Chalfont, UK) and Bio-Rad protein assay reagent from Bio-Rad Laboratories GmbH (Munich, Germany). MXB autoradiography film (blue sensitive: 18 × 24 cm²) was obtained from Genetic Research Instrumentation Ltd. (Braintree, UK). Marvel original dried skimmed milk was purchased from Chivers Ireland Ltd. (Dublin, Ireland). Bovine serum albumen (BSA), bromophenol blue (99%, UV-VIS), DMSO (99%), gentamycin sulfate, glycerol (99%), glycine (99%), N,N,N',N'-Tetramethyl-ethylenediamine (TEMED, 99%), positive control lysate for COX-2 (Human cells-13 lysate, 250 µg in 0.1 mL), sodium bicarbonate (99%), sodium chloride (NaCl, 99.9%), sodium dodecyl sulphate (SDS), tris (hydroxymethyl)methylamine (Tris base, 99.8%), Thermo Scientific SuperSignal® West Dura Extended Duration Substrate, filter paper QL100 (equivalent to Whatman Grade 1), nitrocellulose transfer membrane (Whatman Protran® BA85 with pore size of 0.45 µm) and all other solvents were of analytical grade or equivalent obtained from Fisher Scientific (Loughborough, UK).

Freshly excised porcine ears were obtained from a local abattoir prior to steam cleaning and immersed in iced HEPES-buffered Hanks' balanced salt (HBHBS) solution upon excision, to help maintain viability. The solution was made up of Hanks' balanced salt buffer (9.7 g), HEPES (6 mg), and sodium bicarbonate (0.35 g) in 1 L de-ionised water to facilitate extended skin viability, and thus maintain skin metabolism activities, during transportation from the abattoir to the laboratory. The skin was used within 3 h of slaughter.

7.2.2 Methods

7.2.2.1 Western Blot Analysis

Western blotting is a technique used to identify and locate proteins or enzymes of interest in a given sample of tissue homogenate or extract, based on their ability to bind to specific antibodies. This technique gives information regarding:

- (i) The size of the proteins in comparison to a size marker and
- (ii) The relative expression level in comparison to a control.

7.2.2.1.1 Sample Preparation: Skin Lysates

The freshly excised porcine skin sections were prepared according to the protocol in Section 3.2.2.4.3 and set up in Franz-type glass cells as detailed in Section 3.2.2.5, where treatments were prepared in de-ionised water (**Table 7-2**). The receptor phase, HBHBS - gentamycin was made up of HBSS (9.7 g), HEPES (6 mg), sodium bicarbonate (0.35 g), and gentamycin sulfate (50 mg) in 1 L de-ionised water. The HBHBS was used as it proven able to maintain skin viability for 24 h (Bronaugh, 2007), while gentamycin served a role to inhibit or minimise bacterial growth in the receptor phase. Skin samples were recovered from the diffusion cells 9 h post-application of the treatments. The areas, to which the treatments were applied, were weighed to ~0.4 g of full thickness skin. They were cut into small pieces using a clean blade and homogenised using a Silverson® homogeniser (Silverson Machines Ltd., Chesham, UK) in a lysis buffer (RIPA buffer added with fresh protease inhibitors as listed in **Table 7-3**: PMSF, EDTA, aprotinin, and leupeptin to make up a final volume of 500 µL) to release the protein of interest. The buffer (with inhibitors) should be ice-cold prior to homogenisation and its volume must be determined in relation to the amount of tissue presents. This is to ensure the protein extracted not to be too diluted to prevent loss of protein and large volumes of samples to be loaded onto gels. The homogeniser was rinsed with HBHBS solution after each sample. After 15 min incubation on ice, samples were centrifuged in the Heraeus Multifuge 3 S-R (14,000 rpm, 4°C for 15 min), twice in Eppendorf® tubes. The resulting supernatants were aspirated and stored at -20°C prior to use.

Table 7-2: Treatments applied for the protein immunoblot study.

	Dosing Regimen	Dose (μL)
(i)	Aqueous solution of NIPAM monomer (1% w/v, pH 6.68 ± 0.03) alone	500
(ii)	Aqueous solution of AAc monomer (0.05% v/v, pH 3.10 ± 0.01) alone	500
(iii)	Aqueous solution of CA (5% w/v, pH 1.91 ± 0.01) alone	200
(iv)	Swollen polyNIPAM nanogel alone	500
(v)	Swollen poly(NIPAM-co-AAc)(5%) nanogel alone	500
(vi)	Swollen poly(NIPAM-co-AAc)(5%), followed by aqueous solution of CA (5% w/v)	500 + 200
(vii)	De-ionised water alone	500
(viii)	Aqueous saturated solution of MTX (pH 4.69 ± 0.10) alone	500
(x)	Swollen poly(NIPAM-co-BA) nanogel alone	100

*Applied dose: Monomers – based on the actual concentrations utilised during the nanogel preparations (CHAPTERS 2 and 4), and for other treatments - based on the related *in vitro* permeation investigations (CHAPTERS 3, 5 and 6).

Table 7-3: Cocktail of protease inhibitors added to the RIPA buffer for lysis of tissue samples.

Inhibitor	Protease Inhibited	Stock (stored at -20°C)	Final Concentration in Lysis Buffer
Aprotinin	• Trypsin	Diluted in water, 1 mg mL^{-1}	$5 \mu\text{g mL}^{-1}$
	• Chymotrypsin		
	• Plasmin		
Leupeptin	• Lysosomal	Diluted in water, 0.5 mg mL^{-1}	$5 \mu\text{g mL}^{-1}$
PMSF	• Serine	Diluted in ethanol, 0.1 M	1 mM
	• Cysteine proteases		
EDTA	• Metalloproteases that require Mg^{++} and Mn^{++}	Diluted in water, 0.1 M	1 mM

7.2.2.1.1.1 Protein Estimation

Total protein concentration in the skin lysates was determined using the Bio-Rad protein assay kit (modified Lowry method). BSA was used as the protein standard and a standard curve was produced using dilutions with a range of 0 - 25 $\mu\text{g mL}^{-1}$ BSA in de-ionised water. Sample protein lysates were made by diluting the supernatants of the skin lysates at 1/200 in de-ionised water. Then, 200 μL of the Bio-Rad reagent was added to 800 μL of each diluted lysate sample and BSA standard in 1.5 mL disposable cuvettes. The mixtures were gently mixed and left to stand for ~ 15 min for full colour development. The resulting blue colour was then read at 595 nm using a UV spectrophotometer (CECIL Instruments CE2041 series 2000, Cecil Instruments, Cambridge, UK). The protein concentration in each diluted sample was obtained through extrapolation of the standard BSA curve with $R^2 > 0.99$. The concentration in the total sample was worked out by multiplying with the dilution factor. All samples and standards were prepared in replicates of three ($n=3$).

7.2.2.1.1.2 Protein Denaturation

Antibodies normally recognise only a small portion of the protein of interest and this domain may reside within the 3-D conformation of the protein. To enable access of the antibody to this portion, it is necessary to unfold the protein by denaturing it.

Skin lysates containing 25 μg of soluble proteins were aliquoted to Eppendorf® tubes and diluted in a 1:1 ratio with 2X Laemmli buffer (1.2 mL of 1 M Tris-HCL pH 6.8, 4 mL of 10% w/v SDS, 2 mL glycerol and 0.01% w/v bromophenol blue in de-ionised water to make up a total volume of 10 mL) containing 0.1 M DTT. The mixtures were mixed gently on Eppendorf® Mixer 5432 (Eppendorf®-Netheler-Hinz GmbH, Germany) for 5 min. The lid of the tubes were pierced with a syringe needle before being placed in the heating block at 100°C for 5 min to denaturise the tertiary form of the proteins. Then, the samples were cool down for 5 min and mixed gently at RT before subjected to centrifugation (Heraeus Multifuge 3 S-R, 14,000 rpm

at 4°C for 1 min) to spin the evaporated liquid down the Eppendorf®. The denatured samples were then stored at -20°C or used straight away for Sodium dodecyl sulphate-polyacrylamide gel electrophoresis (SDS-PAGE).

7.2.2.1.2 Gel Electrophoresis

SDS-PAGE was performed using the XCell SureLock™ Mini - Cell (Invitrogen Ltd., Paisley, UK) (**Figure 7-2**) powered by a Powerpac 300 power pack (Bio-Rad Laboratories Ltd., Hemel Hempstead, UK) following the manufacturer's guidelines.

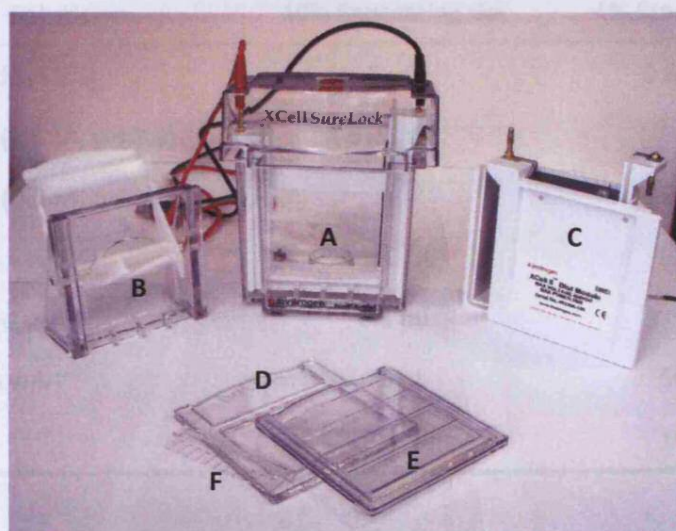


Figure 7-2: Components of XCell SureLock™ Mini - Cell electrophoresis system apparatus.

(A) electrophoresis module consists of a running tank, buffer core, and lid; (B) gel tension wedge; (C) Xcell™ Blot Module; (D) buffer dam; (E) plastic cassette; and (F) comb.

7.2.2.1.2.1 SDS-PAGE

The denatured samples were resolved on 10% SDS-PAGE separating gel and 4% SDS-PAGE stacking gel (**Table 7-4**). The separating gel was cast in a disposable plastic cassette (1.0 mm thick, Invitrogen Ltd., Paisley, UK) which held upright using a pair of bulldog clips as a stand. All the constituents of the separating gel, except the accelerators (APS and TEMED), were prepared in a universal container with gentle

mixing to minimise formation of gas bubbles. APS and TEMED were then added to the gel solution immediately prior to use as these chemicals catalyse the polymerisation of the acrylamide causing the gel to set. The separating gel solution was quickly, but gently, transferred into the cassette using a pipette leaving ~2 cm from top for loading the stacking gel later. The separating solution was then overlaid with de-ionised water to ensure a flat surface obtained when the gel had set and prevent the gel from drying out. The gel was allowed to set at RT for ~30 min.

Table 7-4: Separating and stacking gels used in SDS-PAGE analysis. The preparation can be used to prepare two SDS-PAGE gels.

Solution	10% Separating Gel	4% Stacking Gel
Acrylamide (30%)	5 mL	0.65 mL
Tris base (1.5 M, pH 8.8)	3.75 mL	-
Tris base (0.5 M, pH 6.8)	-	1.25 mL
SDS (10% w/v)	150 μ L	50 μ L
De-ionised water	6.1 mL	3.05 mL
APS (10% w/v)	75 μ L	50 μ L
TEMED	7.5 μ L	10 μ L

De-ionised water was poured out of the cassette and any excess was removed with a filter paper. The stacking gel solution was prepared and transferred on top of the separating gel using a pipette. A 12-well comb (1.0 mm thick, Invitrogen Ltd., Paisley, UK) was immediately inserted and the gel was allowed to set at ambient temperature for ~15 min. After setting, the comb was removed, and the wells were rinsed with de-ionised water before placing the cassette in the electrophoresis tank. Then, the 1X running buffer was used to fill up each well. The running buffer of 1X concentration was prepared by diluting the 10X stock solution (0.25 M Tris base, 1.92 M glycine and 1% SDS with no pH adjustment) with de-ionised water. The samples prepared were loaded into the wells of the stacking gel alongside 2.5 μ L of Full range Rainbow® recombinant protein molecular weight

marker (10 – 250 kDa) and positive control lysate for COX-2. The Rainbow[®] marker enables the determination of the protein size and the positive control lysate used to demonstrate that the protocol is efficient and correct and that the antibody recognised the target which may not be present in the experimental samples. If there was any well not needed, the Laemmli buffer containing no sample was used to load the well. This procedure ensures that each well behaves the same during separation. If an adjacent well is left empty, the adjoining samples will tend to spread laterally during electrophoresis.

The entire inner and outer chambers of the electrophoresis tank were filled with the 1X running buffer. The tank was then connected to the power pack and electrophoresis was performed at a constant voltage 125 V per gel (expected current start at 25 mA per gel) until the tracker dye reaches the bottom of the separating gel (~60 min) as shown in **Figure 7-3**. After electrophoresis, the gel was carefully removed from the cassette. The stacking gel and the bottom part of the gel were carefully cut out and discarded. The separating gel was then transferred carefully to a tray containing transfer buffer to briefly wash off any excess of SDS. The buffer was made up of 40 mL of 25X running buffer (0.3 M Tris base and 2.4 M glycine, no pH adjustment was done), 200 mL methanol and 760 mL de-ionised water.

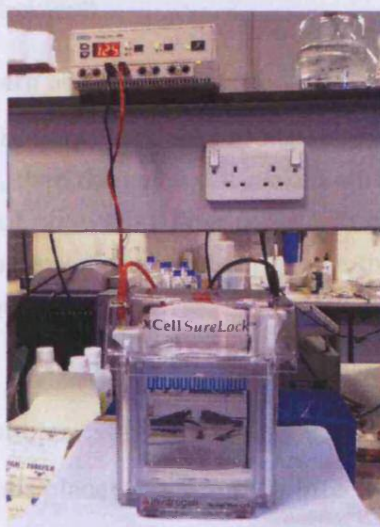


Figure 7-3: Gel electrophoresis set up demonstrating the electrophoresis stage. Sample wells were marked with a marker pen to aid loading of samples.

7.2.2.1.2.2 Protein Blotting

For each developed gel, the proteins were transferred from within the gel onto a nitrocellulose membrane using electric current. In preparation for blotting procedure, two filter papers and a nitrocellulose membrane were cut slightly larger than the size of the gel. The membrane, filter papers and four sponge pads were pre-soaked in the transfer buffer until use. The gel was then assembled as shown in **Figure 7-4**.

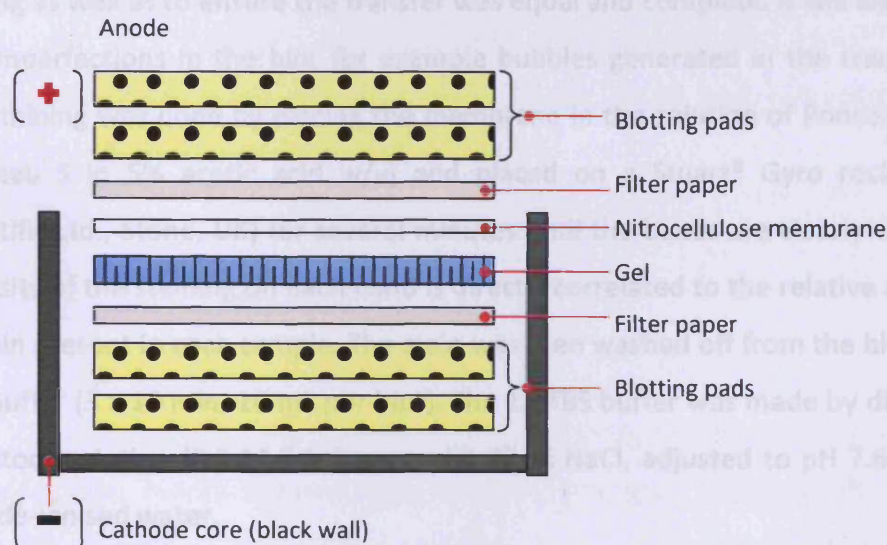


Figure 7-4: Assembly of Western blot 'gel sandwich'.

In a tray filled with transfer buffer, pre-soaked sponge pads are put on top, followed by a piece pre-wetted filter paper, then the gel. A pre-soaked nitrocellulose membrane is laid on top carefully. Another piece of pre-wetted filter paper and sponge pads are put in place. A glass tube is used to gently roll any air bubbles out before the gel sandwich is placed in a blot module and locked in an electrophoresis tank.

Any trapped air bubbles were removed by gently rolling a Pasteur pipette over the surface. It was then placed horizontally into the blotting module such that the gel was on the cathode of the cassette, whereas the membrane was closer to the anode. This was to ensure the proteins migrated from the gel to the membrane. After the gel was fitted into the electrophoresis tank, the transfer buffer was added

into the blotting module just above the assembly and de-ionised water was used to fill up the tank. The blotting was run at 25 V per gel (constant voltage: ~100 mA at start per gel) for 1 h.

7.2.2.1.3 Immunohistochemistry

After the blotting step, the transfer apparatus was disassembled and the nitrocellulose membrane was removed and rinsed twice in de-ionised water. The blot was temporarily stained with Ponceau S solution to observe successful protein loading as well as to ensure the transfer was equal and complete. It will also indicate any imperfections in the blot for example bubbles generated in the transfer step. The staining was done by placing the membrane in the solution of Ponceau S (0.1% Ponceau S in 5% acetic acid w/v) and placed on a Stuart® Gyro rocker (Bibby Scientific Ltd., Stone, UK) for several minutes until the bands are clearly visible. The intensity of the staining on each band is directly correlated to the relative amount of protein present in each sample. The stain was then washed off from the blot with 1X TBS buffer (3 x 10 min, 10 mL per blot). The 1X TBS buffer was made by diluting 10X TBS stock solution (0.2 M Tris base and 1.37 M NaCl, adjusted to pH 7.6 with HCl) with de-ionised water.

7.2.2.1.3.1 Membrane Blocking

Membrane blocking was done in order to block non-specific protein binding on the blot, eliminating false-positive results. The blot was blocked with 5% non-fat dry milk (Marvel) in TBS-Tween® (1X TBS with 0.1% v/v Tween® 20, 10 mL per blot) for 1 h at RT with constant rocking on a platform Stuart® Gyro rocker. After blocking, the milk solution was discarded and the blot was rinsed with TBS-Tween® (3 x 10 min, 10 mL per blot).

7.2.2.1.3.2 Primary and Secondary Antibody Conjugation

Primary antibody specific for the protein of interest was diluted to the required dilution using TBS-Tween®: The blot was incubated in the diluted primary antibody (COX-2, 1/1,000 dilution, 5 mL per blot) at 4°C for overnight incubation with constant gentle agitation on the platform Stuart® Gyro rocker. Later, the blot was washed with TBS-Tween® (3 x 10 min, 10 mL each blot) to remove any unbound primary antibody followed by conjugation with Anti-rabbit IgG, HRP-linked antibody (secondary antibody). The conjugation was carried out by incubating the blot in the diluted secondary antibody (1/10,000 in the TBS-Tween® with 1% w/v Marvel milk, 5 mL per blot) for 1 h under constant agitation on the Stuart® Gyro rocker at RT. The membrane was washed in PBS-Tween® (3 x 10 min, 20 mL each blot) prior to signal detection using chemiluminescence.

7.2.2.1.3.3 Detection of Protein

The blot was transferred into a light-proof x-ray cassette with its protein side facing up was evenly covered with a freshly prepared SuperSignal® West Dura Substrate working solution (300 µL per blot). It was incubated in the reagent for 5 min at RT. A clear plastic wrap was carefully placed on the cassette to cover the blot (avoid formation of bubbles) and the excess reagent was drained with a soft tissue before performing autoradiography. Time of exposure of the blot to autoradiography film varied adequately for an optimal signal and was developed using X-ray developer (X-O-graph Compact X2, X-O-graph Imaging System, Tetbury, UK). The bands corresponding to the protein of interest can be obtained as black bands. Membranes were subsequently washed in TBS-Tween (3 x 10 min, each) and stored in the fridge for up to 14 days.

The bands were scanned and analysed using ImageJ version 1.45b (National Institute of Health, Bethesda, MD). β -actin served as a loading control. Histograms represent the ratio of the protein of interest against β -actin and the control is 100%.

7.2.2.1.3.4 Loading Control

The loading control was used to verify the differences observed on a blot are not because of unequal loading of the wells but because of real changes upon treatment. The expression levels of the loading control should be at a constant level regardless of the treatment applied between different sample lanes.

β -actin, a 42 kDa molecule is normally the most appropriate protein to be used as a loading control. The blot was probed with 1/50,000 β -actin primary mouse antibody for 45 min followed by conjugation with Anti-rabbit IgG, HRP-linked antibody (secondary antibody) for 1 h. Both incubations were done at RT with constant agitation followed by 3 x 10 min washes in TBS-Tween® after every incubation process.

7.2.2.1.4 Data Analysis

The data obtained were recorded and analysed using Excel 2007 (Microsoft Office, Microsoft Corp., Redmond, WA) and expressed as a mean \pm SD. Statistical analysis was performed with InStat® for Macintosh, version 3.00 (GraphPad Software Inc., San Diego, CA). Significant differences and comparisons of the means between paired data were made using Student's *t*-test. For multiple comparisons, a one-way ANOVA analysis was carried out with Tukey's post-test to identify statistical significances between groups. Confidence interval was 95% where $p < 0.05$ was considered to be significant.

7.3 RESULTS AND DISCUSSION

A study has been carried out to examine potential pro-inflammatory side-effects of topically applied blank polyNIPAM-based nanogels and monomer components, using an *ex vivo* full-thickness porcine skin experimental model.

7.3.1 Western Blotting Determinations of COX-2 Expression

The skin inflammatory potential of the nanogels and their free monomers was determined using Western blotting, a technique in which activity is measured as a function of COX-2 expression induced in skin, post-topical exposure to the respected samples. In this assay, the samples were defined as positive (pro-inflammatory), if the level of COX-2 expression was greater than the recorded concurrent vehicle-treated control. All samples were formulated in the same vehicle, i.e. de-ionised water. COX-2 expression is associated with inflammatory reaction. Thus, any treatments that could increase the COX-2 level indicate inflammation in the skin tissue. Western blot analysis of the proteins was carried out on full-thickness porcine skin treated for 9 h. Quantification of the COX-2 expression was achieved by normalising the values with β -actin protein. MTX was used as a negative control and expected to cause reduction in COX-2 expression due to its anti-inflammatory property. In the current study, two nanogels of interest were investigated – poly(NIPAM-co-BA) and poly(NIPAM-co-AAc)(5%), as both nanogels were shown to enhanced the delivery of the model permeants by efficiently transporting the permeants across the SC (CHAPTERS 3 and 6).

7.3.1.1 Poly(NIPAM-co-AAc)(5%) Nanogel

The blots obtained for the poly(NIPAM-co-AAc)(5%) nanogel, its monomers (NIPAM and AAc), pH modulator (aqueous solution of CA) and control nanogel (polyNIPAM) are shown in [Figure 7-5](#). There was no significance difference between treatments in comparison to the skin treated with only vehicle (control) ($p=0.5123$). The poly(NIPAM-co-AAc)(5%) nanogel caused a slightly higher COX-2 expression by only 17%, and it is consider insignificant ($p=0.1578$). This promising results prove that the poly(NIPAM-co-AAc)(5%) nanogel is not pro-inflammatory even in the presence of aqueous CA solution (pH modulator). A similar result was exhibited by the polyNIPAM ($p=0.1458$). The non-inflammatory effect exhibited by the poly(NIPAM-co-AAc)(5%) and polyNIPAM nanogels could be possibly due to the absence of any

reactive constituents which might induce any interactions with skin components. The results obtained can be further supported by one of the recent publications, where polyNIPAM nanoparticles were assessed for cytotoxicity effect in a HaCaT cell line which served as a dermal model (Naha et al., 2010a). The authors discovered that, the particles were internalised in the cells and predominantly localised in the lysosomes. However, they did not significantly induce cytotoxicity even over a broad concentration range (25 – 1000 $\mu\text{g mL}^{-1}$). Based on the data in this study, it can be inferred that the poly(NIPAM-co-AAc)(5%) nanogel was found to be non-pro-inflammatory to the skin. However, extensive studies must be carried out to get a conclusive result regarding its compatibility with the tissue.

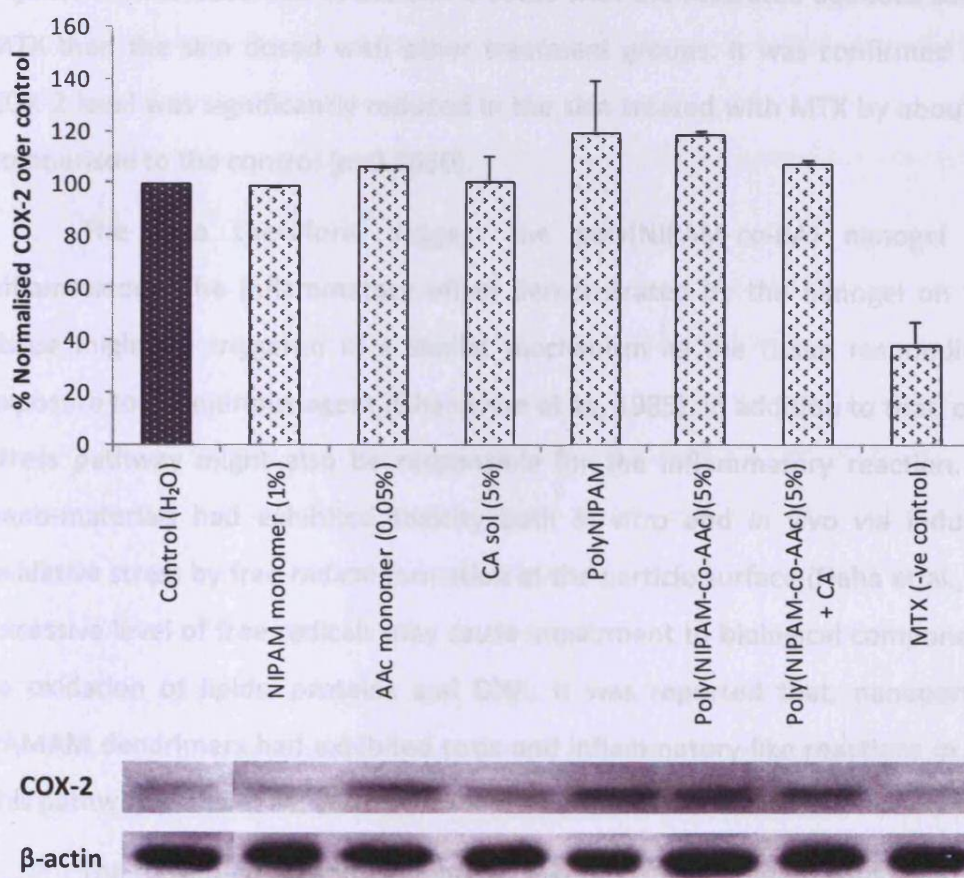


Figure 7-5: COX-2 protein expression by Western blot analysis. Porcine full-thickness skin was treated with the following – control (de-ionised water); NIPAM monomer (1% w/v); AAc monomer (0.05% v/v); aqueous solution of CA (5% w/v); polyNIPAM; poly(NIPAM-co-AAc)(5%); poly(NIPAM-co-AAc)(5%) followed by CA solution; and MTX – negative control at 6 h. The results were normalised using β -actin and level in control was arbitrarily assigned a value of 100%, (n=3, \pm SD). $p < 0.5123$ between treatment groups

7.3.1.2 Poly(NIPAM-co-BA) Nanogel

Immediately noticeable from the densitometric analysis of the resulting bands for COX-2 at ~72 kDa, as shown in [Figure 7-6](#) is that this nanogel is significantly pro-inflammatory. The analysis exhibited a marked induction of COX-2 protein by the nanogel, with COX-2 expression of 67% higher than the control, i.e. skin treated with the vehicle alone ($p=0.0035$). This was followed by the polyNIPAM with COX-2 level of 18% higher than the control ($p=0.1458$). Surprisingly, the aqueous solution of NIPAM monomer (1%) was found not to be pro-inflammatory, as its COX-2 expression level was about the same as the control ($p=0.8905$). Much less intense expression was observed in the skin treated with the saturated aqueous solution of MTX than the skin dosed with other treatment groups. It was confirmed that the COX-2 level was significantly reduced in the skin treated with MTX by about 63% in comparison to the control ($p=0.0060$).

The data therefore, suggest the poly(NIPAM-co-BA) nanogel is pro-inflammatory. The inflammatory effect demonstrated by the nanogel on the skin tissue might be triggered in a similar mechanism as the tissue responding after exposure to an injurious agent (Ghanayem et al., 1985). In addition to that, oxidative stress pathway might also be responsible for the inflammatory reaction. Several nano-materials had exhibited toxicity both *in vitro* and *in vivo* via induction of oxidative stress by free radical formation at the particle surface (Naha et al., 2010a). Excessive level of free radicals may cause impairment to biological components due to oxidation of lipids, proteins and DNA. It was reported that, nanoparticles of PAMAM dendrimers had exhibited toxic and inflammatory-like reactions in cells via this pathway (Naha et al., 2010b).

The observed pro-inflammatory response was unexpected but may be explained by several factors, including a hydrophobicity factor. The poly(NIPAM-co-BA) was prepared by copolymerising the NIPAM with the BA co-monomer, which aimed to reduce the LCST of the resultant copolymer compared to the polyNIPAM, by increasing its overall hydrophobicity. Thus, the nanogel was more hydrophobic in comparison to the poly(NIPAM-co-AAc)(5%), owing to its extra hydrocarbon chain

originated from the BA co-monomer. In a study conducted aimed to investigate cell attachment and detachment control with temperature-induced alteration of surface properties with grafted polyNIPAM copolymers, it was reported that the polymers caused deterioration of cellular metabolic functions at lower temperatures, when they were in a hydrophobic state (Tsuda et al., 2004). This condition is suggested due to cell-and protein-adhesion behaviour of the polymers. Individual functional groups have been demonstrated to affect protein adsorption, cellular response and cell-biomaterial interaction (Lynch et al., 2005). Surfaces displaying methyl groups ($-\text{CH}_3$) bound to proteins more firmly in comparison to surfaces displaying hydroxyl groups ($-\text{OH}$). This interaction may trigger immune response, as shown in another independent study, where the methyl groups were found to trigger immune response by increasing the adhesion of inflammatory cells. In the current study, the BA region of the poly(NIPAM-co-BA) possessed methyl groups belongs to the butyl hydrocarbon, whereas the poly(NIPAM-co-AAc)(5%) possessed carboxyl groups originating from the AAc residues.

Apart from the above factors, the samples obtained for this study were originated from the *in vitro* experiment with static diffusion cells. A potential disadvantage of the static diffusion cells is that accumulation of penetrants may occur both in the skin and receptor chambers in comparison to *in vivo* models with more complex systems (e.g. blood clearance and presence of enzyme activities) (Chilcott et al., 2001). Thus, the likelihood to produce the observed effect is higher in the *in vitro* model compared to the *in vivo* model.

Referring to the *in vitro* study of the MTX-loaded poly(NIPAM-co-BA) nanogel in CHAPTER 3, it was demonstrated that the nanogel was capable of delivering MTX across the epidermis in levels that significantly reduce the biosynthesis of prostaglandin E₂ (PGE₂), a key inflammation mediator. Thus the observed reduced level of PGE₂ was due to the enhanced delivery of MTX, which overwhelmed the inflammatory effect produced by the nanogel.

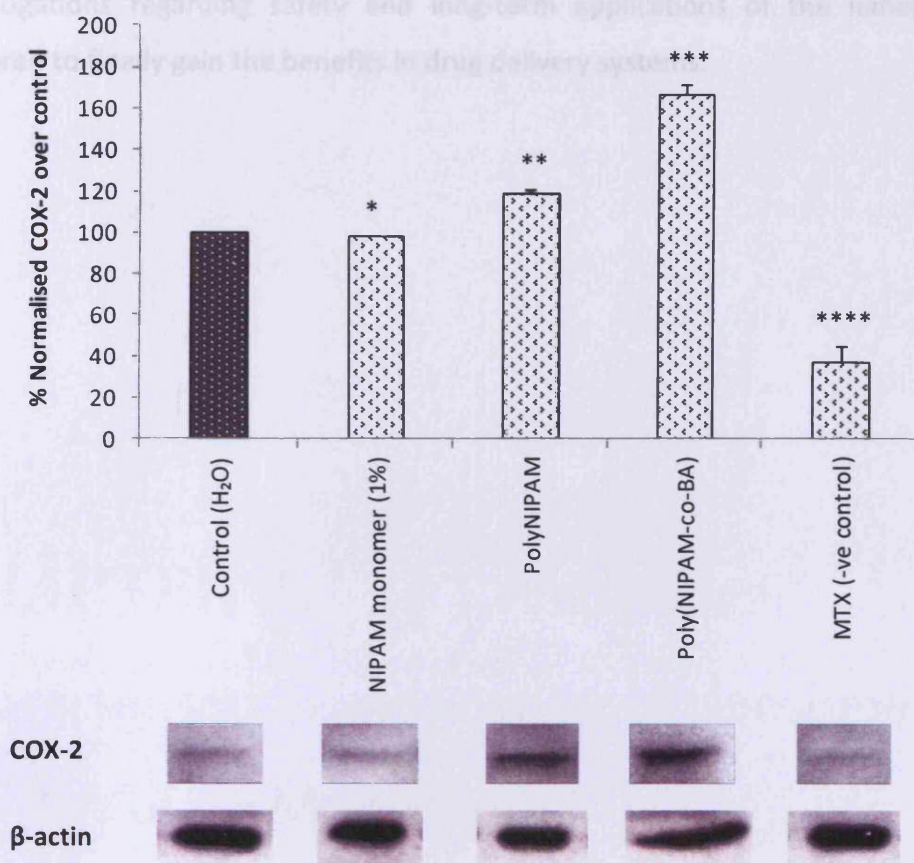


Figure 7-6: Western blotting and densitometric analysis of COX-2 protein expression. Porcine full-thickness skin was treated for 9 h with the following – control (de-ionised water); NIPAM monomer (1% w/v); polyNIPAM; poly(NIPAM-co-BA); and MTX (negative control); Results were normalised using β -actin and level in control was arbitrarily assigned a value of 100% ($n=3$, \pm SD). (* $p=0.8905$, ** $p=0.1458$, *** $p=0.0035$ and **** $p=0.0060$, vs. control treatment)

7.4 CONCLUSION

The poly(NIPAM-co-BA) nanogel was found to induce inflammation reaction when applied topically, reflected by higher COX-2 expression than the control treatment. The data obtained for the poly(NIPAM-co-AAc)(5%) nanogel, on the other hand, indicated that the particles are compatible with skin, even in the presence of aqueous CA solution serving as an external pH modulator. This promising results, further support the potential use of the multi-responsive poly(NIPAM-co-AAc)(5%) nanogel for triggered- or controlled- drug delivery applications. However, rigorous

investigations regarding safety and long-term applications of the nanogels are required to finally gain the benefits in drug delivery systems.

CHAPTER 8 | Preparation,
Characterisation and Loading of Liposomes as
Carriers of pH Modulator

8.1 INTRODUCTION

Liposomes are lipid molecules that form spontaneously under suitable conditions to yield spherical, concentric phospholipid bimolecular layers in the form of vesicles (Balazs and Godbey, 2011; Taylor and Morris, 1995). They have a number of interesting properties including the ability to entrap other chemical species, and may be used as carriers for drugs, including those administered topically. Liposomes can be prepared with a wide range of lipids, including diacylphosphatidylcholine (lecithin), distearoylphosphatidylcholine (DSPC), phosphatidylcholine (PC), dipalmitoylphosphatidylcholine (DPPC) and sphingomyelin, which may be pure lipid or lipid blends. Depending on the lipids used, liposomes possess different properties, most notably in the aspect of phase transition temperatures (Taylor and Morris, 1995). In the current work, liposomes were explored as carriers for modulatory agent.

8.1.1 Preparation of Liposomes

Several techniques for producing liposomes have been proposed and established over the years, such as reverse-phase evaporation, thin-film hydration, ethanol injection and freeze-thaw (Chatterjee and Banerjee, 2002; Ranade and Cannon, 2011).

The most simple, rapid and common technique is the hydration of a lipid film where, a thin film of lipids is deposited onto the walls of a vessel (Ranade and Hollinger, 2003) – in this technique, the required proportions of lipid is first dissolved in a volatile organic solvent (e.g. chloroform, diethyl ether or methanol) to give a lipid solution. The volatile solvent is evaporated to obtain a thin lipid film, before the film is rehydrated with water, buffer or an aqueous solution containing the hydrophilic material to be entrapped within the liposome vesicles. If the film is rehydrated at temperatures above the phase transition temperature of the lipids, then multilamellar vesicles (MLV) will form spontaneously. These large structures,

typically ranging from 0.1 – 10 μm in diameters, have multiple lipid bilayers surrounding the aqueous core. The size and lamellarity of these MLVs are difficult to control, and hence these structures are subjected to sonication or extrusion through membrane filters to form large unilamellar vesicles (LUV, generally 1 – 5 μm in diameters) or small unilamellar vesicles (SUV, usually 0.1 – 0.5 μm in diameters).

8.1.2 Loading Compounds into Liposomes

The loading of compounds into liposomes can be achieved using the following techniques (Chrai et al., 2001):

- (i) Thin lipid film encapsulation technique is suitable for hydrophilic compounds which involve hydration of a lipid film using an aqueous solution of the desired compound. The dissolved compound resides in the inter-lamellar spaces (Figure 8-1);
- (ii) Partitioning – a hydrophobic compound is dissolved along with the lipids in a suitable organic solvent. Then, the solution is either dried first or added directly to the aqueous phase, and the residual solvent is removed under vacuum. The compound will be located in the intra-bilayer space (Figure 8-1), where the acyl chains of the phospholipids provide a solubilising environment for the compound; or
- (iii) The 'reverse loading' method, which works based on the principle that certain compounds may exist in both charged and uncharged states depending on the pH of their environment. Initially, the compound is added to an aqueous phase in its uncharged form to ease its permeation into liposome vesicles through lipid bilayers. Following that, the internal pH of the vesicles is adjusted to create a charge on the compound. Once charged, the compound will reside inside the vesicles, as its increased lipophilicity will inhibit its passage through the bilayer membrane to return to the external medium.

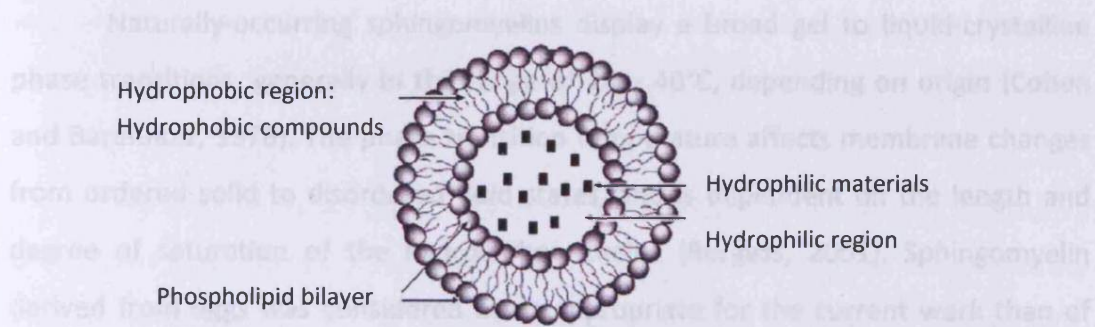


Figure 8-1: Hydrophilic and hydrophobic compounds encapsulation by a liposome vesicle. Adapted from (Pattnaik and Ray, 2009).

8.1.3 Sphingomyelin Liposomes

In the current study, the liposomes were produced from sphingomyelin, which is a type of sphingolipid consisting of a ceramide core unit (sphingosine bonded to a fatty acid via an amide linkage) with an attached polar head group, which is either phosphorylcholine or phosphoethanolamine. The general structure of sphingomyelin with phosphorylcholine as the head group is illustrated in **Figure 8-2**. Sphingomyelin is a ubiquitous component of animal cell membranes (Riboni et al., 2010). It is the most abundant sphingolipid and represents almost 85% of all sphingolipids in humans.

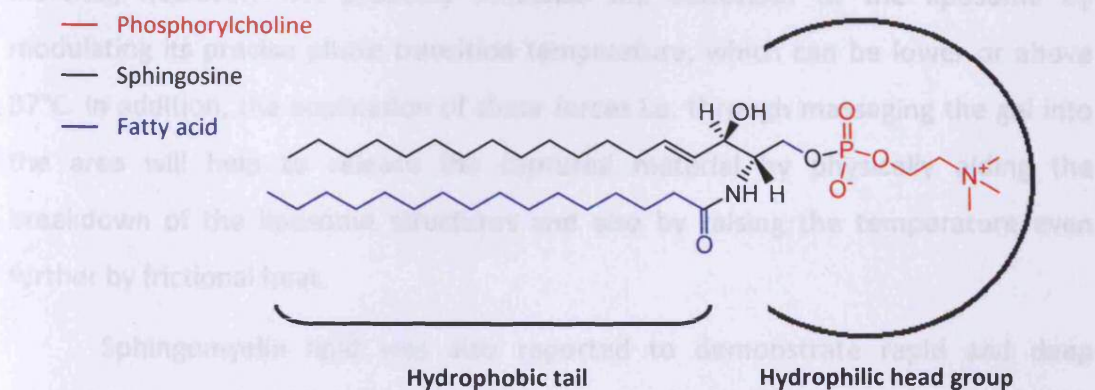


Figure 8-2: Chemical structure of sphingomyelin.

Naturally-occurring sphingomyelins display a broad gel to liquid-crystalline phase transitions, generally in the range of 28 – 40°C, depending on origin (Cohen and Barenholz, 1978). The phase transition temperature affects membrane changes from ordered solid to disordered fluid states, and is dependent on the length and degree of saturation of the hydrocarbon chains (Burgess, 2001). Sphingomyelin derived from eggs was considered more appropriate for the current work than of other types of lipids, such as PC and DPPC which have a reported phase transition temperature of ~41°C and ~21°C, respectively (Sulkowski et al., 2005). The egg sphingomyelin has a phase transition temperature of ~37°C, which is similar to the human physiological temperature (Rosen, 2005). Hypothetically, at temperatures below 37°C, the sphingomyelin bilayer is in a solid state due to the presence of palmitic acid (C₁₆H₃₂O₂), a saturated fatty acid in its structure. Thus, leakage of the entrapped material from the sphingomyelin liposome should be minimal. When the temperature is raised to and above 37°C, the liposome undergoes gel-to-liquid crystalline phase transition. This is accompanied by a loss of order in the liposome membrane structure, and change in bilayer thickness and density. These processes lead to an abrupt increase in membrane fluidity allowing the material contained within to escape, consequently activating the nanogel particles.

A transition phase of 37°C is ideal for a topical system, as it is slightly above the average surface temperature of human skin (≥ 32°C) and therefore, entrapped material can escape when the formulation is applied *in vivo*. The encapsulated material, however, will probably influence the behaviour of the liposome by modulating its precise phase transition temperature, which can be lower or above 37°C. In addition, the application of shear forces i.e. through massaging the gel into the area will help to release the captured material by physically aiding the breakdown of the liposome structures and also by raising the temperature even further by frictional heat.

Sphingomyelin lipid was also reported to demonstrate rapid and deep penetration into the dermal layer within 30 min post-application (Betz et al., 2001). Based on the CLSM images, it was suggested that the hair follicles played a role for the transport of the sphingomyelin liposome into the skin. However, the observation

was limited to the level of phospholipid molecules rather than the entire liposome vesicles due to the limited CLSM function, which only captured fluorescence material.

The primary purpose of the liposomal encapsulation is somewhat different in the current study, as deep penetration of the lipid vesicles into the skin is not our primary concern. The aim of the current study was to prepare a sphingomyelin based-liposome to probe whether they would be an appropriate means of isolating the pH modulator molecules from the nanogel particles until required. CA was selected as a model to be encapsulated in the aqueous core of the “blank” liposome vesicles to form a CA-loaded liposome, aimed to regulate the poly(NIPAM-co-AAc)(5%) nanogel carrier function by exploiting its pH-activation–de-swelling property. The concept is illustrated in **Figure 8-3**. To that end, sphingomyelin-based liposome vesicles were prepared by a thin film hydration method and evaluated for its physicochemical characteristics, such as vesicle size and size distribution, EE (%), and stability.

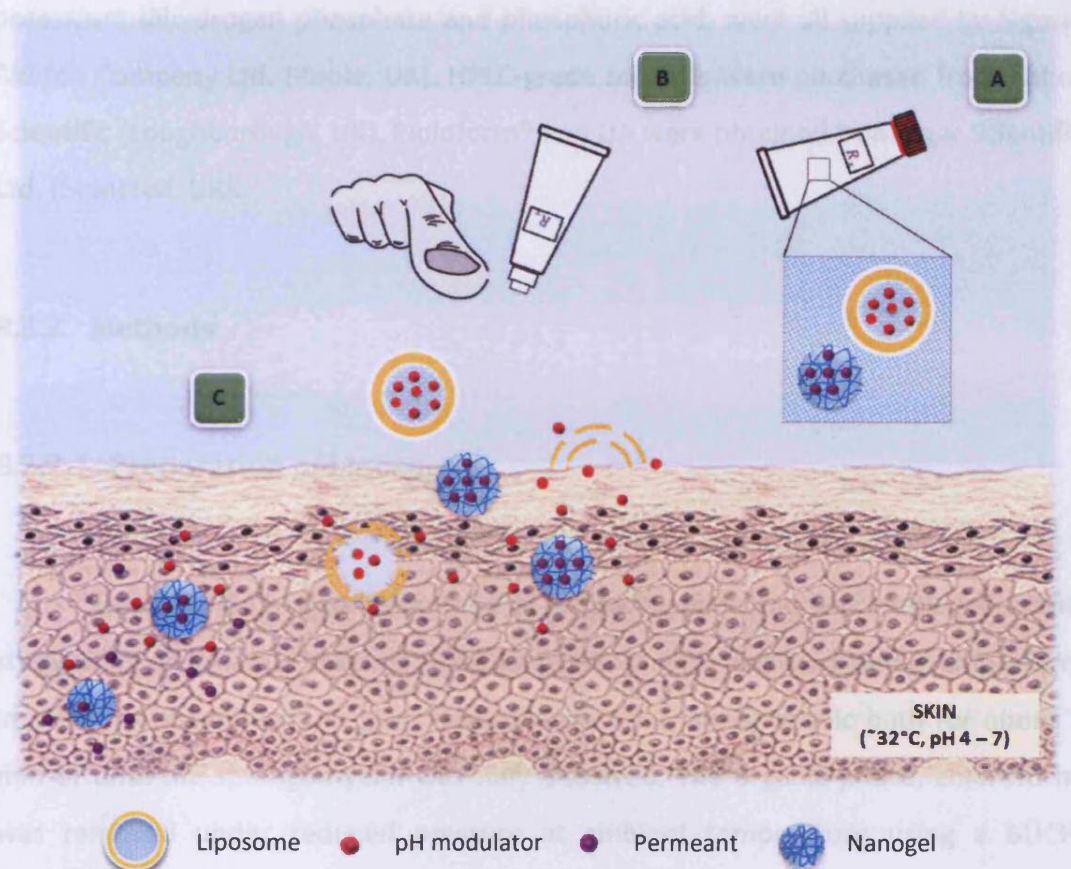


Figure 8-3: Schematic diagram of pH-modulator loaded-liposome vesicles in a proposed single compartment system.

(A) Two components, i.e. permeant-loaded nanogel particles and pH modulator-loaded liposome vesicles are formulated within a single tube, without any interactions take place under storage condition prior to use; (B) once applied onto the skin, the thermally labile sphingomyelin vesicle becomes leaky and releases its encapsulated pH modulator molecules *in situ*, ideally in the upper layer of skin; and (C) the acidic environment created by the pH modulator subsequently modulate the nanogel particles by causing the structure to collapse and expel its loaded-permeant. In addition, the particles are also simultaneously modulated by a temperature stimulus provided by the skin ($\sim 32^{\circ}\text{C}$).

8.2 MATERIALS AND METHODS

8.2.1 Materials

Egg-yolk sphingomyelin (LIPOID E SM, >98%, MW: 703) was a gift from Lipoid GmbH (Ludwigshafen, Germany) and was used as received. CA anhydrous (99.5%),

potassium dihydrogen phosphate and phosphoric acid, were all supplied by Sigma-Aldrich Company Ltd. (Poole, UK). HPLC-grade solvents were purchased from Fisher Scientific (Loughborough, UK). Pioloform® and UA were obtained from Agar Scientific Ltd. (Stansted, UK).

8.2.2 Methods

8.2.2.1 Preparation of Liposomes

The thin film hydration method of producing liposome was employed in this study using an in-house method. Sphingomyelin (2 mM) was dissolved in chloroform in a 250 mL round bottom glass flask and placed in an ultrasonic bath for about 5 min or until the sphingomyelin was fully dissolved. The organic phase, chloroform, was removed under reduced pressure at ambient temperature using a BÜCHI Rotovapor R-114 (BÜCHI Labortechnik AG, Flawil, Switzerland), thus forming a thin, dry lipid film around the inner face of the flask. In order to ensure that all residues of chloroform had been removed from the lipid mixture, the film was placed under high vacuum for 4 h before the encapsulation of the aqueous phase was undertaken.

The dried lipid film was hydrated with 5 mL of a pre-warmed (~45°C) aqueous CA solution (5% w/v) and the flask was agitated vigorously until all of the film had been re-suspended in the aqueous phase (i.e. no lipid film was visible on the flask wall). The liposome was further hydrated by low speed rotation at ~45°C, exceeding that of the sphingomyelin transition temperature (~37°C) using a rotary evaporator equipped with a BÜCHI water bath B-480 (BÜCHI Labortechnik AG, Flawil, Switzerland) under atmospheric pressure for 1 h. A temperature of 45°C was necessary to maintain the lipids in a gel-like state in order to maximise entrapment of CA inside the vesicles. Following this, the suspension was stored at 2 – 4°C overnight. Non-encapsulated CA was removed by centrifugation in the Beckman Coulter Avanti® J-25 at 50,000 x *g*, 4°C for 1 h. The resulting liposome pellets formed at the bottom of the tubes were washed with de-ionised water by repeated steps of

re-dispersion, centrifugation (50,000 x *g* for 1 h at 4°C) and decantation, after which the pellets were stored at 2 – 4°C and protected from light prior to use.

Unloaded liposome vesicles which served as a control were prepared in a similar manner as described above with the same volume of de-ionised water added during the film hydration step.

8.2.2.2 Determination of EE

The amount of CA successfully entrapped by liposome vesicles was presented as EE (%) and determined according to a protocol adapted from the one originally established by Ishii and Nagasaka (Ishii and Nagasaka, 2001; Nii and Ishii, 2005). The liposome batch was divided into two portions as described in **Figure 8-4**. Firstly, ethanol was added to a liposome pellet causing lysis of the structures (observed as a clear solution) and therefore, completely releasing the encapsulated CA into surrounding media. The resulting solution was immediately centrifuged to remove liposomal debris, before the supernatant was assayed by HPLC (Section 8.2.2.3). As the HPLC method was considered unsuitable for assaying CA in ethanol, the supernatant was evaporated beforehand and the CA remaining in the tube was reconstituted with de-ionised water. For the second step, the liposome pellet was suspended in de-ionised water in order to measure the amount of CA in the external phase of the intact liposome. The supernatant obtained after centrifugation was diluted 5-fold with de-ionised water. The concentration of CA in both samples was determined by HPLC in triplicate (n=3). The percentage of EE was calculated according to the Equation 3-1 described in CHAPTER 3.

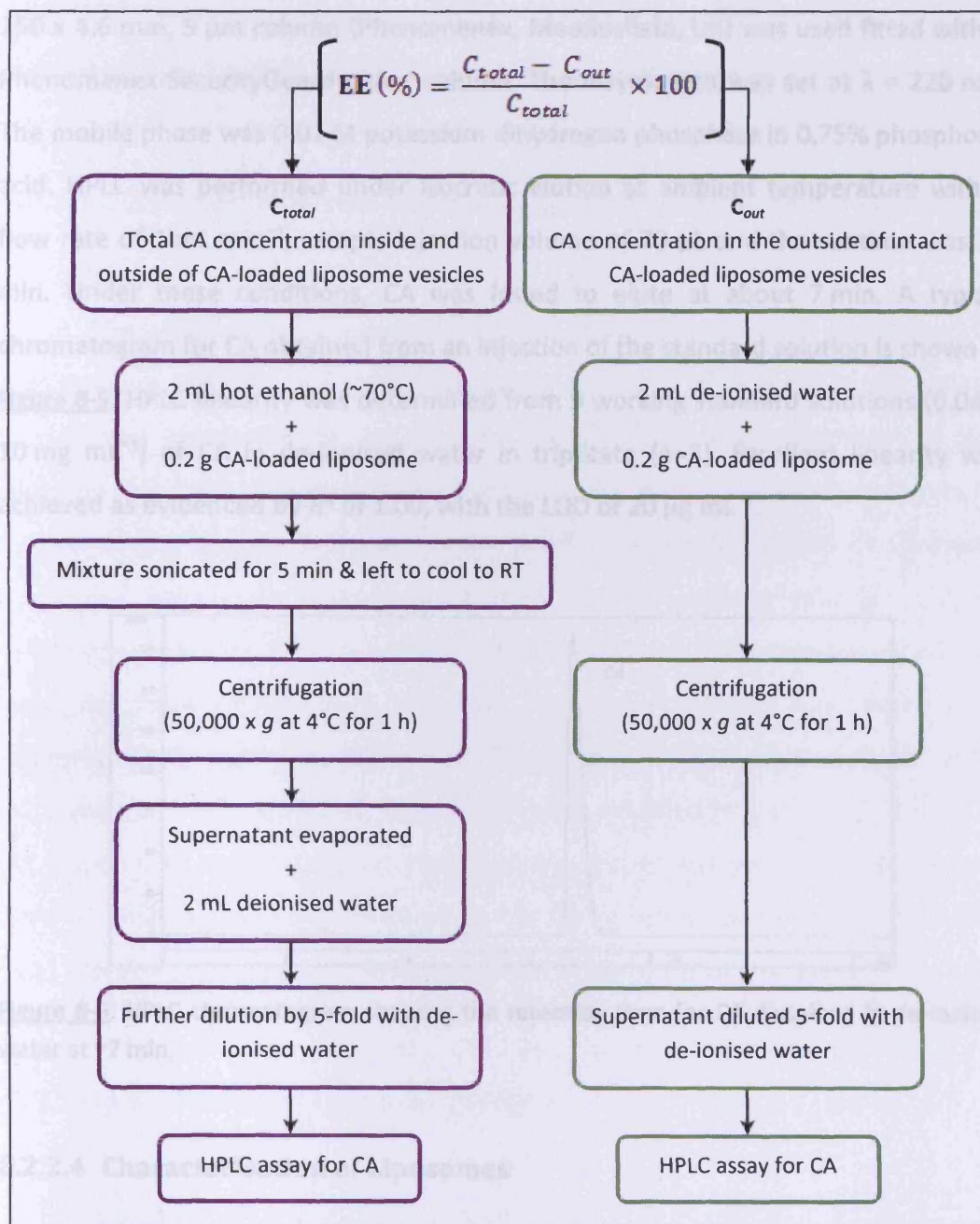


Figure 8-4: Flow chart describing the procedures for EE determination of CA.

8.2.2.3 HPLC Analysis of CA

Quantitative analysis of the CA content in the liposomes was performed by reversed-phase HPLC using an Agilent 1100 series automated system with Agilent ChemStation software (Agilent Technologies, Santa Clara, CA). A Gemini-NX C₁₈ ODS

250 x 4.6 mm, 5 μm column (Phenomenex, Macclesfield, UK) was used fitted with a Phenomenex SecurityGuard guard column. The wavelength was set at $\lambda = 220 \text{ nm}$. The mobile phase was 0.01 M potassium dihydrogen phosphate in 0.75% phosphoric acid. HPLC was performed under isocratic elution at ambient temperature with a flow rate of 1 mL min^{-1} , sample injection volume of $20 \mu\text{L}$ and the runtime was 12 min. Under these conditions, CA was found to elute at about 7 min. A typical chromatogram for CA obtained from an injection of the standard solution is shown in **Figure 8-5**. HPLC linearity was determined from 9 working standard solutions ($0.04 - 10 \text{ mg mL}^{-1}$) of CA in de-ionised water in triplicate ($n=3$). Excellent linearity was achieved as evidenced by R^2 of 1.00, with the LOD of $20 \mu\text{g mL}^{-1}$.

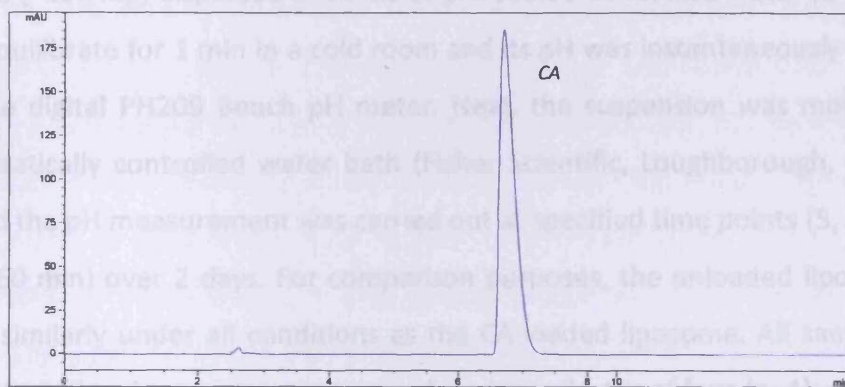


Figure 8-5: HPLC chromatogram showing the retention time for CA dissolved in de-ionised water at $\sim 7 \text{ min}$.

8.2.2.4.3 Evaluation of Liposome Stability

8.2.2.4 Characterisation of Liposomes

8.2.2.4.1 Vesicle Size and Size Distribution

One of the most commonly used methods to determine size and size distribution of the liposome vesicles is laser light scattering analysis (Ranade and Cannon, 2011). The analysis was carried out using Malvern Mastersizer 2000 at ambient temperature in replicates of three ($n=3$). Concentrations in the range of 1 – 5% w/v are ideally suited for most liposome size measurements. Thus, liposome suspensions were prepared at a concentration of 5% w/v in de-ionised water. For the

liposomes - the minimum, maximum and hydrodynamic (volume weighed mean) diameters of the vesicles, as well as span and uniformity values were reported.

8.2.2.4.2 Release of CA from Degrading Spingomyelin Liposome Vesicles

The ability of the liposome to release the encapsulated pH modulator, CA, into the surrounding media once applied onto the skin is of key importance and was investigated by monitoring pH of the CA-loaded liposomal suspension at 32°C (average skin surface temperature). Hypothetically, a decrease in pH indicates the leaking of the vesicles and CA release. Briefly, the purified pellet of CA-loaded liposome (~100 mg) dispersed in 10 mL of pre-cooled de-ionised water (2 – 4°C) was left to equilibrate for 1 min in a cold room and its pH was instantaneously measured using the digital PH209 Bench pH meter. Next, the suspension was moved into a thermostatically controlled water bath (Fisher Scientific, Loughborough, UK) set at 32°C and the pH measurement was carried out at specified time points (5, 10, 15, 30, 45 and 60 min) over 2 days. For comparison purposes, the unloaded liposome was treated similarly under all conditions as the CA-loaded liposome. All samples were light protected and measurements were done in replicates of four (n=4).

8.2.2.4.3 Evaluation of Liposome Stability

Liposome vesicles are considered unstable structures. They are known to be sensitive to fusion (grow into bigger vesicles), aggregation, degradation and leakage of the encapsulated substance during storage (Ranade and Cannon, 2011). The extent to which the liposome membrane retains its integrity in the acidic environment of its core region created by the associated or entrapped CA is again crucial, in order to be effective as a potential carrier for the pH modulator. A stability study was conducted in an attempt to establish that CA was effectively entrapped under storage condition (2 – 4°C) and during handling at ambient temperature (i.e. liposome vesicles were not leaky). A thermal stimulus (32°C) was also applied to the

liposomal suspension in order to model membrane integrity upon application onto the skin. It was crucial to ensure the liposome vesicles dump their contents into the external environment at ~32°C in order to activate the nanogel particles. Therefore, the effect of temperature and pH on the physical stability of the liposome prepared from pure sphingomyelin was evaluated by a laser light diffraction system and TEM observation.

8.2.2.4.3.1 Vesicle Size and Size Distribution

The stability of CA-loaded liposome was evaluated by monitoring its vesicle size and size distribution, as a function of a storage time (30 days). A fresh liposomal suspension (5% w/v in de-ionised water) was transferred into amber bottles, bubbled with nitrogen gas to remove traces of oxygen and sealed prior to storage either in a refrigerator at 2 – 4°C or left on a bench for RT environment. At predetermined time intervals (i.e. day -0, -1, -7, -20 and -30), samples were collected and subjected to measurement by Malvern Mastersizer 2000. Measurements on day-0 (baseline) were made 1 h after storage under the respected temperatures. Unloaded liposome served as a control for this study. All measurements were carried out in three replicates (n=3).

A further set of stability study was carried out, where the CA-loaded liposomal suspension was maintained at 32°C (skin surface temperature) and 40°C (maximal heat effect) to check for loss of structural integrity upon heating to the respected temperatures. From a topical delivery perspective, 32°C is the key requirement where the liposome vesicles should significantly liberate its encapsulated material into surrounding environment, consequently activating pH-responsive nanogel particles. The samples were incubated for 1 h in the thermostatically controlled water bath. The shorter incubation period was due to the hypothesis that, if the liposome structures would experience any damage at those temperatures, the effect should be rapid. All measurements were made in triplicate (n=3). Unloaded liposome served as a control and treated in the same manner as the CA-loaded liposome.

8.2.2.4.3.2 TEM

The effect of temperature and pH on the outer morphology of the CA-loaded liposome, post-treated at particular temperatures over a period of 7 days, was examined by TEM. To minimise overlapping of the lipid vesicles observed under the microscope, a liposomal suspension was freshly prepared in de-ionised water at 0.1% w/v concentration. Samples of the suspension were then stored at 2 – 4°C (fridge), RT (on a laboratory bench) or 32°C (thermostatically controlled water bath) in replicates of three (n=3). Samples for TEM were prepared according to the protocol in Section 4.2.2.3.4.2.1, before being examined and photographed on day-0 (1 h after incubation at the respected temperatures) and day-7. Unloaded liposome served as a control and treated in a similar way as the loaded liposome.

8.2.2.4.4 Thermal Analysis: Phase Transition

In order for the CA-loaded liposome to activate the nanogel particles efficiently, it is crucial for the vesicles to have adequate thermal-responsive property reflected by undergoing thermally-induced phase transition at a particular temperature range ($32^{\circ}\text{C} \leq T \leq 37^{\circ}\text{C}$). The primary aim of this study was to investigate the behaviour of the sphingomyelin liposome in several different environments.

Samples were prepared by dispersing concentrated CA-loaded and unloaded (control) liposomes in de-ionised water at 10% w/v. The resulting suspensions were left to equilibrate for 30 min at 2 – 4°C environment prior to analysis. A thermal scan was performed on the samples from 4 – 50°C at a scanning rate of $1^{\circ}\text{C min}^{-1}$, with an equilibrium period of 2 min. A standard DSC protocol and thermogram interpretation were described in Section 2.2.2.3.3.

8.2.2.5 Data Analysis

The data obtained were recorded and analysed using Excel 2010 (Microsoft Office, Microsoft Corp., Redmond, WA) and expressed as a mean \pm SD. Statistical test was carried out with InStat® for Macintosh, version 3.00 (GraphPad Software Inc., San Diego, CA). Significant differences and comparisons between paired means were made using Student's *t*-test. Analysis using a one-way ANOVA was performed, followed by Tukey-Kramer test for multiple comparisons among several groups. Confidence interval was 95% where $p < 0.05$ was considered to be significant.

8.2.3 RESULTS AND DISCUSSION

8.2.3.1 EE of Liposome

Encapsulating a high level of pH modulator was one of the most desirable properties in the current study. The concentration of CA in the liposome was determined by HPLC after disruption of the structures in ethanol at 1:1 ratio (Section 8.2.2.2). The total CA used during the preparation of liposomes was 1 mL of 5% aqueous solution of CA, which equals to 50 mg. Thus, the EE of CA-loaded liposome was found to be 5.3%.

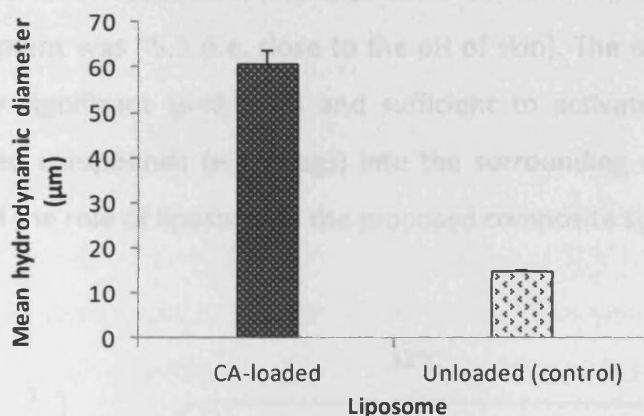
8.2.3.2 Liposome Characterisation

8.2.3.2.1 Vesicle Size and Size Distribution

The mean hydrodynamic diameter of the CA-loaded and unloaded liposome vesicles were found to be 60.73 ± 1.68 and 15.02 ± 0.11 μm respectively, as summarised in [Figure 8-6](#). The liposome vesicles containing CA were significantly

larger in size than the unloaded vesicles by about 4-fold ($p < 0.0001$), suggesting entrapment of CA molecules into the vesicles.

Both loaded- and unloaded-liposomes demonstrated unimodal size distributions with broad vesicle size characteristics as shown by their minimal and maximum vesicle diameters. Furthermore, the liposomes exhibited a rather high polydispersity i.e. non homogenous size distribution, as reflected by their span and uniformity distribution values. As the vesicles were intended to serve as carriers for pH modulator molecules, there are no specific concerns regarding the vesicle size and uniformity for enhanced skin permeation.



Liposome	Vesicle Diameter (µm)		Span	Uniformity
	Minimum	Maximum		
CA-loaded	17.21 ± 0.85	112.81 ± 8.14	2.31 ± 0.41	0.84 ± 0.12
Unloaded	4.93 ± 0.06	28.24 ± 0.35	1.81 ± 0.06	0.57 ± 0.004

Figure 8-6: Vesicle size analysis of CA-loaded liposome measured by laser light diffraction analyser at room temperature; unloaded liposome served as control; span and uniformity data represent polydispersity of the samples ($n=3$, \pm SD). $p < 0.0001$ vs. control

8.2.3.2.2 Release of CA from Degrading Sphingomyelin Liposome Vesicles

Figure 8-7 presents pH values of the CA-loaded liposomal suspension determined over a period of 60 min. At 2 – 4°C the suspensions of CA-loaded and

unloaded liposomes were measured as pH 4.70 and pH 4.82, respectively. Next, the same suspensions were transferred to a water bath of 32°C and maintained for 48 h. From the graph, it can be observed that the CA-loaded liposomal suspension demonstrated a sharp decline in pH by 21.9% (pH 4.70 → pH 3.67) after 5 min of storage at 32°C ($p < 0.0001$). Such a response is associated with a release of the encapsulated CA molecules by the liposome vesicles into the environmental media due to the loss of liposome structural integrity.

Based on **Figure 8-7**, the release of CA provided an acidic environment of pH 3.67. Correlating this data with the hydrodynamic diameter of poly(NIPAM-co-AAc)(5%) nanogel in response to pH changes (**Figure 4-9**), such condition may induced a diameter reduction of about 8.6% ($693 \pm 11 \text{ nm} \rightarrow 633 \pm 8 \text{ nm}$), assuming the pH of original environment was ~ 5.5 (i.e. close to the pH of skin). The diameter change is considered very significant ($p = 0.0015$) and sufficient to activate de-swelling and release of loaded compounds (e.g. drugs) into the surrounding environment. This result supported the role of liposome in the proposed composite system.

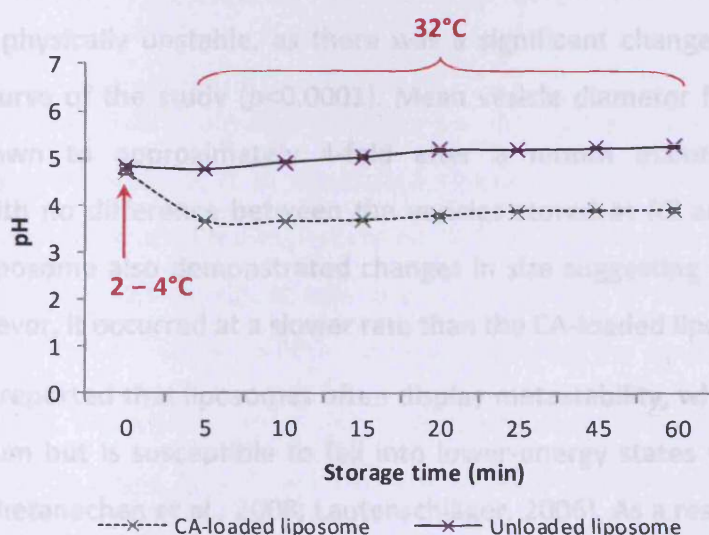


Figure 8-7: pH of CA-loaded liposome, as a function of time (min). Value at the baseline (0 min) obtained while the suspension was maintained at 2 – 4°C, followed by heat application of 32°C for 48 h; unloaded liposome served as control ($n=4, \pm \text{SD}$). $p < 0.0001$, vs. control

8.2.3.3 Evaluation of Liposome Stability

8.2.3.3.1 Vesicle Size and Size Distribution

A stability study was conducted in order to establish that CA was effectively entrapped under storage conditions over a period of 30 days. The mean hydrodynamic vesicle diameter, size distribution (i.e. minimum and maximum diameter) and polydispersity of the aqueous dispersions of CA-loaded and control liposomes maintained at 2 – 4°C are presented in [Figure 8-8](#) and [Table 8-1](#). Additionally, identical samples were maintained at RT and the data obtained are presented in [Figure 8-9](#) and [Table 8-2](#). In all cases, both liposome types exhibited a broad size distribution based on their minimum and maximum vesicle diameters. In addition, they exhibited a considerably moderate polydispersity as shown by their span and uniformity values.

The physical stability of liposome products is a function of integrity and size distribution of the lipid vesicles. Samples of the loaded liposome stored at 2 – 4°C and RT were physically unstable, as there was a significant change in vesicle size during the course of the study ($p < 0.0001$). Mean vesicle diameter for the samples decreased down to approximately 4-fold after a month maintained at both conditions, with no difference between the vesicles stored at RT and refrigerator. The control liposome also demonstrated changes in size suggesting lack of physical stability. However, it occurred at a slower rate than the CA-loaded liposome.

It was reported that liposomes often display metastability, where the system is in equilibrium but is susceptible to fall into lower-energy states with only slight interaction (Chetanachan et al., 2008; Lautenschläger, 2006). As a result, the vesicles are prone to change their lamellarity, size, size distribution, and shape over time. For example, small vesicles tend to form larger ones and large vesicles to smaller ones. Furthermore, liposome vesicles are susceptible to degradation processes, particularly oxidation and hydrolysis of its membrane (Ranade and Cannon, 2011). Oxidation most probably played a minor role to the instability of the liposome, since

the samples were sparged with nitrogen gas to create an inert atmosphere prior being subjected to the experimental storage conditions. In the case of loaded-liposome vesicles, their acidic internal environment might exacerbate lipid stability problems by inducing hydrolysis of the acyl chains in the lipid components (Mayer et al., 1993; Nacka et al., 2001) and thus, could disrupt a large proportion of their structures. Hydrolysis caused the liposome membrane to become permeable which generate osmotic forces, leading to evacuation of its content into the media environment, reflected by reduced vesicle size. The process depends on the pH and temperature conditions the liposome product experienced, and this may also impact the functionality with possible faster release and reduced stability.

Another possible reason for the reduced vesicle size could be attributed to protonation of the phospholipid polar heads of the liposome bilayer membrane in the acidic environment (Ariën et al., 1994; Cevc, 1993). At low pH, below the pK_a value of the phosphate group ($pH < pK_a \leq 1 - 2$), bilayers of the phosphorylcholine (polar lipid of the sphingomyelin molecule) become partly dehydrated and tend to form a new phase, possibly a non-bilayer type. This event would render them less likely to form tightly pack structure, resulting in increased membrane permeability and CA leakage.

There were visible physical changes to the liposomal suspensions. CA appeared to solubilise the lipid as the turbid suspension turned into a colourless solution with an oil-like appearance, where no visible turbidity after several days of storage either at 2 – 4°C or RT. It was also accompanied by formation of white coloured sediment at the bottom of the container following the incubation period.

In addition, a set of liposome suspensions was maintained at 32°C and 40°C for 1 h as shown in [Figure 8-10](#). There was a substantial reduction in diameter and size distribution of the loaded liposome after 1 h maintained at 32°C and 40°C in comparison to the sample maintained at 2 – 4°C ($p < 0.0001$), as presented in [Table 8-3](#) indicating a loss of structural integrity.

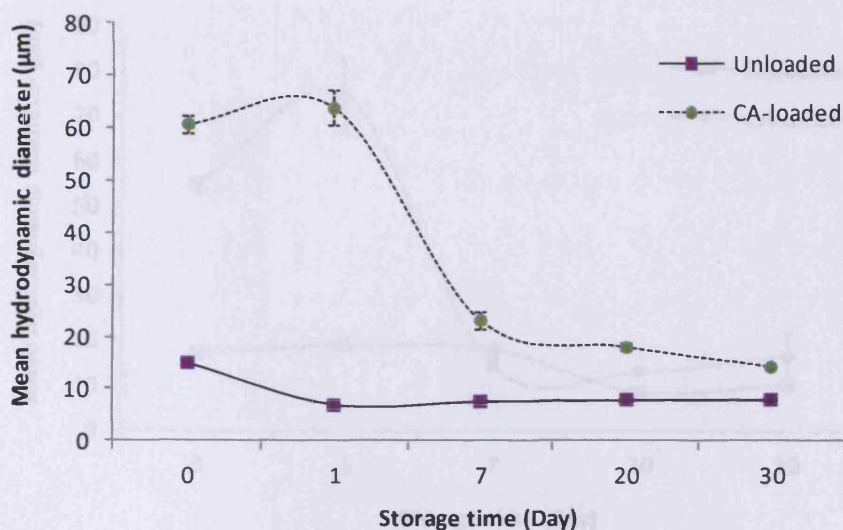


Figure 8-8: Mean hydrodynamic diameter of CA-loaded liposome vesicles (green) following maintenance at 2 – 4°C for 30 days; unloaded liposome served as control (purple) (n=3, ± SD).

Table 8-1: Vesicle size analysis of CA-loaded liposome following maintenance at 2 – 4°C for 30 days; unloaded liposome served as control (n=3, ± SD).

Liposome	Day	Vesicle Diameter (µm)		Span	Uniformity
		Minimum	Maximum		
CA-loaded	0	17.21 ± 0.85	112.81 ± 14.10	2.31 ± 0.41	0.84 ± 0.12
	1	12.36 ± 1.92	144.91 ± 10.59	3.32 ± 0.09	1.13 ± 0.01
	7	5.05 ± 0.04	47.57 ± 29.23	3.41 ± 1.99	1.28 ± 0.10
	20	5.88 ± 0.45	26.13 ± 2.73	1.66 ± 0.23	0.81 ± 0.25
	30	6.85 ± 0.02	23.50 ± 0.20	1.29 ± 0.01	0.40 ± 0.004
Unloaded (control)	0	4.93 ± 0.06	28.24 ± 0.35	1.81 ± 0.06	0.57 ± 0.004
	1	3.04 ± 0.02	12.32 ± 0.28	1.55 ± 0.02	0.48 ± 0.01
	7	3.24 ± 0.06	13.57 ± 0.10	1.60 ± 0.004	0.50 ± 0.001
	20	3.31 ± 0.001	14.03 ± 7.85	1.59 ± 0.01	0.49 ± 0.002
	30	3.35 ± 0.03	14.02 ± 0.68	1.57 ± 0.08	0.49 ± 0.02

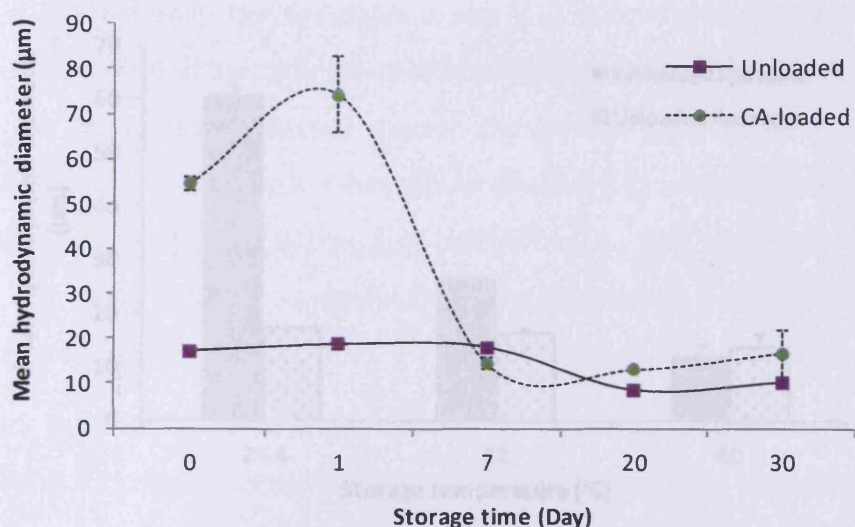


Figure 8-9: Mean hydrodynamic diameter of CA-loaded liposome vesicles (green) following maintenance at RT (~25°C) for 30 days; unloaded liposome served as control (purple) (n=3, ± SD).

Table 8-2: Vesicle size analysis of CA-loaded liposome following maintenance at RT for 30 days; unloaded liposome served as control (n=3, ± SD).

Liposome	Day	Vesicle Diameter (µm)		Span	Uniformity
		Minimum	Maximum		
CA-loaded	0	14.97 ± 1.59	103.92 ± 10.41	2.50 ± 0.51	0.91 ± 0.19
	1	16.29 ± 0.77	173.04 ± 50.95	3.48 ± 0.75	1.08 ± 0.17
	7	5.05 ± 0.12	23.32 ± 2.83	1.70 ± 0.23	0.68 ± 0.20
	20	6.29 ± 0.06	21.29 ± 0.17	1.27 ± 0.003	0.40 ± 0.001
	30	5.73 ± 0.35	27.30 ± 21.32	1.85 ± 1.05	0.76 ± 2.33
Unloaded (control)	0	4.19 ± 0.08	35.16 ± 0.73	2.20 ± 0.12	0.71 ± 0.04
	1	4.41 ± 0.01	37.06 ± 0.02	2.03 ± 0.01	0.64 ± 0.003
	7	4.65 ± 0.05	35.33 ± 0.09	1.97 ± 0.02	0.62 ± 0.01
	20	3.06 ± 0.01	16.51 ± 0.39	2.09 ± 0.04	0.68 ± 0.03
	30	3.81 ± 0.02	19.40 ± 0.08	1.89 ± 0.02	0.59 ± 0.01

The TEM observations of CA-loaded and control liposomes have revealed that they were generally formed in clusters as shown in **Figure 8-11**, **Figure 8-12**, **Figure 8-13** and **Figure 8-14**. The liposomes in clusters are of variable sizes and shapes (spherical).

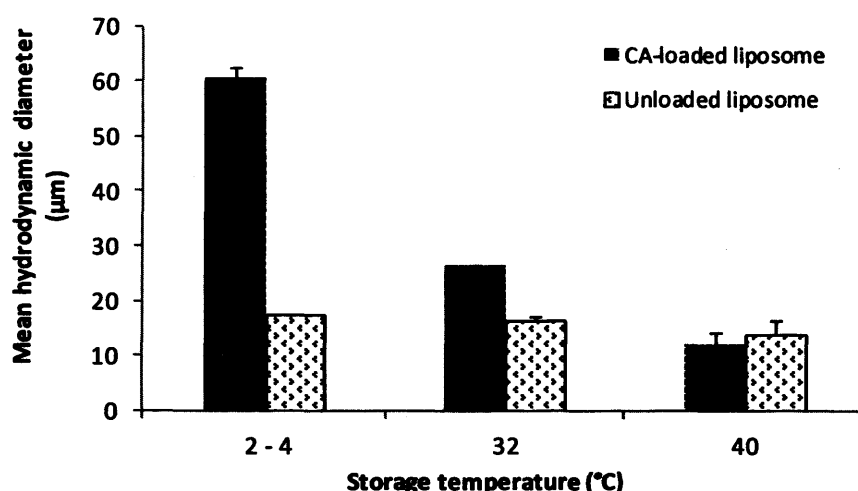


Figure 8-10: Mean hydrodynamic diameter of CA-loaded liposome determined after 1 h storage at 2 – 4°C, 32°C and 40°C; unloaded liposome served as control (n=3, ± SD). $p < 0.0001$ between treatments

Table 8-3: Vesicle size analysis of CA-loaded liposome following maintenance at 2 – 4°C, 32°C and 40°C for 1 h; unloaded liposome served as control (n=3, ± SD).

Liposome	Storage (°C)	Vesicle Diameter (µm)		Span	Uniformity
		Minimum	Maximum		
CA-loaded	2 – 4	17.21 ± 0.85	112.81 ± 8.14	2.31 ± 0.41	0.84 ± 0.12
	32	8.42 ± 0.06	48.48 ± 1.11	1.71 ± 0.04	0.53 ± 0.01
	40	4.11 ± 0.20	21.89 ± 3.21	1.95 ± 0.51	0.66 ± 0.21
Unloaded (control)	2 – 4	7.52 ± 0.20	29.88 ± 0.59	1.41 ± 0.01	0.44 ± 0.002
	32	7.30 ± 0.24	28.08 ± 1.12	1.38 ± 0.06	6.43 ± 0.02
	40	6.49 ± 0.02	27.84 ± 0.38	1.49 ± 0.03	0.46 ± 0.01

8.2.3.3.2 TEM Investigation

The TEM observations of CA-loaded and control liposomes have revealed that they were generally formed in clusters as shown in [Figure 8-11](#), [Figure 8-12](#), [Figure 8-13](#) and [Figure 8-14](#). The liposomes in clusters are of variable sizes and shapes (spherical,

elliptical and hexagonal). This variability in size is consistent with the data obtained from the size analysis of the samples using laser light scattering (Section in 8.2.3.2.1). Most of the liposomes in clusters appear compressed side-to-side against each other, leading to the formation of hexagonal structures in a honeycomb-like lattice which can be seen in [Figure 8-11\(A & B\)](#). Furthermore, their interfaces show high intensity of uranyl stained, suggesting their multilamellar membranes property ([Figure 8-11](#) and [Figure 8-12](#)).

The previous stability study using the laser light scattering instrument (Section 8.2.3.3.1) has demonstrated that within one week of the experimental time frame, liposome vesicles exhibited a significant reduction in size with no further substantial changes. Based on these findings, the TEM investigation was conducted using the same time scale. The TEM results showed that both high temperature and long term storage had an adverse effect on the morphology of liposome vesicles. The CA-loaded liposome samples stored at temperatures, (2 – 4)°C and 25°C (RT) showed no apparent structure alteration on day-1 of study, as shown in [Figure 8-11\(A & B\)](#) and [Figure 8-13\(A & B\)](#), respectively. However, significant structure alterations were observed in the samples that were stored for 7 days at those temperatures [[Figure 8-11\(C & D\)](#) and [Figure 8-13\(C & D\)](#)]. Moreover, those stored at a much higher temperature (32°C) even for a short period of time (1 h) exhibited severe morphological alterations ([Figure 8-15](#)). In most cases, the affected liposomes were broken into small fragments, resulting in a substantial leakage of the encapsulated materials. It is noteworthy, overtime no further alterations was observed, supporting that 1 h exposure at 32°C was sufficient to cause maximal structural alteration to the liposomes. In all cases, similar observations were observed for the control liposome vesicles ([Figure 8-12](#), [Figure 8-14](#) and [Figure 8-16](#)).

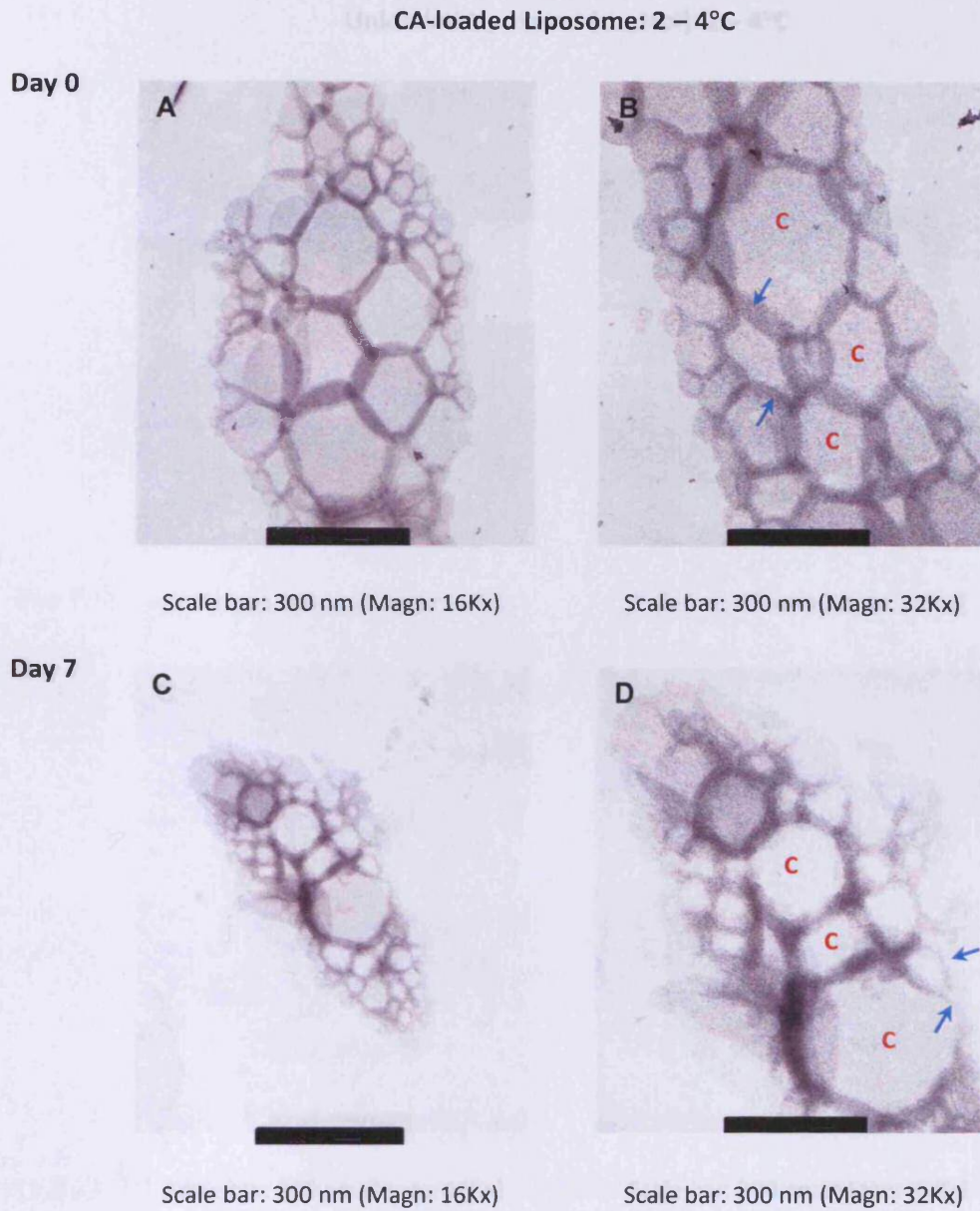


Figure 8-11: TEM images of CA-loaded liposome vesicles maintained at 2 – 4°C taken on day-0 (baseline) and day-7; samples were negatively-stained with aqueous UA 2%.

(A & B) : No apparent structural alterations with intact and well defined lamellar membranes (→). Thick and darkly-stained interfaces (→) lining uniformly light grey-stained compartments (C).

(C & D) : Lamellar membranes (→) poorly defined and broken in places through which encapsulated materials leak out from the compartment (C) and as a result, liposome vesicles appear empty (discolouration of the compartment).

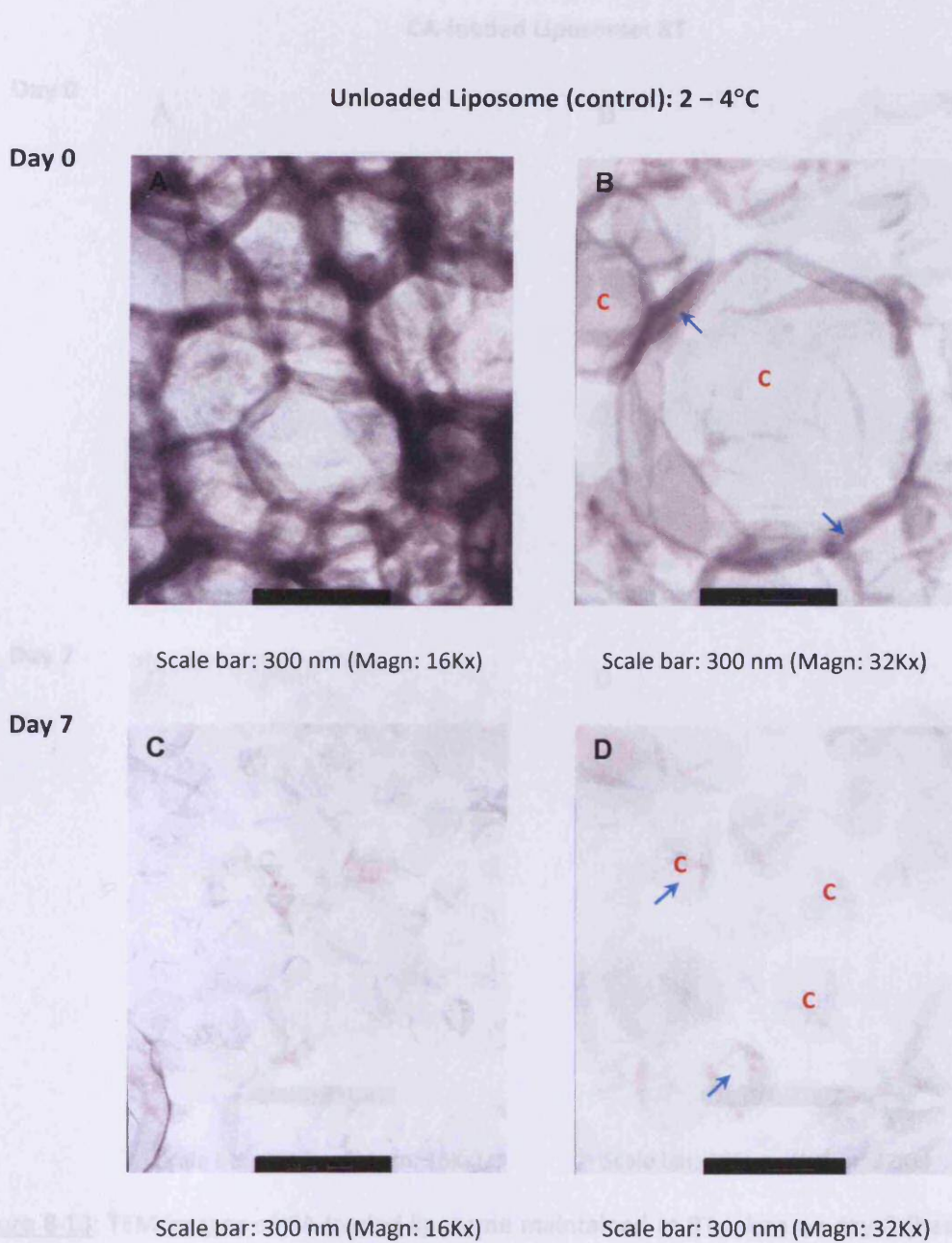


Figure 8-12: TEM images of unloaded liposome (control) maintained at 2 – 4°C taken on day-0 (baseline) and day-7; samples were negatively stained with aqueous UA 2%.

Figure 8-12: TEM images of unloaded liposome (control) maintained at 2 – 4°C taken on day-0 (baseline) and day-7; samples were negatively stained with aqueous UA 2%.

(A & B) : No apparent morphological changes. Liposome vesicles (C) retain their structure – dark lamellar membranes (→) shown by dark image staining.

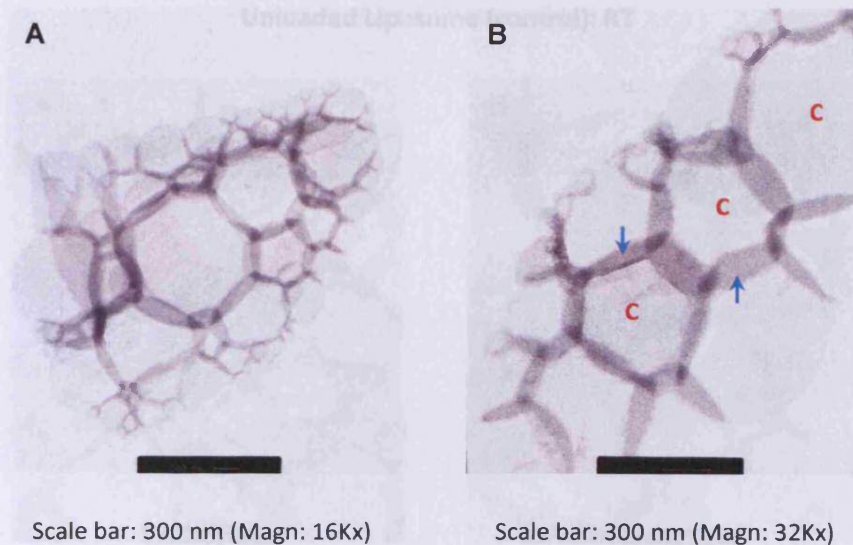
(A & B) : Lamellar membranes appear intact; strong uranyl stained density signifies multilamellar structure (→). Most vesicles still retained their content.

(C & D) : Morphological changes (less intact) presence of broken lipid film and

(C & D) : Structural alterations are observed. Liposome vesicles (C) appear broken and show typical shrinkage features (→). The vesicles membranes appear very pale (low staining intensity) due to leakage of content.

CA-loaded Liposome: RT

Day 0



Day 7

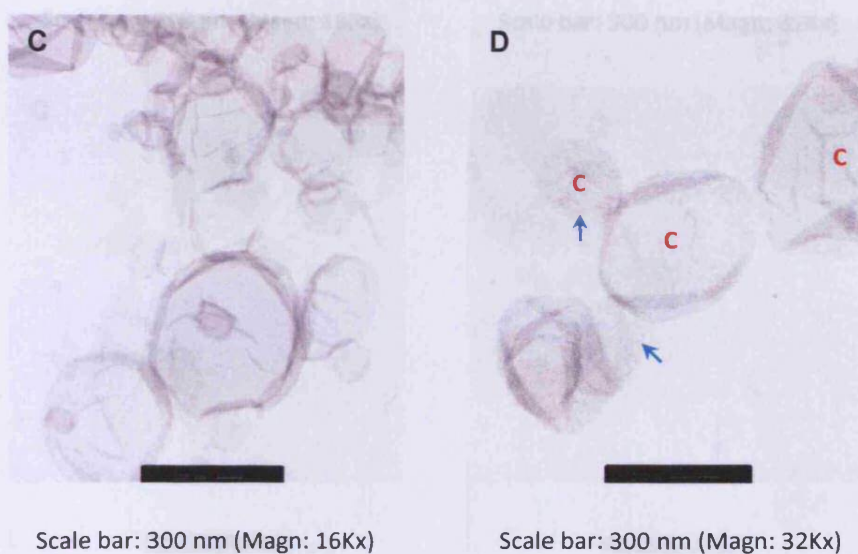
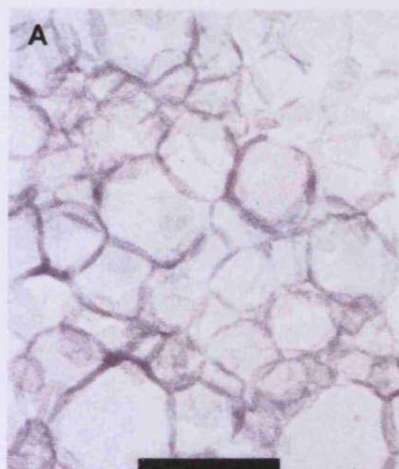


Figure 8-13: TEM images of CA-loaded liposome maintained at RT taken on day-0 (baseline) and day-7; samples were negatively-stained with aqueous UA 2%.

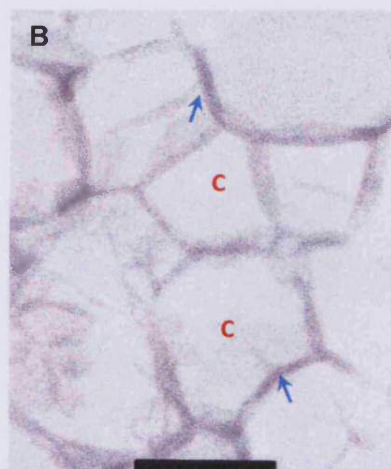
- (A & B) : No apparent morphological changes. Liposome vesicles (C) retain their structure - thick lamellar membranes (→) shown by dark uranyl staining remain intact.
- (C & D) : Morphological changes taking place; presence of broken lipid film and fragments (→) in the liposome vesicles (C) are evidence that the structures are altered and lost their structural integrity. As a result, encapsulated materials leak out into the surrounding medium.

Unloaded Liposome (control): RT

Day 0

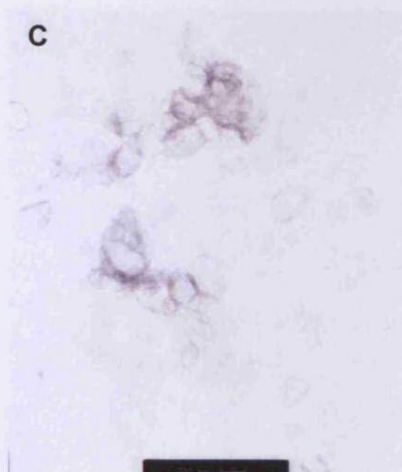


Scale bar: 300 nm (Magn: 16Kx)

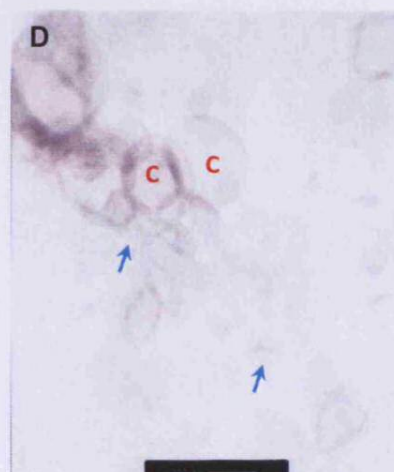


Scale bar: 300 nm (Magn: 32Kx)

Day 7



Scale bar: 300 nm (Magn: 16Kx)



Scale bar: 300 nm (Magn: 32Kx)

Figure 8-14: TEM images of unloaded liposome (control) maintained at RT taken on day-0 (baseline) and day-7; samples were negatively-stained with aqueous UA 2%.

- (A & B) : No apparent structural changes. Liposome vesicles (C) appear in a honeycomb-like arrangement with their membrane remained intact (→).
- (C & D) : Structural alterations take place; liposome vesicles lose their honeycomb structural arrangement and their membranes appear broken.

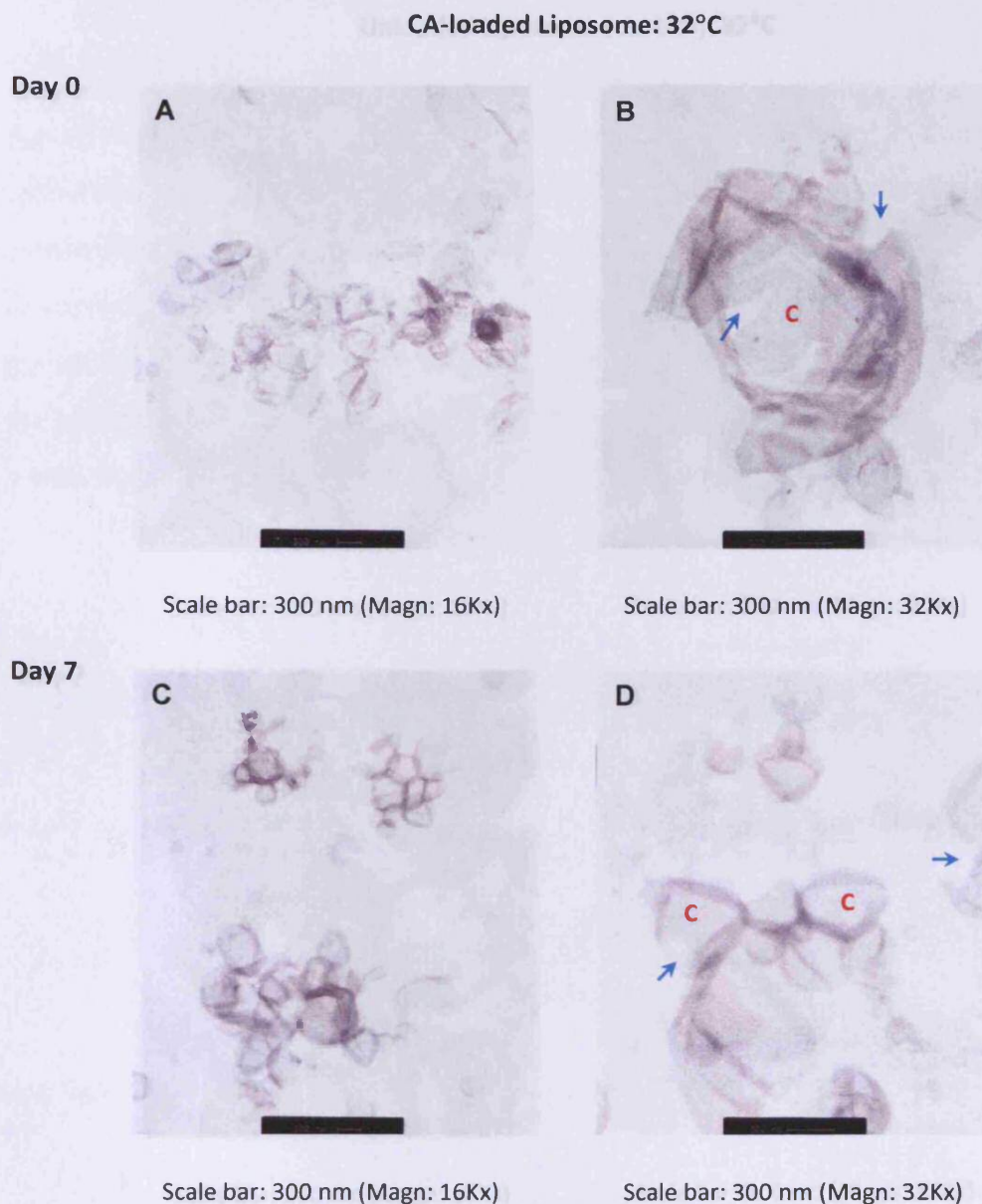


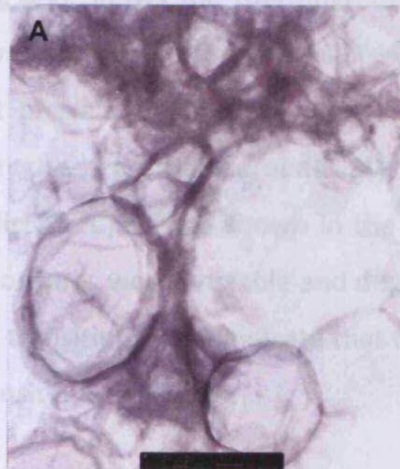
Figure 8-15: TEM images of CA-loaded liposome taken on day-0 (baseline) and day-7 of storage at 32°C; samples were negatively-stained with aqueous UA 2%.

- (A & B) : Absolute structural alterations – liposome membranes (C) appear broken (→) leads to release of encapsulated materials, CA.
- (C & D) : Morphological changes with absolute broken lamellar membranes (→).

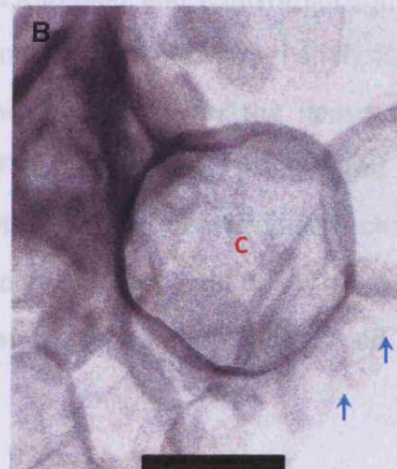
8.2.3.4 Thermal Analysis: Phase Transition

Unloaded Liposome (control): 32°C

Day 0

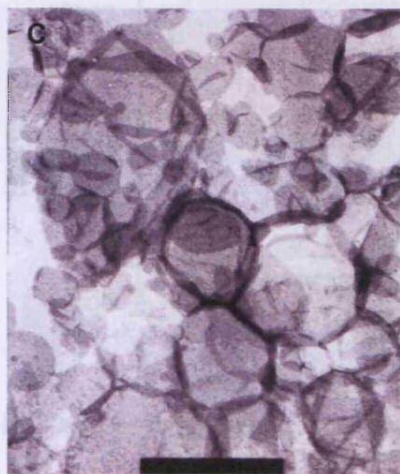


Scale bar: 300 nm (Magn: 16Kx)

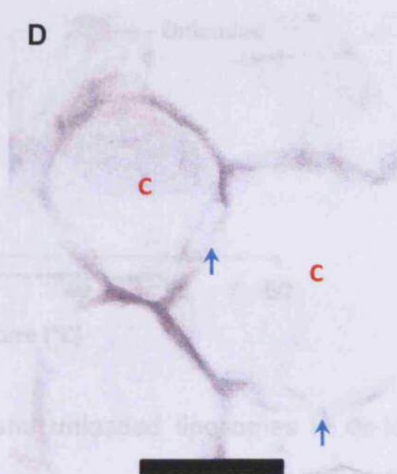


Scale bar: 300 nm (Magn: 32Kx)

Day 7



Scale bar: 300 nm (Magn: 16Kx)



Scale bar: 300 nm (Magn: 32Kx)

Figure 8-16: TEM images of unloaded liposome (control) taken on day-0 (baseline) and day-7 of storage at 32°C; samples were negatively-stained with aqueous UA 2%.

(A & B) : Structural alteration – membrane thinning as shown by lack of uranyl staining (→).

(C & D) : Severe structure changes. Liposome membranes appear thin and fragmented (→); loss of content as shown by discolouration in the vesicle structures (C).

8.2.3.4 Thermal Analysis: Phase Transition

Figure 8-17 shows the thermograms of CA-loaded and control liposomes in de-ionised water. Both liposomes exhibited a similar profile of thermal analysis, with no apparent phase transition taking place. It was expected for the liposomes to demonstrate the transition around 30 – 37°C, lower than a hydrated pure sphingomyelin (37°C). It was shown in the previous section of the current chapter, that both liposomes were unstable and degraded into broken lipid film. The absence of the phase transition might indicate that the samples were already degraded; thus, no phase transition took place.

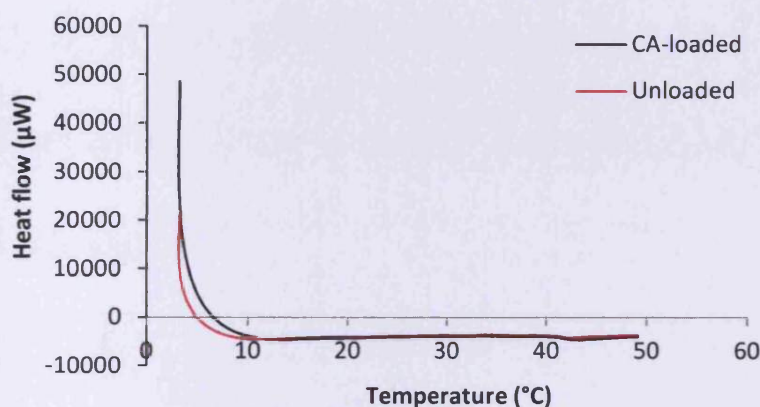


Figure 8-17: MC-DSC thermograms of CA-loaded and unloaded liposomes in de-ionised water.

8.3 CONCLUSION

For liposomes to be effective as pH modulator carriers, it has to be stable against the acidic environment ($\sim\text{pH } 2$) presented by the entrapment of the pH regulator, CA. The lipid vesicles synthesised using pure sphingomyelin were found to be unstable during storage both in the absence or presence of the pH regulator, CA molecules. This was characterised by time-dependant reduction of the vesicle size and the appearance of thin and absolute broken membranes. Moreover, the

calorimetric analysis performed on the liposome samples, detected no significant phase transitions possibly due to the samples contained mixtures of lipid fragments, instead of stable sphingomyelin bilayers.

Further study is required to synthesise and formulate liposomes which are stable enough to retain the acidic encapsulated material during storage, but can abruptly release their content once triggered by the thermal stimulus of skin origin (32°C). This can be possibly achieved by incorporating different types of lipids at particular ratios.

CHAPTER 9 | Composite Topical
Delivery System: pH Modulator-loaded
Liposome and Drug-loaded Poly(NIPAM-co-
AAc) Nanogel

9.1 INTRODUCTION

This chapter concerns the design of a composite topical drug delivery system consisting of a pH modulator-loaded liposome and drug-loaded ionic nanogel. It was found (CHAPTER 8) that the reaction between the two components may be significantly modulated by changes in their environmental temperature, where appropriate heat application could cause the liposome vesicles to liberate their content, subsequently activate the loaded-nanogel particles to expel their content into the surrounding medium. Ideally, the composite system should provide the stability of both components separately, yet in a manner that they can be readily integrated once applied to the skin area. There are two major approaches that can be considered in solving this challenge, either through multiple compartment or single compartment formulations.

Single compartment products are designed for the storage of stable, non-reactive formulations, and are very widely used. However, a multiple compartment formulation refers to an approach whereby two or more components are maintained under physical separation conditions prior to use. For example, the multiple chamber system ReGenesis known as the “SnapPack” displayed in [Figure 9-1\(A\)](#) and [Figure 9-1\(B\)](#) (Rosen, 2005), is composed of two or more plastic reservoirs filled with their respective formulations, heat-sealed to a flat card or plastic board which has a scored line, the purpose of which is to break open the chambers prior to application. Another example is the TanDerm™ pack – a double action wipe, where two separate applicator pads impregnated with different formulations are attached side by side to a slim pouch, as shown in [Figure 9-1\(C\)](#) (Rosen, 2005). The individual formulations will be in contact once the wipe was placed against the skin and wiped over the desired area in a circular motion to mix the formulations.

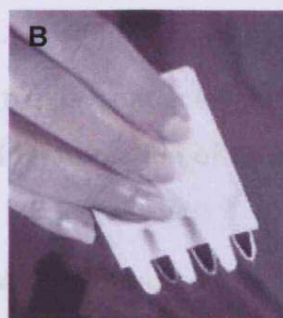
The current study involved the development of a novel smart single compartment system, whereby the two reactive components are formulated within a single tube, yet without any interaction under storage condition prior to use. This type of system would be advantageous in terms of being consumer friendly with no

metering or mixing step necessary; cheaper to manufacturer (e.g. a single regular tube or container); and environmentally friendly, as less amount of waste produced. To develop a single compartment product presents substantially greater challenges than a multi compartment product, as it is essential to effectively separate the two reactive components within the compartment until required for use.

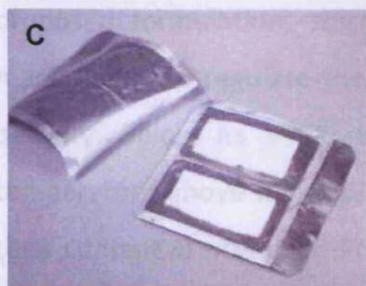
In this study, we considered the potential liposome vesicles for the selective sequestration of one compartment system under storage conditions, employing specific thermally-induced phase transitions as the mechanism to allow contact between two reacting components.



SnapPack – to create a dispensing comb and break open each individual compartment, the board was “snap” along the scored line.



Formulations were dispensed by pressing the SnapPack compartments.



TanDerm™ applicator pads are kept separate until use.

Figure 9-1: Multiple compartment systems – (A & B) SnapPack and (C) TanDerm™ (Rosen, 2005).

9.1.1 Formulation Design of a pH Modulator-loaded Liposome and Drug-loaded Poly(NIPAM-co-AAc) Nanogel – Skin Composite System

The proposed pH modulator-loaded liposome – nanogel single compartment system was designed based on the concept of two components (i.e. liposome and nanogel) present in a single formulation without any interactions under storage conditions. The proposed system was designed according to the technology disclosed in the recent patent obtained by our group (Denyer et al., 2007), involving the entrapment of ferrous sulfate (Fe_2SO_4) in liposome vesicles which were proven to effectively isolate the Fe_2SO_4 from the phytochemical constituents of pomegranate rind extract (PRE) in the extra liposomal matrix. The loaded-liposome vesicles were stable at refrigerated condition ($2 - 4^\circ\text{C}$), but degraded when heated to 32°C , liberating Fe_2SO_4 into the surrounding media containing PRE (interaction between PRE and ferrous ion was characterised by formation of a visible black by-product).

Dealing with the primary component of the proposed system first – the nanogel particulates were proposed to serve as carriers for active ingredients (e.g. drugs and cosmetics) to be delivered and localised into the skin layers. The pH- and temperature-sensitive poly(NIPAM-co-AAc)(5%) nanogel was selected for the proposed formulation, since its multiple stimuli-responsive properties could be manipulated to regulate the function of the nanogel, as a suitable carrier for drug delivery. Below its VPTT, the particles are highly swollen whereas raising the temperature above it, causes the particles to instantaneously collapse, forcing out their content *in situ*. In addition to the concept of the nanogel temperature-induced content release, its pH-sensitive property could provide additive effect by triggering further collapse of the structure upon interaction with a suitable acidic pH modulator. The poly(NIPAM-co-AAc)(5%) nanogel particles were successfully demonstrated to be responsive towards temperature and pH changes in their aqueous surrounding media (CHAPTER 4). Additionally, the particles of poly(NIPAM-co-AAc)(5%) nanogel were found able to penetrate the skin and migrate across the epidermis as demonstrated in CHAPTER 5.

As regards to the second component – liposomes were used to encapsulate a pH-modulator which was required for regulating the form of the nanogel particles. In the current study liposomes of sphingomyelin, as prepared in CHAPTER 8, were selected as a part of the composite system. The primary purpose of the liposomal encapsulation is somewhat different in the current study, as there is no need for the lipid vesicles to penetrate deep into the skin. They are utilised to formulate a storage compartment, which later would breakdown in the upper layers of the skin, as a consequence of increased environmental temperature, thus facilitating the mixing of the two components of the proposed system to take place. As discussed in CHAPTER 5, 6 and 8, CA was used as a pH-modulator model in an attempt to enhance and optimise the release of permeant by the loaded-nanogel in addition to temperature-activation. Even though the CA-loaded liposome vesicles were found to be unstable under the conditions studied in CHAPTER 8, the current study was carried out to determine whether a novel single formulation of liposome and nanogel might be feasible at all.

The key requirement of the composite system is to maintain the two entities in stable isolation over a useful shelf life. In this chapter, the stability of the composite system was studied by assessing the variance in particle sizes over a period of time. This was achieved by means of laser light scattering analysis and microscope observation (TEM).

9.2 MATERIALS AND METHODS

9.2.1 Materials

CA anhydrous (99.5%) was supplied by Sigma-Aldrich Company Ltd. (Poole, UK) and HPLC-grade solvents were purchased from Fisher Scientific (Loughborough, UK). Pioloform® and UA were obtained from Agar Scientific Ltd. (Stansted, UK). Sphingomyelin liposomes were prepared according to the protocol in Section 8.2.2.1. Materials used for synthesis of poly(NIPAM-co-AAc)(5%) and polyNIPAM nanogels

were described in Section 4.2.1 and the nanogels were synthesised as detailed in Section 4.2.2.1.

9.2.2 Methods

9.2.2.1 Effect of pH Modulator and Temperature Concomitantly on Poly(NIPAM-co-AAc)(5%) Nanogel

This study was carried out to evaluate the effect of pH and temperature stimuli when applied simultaneously on the poly(NIPAM-co-AAc)(5%) nanogel, simulating the actual condition upon application on the skin. The pH modulator was applied directly on to the swollen nanogel without being encapsulated in the liposome structure. The effect was evaluated based on the assumption that, a reduction in particle diameter of the nanogel reflected the release of their internal content into external medium.

The particle diameter and size distribution of the nanogel particles were determined at ambient temperature using Malvern Mastersizer 2000. Initially, samples were prepared by thoroughly mixing the concentrated swollen nanogel and CA solution (5% w/v) in a ratio of 5:2 similar to the dosing procedures described in CHAPTER 5. Since the resulting mixture was too concentrated for particle size analysis, it was diluted 5-fold with de-ionised water. Identical samples in replicates of three (n=3) were prepared and maintained for 1 h as listed in [Table 9-1](#).

Table 9-1: Storage conditions for polyNIPAM-based nanogel particles to investigate temperature-responsive effect.

Temperature (°C)	Rationale	Storage
2 – 4	Storage condition	Cold room
~25	RT – handling and analysis	Laboratory bench
32	Average skin surface temperature	Thermostatically controlled water bath
37	Average physiological temperature and maximal effect	Thermostatically controlled water bath

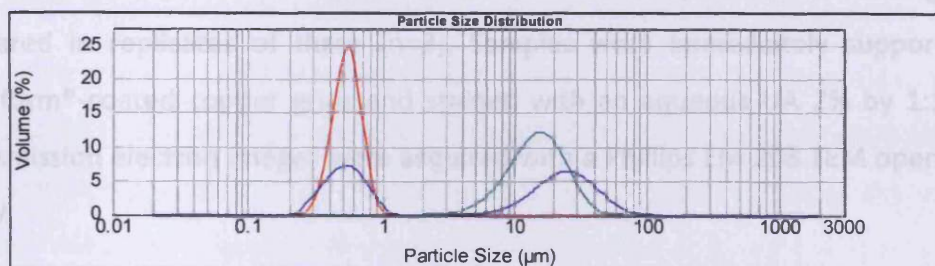
9.2.2.2 CA-loaded Liposome – activated – poly(NIPAM-co-AAc)(5%) Nanogel – skin Composite System

In order for the poly(NIPAM-co-AAc)(5%) nanogel particles to function ideally as drug carriers, it is necessary for the CA-loaded liposome vesicles to efficiently release the CA molecules to their surroundings when applied onto the skin once the lamellar structure begins to decompose. The released CA molecules further increase the acidic environment of the skin, leading to activation of the nanogel particles by causing the particles to collapse and expel the encapsulated material. In addition, the particles can be activated simultaneously by a thermal stimulus originated from the skin (~32°C), aiding the release of more encapsulated material.

9.2.2.2.1 Particle Size Distribution and Stability Evaluation

The proposed system is a mixture of liposome and nanogel with different particle size distributions. Thus, two distinct individual curves were anticipated, which below 1 µm range for the nanogel particles and above 1 µm range for the liposome as shown in [Figure 9-2](#). The nanogel particles were confirmed to exhibit a particle size distribution curve less than 1 µm, as proven in the nanogel

characterisation, 4.3.1.1. For this study, we took the view that under stable conditions, where no interaction took place between the nanogel and liposome, these two individual curves should remain separated. However, if there was any form of interaction, the curves might shift significantly or fuse and form a single peak. Since multiple distribution curves were obtained as the end result, the particle analysis profile generated by the laser light diffraction system could not be evaluated quantitatively. This is because the instrument could not differentiate that each curve originated from different components contained in a mixture. Therefore, the evaluation could only be carried out qualitatively according to the distribution curve images.



- Poly(NIPAM-co-AAc)(5%) nanogel alone
- Unloaded liposome (control) alone
- Mixture of poly(NIPAM-co-AAc)(5%) + Unloaded liposome

Figure 9-2: Particle size distribution curves illustrating poly(NIPAM-co-AAc)(5%) nanogel, unloaded liposome and freshly prepared mixture of both measured at RT using a laser light diffraction system.

A short-term stability study was undertaken on a mixture of liposome and nanogel. Samples were prepared by mixing equal volumes (1:1) of the liposomal suspension (5% w/v) and nanogel dispersant (1% w/v) as follows:

- (i) CA-loaded liposome + Poly(NIPAM-co-AAc)(5%) nanogel
- (ii) Unloaded liposome + Poly(NIPAM-co-AAc)(5%) nanogel

Each mixture was prepared in replicates of three ($n=3$). The study was carried out according to the stability study protocol described in Section 8.2.2.4.3.1, where the samples maintained at 2 – 4°C and RT over 30 days. Samples containing unloaded liposome served as a control.

9.2.2.2.2 TEM Investigation

TEM investigation was carried out to provide visual proof regarding any possible interaction between the nanogel particles and liposome vesicles co-exist in a single formulation during storage and upon application onto the skin. Identical samples in nature as tested in the previous stability test were prepared (Section 9.2.2.2.1). Equal volumes (1:1) of the 1% w/v nanogel dispersant and 0.2% w/v liposome suspension were mixed together at RT for 5 min and stored either at 2 – 4°C (cold room) or 32°C (thermostatically controlled water bath – Fisher Scientific, Loughborough, UK) for 1 h. Additionally, the sample prepared for 2 – 4°C served as a baseline for the 32°C condition. Each combination of liposome and nanogel was prepared in replicates of three (n=3). Samples were immediately supported on Pioloform®-coated copper grids and stained with an aqueous UA 2% by 1:1 ratio. Transmission electron images were acquired with a Phillips EM 208 TEM operated at 80 kV.

9.2.2.3 Data Analysis

The data obtained were recorded and analysed using Excel 2010 (Microsoft Office, Microsoft Corp., Redmond, WA) and expressed as a mean \pm SD. Statistical test was carried out with InStat® for Macintosh, version 3.00 (GraphPad Software Inc., San Diego, CA). Significant differences and comparisons were made employing Student's t-test. Confidence interval was 95% where $p < 0.05$ was considered to be significant.

9.3 RESULTS AND DISCUSSION

9.3.1 Effect of pH Modulator and Temperature Concomitantly on Poly(NIPAM-co-AAc)(5%) Nanogel

The study was undertaken to determine the effect of temperature and pH modulator when applied simultaneously to the poly(NIPAM-co-AAc)(5%) nanogel. The response was evaluated based on the measured hydrodynamic particle size and visual observation. **Figure 9-3** shows images of the poly(NIPAM-co-AAc)(5%) nanogel in a series of increasing temperature in a CA solution of ~pH 2, where the nanogel underwent a conformational transition.

Since the poly(NIPAM-co-AAc)(5%) contained NIPAM segments, it was expected that the nanogel particles responded to the increasing environmental temperature by experiencing volume loss. It can be observed that the nanogel particles remained dispersed in the acidic environment at 2 – 4°C and RT (~25°C). However, evidence for particle aggregation was observed in the identical samples upon heating to 32°C (**Figure 9-3-C**) and 37°C (**Figure 9-3-D**), making the particle analysis impossible. Initially, the turbidity became progressively intense with a 'gritty' appearance being noted – characteristic of an aggregation, with larger aggregation forming later, sticking to the walls of the glass vial. The phenomenon was temperature-induced since it was found to be reversible. On cooling, the solvency of the dispersion improved and by gently inverting the glass vial several times, the flocculated particles re-dispersed as shown in **Figure 9-4**. This temperature-induced aggregation of the particles and subsequent re-dispersion on cooling was repeated several times with the process remaining fully reversible. In the absence of CA, the aqueous dispersion nanogel appeared turbid only when heated to or above 32°C, with no evidence of aggregation (**Figure 9-5**).

One explanation for this behaviour is that under the acidic condition of pH 2, where carboxyl groups (—COOH) of AAc segments within the nanogel structure were in associated form (neutral), the resulting absence of charges caused the particles to

be less hydrophilic and adopt a compact structure. At this state, the swelling and de-swelling mechanism of the nanogel is primarily governed by the NIPAM segments of the nanogel:

- (i) Hydrogen bonding between solvent molecules and the hydrophilic amide of the NIPAM segments, and
- (ii) Hydrophobic interaction between the solvent molecules and the hydrophobic isopropyl NIPAM segments.

At hydrophobic state in response to the acidic environment, the hydrogen bonding between the solvent molecules and the amide groups were reduced, and thus, there were less hydrogen bonds to be broken as temperature increased, less energy required to break the bonds causing the nanogel to exhibit phase transition at lower temperature (Khan, 2007). In addition, at lower pH the carboxyl group of AAc would possibly interact with the amide group of NIPAM ($-\text{CONH}$) through hydrogen bonding, and that could also contribute to the reducing of interaction between the solvent and nanogel, thus reducing of its LCST (Khan, 2007; Kokufuta et al., 1998).

The precipitation of the nanogel was progressively induced as the environmental temperature exceeded its LCST, which was predominantly driven by the hydrophobic interactions between the isopropyl side groups of the NIPAM units. The interactions caused the NIPAM units to aggregate leading to removal of its content by increasing the flow rate of water out of the nanogel particles then drew the whole network to a further collapsed state. When the NIPAM units aggregated at higher temperatures, incorporated segments which maintained hydration, i.e. amide residues of the NIPAM also restricted the de-swelling of particles synchronously. Even though the two forces are opposing, the hydrophobic forces apparently overwhelmed the hydrophilic forces in the matrices.

On changing the temperature from RT to 32°C, the de-swelling was observed to be completed within a very a short time scale, occurring in less than a minute. When the nanogel was removed from 32°C condition and left to cool at RT, the process was reversible, but took longer to be re-dispersed which was slower than

the de-swelling process. This could be possibly due to formation of entangled networks within the particles during the collapsed state, and thus more time required attaining their original conformation and hydration state.

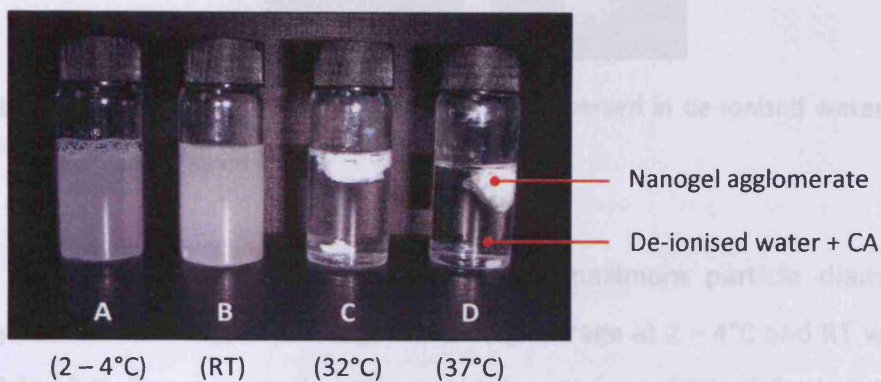


Figure 9-3: Images of diluted mixtures of poly(NIPAM-co-AAc)(5%) and CA solution (5% w/v) after maintained at various temperatures. From left at (A) 2 – 4°C; (B) RT (~25°C); (C) 32°C; and (D) 37°C.

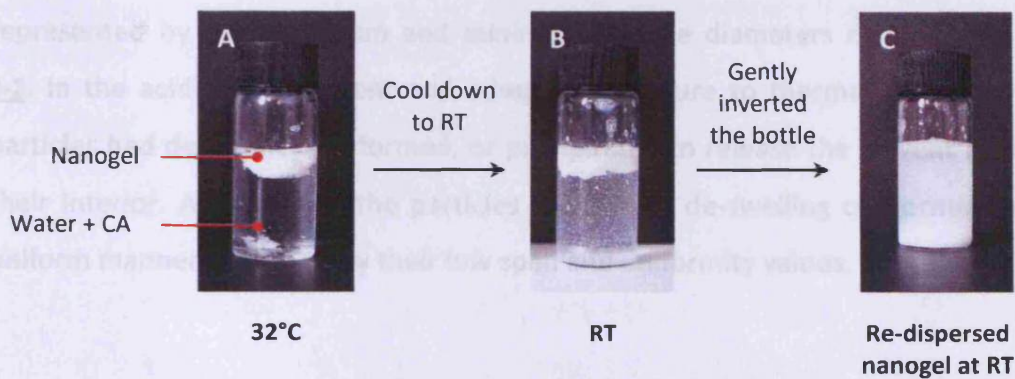


Figure 9-4: Images of poly(NIPAM-co-AAc)(5%) suspension at – (A) 32°C; (B) 5 min after cooling down at RT; and (C) after gently shaken to re-disperse the agglomerates.

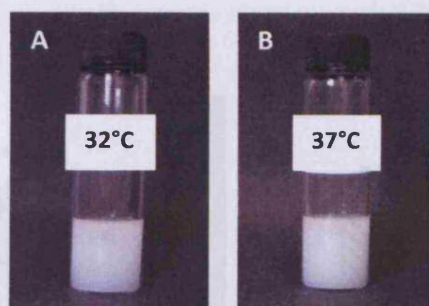


Figure 9-5: Images of poly(NIPAM-co-AAc)(5%) dispersed in de-ionised water in absence of CA solution maintained at (A) 32°C and (B) 37°C.

Mean hydrodynamic, minimum and maximum particle diameters of the poly(NIPAM-co-AAc)(5%) nanogel following storage at 2 – 4°C and RT were recorded in [Table 9-2](#). It was seen that the nanogel particles exhibited further de-swelling in the presence of CA. Under both storage conditions, the nanogel particles showed statistically significant differences in size reduction compared to the control (absence of CA), with $p < 0.0001$ for each condition as shown graphically in [Figure 9-6](#). The difference could also be observed based on their particle size distributions represented by the maximum and minimum particle diameters displayed in [Table 9-2](#). In the acidic environment and adequate exposure to thermal stimulus, these particles had de-swollen, deformed, or precipitated to release the solvent loaded in their interior. Additionally, the particles underwent de-swelling conformation in a uniform manner, reflected by their low span and uniformity values.

2-4°C	Nanogel	501 ± 15	989 ± 27	0.61 ± 0.01	0.39 ± 0.02
RT	Nanogel + CA	274 ± 14	684 ± 14	0.50 ± 0.04	0.28 ± 0.01
	Nanogel	381 ± 17	842 ± 22	0.61 ± 0.02	0.29 ± 0.01

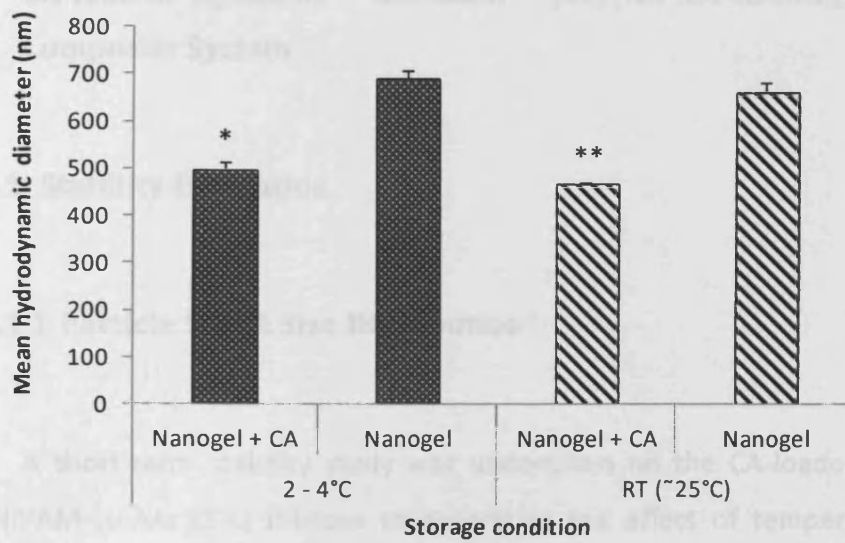


Figure 9-6: Mean hydrodynamic diameters of poly(NIPAM-co-AAc)(5%) dispersed in de-ionised water, followed by addition of CA solution (5% w/v) and maintained at different temperatures; nanogel sample in the absence of CA served as control (n=3, ± SD). * $p=0.0001$ and ** $p=0.0001$, vs. control.

Table 9-2: Particle analysis profile of poly(NIPAM-co-AAc)(5%) nanogel followed by addition of CA solution (5% w/v) and maintained either at 2 – 4°C or RT (n=3, ± SD); nanogel sample in the absence of CA served as control.

Storage (°C)	Sample	Particle Diameter (nm)		Span	Uniformity
		Minimum	Maximum		
2 – 4	Nanogel + CA	320 ± 9	691 ± 19	0.76 ± 0.02	0.24 ± 0.01
	Nanogel	501 ± 15	909 ± 23	0.61 ± 0.01	0.19 ± 0.004
RT	Nanogel + CA	274 ± 14	684 ± 19	0.90 ± 0.08	0.28 ± 0.02
	Nanogel	461 ± 12	842 ± 22	0.61 ± 0.002	0.20 ± 0.01

9.3.2 CA-loaded Liposome – activated – poly(NIPAM-co-AAc)(5%) – skin Composite System

9.3.2.1 Stability Evaluation

9.3.2.1.1 Particle Size & Size Distribution

A short-term stability study was undertaken on the CA-loaded liposome – poly(NIPAM-co-AAc)(5%) mixture to determine the effect of temperature on the integrity of CA-loaded liposome structure and ultimately on the nanogel particles.

For the sample containing CA-loaded liposome and nanogel, the baseline measurement presented a single curve instead of two distinctive curves, regardless the storage temperatures, 2 – 4°C [Figure 9-7(A)] or RT [Figure 9-8(A)], suggesting possible interactions between those two components. Since the baseline measurement was carried out on the freshly made sample and only 1 h after incubation, the interaction between those two components was considered to be instant.

In contrast, the control preparation (unloaded liposome and nanogel) exhibited the expected feature, i.e. two individual curves as shown in Figure 9-7(B) and Figure 9-8(B). Over time, the characteristic peaks of the samples maintained at 2 – 4°C disappeared, and shifted to form a single peak with a greater size distribution. For the samples maintained at RT, the individual curves were retained over the course of the study.

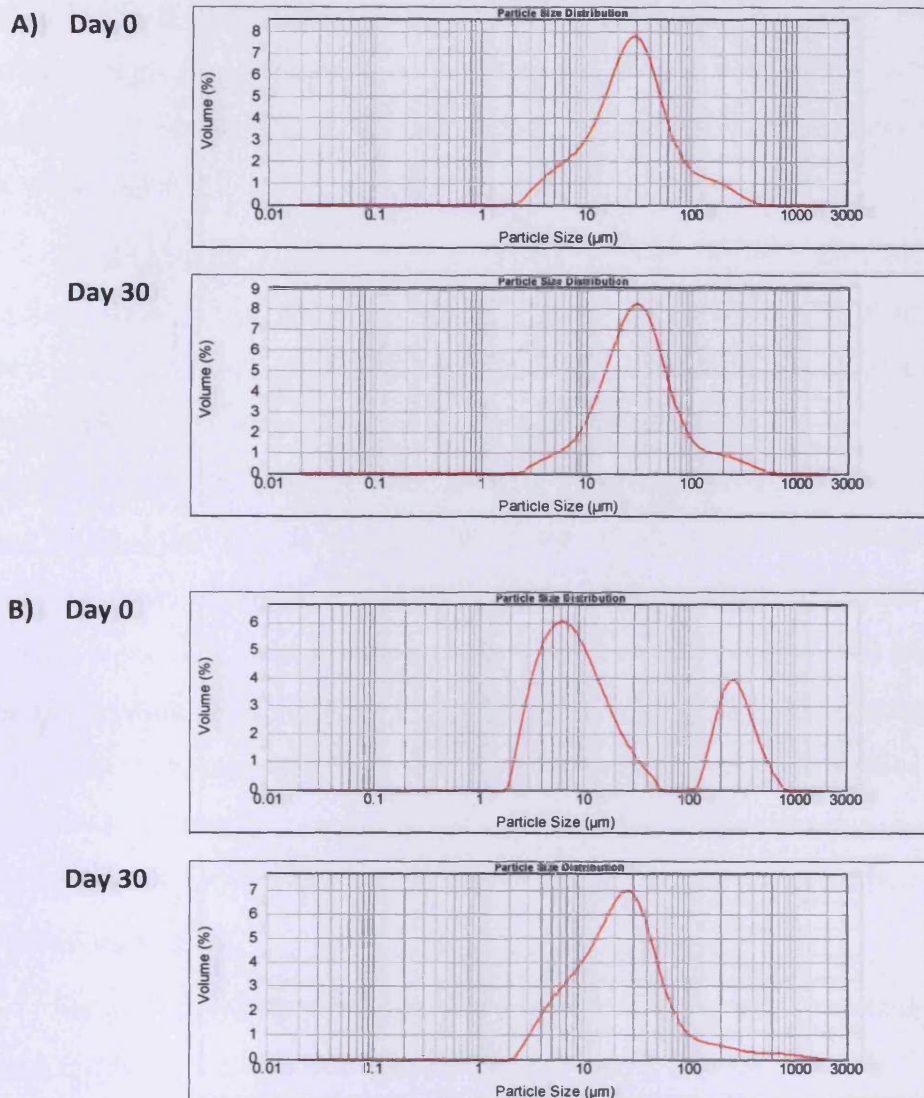


Figure 9-7: Particle size distribution curve for a mixture containing a nanogel and liposome – (A) CA-loaded liposome and poly(NIPAM-co-AAc)(5%) and (B) unloaded liposome and poly(NIPAM-co-AAc)(5%) maintained at 2 – 4°C measured on day-0 and day-30. Sample (B) containing the unloaded liposome served as control.

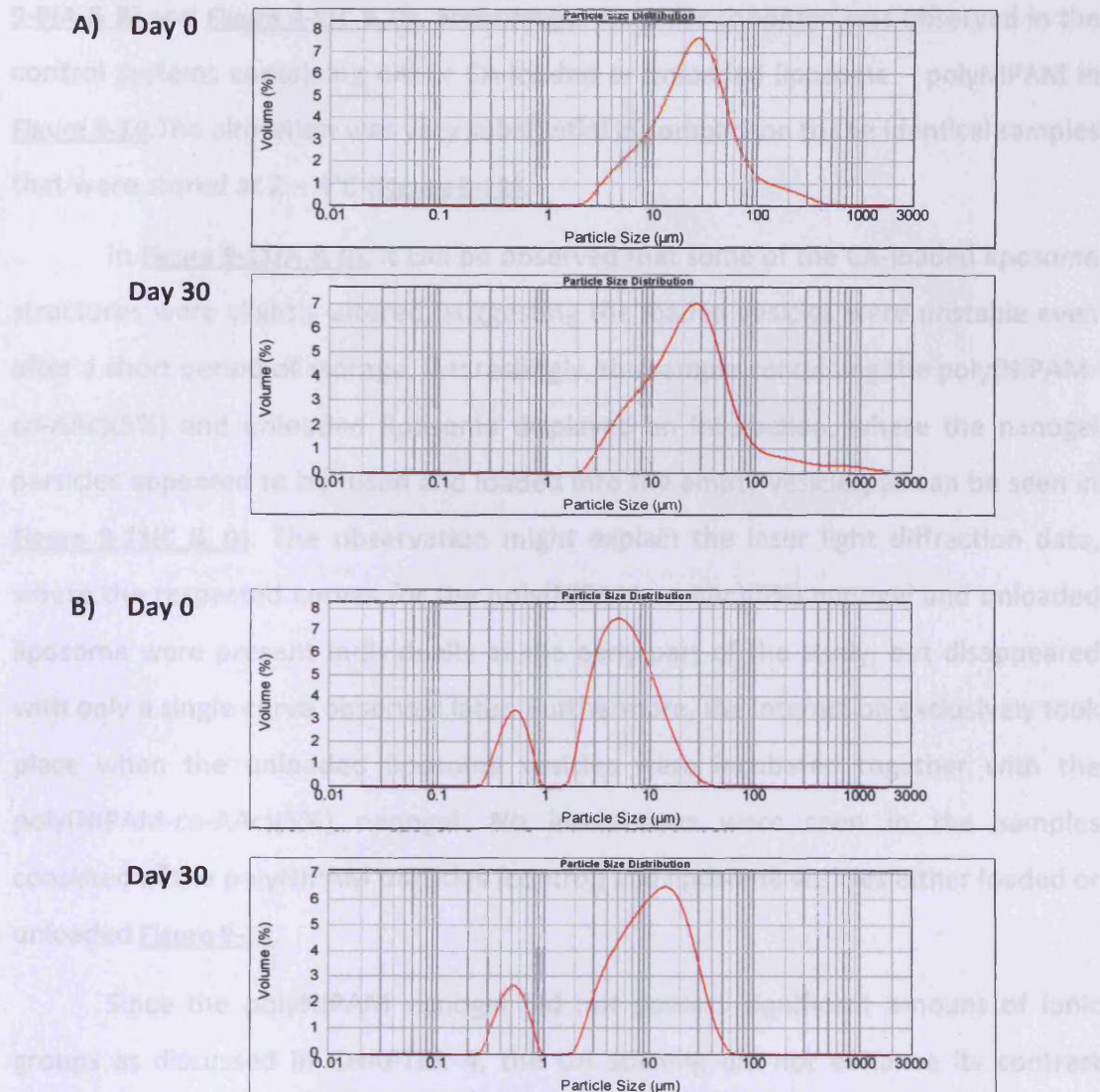


Figure 9-8: Particle size distribution curve for a mixture containing a nanogel and liposome – (A) CA-loaded liposome and poly(NIPAM-co-AAc)(5%) and (B) unloaded liposome and poly(NIPAM-co-AAc)(5%) maintained at RT measured on day-0 and day-30. Sample (B) containing the unloaded liposome served as control.

9.3.2.1.2 TEM Investigation

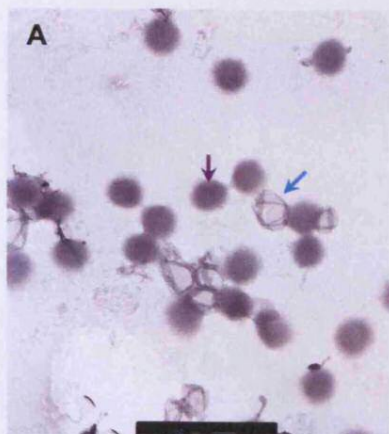
Figure 9-9 shows the TEM images of the proposed single compartment system where the nanogel and liposome were present within a single formulation following storage at 32°C for 1 h. The liposome structures were noticeably altered, characterised by their loss of bilayer membrane and broken lipid film after being

exposed to heat of 32°C regardless with or without presence of CA as shown in **Figure 9-9(A & B)** and **Figure 9-9(C & D)**, accordingly. A similar condition was observed in the control systems containing either CA-loaded or unloaded liposome – polyNIPAM in **Figure 9-10**. The alteration was very substantial in comparison to the identical samples that were stored at 2 – 4°C (**Figure 9-11**).

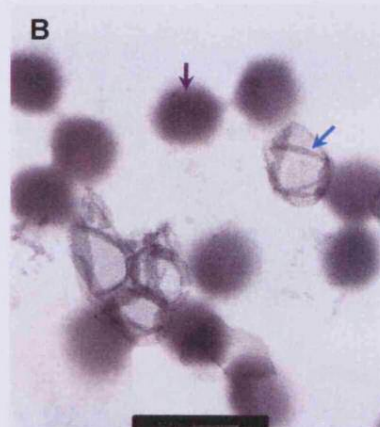
In **Figure 9-11(A & B)**, it can be observed that some of the CA-loaded liposome structures were slightly altered, suggesting the loaded vesicles were unstable even after a short period of storage. Interestingly, the sample containing the poly(NIPAM-co-AAc)(5%) and unloaded liposome displayed an interaction, where the nanogel particles appeared to be fused and loaded into the empty vesicles, as can be seen in **Figure 9-11(C & D)**. The observation might explain the laser light diffraction data, where the respected curves for the poly(NIPAM-co-AAc)(5%) nanogel and unloaded liposome were present individually at the early part of the study, but disappeared with only a single curve observed later. Furthermore, the interaction exclusively took place when the unloaded liposome vesicles were incubated together with the poly(NIPAM-co-AAc)(5%) nanogel. No interactions were seen in the samples consisted of the polyNIPAM particles (control) and liposome vesicles either loaded or unloaded **Figure 9-12**.

Since the polyNIPAM nanogel did not possess significant amount of ionic groups as discussed in CHAPTER 4, the UA staining did not enhance its contrast causing difficulty to visualise the particles discretely in comparison to the poly(NIPAM-co-AAc)(5%) and liposomes.

CA-loaded Liposome + Poly(NIPAM-co-AAc)(5%): 32°C

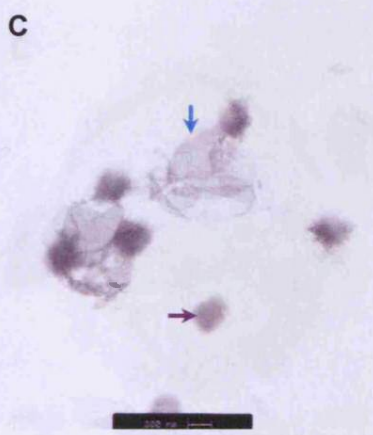


Scale bar: 300 nm (Magn: 16Kx)

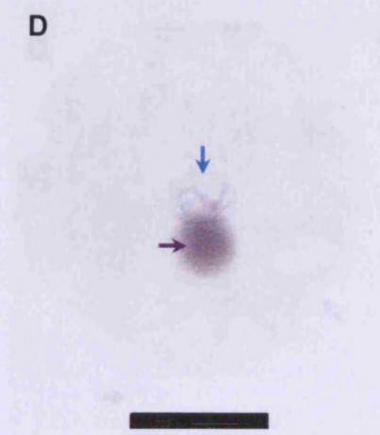


Scale bar: 300 nm (Magn: 32Kx)

Unloaded Liposome + Poly(NIPAM-co-AAc)(5%): 32°C



Scale bar: 300 nm (Magn: 16Kx)



Scale bar: 300 nm (Magn: 32Kx)

Figure 9-9: TEM images of a proposed single compartment system where poly(NIPAM-co-AAc)(5%) and CA-loaded liposome exist within a single formulation, maintained at 32°C for 1 h; samples containing unloaded liposome served as control; all samples were negatively stained with aqueous UA 2% (→ Nanogel; → Liposome).

A – D : Liposomes (→) show substantial morphology alterations; lipid film and fragments can be seen scattered in places in both samples containing CA-loaded or unloaded liposomes – poly(NIPAM-co-AAc)(5%). The nanogel particles (→) are densely stained and can be seen either attached or floated in close vicinity to the fragmented liposome vesicles.

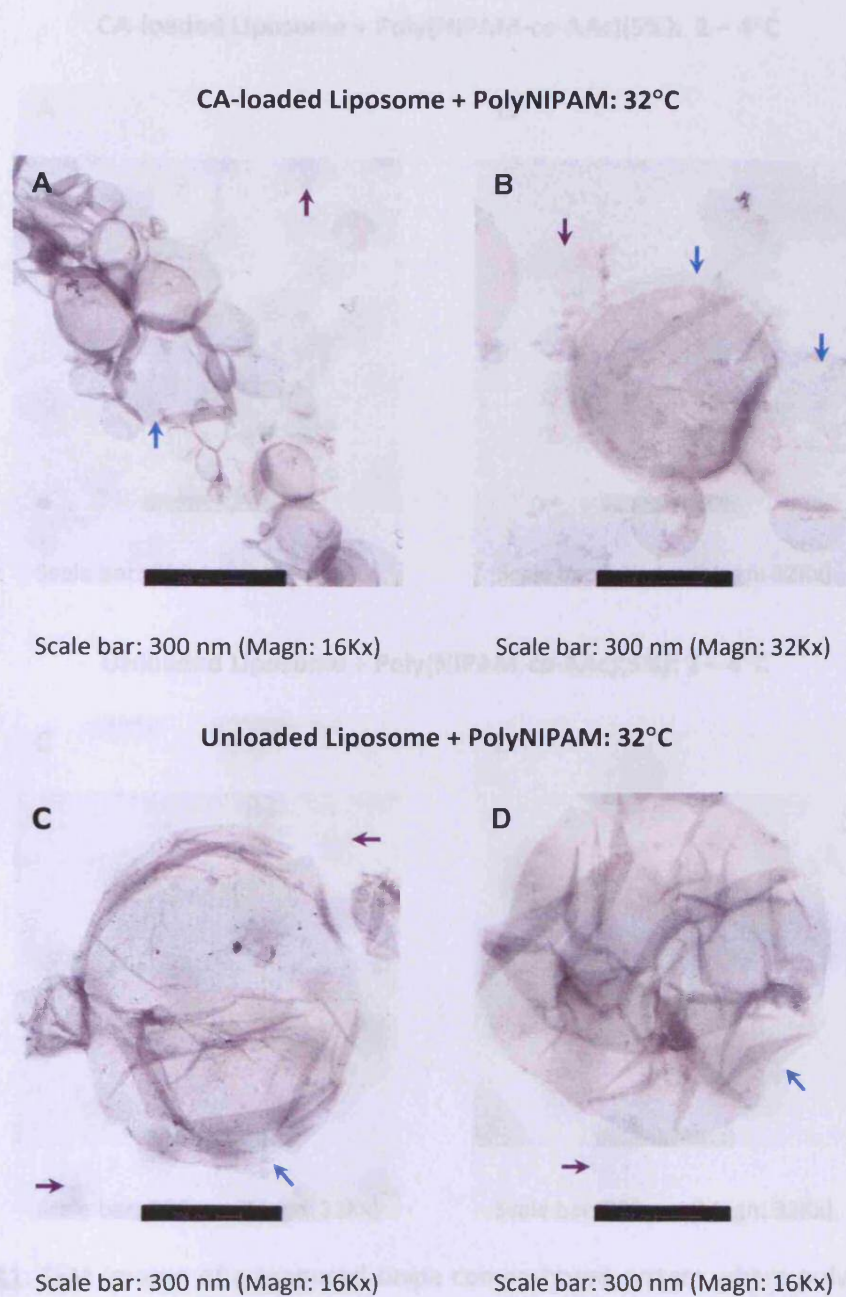
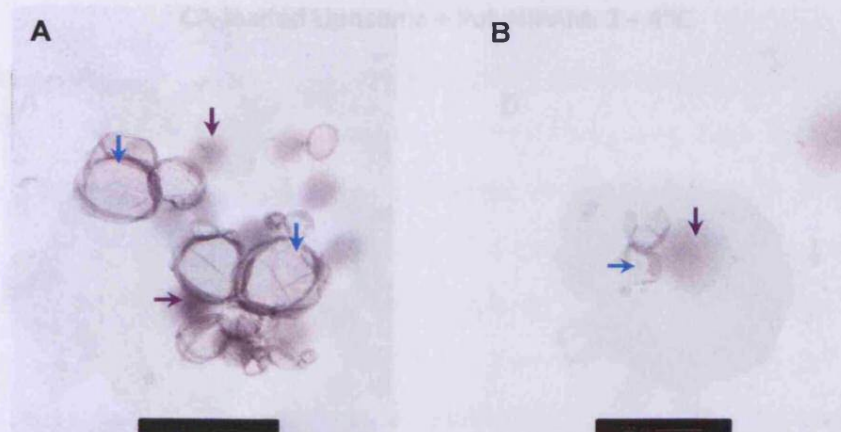


Figure 9-10: TEM images of control (A & B) CA-loaded liposome – polyNIPAM and (C & D) unloaded liposome – polyNIPAM systems maintained at 32°C for 1 h; all samples were negatively-stained with aqueous UA 2% (→ Nanogel; → Liposome).

A – D : Clusters of either CA-loaded or unloaded liposome vesicles (→) with lightly-stained background of polyNIPAM nanogel particles (→).

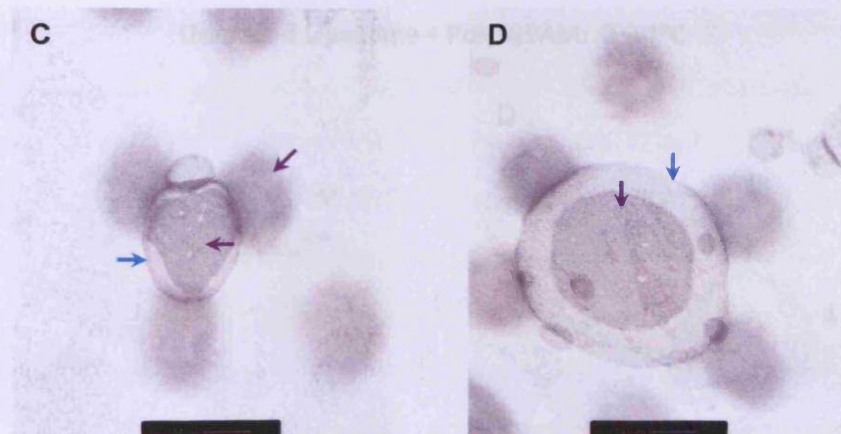
CA-loaded Liposome + Poly(NIPAM-co-AAc)(5%): 2 – 4°C



Scale bar: 300 nm (Magn: 16Kx)

Scale bar: 300 nm (Magn: 32Kx)

Unloaded Liposome + Poly(NIPAM-co-AAc)(5%): 2 – 4°C



Scale bar: 300 nm (Magn: 32Kx)

Scale bar: 300 nm (Magn: 32Kx)

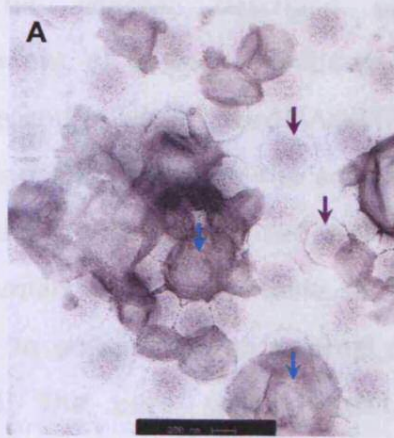
Figure 9-11: TEM images of a proposed single compartment system where poly(NIPAM-co-AAc)(5%) and CA-loaded liposome exist within a single formulation, maintained at 2 – 4°C for 24 h; all samples were negatively-stained with aqueous UA 2% (→ Nanogel; → Liposome).

A & B : Particles of poly(NIPAM-co-AAc)(5%) nanogel (→) appear attached to the broken vesicles of CA-loaded liposome (→).

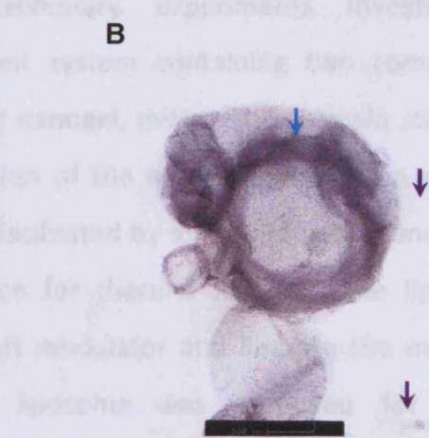
C & D : Unloaded liposome-poly(NIPAM-co-AAc)(5%) appear in a well-formed complex, consisting of several nanogel particles (→) that either attached to or loaded into the larger liposome vesicles (→).

9.4. CONCLUSION

CA-loaded Liposome + PolyNIPAM: 2 – 4°C

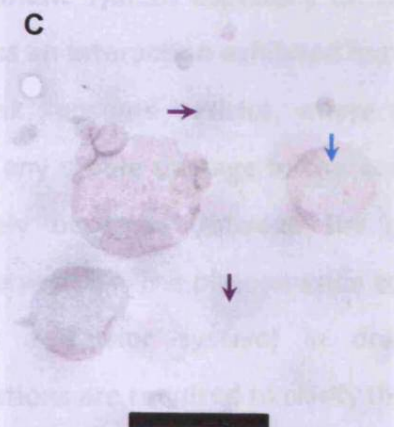


Scale bar: 300 nm (Magn: 16Kx)

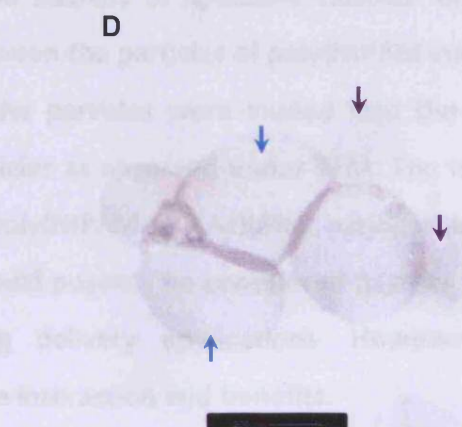


Scale bar: 300 nm (Magn: 32Kx)

Unloaded Liposome + PolyNIPAM: 2 – 4°C



Scale bar: 300 nm (Magn: 16Kx)



Scale bar: 300 nm (Magn: 32Kx)

Figure 9-12: TEM images of control (A & B) CA-loaded liposome – polyNIPAM and (C & D) unloaded liposome – polyNIPAM systems maintained at 2 – 4°C for 1 h; all samples were negatively-stained with aqueous UA 2% (→ Nanogel; → Liposome).

- A & B : Clusters of the polyNIPAM particles (→) and CA-loaded liposome vesicles (→). Some of the liposome vesicles still retain their typical lamellar membranes.
- C & D : Most of the liposome vesicles shown damaged membranes (→) and the pale-stained polyNIPAM nanogel particles (→) are seen in the background.

9.4 CONCLUSION

This chapter described preliminary experiments investigating the development of a single compartment system containing two components i.e. liposome and poly(NIPAM-co-AAc)(5%) nanogel, designed to remain stable until its application onto the skin. The activation of the nanogel particles to release their therapeutic payload is intended to be facilitated by external thermal and pH stimuli. Since human skin is a suitable source for thermal stimulus, the liposome was selected to encapsulate an external pH modulator and liberate the material once required. The pure sphingomyelin liposome was proposed for the single compartment system, however, it was found to be unsuitable due to instability. Lipid fragments were observed in the samples stored at 2 – 4°C and ambient temperature.

Further investigations are required to improve the proposed single compartment system especially on the stability of liposome vesicles. In addition, there was an interaction exhibited between the particles of poly(NIPAM-co-AAc)(5%) and blank liposome vesicles, where the particles were loaded into the liposome without any visible damage to the vesicles as observed under TEM. The interaction exclusively occurred between the poly(NIPAM-co-AAc)(5%) nanogel and blank liposome vesicles. The phenomenon could possibly be considered to offer potentials (e.g. as a carrier system) in drug delivery applications. However, further investigations are required to clarify the interaction and benefits.

CHAPTER 10 | General Discussion

10.1 GENERAL DISCUSSION

Over the years, substantial research, consequent publications, patents and product development studies on the homopolymer polyNIPAM, and its copolymers have been reported. Despite a long history of investigation, there are limited scientific studies describing polyNIPAM-based nanogel particles, as carriers for controlled- or triggered-drug delivery across the skin, which was therefore the major topic of investigation in this thesis.

The objective of this thesis was to investigate the potential of multiple stimuli-responsive co-polymers polyNIPAM, with a view to serve as carriers for drug delivery by topical route of administration. The characteristics of nanogels can be exploited for drug delivery applications to attain adequate localisation of actives within the skin, to enhance the local effect or to increase the penetration through the SC.

A multi-responsive temperature- and pH-modulated type polyNIPAM-based polymer of nanoscale size was proposed. By inducing a change in their swelling/deswelling behaviour, which directly correlates to the release of the incorporated materials, a triggered-release carrier system can be developed. In this regard, the environmental sensitivity of the polymer is advantageous, and can be tailored according to the selected skin characteristics:

- (i) Particulates of submicron size ($< 1 \mu\text{m}$) are suitable candidates for transdermal delivery, as generally discussed in CHAPTER 1;
- (ii) Temperature-responsive – skin has an average surface temperature of 32°C and thus, could serve as a source of thermal stimulus; and
- (iii) pH-responsive – skin provides a weak acidic environment of pH 4 – 7.

Active ingredients were hypothesised to be loaded into the nanogel particles under one set of conditions, where it is swollen the most ($T < \text{LCST}$ and $\text{pH} > \text{pK}_a$ of the functional groups) and expel the actives once their structures collapse due to changes in the environmental medium ($T > \text{LCST}$ and $\text{pH} < \text{pK}_a$ of the functional groups). Application of an external pH modulator was suggested to create a stronger

acidic medium, in addition to the skin acidic environment. To establish the above aim, a single compartment system comprised of a multi-responsive nanogel and a thermally labile liposome was proposed. The liposome was used to isolate the external pH modulator from in contact with the nanogel until required.

At the beginning of the study, a series of temperature-responsive polyNIPAM-based gels of nanoscale size were synthesised by the SFEP technique (CHAPTER 2). The nanogels were synthesised based on several different parameters in terms of co-monomer incorporation, pH of the reaction mixture, and stirring rate during the polymerisation. Furthermore, CHAPTER 2 focussed on the experimental procedures used to characterise the nanogel particles in terms of particle size, size distribution, thermal analysis, swelling/de-swelling capacity and morphology. The copolymer polyNIPAM co-butyl acrylate termed as poly(NIPAM-co-BA) was found to exhibit the most dramatic changes of its swelling/ de-swelling behaviour in response to changes in surrounding temperature.

Following that, the poly(NIPAM-co-BA) nanogel was investigated for its loading and release efficiency using a model permeant (MTX), as described in CHAPTER 3. It was found that the nanogel was capable of delivering MTX across *ex vivo* porcine epidermis in levels that significantly reduce the biosynthesis of PGE₂, a key inflammatory mediator. MTX possesses anti-inflammatory properties, thus reduction in the PGE₂ expression was used as an indirect marker of successful delivery of the agent across skin. Both delivery and biological activity of MTX were further enhanced by the addition of Na₂CO₃, which was found not to be pro-inflammatory. The enhancement effect produced by the base was found not related to the nanogel particles, as the nanogel did not possess any significant level of ionic functional groups, thus, lack of pH-responsive effect. The enhancement effect believed to be due to *in situ* solubilisation of the MTX in basic condition and dissolution from within the nanoparticles already deposited within the skin.

In an attempt to achieve higher release of loaded permeant, a multiple stimuli responsive nanogels, temperature- and pH-responsive, were synthesised in CHAPTER 4. The pH-induced conformational changes offered additional 'triggering' variables for use in the systems for controlled-release agents in topical delivery

applications. Simultaneous temperature- and pH-triggering effects may contribute to enhanced swelling/de-swelling capacity than each stimulus individually. Temperature- and pH- responsive nanogels as drug delivery carriers have a unique set of properties that ideally fit conditions of drug transport via skin routes of administration. Such material offers considerable advantages over their homopolymer analogue (polyNIPAM), which are only sensitive to temperature changes. The nanogels were prepared by incorporating varying amounts of hydrophilic AAc co-monomer (0%, 2% and 5% w/v) into polyNIPAM to form poly(NIPAM-co-AAc). The poly(NIPAM-co-AAc)(5%) dispersed in aqueous media was found to be the most responsive by exhibiting the most pronounced swelling/de-swelling capacity in response to pH and temperature stimuli. It also exhibited a uniform distribution of AAc functional groups, as shown by negative-staining technique with aqueous uranyl acetate (UA) 2%.

To be considered as potential carriers for drug delivery via skin, it is necessary to prove that the particles of nanogel are able to traverse across the principle barrier of the skin, SC, following their topical application. The thermal analysis data demonstrated that the addition of external pH modulator (CA) into the aqueous dispersion of poly(NIPAM-co-AAc)(5%), resulted in a significant decrease of its LCST from 37°C to 31°C; thus, enhanced its degree of de-swelling at 32°C (skin surface temperature). *In vitro* migration, followed by electron microscope imaging was carried out to probe the migration of the intact empty nanogel particles across the porcine epidermis with and without the addition of aqueous solution of CA (see CHAPTER 5). Although non conclusive, it is possible that the particles of poly(NIPAM-co-AAc)(5%) and polyNIPAM are capable of penetrating the skin and migrating across the epidermis, as shown by the presence of the particulates in the diffusion cell receptor phases. However, the anticipated effect of external pH modulator in modulating the permeation of particles was found to be marginal.

Following the promising results of the penetration studies for poly(NIPAM-co-AAc)(5%) and polyNIPAM particles, loading and release studies of model permeants by the respected nanogels were carried out in CHAPTER 6. The loading was done via a “breathing-in” technique, with model permeants of cosmetic peptides and

caffeine. Poly(NIPAM-co-AAc)(5%) and polyNIPAM nanogels facilitate the skin permeation of loaded permeants and therefore, have the potential to act as carriers for topically applied compounds intended for skin conditions or transdermal. The studies indicate that the hydrophilic/hydrophobic balance of the nanogels does influence the corresponding loading level of permeants with respect to water/octanol partition co-efficient of the permeants.

A study was undertaken to investigate potential side-effects following topical application of the poly(NIPAM-co-BA), poly(NIPAM-co-AAc)(5%) and control polyNIPAM in comparison to their monomers at the tissue level. Both poly(NIPAM-co-AAc)(5%) and polyNIPAM were found not to induce significant inflammatory reactions post-topical application, suggesting their compatibility with skin. However, the Western blotting results demonstrated that the poly(NIPAM-co-BA) was pro-inflammatory to the skin. This could be largely due to increased hydrophobicity, as a result of the hydrocarbon side chain of the butyl co-monomer.

As stated earlier, the proposed single compartment system involves a second key component, the pH modulator-loaded liposome. In CHAPTER 8, the liposome vesicles of pure sphingomyelin were prepared for encapsulation of an external pH modulator, CA. However, the loaded-liposome was found to be unstable within the acidic environment (~pH 2) presented by the CA solution during storage condition, characterised by a time-dependant reduction of the vesicle size and the appearance of broken lipid fragments. The lipid type and drug lipid ratio might be the most important factors in determining the stability and functionality of the product, while the pH and temperature conditions are the most important environmental conditions to be considered.

For the final part of the study, a preliminary investigation into developing a single compartment system containing two components i.e. liposome and poly(NIPAM-co-AAc)(5%) nanogel, designed to remain stable until its application onto the skin was carried out. However, the system was found to be unstable primarily due to the instability posed by the liposome vesicles. Interestingly, the particles of poly(NIPAM-co-AAc) were found to gain access to the empty liposome

vesicles, with no physical alteration to the structure of vesicles observed, i.e. absence of lipid films or fragments.

In summary, the advantages and limitations of the polyNIPAM-based nanogels particularly poly(NIPAM-co-AAc)(5%) as carriers in topical delivery have been investigated and supported by the data in this thesis. The particles of nanogel demonstrated an enhanced delivery of model permeants across the skin relative to the saturated aqueous solution of the free permeants. However, the proposed composite system was found to be lacking in stability, primarily due to the liposome component especially CA-loaded liposome. The pure sphingomyelin liposome was found to be unstable under storage conditions; thus, unable to retain the encapsulated pH modulator molecules. Even though the application of the external pH modulator was found to be insignificant to the activation of the nanogel particles, the approach still can be consider for other types of dual-action systems.

10.2 FUTURE WORK

Given the initial progress made and encouraging results obtained with this thesis on triggered-permeants release from nanogels, further investigations are required. Further works are required to elucidate the mechanism involve in penetration of the particulates across the SC. Apart from that, investigations regarding their possible safety potentials are one of the primary concerns. Biocompatibility at cellular level such as sensitisation study will give some further insights in terms of safety level. In addition, *in vivo* work on animals could also be undertaken to determine the clinical efficacy achieved, as a result of enhanced delivery by the nanogels to further establish potential clinical benefits. Studies should be done to improve the design of the liposome – skin – nanogel composite system. Liposome preparations with improved stability profiles are one of the main concerns for the composite system.

10.3 CONCLUDING REMARKS

The hypothesis that the polyNIPAM-based nanogel particles would result in improved topical delivery has been demonstrated. This work focused on the development of a pH modulator-loaded liposome – skin – polyNIPAM-based nanogel composite system. This novel smart drug delivery system is within reach, provided the pH modulator-loaded liposome can be adequately stabilised.

REFERENCES

- Abu Samah, N.H., Heard, C.M., 2011. Topically applied KTTKS: a review. *Int. J. Cosmet. Sci.*, (corrected proof).
- Agarwal, K., Lange, A.-C., Beck, H., 2007. Thermal imaging in healthy humans – what is “normal” skin temperature? [online]. Available at: <http://www.goinfrared.com/media/2007-005Agarwal.pdf> [Accessed: 28 January 2011].
- Agbugba, C.B., Hendriksen, B.A., Chowdhry, B.Z., Snowden, M.J., 1998. The redispersibility and physico-chemical properties of freeze-dried colloidal microgels. *Colloids Surf. A Physicochem. Eng. Asp.* 137, 155-164.
- Aguilar, M.R., Elvira, C., Gallardo, A., Vázquez, B., Román, J.S., 2007. Smart polymers and their applications as biomaterials, in: Ashammakhi, N., Reis, R.L., Chiellini, E. (Eds.), *Topics in Tissue Engineering*. University of Oulu, Finland, pp. 1-27.
- Ali, M.F., Salah, M., Rafea, M., Saleh, N., 2008. Liposomal methotrexate hydrogel for treatment of localized psoriasis: preparation, characterization and laser targeting. *Med. Sci. Monit.* 14, PI66-74.
- Alvarez-Figueroa, M.J., Delgado-Charro, M.B., Blanco-Méndez, J., 2001. Passive and iontophoretic transdermal penetration of methotrexate. *Int. J. Pharm.* 212, 101-107.
- Alvarez-Román, R., Naik, A., Kalia, Y.N., Fessi, H., Guy, R.H., 2004a. Visualization of skin penetration using confocal laser scanning microscopy. *Eur. J. Pharm. Biopharm.* 58, 301-316.
- Alvarez-Román, R., Naik, A., Kalia, Y.N., Guy, R.H., Fessi, H., 2004b. Enhancement of topical delivery from biodegradable nanoparticles. *Pharm. Res.* 21, 1818-1825.
- Alvarez-Román, R., Naik, A., Kalia, Y.N., Guy, R.H., Fessi, H., 2004c. Skin penetration and distribution of polymeric nanoparticles. *J. Controlled Release* 99, 53-62.
- Amalvy, J.I., Wanless, E.J., Li, Y., Michailidou, V., Armes, S.P., Duccini, Y., 2004. Synthesis and characterization of novel pH-responsive microgels based on tertiary amine methacrylates. *Langmuir* 20, 8992-8999.
- Ankareddi, I., Bailey, M.M., Brazel, C.S., Rasco, J.F., Hood, R.D., 2008. Developmental toxicity assessment of thermoresponsive poly(*N*-isopropylacrylamide-co-acrylamide) oligomers in CD-1 mice. *Birth Defects Res. B Dev. Reprod. Toxicol.* 83, 112-116.
- Ariën, A., Henry-Toulmé, N., Dupuy, B., 1994. Calcitonin-loaded liposomes: stability under acidic conditions and bile salts-induced disruption resulting in calcitonin-phospholipid complex formation. *Biochim. Biophys. Acta* 1193, 93-100.
- Aungst, B.J., Blake, J.A., Hussain, M.A., 1990. Contributions of drug solubilization, partitioning, barrier disruption, and solvent permeation to the enhancement of skin permeation of various compounds with fatty acids and amines. *Pharm. Res.* 7, 712-718.
- Balazs, D.A., Godbey, W., 2011. Liposomes for use in gene delivery. *J. Drug. Deliv.* 2011, 1-12.

- Bangham, A.D., Standish, M.M., Miller, N., 1965. Cation permeability of phospholipid model membranes: effect of narcotics. *Nature* 208, 1295-1297.
- Baroli, B., 2010. Penetration of nanoparticles and nanomaterials in the skin: fiction or reality? *J. Pharm. Sci.* 99, 21-50.
- Baumann, L., Saghari, S., 2009. Basic science of the dermis, in: Baumann, L. (Ed.), *Cosmetic Dermatology: Principles and Practice*, second ed. McGraw-Hill Companies, New York, pp. 8-13.
- Beltran, S., Baker, J.P., Hooper, H.H., Blanch, H.W., Prausnitz, J.M., 1991. Swelling equilibria for weakly ionizable, temperature-sensitive hydrogels. *Macromolecules* 24, 549-551.
- Benson, H., Caccetta, R., Chen, Y., Kearns, P., Toth, I., 2003. Transdermal delivery of a tetrapeptide: evaluation of passive diffusion. *Int. J. Pept. Res. Ther.* 10, 615-620.
- Benson, H.A., 2005. Transdermal drug delivery: penetration enhancement techniques. *Curr. Drug Deliv.* 2, 23-33.
- Berti, J.J., Lipsky, J.J., 1995. Transcutaneous drug delivery: a practical review. *Mayo Clinic Proceedings* 70, 581-586.
- Betz, G., Imboden, R., Imanidis, G., 2001. Interaction of liposome formulations with human skin *in vitro*. *Int. J. Pharm.* 229, 117-129.
- Bhalerao, S.S., Raje Harshal, A., 2003. Preparation, optimization, characterization, and stability studies of salicylic acid liposomes. *Drug Dev. Ind. Pharm.* 29, 451-467.
- Boderke, P., Merkle, H.P., Cullander, C., Ponec, M., Bodde, H.E., 1997. Localization of aminopeptidase activity in freshly excised human skin: direct visualization by confocal laser scanning microscopy. *J. Investig. Dermatol.* 108, 83-86.
- Bradley, M., Ramos, J., Vincent, B., 2005. Equilibrium and kinetic aspects of the uptake of poly(ethylene oxide) by copolymer microgel particles of *N*-isopropylacrylamide and acrylic acid. *Langmuir* 21, 1209-1215.
- Brain, K.R., Hadgraft, J., Lewis, D., Allan, G., 1991. The influence of azone[®] on the percutaneous absorption of methotrexate. *Int. J. Pharm.* 71, R9-R11.
- Bromberg, L.E., Ron, E.S., 1998. Temperature-responsive gels and thermogelling polymer matrices for protein and peptide delivery. *Adv. Drug Delivery Rev.* 31, 197-221.
- Bronaugh, R.L., 2007. Methods for *in vitro* skin metabolism studies, in: Zhai, H., Wilhelm, K.-P., Maibach, H.I. (Eds.), *Marzulli and Maibach's Dermatotoxicology*. Taylor & Francis Ltd., Boca Raton, pp. 373-376.
- Bronaugh, R.L., Maibach, H.I., 2005. *Percutaneous Absorption: Drugs, Cosmetics, Mechanisms, Methodology*, fourth ed. Taylor & Francis, Boca Raton; London.
- Brown, M.B., Martin, G.P., Jones, S.A., Akomeah, F.K., 2006. Dermal and transdermal drug delivery systems: current and future prospects. *Drug Delivery* 13, 175-187.
- Burgess, D.J., 2001. Regulatory science of liposome drug products. US FDA, Florida.

- Cayman Chemical Company, 2011. Schematic of the ACE™ EIA, in: Prostaglandin E₂ EIA kit - Monoclonal, 01/24/2011 ed. Cayman Chemical Company, Ann Arbor.
- Cevc, G., 1993. Lipid properties as a basis for membrane modeling and rational liposome design, in: Gregoriadis, G. (Ed.), *Liposome Technology - Liposome Preparation and Related Techniques*, second ed. CRC Press, Boca Raton, pp. 2-31.
- Cevc, G., Schätzlein, A., Blume, G., 1995. Transdermal drug carriers: basic properties, optimization and transfer efficiency in the case of epicutaneously applied peptides. *J. Controlled Release* 36, 3-16.
- Chai, Z., Zheng, X., Sun, X., 2003. Preparation of polymer microspheres from solutions. *J. Polym. Sci. B Polym. Phys.* 41, 159-165.
- Chatterjee, S., Banerjee, D.K., 2002. Preparation, isolation and characterisation of liposomes containing natural and synthetic lipids, in: Basu, S.C., Basu, M. (Eds.), *Liposome Methods and Protocols - Methods in Molecular Biology*. Humana Press Inc, Totowa, pp. 1-16.
- Chetanachan, P., Akarachalanon, P., Worawirunwong, D., Dararutana, P., Bangtrakulnonth, A., Bunjop, M., Kongmuang, S., 2008. Ultrastructural characterization of liposomes using transmission electron microscope. *Adv. Mat. Res.* 55-57, 709-711.
- Chilcott, R.P., Jenner, J., Hotchkiss, S.A.M., Rice, P., 2001. In vitro skin absorption and decontamination of sulphur mustard: comparison of human and pig-ear skin. *J. Appl. Toxicol.* 21, 279-283.
- Chrai, S.S., Murari, R., Ahmad, I., 2001. Liposomes: a review part I: manufacturing issues. *BioPharm* 14, 10-14.
- Christensen, M.L., Keiding, K., 2005. Study of the compositional heterogeneity in poly(*N*-isopropylacrylamide-acrylic acid) microgels by potentiometric titration experiments. *Colloids Surf. A Physicochem. Eng. Asp.* 252, 61-69.
- Chung, J.H., Seo, J.Y., Choi, H.R., Lee, M.K., Youn, C.S., Rhie, G., Cho, K.H., Kim, K.H., Park, K.C., Eun, H.C., 2001. Modulation of skin collagen metabolism in aged and photoaged human skin *in vivo*. *J. Invest. Dermatol.* 117, 1218-1224.
- Cohen, R., Barenholz, Y., 1978. Correlation between the thermotropic behavior of sphingomyelin liposomes and sphingomyelin hydrolysis by sphingomyelinase of *Staphylococcus aureus*. *Biochim. Biophys. Acta* 509, 181-187.
- Collins, P., Rogers, S., 1992. The efficacy of methotrexate in psoriasis - a review of 40 cases. *Clin. Exp. Dermatol.* 17, 257-260.
- Contri, R.V., Fiel, L.A., Pohlmann, A.R., Guterres, S.S., Beck, R.C.R., 2011. Transport of substances and nanoparticles across the skin and *in vitro* models to evaluate skin permeation and/or penetration, in: Beck, R., Guterres, S., Pohlmann, A.R. (Eds.), *Nanocosmetics and Nanomedicines: New Approaches for Skin Care*. Springer-Verlag Berlin Heidelberg, New York, p. 9.
- Cosmetic Ingredient Review, 2010. Cosmetic ingredients found safe as used (1089 total, through September, 2010). Cosmetic Ingredient Review, Washington.

- Crofford, L.J., 1997. COX-1 and COX-2 tissue expression: implications and predictions. *J. Rheumatol.* 49, 15-19.
- Crowther, H.M., Vincent, B., 1998. Swelling behavior of poly-*N*-isopropylacrylamide microgel particles in alcoholic solutions. *Colloid Polym. Sci.* 276, 46-51.
- da Silva, R., Ganzarolli de Oliveira, M., 2007. Effect of the cross-linking degree on the morphology of poly(NIPAAm-co-AAc) hydrogels. *Polymer* 48, 4114-4122.
- Das, M., 2008. Stimulus-responsive microgels: Design, properties and applications. University of Toronto, Toronto.
- Das, M., Zhang, H., Kumacheva, E., 2006. Microgels: old materials with new applications. *Annu. Rev. Mater. Res.* 36, 117-142.
- Davison, Z., Nicholson, R.I., Maillard, J.Y., Denyer, S.P., Heard, C.M., 2009. Control of microbial contamination of Franz diffusion cell receptor phase in the development of transcutaneous breast cancer therapeutics. *Lett. Appl. Microbiol.* 49, 456-460.
- Dearman, R.J., Betts, C.J., Farr, C., McLaughlin, J., Berdasco, N., Wiench, K., Kimber, I., 2007. Comparative analysis of skin sensitization potency of acrylates (methyl acrylate, ethyl acrylate, butyl acrylate, and ethylhexyl acrylate) using the local lymph node assay. *Contact Dermatitis* 57, 242-247.
- deBethizy, J.D., Udinsky, J.R., Scribner, H.E., Frederick, C.B., 1987. The disposition and metabolism of acrylic acid and ethyl acrylate in male Sprague-Dawley rats. *Fundam. Appl. Toxicol.* 8, 549-561.
- Denyer, S.P., Bowen, J.L., Heard, C.M., 2007. Novel therapeutic delivery system - United Kingdom. Patent GB2437806, United Kingdom Intellectual Property Office (IPO).
- Desai, A., 2007. Topical and transdermal delivery systems, in: Desai, A., Lee, M. (Eds.), *Drug Delivery Systems in Pharmaceutical Care*. American Society of Health-System Pharmacists, Bethesda, pp. 43-58.
- Dick, I.P., Scott, R.C., 1992. Pig ear skin as an *in-vitro* model for human skin permeability. *J. Pharm. Pharmacol.* 44, 640-645.
- Diegelmann, R.F., 2001. Collagen metabolism. *Wounds* 13, 177-182.
- Don, T.-M., Huang, M.-L., Chiu, A.-C., Kuo, K.-H., Chiu, W.-Y., Chiu, L.-H., 2008. Preparation of thermo-responsive acrylic hydrogels useful for the application in transdermal drug delivery systems. *Mater. Chem. Phys.* 107, 266-273.
- Dong, L.-C., Hoffman, A.S., 1991. A novel approach for preparation of pH-sensitive hydrogels for enteric drug delivery. *J. Controlled Release* 15, 141-152.
- Dowding, P.J., Vincent, B., Williams, E., 2000. Preparation and swelling properties of poly(NIPAM) "minigel" particles prepared by inverse suspension polymerization. *J. Colloid Interface Sci.* 221, 268-272.

- Draeos, Z.D., 2002. Glycolic acid and other superficial peels, in: Lowe, N.J. (Ed.), *Textbook of Facial Rejuvenation: The Art of Minimally Invasive Combination Therapy*. Martin Dunitz, Taylor & Francis Group plc, London, pp. 49-59.
- Eeckman, F., Moës, A.J., Amighi, K., 2004. Synthesis and characterization of thermosensitive copolymers for oral controlled drug delivery. *Eur. Polym. J.* 40, 873-881.
- Egger, G., Satanton, R., Cameron-Smith, D., 2003. Alternative treatments for weight loss: range, rationale, and effectiveness, in: Medeiros-Neto, G., Halpern, A., Bouchard, C. (Eds.), *Progress in Obesity Research: No. 9: Proceedings of the 9th International Congress on Obesity*. John Libbey Eurotext, Surrey, pp. 922-926.
- El Maghraby, G.M., Barry, B.W., Williams, A.C., 2008. Liposomes and skin: from drug delivery to model membranes. *Eur. J. Pharm. Sci.* 34, 203-222.
- Eliassaf, J., 1978. Aqueous solutions of poly(*N*-isopropylacrylamide). *J. Appl. Polym. Sci.* 22, 873-874.
- Eskicirak, B., Zemheri, E., Cerkezoglu, A., 2006. The treatment of psoriasis vulgaris: 1% topical methotrexate gel. *Int. J. Dermatol.* 45, 965-969.
- Fasano, W.J., Manning, L.A., Green, J.W., 2002. Rapid integrity assessment of rat and human epidermal membranes for *in vitro* dermal regulatory testing: Correlation of electrical resistance with tritiated water permeability. *Toxicol. in Vitro* 16, 731-740.
- FitzGerald, P.A., Amalvy, J.I., Armes, S.P., Wanless, E.J., 2008. Film-forming microgels for pH-triggered capture and release. *Langmuir* 24, 10228-10234.
- Flory, P.J., Rehner, J., 1943. Statistical mechanics of cross-linked polymer networks II. Swelling. *J. Chem. Phys.* 11, 521-526.
- Flynn, G.L., 2002. Cutaneous and transdermal delivery - process and systems of delivery, in: Banker, G.S., Rhodes, C.T. (Eds.), *Modern Pharmaceutics*, fourth revised ed. Informa Healthcare, New York, pp. 187-235.
- Foldvari, M., 2000. Non-invasive administration of drugs through the skin: challenges in delivery system design. *Pharm. Sci. Technol. Today.* 3, 417-425.
- Futagami, A., Ishizaki, M., Fukuda, Y., Kawana, S., Yamanaka, N., 2002. Wound healing involves induction of cyclooxygenase-2 expression in rat skin. *Lab. Invest.* 82, 1503-1513.
- Galaev, I., Mattiasson, B., 2007. *Smart Polymers - Applications in Biotechnology and Biomedicine*, second revised ed. Taylor & Francis, Boca Raton.
- Gan, T., Guan, Y., Zhang, Y., 2010. Thermogelable PNIPAM microgel dispersion as 3D cell scaffold: effect of syneresis. *J. Mater. Chem.* 20, 5937-5944.
- Gehrke, S.H., Uhden, L.H., McBride, J.F., 1998. Enhanced loading and activity retention of bioactive proteins in hydrogel delivery systems. *J. Controlled Release* 55, 21-33.
- Ghanayem, B.I., Maronpot, R.R., Matthews, H.B., 1985. Ethyl acrylate-induced gastric toxicity: II. Structure-toxicity relationships and mechanism. *Toxicol. Appl. Pharmacol.* 80, 336-344.

- Goldovsky, M., Zhai, H., Dika, E., Maibach, H.I., 2006. Safety assays in skin pharmacology, in: Vogel, H.G., Hock, F.J., Maas, J., Mayer, D. (Eds.), *Drug Discovery and Evaluation: Safety and Pharmacokinetic Assays*. Springer-Verlag Berlin Heidelberg, New York, p. 366.
- Gorouhi, F., Maibach, H.I., 2009. Role of topical peptides in preventing or treating aged skin. *Int. J. Cosmet. Sci.* 31, 327-345.
- Gracia, L.H., Snowden, M.J., 2007. Preparation, properties and applications of colloidal microgels, in: Williams, P.A. (Ed.), *Handbook of Industrial Water Soluble Polymers*. Blackwell Publishing Ltd, Oxford, pp. 268-297.
- Griffin, J.M., Robb, I., Bismarck, A., 2007. Preparation and characterization of surfactant-free stimuli-sensitive microgel dispersions. *J. Appl. Polym. Sci.* 104, 1912-1919.
- Guterres, S.S., Alves, M.P., Pohlmann, A.R., 2007. Polymeric nanoparticles, nanospheres and nanocapsules, for cutaneous applications. *Drug Target Insights* 2, 147-157.
- Guy, R.H., 1996. Current status and future prospects of transdermal drug delivery. *Pharm. Res.* 13, 1765-1769.
- Hadgraft, J., 2004. Skin deep. *Eur. J. Pharm. Biopharm.* 58, 291-299.
- Hadgraft, J., Guy, R.H., 1989. *Transdermal Drug Delivery: Developmental Issues and Research Initiatives*. Marcel Dekker, New York.
- Hall, R.J., Pinkrah, V.T., Chowdhry, B.Z., Snowden, M.J., 2004. Heteroaggregation studies of mixed cationic co-polymer/anionic homopolymer microgel dispersions. *Colloids Surf. A Physicochem. Eng. Asp.* 233, 25-38.
- Hallensleben, M.L., 2004. Crosslinking and polymer networks, in: Kricheldorf, H.R., Nuyken, O., Swift, G. (Eds.), *Handbook of Polymer Synthesis*, second ed. Taylor & Francis, London, pp. 841-880.
- Hayat, M.A., 2000. *Principles and Techniques of Electron Microscopy: Biological Application*, fourth ed. Cambridge University Press, Cambridge.
- Heard, C.M., Kung, D., Thomas, C.P., 2006. Skin penetration enhancement of mefenamic acid by ethanol and 1,8-cineole can be explained by the "pull" effect. *Int. J. Pharm.* 321, 167-170.
- Heard, C.M., Screen, C., 2008. Probing the permeation enhancement of mefenamic acid by ethanol across full-thickness skin, heat-separated epidermal membrane and heat-separated dermal membrane. *Int. J. Pharm.* 349, 323-325.
- Hellweg, T., 2003. Properties of NIPAM-based intelligent microgel particles: investigated using scattering methods, in: Liz-Marzan, L.M., Kamat, P.V. (Eds.), *Nanoscale Materials*. Kluwer Academic Publishers, Dordrecht, pp. 209-225.
- Hernández, G.L., Volpert, O.V., Íñiguez, M.A., Lorenzo, E., Martínez-Martínez, S., Grau, R., Fresno, M., Redondo, J.M., 2001. Selective inhibition of vascular endothelial growth factor – mediated angiogenesis by cyclosporin A. *J. Exp. Med.* 193, 607-620.
- Hideji, T., Kazuo, H., 1982. Structure-toxicity relationship of acrylates and methacrylates. *Toxicol. Lett.* 11, 125-129.

- Hoare, T., McLean, D., 2006. Kinetic prediction of functional group distributions in thermosensitive microgels. *J. Phys. Chem. B* 110, 20327-20336.
- Hoare, T., Pelton, R., 2004a. Functional group distributions in carboxylic acid containing poly(*N*-isopropylacrylamide) microgels. *Langmuir* 20, 2123-2133.
- Hoare, T., Pelton, R., 2004b. Highly pH and temperature responsive microgels functionalized with vinylacetic acid. *Macromolecules* 37, 2544-2550.
- Hoare, T., Pelton, R., 2007. Functionalized microgel swelling: comparing theory and experiment. *J. Phys. Chem. B* 111, 11895-11906.
- Hoare, T., Pelton, R., 2008a. Characterizing charge and crosslinker distributions in polyelectrolyte microgels. *Curr. Opin. Colloid Interface Sci.* 13, 413-428.
- Hoare, T., Pelton, R., 2008b. Impact of microgel morphology on functionalized microgel-drug interactions. *Langmuir* 24, 1005-1012.
- Hoffman, A.S., 1995. "Intelligent" polymers in medicine and biotechnology. *Artificial Organs* 19, 458-467.
- Houk, J., Guy, R.H., 1988. Membrane models for skin penetration studies. *Chem. Rev.* 88, 455-472.
- Huang, X., Brazel, C.S., 2001. On the importance and mechanisms of burst release in matrix-controlled drug delivery systems. *J. Controlled Release* 73, 121-136.
- Ishii, F., Nagasaka, Y., 2001. Simple and convenient method for estimation of marker entrapped in liposomes. *J. Dispersion Sci. Technol.* 22, 97 - 101.
- IUPAC Macromolecular Division, 1996. Commission on macromolecular nomenclature, recommendation. *Pure Appl. Chem.* 68, 2287-2311.
- Jagur-Grodzinski, J., 2010. Polymeric gels and hydrogels for biomedical and pharmaceutical applications. *Polym. Adv. Technol.* 21, 27-47.
- Kabanov, A.V., Vinogradov, S.V., 2008. Nanogels as pharmaceutical carriers, in: Torchilin, V.P. (Ed.), *Multifunctional Pharmaceutical Nanocarriers*. Springer-Verlag New York Inc, New York, pp. 67-80.
- Kaneda, I., Vincent, B., 2004. Swelling behavior of PMMA-g-PEO microgel particles by organic solvents. *J. Colloid Interface Sci.* 274, 49-54.
- Kawaguchi, H., Fujimoto, K., Mizuhara, Y., 1992. Hydrogel microspheres III. Temperature-dependent adsorption of proteins on poly-*N*-isopropylacrylamide hydrogel microspheres. *Colloid Polym. Sci.* 270, 53-57.
- Keerl, M., Richtering, W., 2007. Synergistic depression of volume phase transition temperature in copolymer microgels. *Colloid Polym. Sci.* 285, 471-474.
- Khan, A., 2007. Preparation and characterization of *N*-isopropylacrylamide/acrylic acid copolymer core-shell microgel particles. *J. Colloid Interface Sci.* 313, 697-704.

- Khare, A.R., Peppas, N.A., 1995. Swelling/deswelling of anionic copolymer gels. *Biomaterials* 16, 559-567.
- Kim, S.W., Bae, Y.H., Okano, T., 1992. Hydrogels: Swelling, drug loading, and release. *Pharm. Res.* 9, 283-290.
- Kligman, A.M., Christophers, E., 1963. Preparation of isolated sheets of human stratum corneum. *Arch. Dermatol.* 88, 702-705.
- Knorr, F., Lademann, J., Patzelt, A., Sterry, W., Blume-Peytavi, U., Vogt, A., 2009. Follicular transport route - research progress and future perspectives. *Eur. J. Pharm. Biopharm.* 71, 173-180.
- Kokufuta, E., Wang, B., Yoshida, R., Khokhlov, A.R., Hirata, M., 1998. Volume phase transition of polyelectrolyte gels with different charge distributions. *Macromolecules* 31, 6878-6884.
- Kratz, K., Hellweg, T., Eimer, W., 2000. Influence of charge density on the swelling of colloidal poly(*N*-isopropylacrylamide-co-acrylic acid) microgels. *Colloids Surf. A Physicochem. Eng. Asp.* 170, 137-149.
- Kratz, K., Hellweg, T., Eimer, W., 2001. Structural changes in PNIPAM microgel particles as seen by SANS, DLS, and EM techniques. *Polymer* 42, 6631-6639.
- Lademann, J., Knorr, F., Richter, H., Blume-Peytavi, U., Vogt, A., Antoniou, C., Sterry, W., Patzelt, A., 2008. Hair follicles – an efficient storage and penetration pathway for topically applied substances. *Skin Pharmacol. Physiol.* 21, 150-155.
- Lademann, J., Patzelt, A., Richter, H., Antoniou, C., Sterry, W., Knorr, F., 2009. Determination of the cuticula thickness of human and porcine hairs and their potential influence on the penetration of nanoparticles into the hair follicles. *J. Biomedical Optics* 14, 021014.
- Lademann, J., Richter, H., Schanzer, S., Knorr, F., Meinke, M., Sterry, W., Patzelt, A., 2011. Penetration and storage of particles in human skin: perspectives and safety aspects. *Eur. J. Pharm. Biopharm.* 77, 465-468.
- Lademann, J., Richter, H., Teichmann, A., Otberg, N., Blume-Peytavi, U., Luengo, J., Weiß, B., Schaefer, U.F., Lehr, C.-M., Wepf, R., Sterry, W., 2007. Nanoparticles - an efficient carrier for drug delivery into the hair follicles. *Eur. J. Pharm. Biopharm.* 66, 159-164.
- Lambers, H., Piessens, S., Bloem, A., Pronk, H., Finkel, P., 2006. Natural skin surface pH is on average below 5, which is beneficial for its resident flora. *Int. J. Cosmet. Sci.* 28, 359-370.
- Langer, R., Peppas, N., A. , 2003. Advances in biomaterials, drug delivery, and bionanotechnology. *AIChE J.* 49, 2990-3006.
- Lau, W.M., White, A.W., Gallagher, S.J., Donaldson, M., McNaughton, G., Heard, C.M., 2008. Scope and limitations of the co-drug approach to topical drug delivery. *Curr. Pharm. Des.* 14, 794-802.
- Lauer, A.C., Ramachandran, C., Lieb, L.M., Niemiec, S., Weiner, N.D., 1996. Targeted delivery to the pilosebaceous unit via liposomes. *Adv. Drug Delivery Rev.* 18, 311-324.

- Lautenschläger, H., 2006. Liposomes, in: Barel, A.O., Paye, M., Maibach, H.I. (Eds.), *Handbook of Cosmetic Science and Technology*. CRC Press Taylor & Francis Group, Boca Raton, pp. 155-163.
- Lee, C.-F., Lin, C.-C., Chiu, W.-Y., 2008. Thermosensitive and control release behavior of poly (*N*-isopropylacrylamide-co-acrylic acid) latex particles. *J. Polym. Sci. A Polym. Chem.* 46, 5734-5741.
- Leong, J., Hughes-Fulford, M., Rakhlin, N., Habib, A., Maclouf, J., Goldyne, M.E., 1996. Cyclooxygenases in human and mouse skin and cultured human keratinocytes: association of COX-2 expression with human keratinocyte differentiation. *Exp. Cell Res.* 224, 79-87.
- Lin, C.-L., Chiu, W.-Y., Lee, C.-F., 2006. Preparation, morphology, and thermoresponsive properties of poly(*N*-isopropylacrylamide)-based copolymer microgels. *J. Polym. Sci. A Polym. Chem.* 44, 356-370.
- Lintner, K., Peschard, O., 2000. Biologically active peptides: from a laboratory bench curiosity to a functional skin care product. *Int. J. Cosmet. Sci.* 22, 207-218.
- Lopez, V.C., Hadgraft, J., Snowden, M.J., 2005. The use of colloidal microgels as a (trans)dermal drug delivery system. *Int. J. Pharm.* 292, 137-147.
- Lopez, V.C., Raghavan, S.L., Snowden, M.J., 2004. Colloidal microgels as transdermal delivery systems. *React. Funct. Polym.* 58, 175-185.
- Lupo, M.P., Cole, A.L., 2007. Cosmeceutical peptides. *Dermatol. Ther.* 20, 343-349.
- Lynch, I., Blute, I.A., Zhmud, B., MacArtain, P., Tosoletto, M., Allen, L.T., Byrne, H.J., Farrell, G.F., Keenan, A.K., Gallagher, W.M., Dawson, K.A., 2005. Correlation of the adhesive properties of cells to *N*-isopropylacrylamide/*N*-tert-butylacrylamide copolymer surfaces with changes in surface structure using contact angle measurements, molecular simulations, and Raman spectroscopy. *Chem. Mater.* 17, 3889-3898.
- Ma, X., Xi, J., Zhao, X., Tang, X., 2005. Deswelling comparison of temperature-sensitive poly(*N*-isopropylacrylamide) microgels containing functional -OH groups with different hydrophilic long side chains. *J. Polym. Sci. B Polym. Phys.* 43, 3575-3583.
- Maghraby, G.M.M.E., Williams, A.C., Barry, B.W., 2006. Can drug-bearing liposomes penetrate intact skin? *Journal of Pharmacy and Pharmacology* 58, 415-429.
- Mahalingam, R., Li, X., Jasti, B.R., 2008. Semisolid dosages: ointments, creams, and gels, in: Gad, S.C. (Ed.), *Pharmaceutical Manufacturing Handbook: Production and Processes*. Wiley, John & Sons, Incorporated, New Jersey, p. 306.
- Makino, K., Agata, H., Ohshima, H., 2000. Dependence of temperature-sensitivity of poly(*N*-isopropylacrylamide-co-acrylic acid) hydrogel microspheres upon their sizes. *J. Colloid Interface Sci.* 230, 128-134.
- Makino, K., Kado, H., Ohshima, H., 2001. Aggregation behavior of poly(*N*-isopropylacrylamide) microspheres. *Colloids Surf. B Biointerfaces* 20, 347-353.

- Malonne, H., Eeckman, F., Fontaine, D., Otto, A., Vos, L.D., Moës, A., Fontaine, J., Amighi, K., 2005. Preparation of poly(*N*-isopropylacrylamide) copolymers and preliminary assessment of their acute and subacute toxicity in mice. *Eur. J. Pharm. Biopharm.* 61, 188-194.
- Malvern Instruments Ltd., 2007. Mastersizer 2000 User Manual MAN0384 Issue 1.0 ed. Malvern Instruments Ltd., Malvern.
- Marks, F., Fürstenberger, G., Müller-Decker, K., 1998. Arachidonic acid metabolism as a reporter of skin irritancy and target of cancer chemoprevention. *Toxicol. Lett.* 96-97, 111-118.
- Maroon, J.C., Bost, J.W., Borden, M.K., Lorenz, K.M., Ross, N.A., 2006. Natural antiinflammatory agents for pain relief in athletes. *Neurosurg Focus.* 21, E11.
- Marshak, D.R., Kadonaga, J.T., Burgess, R.R., Knuth, M.W., Brennan, W.A., Lin, S.-H., 1995. *Strategies for Protein Purification and Characterization: A Laboratory Course Manual.* Cold Spring Harbor Laboratory Press, New York.
- Mayer, L.D., Madden, T.D., Bally, M.B., Cullis, P.R., 1993. pH Gradient-mediated drug entrapment in liposomes, in: Gregoriadis, G. (Ed.), *Liposome Technology Entrapment of Drugs and Other Materials*, second ed. CRC Press, Boca Raton, pp. 27-42.
- McCullough, J.L., Snyder, D.S., Weinstein, G.D., Friedland, A., Stein, B., 1976. Factors affecting human percutaneous penetration of methotrexate and its analogues *in vitro*. *J. Investig. Dermatol.* 66, 103-107.
- Mendelsohn, R., Flach, C.R., Moore, D.J., 2006. Determination of molecular conformation and permeation in skin via IR spectroscopy, microscopy, and imaging. *Biochim. Biophys. Acta* 1758, 923-933.
- Mezei, M., Gulasekharan, V., 1980. Liposomes - a selective drug delivery system for the topical route of administration I. Lotion dosage form. *Life Sci.* 26, 1473-1477.
- Minoo-Rabeeh-Hobabi, Hassanzadeh, D., Azarmi, S., Entezami, A.A., 2007. Effect of synthesis method and buffer composition on the LCST of a smart copolymer of *N*-isopropylacrylamide and acrylic acid. *Polym. Adv. Technol.* 18, 986-992.
- Mitragotri, S., 2003. Modeling skin permeability to hydrophilic and hydrophobic solutes based on four permeation pathways. *J. Controlled Release* 86, 69-92.
- Mitragotri, S., 2007. Temperature dependence of skin permeability to hydrophilic and hydrophobic solutes. *J. Pharm. Sci.* 96, 1832-1839.
- Mizoguchi, K., Ida, J., Matsuyama, T., Yamamoto, H., 2010. Straight-chained thermo-responsive polymer with high chelating group content for heavy metal ion recovery. *Sep. Purif. Technol.* 75, 69-75.
- Moser, K., Kriwet, K., Naik, A., Kalia, Y.N., Guy, R.H., 2001. Passive skin penetration enhancement and its quantification *in vitro*. *Eur. J. Pharm. Biopharm.* 52, 103-112.
- Murray, M.J., Snowden, M.J., 1995. The preparation, characterisation and applications of colloidal microgels. *Adv. Colloid Interface Sci.* 54, 73-91.

- Murthy, N., Xu, M., Schuck, S., Kunisawa, J., Shastri, N., Fréchet, J.M.J., 2003. A macromolecular delivery vehicle for protein-based vaccines: acid-degradable protein-loaded microgels. *Proc. Nat. Acad. Sci. USA* 100, 4995-5000.
- Nacka, F., Cansell, M., Gouygou, J.P., Gerbeaud, C., Méléard, P., Entressangles, B., 2001. Physical and chemical stability of marine lipid-based liposomes under acid conditions. *Colloids Surf. B Biointerfaces* 20, 257-266.
- Naha, P.C., Bhattacharya, K., Tenuta, T., Dawson, K.A., Lynch, I., Gracia, A., Lyng, F.M., Byrne, H.J., 2010a. Intracellular localisation, geno- and cytotoxic response of poly-N-isopropylacrylamide (PNIPAM) nanoparticles to human keratinocyte (HaCaT) and colon cells (SW 480). *Toxicol. Lett.* 198, 134-143.
- Naha, P.C., Davoren, M., Lyng, F.M., Byrne, H.J., 2010b. Reactive oxygen species (ROS) induced cytokine production and cytotoxicity of PAMAM dendrimers in J774A.1 cells. *Toxicol. Appl. Pharmacol.* 246, 91-99.
- Nakatani, Y., Kudo, I., 2002. Prostaglandin E₂ synthases. *Nippon Yakurigaku Zasshi* 120, 373-378.
- Narawane, L., Lee, V.H.L., 1994. Absorption barrier, in: Boer, A.G.d. (Ed.), *Drug Absorption Enhancement: Concepts, Possibilities, Limitations and Trends*. Harwood-Academic Publishers, Chur, pp. 1-50.
- Nayak, S.P., Lyon, L.A., 2005. Soft nanotechnology with soft nanoparticles. *Angew. Chem. Int. Ed. Engl.* 44, 7686-7708.
- Ness, S.A., 1994. *Surface and Dermal Monitoring for Toxic Exposures*. John Wiley and Sons Ltd, New York.
- Neyret, S., Vincent, B., 1997. The properties of polyampholyte microgel particles prepared by microemulsion polymerization. *Polymer* 38, 6129-6134.
- Nii, T., Ishii, F., 2005. Encapsulation efficiency of water-soluble and insoluble drugs in liposomes prepared by the microencapsulation vesicle method. *Int. J. Pharm.* 298, 198-205.
- NIOSH, 2010. Skin permeation calculator. [online]. Available at: <http://www.cdc.gov/niosh/topics/skin/skinpermcalf.html> [Accessed: 5 September 2010].
- Nolan, C.M., 2005. *Microgel based materials for controlled macromolecule delivery*. Georgia Institute of Technology, Georgia.
- Nolan, C.M., Serpe, M.J., Lyon, L.A., 2004. Thermally modulated insulin release from microgel thin films. *Biomacromolecules* 5, 1940-1946.
- Nur, H., Pinkrah, V.T., Mitchell, J.C., Benée, L.S., Snowden, M.J., 2010. Synthesis and properties of polyelectrolyte microgel particles. *Adv. Colloid Interface Sci.* 158, 15-20.
- ObservatoryNANO, 2008. *Nanotechnology in cosmetics*, 21 November 2008 ed. ObservatoryNANO.
- Odian, G., 2004. *Principles of Polymerization*, fourth ed. Wiley, John & Sons Inc, New Jersey.

- Oh, J.K., Drumright, R., Siegwart, D.J., Matyjaszewski, K., 2008. The development of microgels/nanogels for drug delivery applications. *Prog. Polym. Sci.* 33, 448-477.
- Oh, J.K., Lee, D.I., Park, J.M., 2009. Biopolymer-based microgels/nanogels for drug delivery applications. *Prog. Polym. Sci.* 34, 1261-1282.
- Oikarinen, A., 2004. Connective tissue and aging. *Int. J. Cosmet. Sci.* 26, 107-107.
- Otberg, N., Richter, H., Schaefer, H., Blume-Peytavi, U., Sterry, W., Lademann, J., 2004. Variations of hair follicle size and distribution in different body sites. *J. Investig. Dermatol.* 122, 14-19.
- Otto, D.P., M. de Villiers, M., 2009. Physicochemical principles of nanosized drug delivery systems, in: Villiers, M.M.d., Aramwit, P., Kwon, G.S. (Eds.), *Nanotechnology in Drug Delivery*. Springer-Verlag New York Inc, New York, pp. 3-34.
- Paige, D., 2005. Skin disease, in: Kumar, P.J., Clark, M.L. (Eds.), *Kumar and Clark Clinical Medicine*, sixth ed. Elsevier Health Sciences, London, pp. 1315-1317.
- Panayiotou, M., Pöhner, C., Vandevyver, C., Wandrey, C., Hilbrig, F., Freitag, R., 2007. Synthesis and characterisation of thermo-responsive poly(*N,N'*-diethylacrylamide) microgels. *React. Funct. Polym.* 67, 807-819.
- Pattnaik, P., Ray, T., 2009. Improving liposome integrity and easing bottlenecks to production. *Pharmaceutical Technology Europe* 22, 24-28.
- Patzelt, A., Richter, H., Knorr, F., Schäfer, U., Lehr, C.-M., Dähne, L., Sterry, W., Lademann, J., 2011. Selective follicular targeting by modification of the particle sizes. *J. Controlled Release* 150, 45-48.
- Pelton, R., 2000. Temperature-sensitive aqueous microgels. *Adv. Colloid Interface Sci.* 85, 1-33.
- Pelton, R.H., Chibante, P., 1986. Preparation of aqueous latices with *N*-isopropylacrylamide. *Colloids Surf.* 20, 247-256.
- Peppas, N.A., Bures, P., Leobandung, W., Ichikawa, H., 2000. Hydrogels in pharmaceutical formulations. *Eur. J. Pharm. Biopharm.* 50, 27-46.
- Pillai, O., Nair, V., Panchagnula, R., 2004. Transdermal iontophoresis of insulin: IV. Influence of chemical enhancers. *Int. J. Pharm.* 269, 109-120.
- Pinkrah, V.T., Beezer, A.E., Chowdhry, B.Z., Gracia, L.H., Mitchell, J.C., Snowden, M.J., 2004. Thermodynamic considerations of microgel swelling behavior. *Langmuir* 20, 8531-8536.
- Potts, R.O., Guy, R.H., 1992. Predicting skin permeability. *Pharm. Res.* 9, 663-669.
- Pouillot, A., Dayan, N., Polla, A.S., Polla, L.L., Polla, B.S., 2008. The stratum corneum: a double paradox. *J. Cosmet. Dermatol.* 7, 143-148.
- Prausnitz, M.R., Mitragotri, S., Langer, R., 2004. Current status and future potential of transdermal drug delivery. *Nat Rev Drug Discov* 3, 115-124.

- Prow, T.W., Grice, J.E., Lin, L.L., Faye, R., Butler, M., Becker, W., Wurm, E.M.T., Yoong, C., Robertson, T.A., Soyer, H.P., Roberts, M.S., 2011. Nanoparticles and microparticles for skin drug delivery. *Adv. Drug Delivery Rev.* 63, 470-491.
- Pugh, W.J., Roberts, M.S., Hadgraft, J., 1996. Epidermal permeability - penetrant structure relationships: 3. The effect of hydrogen bonding interactions and molecular size on diffusion across the stratum corneum. *Int. J. Pharm.* 138, 149-165.
- Rajakariar, R., Yaqoob, M.M., Gilroy, D.W., 2006. COX-2 in inflammation and resolution. *Mol. Interv.* 6, 199-207.
- Ranade, V.V., Cannon, J.B., 2011. *Drug Delivery Systems*, third ed. CRC Press, Boca Raton.
- Ranade, V.V., Hollinger, M.A., 2003. *Drug Delivery Systems*, second revised ed. Taylor & Francis, Boca Raton.
- Reilly, D.M., Parslew, R., Sharpe, G.R., Powell, S., Green, M.R., 2000. Inflammatory mediators in normal, sensitive and diseased skin types. *Acta Derm. Venereol.* 80, 171-174.
- Renwick, A.G., Hillier, K., Waller, D.G., 2001. *Medical pharmacology and therapeutics*, 1st ed. Elsevier Health Sciences, London.
- Riboni, L., Giussani, P., Viani, P., 2010. Sphingolipid transport, in: Chalfant, C., Poeta, M.D. (Eds.), *Sphingolipids as Signaling and Regulatory Molecules*. Springer-Verlag New York Inc, New York, pp. 24-45.
- Rolland, A., Wagner, N., Chatelus, A., Shroot, B., Schaefer, H., 1993. Site-specific drug delivery to pilosebaceous structures using polymeric microspheres. *Pharm. Res.* 10, 1738-1744.
- Rosen, M.R., 2005. *Delivery System Handbook for Personal Care and Cosmetic Products, Personal Care & Cosmetic Technology*. William Andrew Publishing, Norwich.
- Samah, N.A., Williams, N., Heard, C.M., 2010. Nanogel particulates located within diffusion cell receptor phases following topical application demonstrates uptake into and migration across skin. *International Journal of Pharmaceutics* 401, 72-78.
- Sato, K., Kang, W.H., Saga, K., Sato, K.T., 1989. Biology of sweat glands and their disorders. I. Normal sweat gland function. *J. Am. Acad. Dermatol.* 20, 537-563.
- Saunders, B., Vincent, B., 2006. Responsive microgel dispersions, in: Somasundaran, P. (Ed.), *Encyclopedia of Surface and Colloid Science*, second ed. Taylor & Francis, New York, pp. 5430-5444.
- Saunders, B.R., 2004. On the structure of poly(*N*-isopropylacrylamide) microgel particles. *Langmuir* 20, 3925-3932.
- Saunders, B.R., Laajam, N., Daly, E., Teow, S., Hu, X., Stepto, R., 2009. Microgels: from responsive polymer colloids to biomaterials. *Adv. Colloid Interface Sci.* 147-148, 251-262.
- Saunders, B.R., Vincent, B., 1996. Thermal and osmotic deswelling of poly(NIPAM) microgel particles. *J. Chem. Soc., Faraday Trans.* 92, 3385 - 3389.

- Saunders, B.R., Vincent, B., 1999. Microgel particles as model colloids: theory, properties and applications. *Adv. Colloid Interface Sci.* 80, 1-25.
- Schild, H.G., 1992. Poly(*N*-isopropylacrylamide): experiment, theory and application. *Prog. Polym. Sci.* 17, 163-249.
- Schmidt, T., Janik, I., Kadlubowski, S., Ulanski, P., Rosiak, J.M., Reichelt, R., Arndt, K.-F., 2005. Pulsed electron beam irradiation of dilute aqueous poly(vinyl methyl ether) solutions. *Polymer* 46, 9908-9918.
- Schmook, F.P., Meingassner, J.G., Billich, A., 2001. Comparison of human skin or epidermis models with human and animal skin in *in-vitro* percutaneous absorption. *Int. J. Pharm.* 215, 51-56.
- Scientific Committee on Emerging and Newly Identified Health Risks, 2010. Scientific basis for the definition of the term "Nanomaterial", in: Directorate-General for Health & Consumers (Ed.), Scientific Committee on Emerging and Newly Identified Health Risks. European Commission, Brussels.
- Senff, H., Richtering, W., 2000. Influence of cross-link density on rheological properties of temperature-sensitive microgel suspensions. *Colloid Polym. Sci.* 278, 830-840.
- Shibata, A., Nakagawa, K., Yamanoi, H., Tsuduki, T., Sookwong, P., Higuchi, O., Kimura, F., Miyazawa, T., 2010. Sulforaphane suppresses ultraviolet B-induced inflammation in HaCaT keratinocytes and HR-1 hairless mice. *J. Nutr. Biochem.* 21, 702-709.
- Siddiqui, O., Roberts, M.S., Polack, A.E., 1985. Topical absorption of methotrexate: role of dermal transport. *Int. J. Pharm.* 27, 193-203.
- Silver, E.H., Murphy, S.D., 1981. Potentiation of acrylate ester toxicity by prior treatment with the carboxylesterase inhibitor triorthotolyl phosphate (TOTP). *Toxicol. Appl. Pharmacol.* 57, 208-219.
- Simon, G.A., Maibach, H.I., 2000. The pig as an experimental animal model of percutaneous permeation in man: qualitative and quantitative observations – an overview. *Skin Pharmacol. Physiol.* 13, 229-234.
- Snowden, M.J., Chowdhry, B.Z., Vincent, B., Morris, G.E., 1996. Colloidal copolymer microgels of *N*-isopropylacrylamide and acrylic acid: pH, ionic strength and temperature effects. *J. Chem. Soc., Faraday Trans.* 92, 5013-5016.
- Stark, K., Törmä, H., Oliw, E.H., 2006. Co-localization of COX-2, CYP4F8, and mPGES-1 in epidermis with prominent expression of CYP4F8 mRNA in psoriatic lesions. *Prostaglandins Other Lipid Mediat.* 79, 114-125.
- Steinrasser, I., Merkle, H.P., 1995. Dermal metabolism of topically applied drugs: pathways and models reconsidered. *Pharm. Acta Helv.* 70, 3-24.
- Stracke, F., Schneider, M., 2010. Nanoparticulate systems and the dermal barrier, in: Sattler, K.D. (Ed.), *Nanomedicine and Nanorobotics (Handbook of Nanophysics)*. CRC Press, Boca Raton, pp. 1-14.

- Sulkowski, W.W., Pentak, D., Nowak, K., Sulkowska, A., 2005. The influence of temperature, cholesterol content and pH on liposome stability. *J. Mol. Struct.* 744-747, 737-747.
- Swarbrick, J., 2004. *Encyclopedia of Pharmaceutical Technology*, second revised ed. Informa Healthcare, New York.
- Tam, K.C., Ragaram, S., Pelton, R.H., 1994. Interaction of surfactants with poly(*N*-isopropylacrylamide) microgel latexes. *Langmuir* 10, 418-422.
- Tauer, K., 2003. Latex particles, in: Caruso, F. (Ed.), *Colloids and Colloid Assemblies: Synthesis, Modification, Organization and Utilization of Colloid Particles*. Wiley-VCH, Weinheim, pp. 1-51.
- Taylor, K.M.G., Morris, R.M., 1995. Thermal analysis of phase transition behaviour in liposomes. *Thermochim. Acta* 248, 289-301.
- Thomas, C.P., Davison, Z., Heard, C.M., 2007. Probing the skin permeation of fish oil/EPA and ketoprofen-3. Effects on epidermal COX-2 and LOX. *Prostaglandins Leukot. Essent. Fatty Acids* 76, 357-362.
- Thorne, J., Vine, G., Snowden, M., 2011. Microgel applications and commercial considerations. *Colloid Polym. Sci.*, 1-22.
- Tinkle, S.S., Antonini, J.M., Rich, B.A., Roberts, J.R., Salmen, R., DePree, K., Adkins, E.J., 2003. Skin as a route of exposure and sensitization in chronic beryllium disease. *Environ. Health Perspect.* 111, 1202-1208.
- Toll, R., Jacobi, U., Richter, H., Lademann, J., Schaefer, H., Blume-Peytavi, U., 2003. Penetration profile of microspheres in follicular targeting of terminal hair follicles. *J. Investig. Dermatol.* 123, 168-176.
- Trotta, M., Peira, E., Carlotti, M.E., Gallarate, M., 2004. Deformable liposomes for dermal administration of methotrexate. *Int. J. Pharm.* 270, 119-125.
- Tsuda, Y., Kikuchi, A., Yamato, M., Sakurai, Y., Umezu, M., Okano, T., 2004. Control of cell adhesion and detachment using temperature and thermoresponsive copolymer grafted culture surfaces. *J. Biomed. Mater. Res. A* 69A, 70-78.
- US Food & Drug Administration, 1994. CFR - Code of Federal Regulations Title 21, Medical Device Database, 12 December 1994 ed. US Department of Health & Human Services.
- US Food & Drug Administration, 2005. Fentanyl Transdermal System (marketed as Duragesic) Information. [online]. Available at: <http://www.fda.gov/Drugs/DrugSafety/PostmarketDrugSafetyInformationforPatientsandProviders/ucm114961.htm> [Accessed: 6 August 2011].
- US Food and Drug Administration, 2010. Reporting format for nanotechnology-related information in CMC review, 6 June 2010 ed. Center for Drug Evaluation and Research (CDER) Office of Pharmaceutical Science, pp. 1-11.

- Vardaxis, N.J., Brans, T.A., Boon, M.E., Kreis, R.W., Marres, L.M., 1997. Confocal laser scanning microscopy of porcine skin: implications for human wound healing studies. *J Anat.* 190, 601-611.
- Velasco, M.V.R., Tano, C.T.N., Machado-Santelli, G.M., Consiglieri, V.O., Kaneko, T.M., Baby, A.R., 2008. Effects of caffeine and siloxanetriol alginate caffeine, as anticellulite agents, on fatty tissue: histological evaluation. *J. Cosmet. Dermatol.* 7, 23-29.
- Verma, D.D., Verma, S., Blume, G., Fahr, A., 2003. Particle size of liposomes influences dermal delivery of substances into skin. *Int. J. Pharm.* 258, 141-151.
- Vincent, B., 2006. Microgels and core-shell particles, in: Blitz, J., Gun'ko, V. (Eds.), *Surface Chemistry in Biomedical and Environmental Science*. Springer, Dordrecht, pp. 11-22.
- Vogt, A., Mandt, N., Lademann, J., Schaefer, H., Blume-Peytavi, U., 2005. Follicular targeting-a promising tool in selective dermatotherapy. *J. Investig. Dermatol. Symp. Proc.* 10, 252-255.
- Wadajkar, A., Koppolu, B., Rahimi, M., Nguyen, K., 2009. Cytotoxic evaluation of *N*-isopropylacrylamide monomers and temperature-sensitive poly(*N*-isopropylacrylamide) nanoparticles. *J. Nanopart. Res.* 11, 1375-1382.
- Wang, Q., Xu, H., Yang, X., Yang, Y., 2008. Drug release behavior from *in situ* gelatinized thermosensitive nanogel aqueous dispersions. *Int. J. Pharm.* 361, 189-193.
- Warheit, D.B., Sayes, C.M., Reed, K.L., Swain, K.A., 2008. Health effects related to nanoparticle exposures: environmental, health and safety considerations for assessing hazards and risks. *Pharmacol. Ther.* 120, 35-42.
- Weinstein, G.D., McCullough, J.L., Eaglstein, W.H., Golub, A., Cornell, R.C., Stoughton, R.B., Clendenning, W., Zackheim, H., Maibach, H., Kulp, K.R., King, L., Baden, H.P., Taylor, J.S., Deneau, D.D., 1981. A clinical screening program for topical chemotherapeutic drugs in psoriasis. *Arch. Dermatol.* 117, 388-393.
- Williams, A., 2003. *Transdermal and Topical Drug Delivery: From Theory to Clinical Practice*. Pharmaceutical Press, London.
- Woodward, N.C., Chowdhry, B.Z., Snowden, M.J., Leharne, S.A., Griffiths, P.C., Winnington, A.L., 2003. Calorimetric investigation of the influence of cross-linker concentration on the volume phase transition of poly(*N*-isopropylacrylamide) colloidal microgels. *Langmuir* 19, 3202-3211.
- Wu, X., Pelton, R.H., Hamielec, A.E., Woods, D.R., McPhee, W., 1994. The kinetics of poly(*N*-isopropylacrylamide) microgel latex formation. *Colloid Polym. Sci.* 272, 467-477.
- Xia, S., Xu, S., 2005. Ferrous sulfate liposomes: preparation, stability and application in fluid milk. *Food Res. Int.* 38, 289-296.
- Yurdasiper, A., Abdelouahd, N., Ertan, G., Heard, C.M., 2008. Effect of naproxen poly(*N*-isopropylacrylamide) microgel on epidermal cyclooxygenase-2, *APS Skin Forum*. APS, London.

- Zha, L., Li, L., Bao, L., 2007. Synthesis and colloidal stability of poly(*N*-isopropylacrylamide) microgels with different ionic groups on their surfaces. *J. Appl. Polym. Sci.* 103, 3893-3898.
- Zhang, H., Mardyani, S., Chan, W.C.W., Kumacheva, E., 2006. Design of biocompatible chitosan microgels for targeted pH-mediated intracellular release of cancer therapeutics. *Biomacromolecules* 7, 1568-1572.
- Zhang, J.-T., Liu, X.-L., Fahr, A., Jandt, K., 2008. A new strategy to prepare temperature-sensitive poly(*N*-isopropylacrylamide) microgels. *Colloid Polym. Sci.* 286, 1209-1213.
- Zhang, X.-Z., Yang, Y.-Y., Wang, F.-J., Chung, T.-S., 2002. Thermosensitive Poly(*N*-isopropylacrylamide-co-acrylic acid) hydrogels with expanded network structures and improved oscillating swelling & deswelling properties. *Langmuir* 18, 2013-2018.
- Zhang, Y., Zha, L.S., Fu, S.K., 2004. Kinetic analysis of poly(*N*-isopropylacrylamide-co-dimethylaminoethyl methacrylate) microgel latex formation. *J. Appl. Polym. Sci.* 92, 839-846.
- Zhang, Y., Zhu, W., Wang, B., Ding, J., 2005. A novel microgel and associated post-fabrication encapsulation technique of proteins. *J. Controlled Release* 105, 260-268.
- Zondlo, F.M., 2002. Final report on the safety assessment of acrylates copolymer and 33 related cosmetic ingredients. *Int. J. Toxicol.* 21, 1-50.
- Zulfakar, M.H., Abdelouahab, N., Heard, C.M., 2010. Enhanced topical delivery and *ex vivo* anti-inflammatory activity from a betamethasone dipropionate formulation containing fish oil. *Inflamm. Res.* 59, 23-30.

